

Coordination of tissue shape and size in the developing zebrafish neuroepithelium

DISSERTATION

Zur Erlangung des akademischen
Grades

Doctor rerum naturalium
(Dr. rer. nat.)

vorgelegt
der Fakultät Mathematik und Naturwissenschaften
der Technische Universität Dresden

von

Marija Matejčić

geboren am 02.12.1987 in Rijeka, Kroatien

Gutachter 1: Prof. Dr. Stephan Grill

Gutachter 2: Prof. Dr. Carl-Philipp Heisenberg

Eingereicht am: 01.11.2017

Verteidigt am: 23.04.2018

Erklärung entsprechend §5.5 der Promotionsordnung/ Declaration according to §5.5 of the doctorate regulations

**PhD Thesis “Coordination of tissue shape and size in the developing zebrafish neuroepithelium”
submitted by Marija Matejčić**

Hiermit versichere ich, dass ich die vorliegende Arbeit ohne unzulässige Hilfe Dritter und ohne Benutzung anderer als der angegebenen Hilfsmittel angefertigt habe; die aus fremden Quellen direkt oder indirekt übernommenen Gedanken sind als solche kenntlich gemacht. Die Arbeit wurde bisher weder im Inland noch im Ausland in gleicher oder ähnlicher Form einer anderen Prüfungsbehörde vorgelegt.

Die Dissertation wurde im Zeitraum vom 01.11.2013 bis 01.11.2017 verfasst und von Dr. Caren Norden, Max Planck Institute of Molecular Cell Biology and Genetics, Norden group betreut.

Meine Person betreffend erkläre ich hiermit, dass keine früheren erfolglosen Promotionsverfahren stattgefunden haben.

Ich erkenne die Promotionsordnung der Fakultät für Mathematik und Naturwissenschaften, Technische Universität Dresden an.

I herewith declare that I have produced this paper without the prohibited assistance of third parties and without making use of aids other than those specified; notions taken over directly or indirectly from other sources have been identified as such. This paper has not previously been presented in identical or similar form to any other German or foreign examination board.

The thesis work was conducted from 01.11.2013 to 01.11.2017 under the supervision of Dr. Caren Norden at Max Planck Institute of Molecular Cell Biology and Genetics, Norden group.

I declare that I have not undertaken any previous unsuccessful doctorate proceedings.

I declare that I recognize the doctorate regulations of the Fakultät für Mathematik und Naturwissenschaften of the Technische Universität Dresden.

ACKNOWLEDGEMENTS

Many people helped and supported me throughout my PhD education. They all made it possible for me to execute this project and remain motivated. But I have no one to thank more than Caren. I am immensely thankful for such an excellent mentor to take the risk and hire me into her experimental lab when I barely knew how to pipette. I am thankful to her for her creativity, humor and empathy, the most. There were often times when I felt she is living through this project, its questions and challenges along with me and that meant a great deal. Working with a group leader who is human above all else was what ensured I don't give up on the project. It also allowed me the luxury of playing and learning to be a scientist. Caren, stay Caren. Thank you.

Thank you to Guillaume Salbreux, our collaborator, for being very open minded and seeing the simplicity in complex problems. Thank you for explaining the physics to me, often repeating the same thing multiple times. This project would be much shallower without your participation. Furthermore, I want to thank my TAC members, Stephan Grill and Gene Myers. I genuinely enjoyed the annual TAC meetings and looked forward to our discussions each time. Except the 1st one, that is. Both Stephan and Gene provided valuable advice on the project. Also, a big thank-you to Stephan for all the consultations aside from the TAC meetings. Some of his insights in the early stages of the project were essential to keep in going in the direction that it did.

I am grateful that Caren listens to her instinct when choosing employees, which makes the Norden lab a productive, collaborative and passionate place to work in. I am thankful to all of you Nordies for all the discussions, laughs and help throughout these 4 years. Special thanks go to the three lab technicians that taught me everything I now know about lab techniques and helped with experiments. Claudia, Sylvia and Heike, thank you! Claudia, I'm not a molecular biology machine yet, but getting there.

This project would not have been possible without the excellent work of the services and facilities of the MPI-CBG, especially the Light Microscopy Facility, the Image Processing Facility, the Computer Department and the Fish Facility. I am also very grateful to the colleagues and labs that shared expertise, constructs and reagents, especially the Huttner, Grill, Myers, Ninov, Stainier and Jacinto groups.

To my selection colleagues and all other friends that I made at the MPI-CBG: thank you for the laughs, discussions and feedback. I wish I had spent more time with you. I am confident we will continue meeting all around the world in the years to come. And to my friends back in Croatia: always thank you for the constant and everlasting support in all issues in life.

This project has been 4 years of me learning to live science. I this time, I have missed out on many opportunities for friendship, talking mostly to fish. However, Björn, you made Dresden (almost) a home. Thank you for the scientific discussions, for teaching me how to discipline my thoughts and express them more clearly. These are essential traits for a scientist and by this, you helped mold me into one. Thank you. And thank you for life, in general. It would not have been the same without our attacks of laughter at 2 AM.

I dedicate the most special place of this important list to my family. Jure, Ksenija, Ante and Sasa (and Lu): words will never be enough to express my gratitude for your love, support and belief. Thank you for your honesty and all the help throughout the years of my education. You are all so different and each of you taught and continues to teach me so much. Thank you for always keeping me on the right track. The work that I have done here was possible because of you. For this reason, I dedicate this Dissertation to your love.

Observe with imagination and verify with patience.

SUMMARY

During development, tissues have to grow and maintain correct shapes in order to function optimally. This requires precise coordination of changes in tissue size and shape and regulation spanning multiple scales. For example, cells have to coordinate their proliferation, size and shape, with tissue-wide emergent properties such as mechanical constraints. Because of this multitude of factors acting across different scales, the answer to which cell properties give rise to a properly formed tissue is not straightforward. Studies investigating the question of coordination of tissue growth and shape are few and were mostly done in 2D, considering only the apical surface of epithelial tissues as a proxy for tissue-wide 3D behaviors. To circumvent this and to investigate how single cell properties contribute to form of a growing neuroepithelium, I studied tissue growth and shape in the developing zebrafish retinal neuroepithelium. This system allows long tissue-wide 3D live and fixed imaging with subcellular resolution.

The retina is a part of the central nervous system, as well as of the body's optical system and as such shape is essential for its function in proper light propagation and transmission. In addition, this tissue is a conserved and widely spread tissue type, the pseudostratified epithelium (PSE). I first characterized tissue-wide growth and identified cellular contributions to it. Using this dataset, I then tested if over-proliferation might limit growth in the retinal PSE. Here, my results suggest that the mitotic, apical surface is not a constraint to growth, as was previously proposed. Next, analysis of changes in tissue shape during growth revealed that tissue shape is kept constant, due to its cells changing their shape through a 40% increase in cell height. I next investigated if this cell elongation might constrain further increase in tissue size. To test such putative limits to proliferation, I inhibited cell differentiation maintain proliferative growth. The differentiation mutant (*hdac1-/-*) proliferated continuously and eventually its retinal shape was perturbed. This lack of proper shape maintenance was due to the cells not being able to increase their height as in the control, indicating that in the mutant condition, cell height is the major constraint on tissue shape. I identify the timely disappearance of an ECM-dependent basal actin accumulation, as well as cell proliferation, as two critical parameters necessary to allow these changes in cell shape and consequently, maintenance of proper tissue shape during growth.

Overall, my work demonstrates a dynamic cell shape homeostasis in the growing retinal neuroepithelium, necessary in order to maintain tissue shape. I propose that retinal cells need to redefine their major mechanical constraints in order to accommodate changes in tissue volume during development. Findings from this study provide important insight into the poorly understood problem of coordinating shape and size of cell and tissue, which might be applicable to other epithelial tissues, as well.

TABLE OF CONTENTS

LIST OF FIGURES	V
LIST OF TABLES	VI
MOVIE LEGENDS.....	VII
LIST OF ACRONYMS.....	VIII
1 INTRODUCTION	1
1.1 FORM OF BIOLOGICAL SYSTEMS.....	1
1.1.1 Overview of scientific interest in biological form	1
1.2 SIZE CONTROL	4
1.2.1 Autonomous vs. non-autonomous organ growth	4
1.2.2 Growth regulatory mechanisms	7
1.2.3 Future challenges	14
1.3 SHAPE CONTROL.....	15
1.3.1 General introduction	15
1.3.2 Cell-intrinsic changes of tissue shape	18
1.3.3 Cell-extrinsic changes of tissue shape.....	20
1.3.4 Future challenges	21
1.4 COORDINATING CHANGES IN SHAPE AND SIZE.....	21
1.5 PSEUDOSTRATIFIED EPITHELIA.....	24
1.5.1 Main characteristics.....	25
1.5.2 Heterogeneity.....	26
1.5.3 Growth and shape of the PSE.....	28
1.5.4 Mechanics of the PSE.....	29
1.5.5 Future challenges	30
1.6 ZEBRAFISH RETINAL PSE.....	31
1.6.1 Optic cup morphogenesis	31
1.6.2 Neuroepithelial stage.....	32
1.6.3 Differentiation stage.....	33
1.6.4 Variability during retinal development	34
1.7 OBJECTIVE OF THE STUDY	36
2 MATERIALS AND METHODS.....	37
2.1 Zebrafish husbandry	37
2.2 Zebrafish methods.....	37
2.2.1 Transgenic and mutant lines	37
2.2.2 Hdac1 genotyping.....	38
2.2.3 Blastomere transplantation	39

2.2.4	mRNA and plasmid injections	39
2.2.5	Morpholino injections	39
2.2.6	Intravitreal cavity injections.....	40
2.2.7	Heatshock of embryos.....	40
2.2.8	Drug treatments.....	40
2.2.9	Laser ablations	41
2.2.10	Immunostaining.....	41
2.2.11	Cell dissociation and flow cytometry	42
1.3	Image acquisition	43
2.3	Image analysis.....	44
2.3.1	Growth analysis using Imaris 8.....	44
2.3.2	Mitotic density distribution (Script 1).....	44
2.3.3	Division orientation.....	45
2.3.4	Specific growth and shape parameters	45
2.3.5	Actin and nuclear signal intensity distribution (Script 2)	47
2.3.6	Cell cycle analyses	47
2.3.7	Rate of cell division.....	47
2.3.8	Rate of differentiation	48
2.3.9	N/C ratio	48
3	RESULTS	49
3.1	Growth of the retinal neuroepithelium.....	49
3.1.1	Growth analysis workflow	49
3.1.2	Growth decomposition.....	51
3.2	Constant tissue shape is ensured by changes in cell shape	62
3.3	Growth limits in apically constrained PSE.....	64
3.3.1	Availability of apical surface is not a growth constraint to the retinal PSE.....	65
3.4	A brake on tissue thickness in differentiation mutants.....	70
3.4.1	PSE characteristics are maintained in <i>hdac1</i> ^{-/-} retinas	70
3.4.2	Cell height is the major shape constraint in <i>hdac1</i> ^{-/-} mutants	74
3.5	Basal actin accumulation is preserved in <i>hdac1</i> ^{-/-} cells	78
3.5.1	Basal actin accumulation persists in <i>hdac1</i> ^{-/-} mutants	78
3.5.2	Basal actin accumulation disappearance is cell non-autonomous.....	80
3.6	Actin reorganization and proliferation allow cell height increase.....	83
3.6.1	Cell height increase does not dependent on neuronal delamination	83
3.6.2	Cell height increase is proliferation-dependent.....	83
3.6.3	Actin reorganization is necessary for cell height increase	84
4	DISCUSSION.....	87
4.1	GROWTH OF THE ZEBRAFISH RETINAL PSE	88

4.1.1	Two phases of growth in the retinal PSE.....	88
4.1.2	Cell cycle duration as a putative target of mechanoregulation in the retinal PSE.....	90
4.2	COORDINATING GROWTH CONSTRAINTS AND TISSUE SHAPE.....	92
4.2.1	Apical surface availability is not a constraint to retinal PSE growth	92
4.2.2	PSE shape in relation to tissue growth.....	94
4.2.3	Tissue and cell characteristics in the Hdac1-/- retinal PSE.....	95
4.2.4	Nature of the brake on cell height.....	97
4.2.5	ECM-dependence of actin brake	99
4.2.6	Putative regulatory mechanisms for actin brake release.....	101
4.2.7	Physical models for tissue-wide cell height increase	103
4.3	PERSPECTIVES.....	104
4.3.1	3D in vivo analyses of growth and shape as essential datasets for systems and synthetic biology	104
4.3.2	Apico-basal support in thick epithelia.....	105
4.3.3	Timing in retinal PSE development.....	106
4.4	CONCLUSION AND OUTLOOK.....	107
	REFERENCES	109
	APPENDIX.....	123

LIST OF FIGURES

Figure 1: Cell-based modes of tissue growth.....	11
Figure 2: Representative modes of changing tissue shape.....	17
Figure 3: Heterogeneity and universality of pseudostratified epithelia.....	27
Figure 4: Early development of the vertebrate eye.....	32
Figure 5: Development of the zebrafish retinal neuroepithelium.....	34
Figure 6: FACS scatterplots of cells from Tg(SoFa) retinas.....	43
Figure 7: Retinal PSE growth and shape 3D analysis workflow.....	50
Figure 8: Retinal PSE growth is isotropic and homogeneous.....	52
Figure 9: Cell number increase during retinal PSE growth.....	54
Figure 10: Retinal neuronal number increases exponentially, as assessed by live FACS analysis.....	55
Figure 11: Proliferative peak might result from an overall shortening of cell cycles.....	57
Figure 12: Possible differential regulation of S- and G1-stage throughout development.....	59
Figure 13: Decrease in cell size contributes to increasing cell density.....	61
Figure 14: Cell shape changes ensure maintenance of tissue shape.....	63
Figure 15: Availability of apical surface for mitosis is not the growth constraint to the retinal PSE.....	67
Figure 16: Retinal PSE grows in accordance to 3D packing constraint.....	69
Figure 17: Differentiation mutants have perturbed retinal PSE shape.....	70
Figure 18: Retinal cells do not differentiate in the Hdac1 ^{-/-} mutant.....	72
Figure 19: PSE tissue structure and characteristics are preserved in Hdac1 ^{-/-} mutants.....	73
Figure 20: Proliferation is necessary for the folding of the hdac1 ^{-/-} retinal PSE.....	74
Figure 21: Characterization of hdac1 ^{-/-} development.....	75
Figure 22: Hdac1 ^{-/-} retinal PSE changes its shape due to a lack of cell height increase.....	77
Figure 23: Basal actin accumulation persists throughout hdac1 ^{-/-} development.....	79
Figure 24: Basal actin accumulation disappears cell non-autonomously and is ECM-dependent.....	82
Figure 25: Cell height increase depends on proliferation.....	84
Figure 26: Actin concentration at the cell poles might be permissive for cell height increase.....	85
Figure 27: Graphical summary.....	88

LIST OF TABLES

Table 1: A summary of selected studies on tissue growth and shape.	3
Table 2: Zebrafish transgenic lines and mutant used in this study.	38
Table 3: Morpholinos used in this study.	40
Table 4: Chemical inhibitors/drugs used in this study.	41
Table 5: Primary antibodies used in this study.	41
Table 6: Summary of basal actin experiments.	85

MOVIE LEGENDS

See back cover for movies.

- Movie 1: Imaris growth analysis workflow/ The animation is an example of fixed tissue analysis. Blue channel: DRAQ5 (all nuclei). White channel: mitotic cells. Related to Figure 7.
- Movie 2: Abundance of mitotic cells at the apical tissue surface at 42 hpf. Spheres: mitotic cells, White signal: Ath5-GFP. Imaris visualization. Related to Figure 8 and 11.
- Movie 3: Example of a light sheet movie used to manually analyze cell cycle lengths. Nuclei are mosaically labeled by Hsp70::H2B-RFP DNA injection. Time resolution is 5 minutes. Related to Figure 11.
- Movie 4: Light sheet imaging allowed direct observation of *hdac1*^{-/-} tissue development. Note the extreme tissue spread around 46 hpf. Green: RAS-GFP mRNA injection, Magenta: H2B-RFP mRNA injection. Time resolution: 15 minutes. Related to Figure 21.
- Movie 5: Light sheet imaging of *hdac1*^{-/-} development at the time of buckling. Folding starts apically ~50 hpf. Cell membrane marker: RAS-GFP mRNA. Time resolution: 15 minutes. Figure 11 and 15.
- Movie 6: Retinal pigment epithelium does not fold with the retinal PSE tissue in *hdac1*^{-/-}. Magenta dot: PSE cell clone. Green dot: RPE cell. Cell membrane marker: RAS-GFP mRNA. Light sheet imaging. Time resolution: 15 minutes. Related to Figure 21.
- Movie 7: Basal actin accumulation disappears tissue-wide in the WT. Actin marker: Tg(*actb1*::EGFP-UtrCH). Membranes of differentiating Ath5⁺ cells are labeled in faint green (Tg(*Ath5*::RFP)). They start expressing Ath5 ~35 hpf, in the bottom-left region (ventro-nasal patch). Light sheet imaging. Time resolution: 15 minutes. Related to Figure 24.
- Movie 8: *hdac1* MO-injected retina of an embryo treated with 125 μ M Rockout. Basal actin disappears at 37 hpf. Cell height does not increase. Green: EGFP-UtrophinCH mRNA; Magenta: H2B-RFP mRNA. Light sheet imaging. Time resolution: 15 minutes. Related to Figure 25.
- Movie 9: WT retina of an embryo treated with 125 μ M Rockout. Basal actin disappears at 37 hpf. Green: EGFP-UtrophinCH mRNA; Magenta: H2B-RFP mRNA. Basal actin disappears at 37 hpf. Light sheet imaging. Time resolution: 15 minutes. Related to Figure 25.
- Movie 10: Cell height increase does not depend on neuronal delamination. Ath5 MO embryo. Cell height increased past 50 μ m before delamination started. Light sheet imaging. Time resolution: 15 minutes. Related to Figure 25.
- Movie 11: Laser ablation of the lateral cell membrane. Cells collapse along the apico-basal axis towards the cell center. Cortical marker: EGFP-UtrophinCH mRNA injection. Spinning disc imaging. Related to Figure 26.
- Movie 12: Laser ablation of the apical cell membrane. Cells collapse along the apico-basal axis towards the cell center. Cortical marker: Tg(*actb1*::HRAS-GFP). Spinning disc imaging. Related to Figure 26.

LIST OF ACRONYMS

ATP	adenosine-triphosphate
CNS	central nervous system
DAPI	4',6-diamidino-2-phenylindole
DNA	deoxyribonucleic acid
Dpp	decapentaplegic
ECM	extracellular matrix
GFP	green fluorescent protein
H2B	histone 2B
HDAC1	histone-deacetylase 1
hpf	hours post fertilization
HS	heat shock
HU+A	hydroxyurea + aphidicolin
PCNA	proliferating cell nuclear antigen
PH3	phospho-histone 3
PSE	pseudostratified epithelium
RFP	red fluorescent protein
RGC	retinal ganglion cell
RNA	ribonucleic acid
RPC	retinal progenitor cell
RPE	retinal pigment epithelium
SD	standard deviation
SEM	standard error of the mean
Tg	transgenic
TSA	trichostatin-a
WT	wildtype

1 INTRODUCTION

1.1 FORM OF BIOLOGICAL SYSTEMS

One of the most intriguing questions in biology is how a single cell develops into the enormous variety of lifeforms around us. Differences in sizes and shapes are one of the most clearly recognizable properties and allow visual beings to quickly identify lifeforms that surround them. Being more than just a visual identifier, tissue form often directly relates to function. In order to generate a functional complex organism, cells, therefore, have to grow into tissues of a correct size and shape. This is not a trivial task, as a multitude of cellular behaviors needs to be coordinated to each other, to their environment and to emergent tissue- and organism-scale properties. Each developing organism will follow a separate set of rules, that originate at the genomic level and act through different signaling pathways or nutrient gradients. Additionally, intrinsic and extrinsic forces that emerge from the growing tissue, will feed back to the molecular regulatory mechanisms, thus controlling the final form (size and shape, collectively). Only proper integration of these complex cues coming from environmental, systemic, tissue and cellular scales can give rise to an ecologically fit organism that functions optimally. In other words, properties at multiple scales have to be integrated, coordinated and regulated in a robust spatiotemporally controlled manner to result in a reproducible developmental outcome. We are only beginning to understand how this coordination functions in the first place. To contribute to this important task, this thesis deals with the problem of coordinating changes in size and shape during development, which is a prerequisite for proper form to arise. In this section, I introduce different cues and means to govern tissue growth and change tissue shape. I then discuss examples of their coordination and in the end motivate this study.

1.1.1 Overview of scientific interest in biological form

The question of how proper form arises is an old question, dating back to “the dawn of self-awareness” (Gilbert, 2013 preface). This long-standing fascination might stem from the fact that humans are visual beings, with most of our perception of the world coming from visual stimuli. Early development of correct form is relevant to an adult modern human as a tangible personal interest (health), but also as an abstract concept of beauty that “dissolves the boundary between ourselves and the world”, as the poet Richard Jefferies put it.

The earliest recorded interest in biological form is likely found among Babylonian and Ancient Egyptian scripts that mention and discuss congenitally malformed children. Later on, Ancient Greeks studied animal embryos and human corpses, trying to relate organ form to its function, as well as working on classifying known lifeforms based on their morphology.

The “practical skepticism” (Horder, 2001), necessary for a critical, scientific thinking developed only with the Renaissance (14-16th century). As a mathematician, a biologist and a physicist, Leonardo da Vinci was the archetypal *Homo universalis* of the 16th century. He dealt with ideal human proportions (The Vitruvian Man) and malformations that illness can inflict upon them. Allowed to dissect human corpses, da Vinci also studied the morphology of the human fetus (Gilson, 2008). Renaissance research was mostly descriptive, though and no theories on how fetal proportions might develop were proposed. Further morphological and anatomical work remained similarly speculative for as long as until the mid 19th century. In the 17th century, biology was still a descriptive and controversial field, but two main schools arose on the topic of human creation. One argued for preformation, the other for epigenesis (Horder, 2001). Epigenesis revolutionarily proposed that biological form arises gradually through the process of development. By the end of the 17th century, a more experimental approach was on the rise, methods and microscope lenses became better and the idea of epigenesis became established. In the 19th century, after many debates, the Cell theory (1839) was established, identifying cells as basic units of all living things. This opened way to research that was concerned with more unifying principles, i.e., how changes in cells result in observable changes on the tissue level. In the end of the 19th century, Charles Darwin proposed that natural selection resulted in all the different final forms we observe, where the forms fit to live will survive and thrive and the unfit ones would die out during the course of evolution. By the start of the 20th century, biologists thus fully adopted the experimental approach and began to explain how form gradually arises during development and how it might have evolved. At the time while Darwin’s theory was still ‘catching on’, D’Arcy Wentworth Thompson, proclaimed a *Homo universalis* of the 20th century, put forth a theory of development that did not take natural selection nor inheritance into account. In his book, *On Growth and Form* (1917; (D. W. Thompson, 2014 preface by S. J. Gould), Thompson instead proposed that the form of each new organism develops to be fit according to the mechanical environment in its ecological niche. A hundred years later, research is unifying both Thompson’s and Darwin’s theories, provided with a fast-growing pool of evidence on how mechanical forces constrain and direct the development of evolved forms.

Following a burst in experimental methods and data on embryology at the end of the 19th century, 20th century developmental biology relied on increasingly molecular approaches. After the era of biochemistry, cell biology and molecular biology, it was only in the last ~25 years that the research on tissue form experienced a revival. This was in part due to sufficient accumulation of data on single molecular players and signaling pathways during “the molecular era”, that then allowed to investigate more complex questions. In another part, the revival of the field came about thanks to new or improved methods of

study. These include various model systems, imaging (e.g., light sheet imaging, total internal reflection microscopy) and image-analysis techniques, probes (e.g., enhanced fluorophores, fluorescence resonant energy transfer, optogenetics) and biophysical methods (e.g., tensions sensors, laser ablations). Together with the vast amounts of data obtained by more “reductionist” approaches, these methods allowed for interdisciplinary studies of form that span different biological scales and long developmental times. Table 1 summarizes some of the main findings that resulted from such studies of biological form, with main molecular effectors and references to representative studies. Mechanisms controlling tissue size and shape are listed separately, but it should be noted that a change in one can often result in change of the other. E.g., an increase in cell number can lead to the outgrowth of a part of the tissue, depending on the pattern of proliferation (Figure 1A vs. Figure 2B) or external constraints, effectively changing the tissue shape. In Table 1, I referred to newer studies or studies done *in vivo* wherever possible, although some findings were initially made in classical cell culture experiments as far as 50 years ago (e.g., contact inhibition, (Rubin and Stoker, 1967).

Table 1: A summary of selected studies on tissue growth and shape.

*Cell intercalation is a process driven by cellular shape changes. I separate the two in this Table because changes in cell shape during cell intercalation are transient in their nature, compared to e.g., shape changes that drive neural tube invagination, that get stabilized.

Green field: studies of size, orange field: studies of shape.

	Regulation	Molecular factor	Mechanism	System	Model system	Reference
SIZE	Proliferation	Growth factors; Actomyosin; YAP; YAP/beta-catenin	Contact inhibition, anchorage dependence ,...	2D Cell culture; tissue explant	MDCK cells; wing disc	Dong 2007; Schluck 2013; Zhao 2007; Streichan 2014; Benham-Pyle; Mao 2013
	Apoptosis-mediated extrusion	Sphingosine 1-phosphate	Homeostatic cell extrusion	2D culture; In vivo	Human, MDCK, zebrafish	Eisenhoffer 2012;
	Crowding-induced live delamination	Piezo-1, sphingosine 1-phosphate; Myosin II	Cell competition/ Homeostatic cell extrusion	2D cell culture; In vivo	Human, MDCK, zebrafish fin; Fly notum	Eisenhoffer 2012; Marinari 2012
	Cell size	Myc; mTOR, PTEN, miR-29; G1 regulation	Growth rate- or size-sensing	2D cell culture	Drosophila wing; HT29 cells	Johnston 1999; Tumaneng 2012; Cadart, 2017 preprint
	Nutritional/hormonal constraints	Insulin; Mediator complex, Ecdysone	Nutrient delivery	Tissue explant;	Drosophila neuroblasts; wing disc	Homem 2014; Dye 2017 preprint
SHAPE	Division orientation	Mud; Pins; PCP; Dachs; Ecdysone	Spindle positioning	2D Cell culture; In vivo	Drosophila wing disc	Bosveld 2016; Mao 2011; Mao 2013;

					Gibson 2011; Dye 2017
Cell shape	PTEN; Actomyosin; E-cad, N-cad	Differential adhesion-cortical tension; localized constriction	Fixed tissue; 2D Cell culture; In vivo	Drosophila wing; wing disc; mouse neural plate	Etournay 2015; Ma 2017; Grego-Bessa 2016; rev. Lecuit, Lenne 2007
Tissue tension	Actomyosin; alfa-catenin; Talin; YAP/ ARHGAP 18	Differential adhesion-cortical tension	In vivo/ 3D cell culture	Zebrafish fin/ human cells	Yonemura 2010; del Rio 2009; Porazinski 2015
Supracellular structures	PCP: Wnt; JNK/ DPP	Actomyosin cables (short or long)	In vivo	Zebrafish kidney tubule/gastrulation; Drosophila dorsal closure	Lienkamp, 2012; Behrndt 2012; rev. Martin and Goldstein 2014
Cell-rearrangements	A-P segmentation genes; Dachsovs-Dachs	Cell intercalation*; Cell migration; local junctional remodeling	Fixed tissue; In vivo	Drosophila: dorsal thorax; Drosophila germband;	Irvine 1994; Bertet 2004; Bosveld 2012
External physical constraints	ECM/Perlecan/ Collagen IV	ECM patterning	Tissue explant;	Drosophila wing disc; Drosophila follicle	Haigo & Bilder 2011; Ma 2017; Crest 2017; Rev. Morrissey & Sherwood 2015

1.2 SIZE CONTROL

1.2.1 Autonomous vs. non-autonomous organ growth

We still know very little about how animal size is determined. As a body grows, different organs might grow with different rates and times, but still have to generate the right proportions at multiple levels so the organism can function optimally. Cell number and size have to be coordinated with organ growth and organ growth has to be coordinated with systemic growth, environmental cues and developmental transitions (rev. in Andersen et al., 2013). Different organisms employ different growth strategies. Some grow throughout their lifetime (many marine and invertebrate species). In this case, the size of their mature organs does not grow to reach a specific size at a specific point, but rather their growth rate depends on how favorable the environmental cues are. Some species, like planarians, cannot only grow constantly, if nutrition is provided, but can also shrink and lose entire body mass if it is not. Others, mostly terrestrial organisms, grow until they reach a set adult body size (termed determinate growth).

Whichever growth strategy is employed, tissue size has to be spatiotemporally coordinated both with shape generation and cell differentiation to result in a functional organ and a measure of tissue size needs to exist to achieve this. With respect to this, it was

established from salamander grafting experiments already ~80 years ago (Twitty and Schwind, 1931) that tissues measure and determine their size autonomously. Additionally, ~70 years ago, total cell mass, rather than individual cell number or size, was suggested to be the measure of tissue size. In these experiments, if salamander cell size was increased due to polyploidy, the final organ (pronephral duct) was built from fewer cells, but had a comparable size to the organs that consist of monoploid cells (Fankhauser, 1945), indicating that a total organ mass is what is being sensed. Still, a sensor of such a size measure remains elusive and we do not know if it acts on the level of the individual organ (local) or the entire organism (systemic). The following examples shed some light on this problem. If *Drosophila* wing discs are transplanted to another part of the body, they will grow to their correct size (Bryant and Levinson, 1985), suggesting that their size is determined independently of their environment. If wing disc growth is blocked inside the body, however, other organs will grow to be smaller (N. F. Parker and Shingleton, 2011), showcasing that, even though organs might primarily grow autonomously, a system-wide control acts to maintain organismal proportions. This coordination was shown to be governed by the hormone insulin-like-peptide 8 (Dilp8; Colombani et al., 2012; Garelli et al., 2012), regulated by the Hippo signaling pathway (Boone et al., 2016).

Individual organs do not all respond in the same way to growth signals, however and growth rates can be differentially, rather than proportionally, modified as a response to upstream cues. Examples of such differential growth regulation come from fly studies, as well. In *Drosophila*, not all organs slow down their growth during starving conditions, or with lack of growth signals. Two examples include the genital imaginal disc and the brain. Upon starvation, the genital disc becomes more sensitive to growth signals (Tang et al., 2011), while brain growth becomes independent of growth signals (Cheng et al., 2011), as discussed in more detail in the section on nutritional constraints. Therefore, here, by differentially tuning their sensitivity to nutrient availability, different organs respond differently to the same environmental condition. These findings raise the question of whether such differential tissue growth is regulated in a systemic, or in a local, tissue-autonomous manner. Experiments using different mouse fetal organs further highlight the complexity of the problem of proportional growth. If multiple thymus glands are transplanted into a single mouse, each gland will grow to its expected adult size, so the overall final thymus mass will be larger than it should be (Metcalf, 1963). Conversely, the same experiment using spleens will cause each spleen to grow smaller than it should, but the final overall mass of spleen tissue will be normal (Metcalf, 1964). This raises the possibility that the thymus employs an organ-intrinsic measuring tool, similar to the wing disc, while the spleen coordinates its size with the growth of the entire organism. Even though we have many insights into the question of what underlies the size of multicellular systems, we still

do not know which specific organ characteristics make some organs coordinate and others not coordinate their growth with the growth of the system, to result in a fully functional organism.

The above examples suggest that different organs have different master regulators that control their size. Mechanisms underlying most of the mentioned observations are still not known, however and many open questions remain (rev. in Conlon and Raff, 1999), such as how a tissue defines what its correct size is or when it is reached, if it does not simply follow nutrient availability, or what are the exact properties that are measured and how they are sensed to control size? With the number of broad experimental and theoretical studies on growth, as well as explant and organoid cultures on the rise, we will hopefully be able to get closer to a molecular-level understanding of how organ size is determined and how a proportional organism develops.

1.2.1.1 Epithelia as model tissues to study growth

A lot of our knowledge on how tissues grow, as well as how they attain their shape comes from studies on epithelia, one of the four basic animal tissue types (nervous, muscle and connective tissues being the other three types). The salamander pronephros, fly imaginal discs and mouse glands, the growth of which was discussed above are all epithelial tissues and with numerous others, those studies demonstrated that these important tissues allow discoveries spanning the entire animal phylogeny, as well as many organ systems. Epithelia are very abundant tissue types found in all metazoans, both as precursors to various organs and as specialized structural and functional tissues, ranging from the gastric epithelium in Cnidaria, to the skin epithelium or the highly specialized sensory tissues in mammals. Despite having a broad range of functions, epithelial tissues follow conserved organizational principles: they consist of polarized cells that are all attached to each other by various junctional molecules, are often connected through gap junctions and all rest on a thin extracellular lamina. Epithelial cells can be flat, cuboidal or columnar, resulting in different thicknesses of epithelial sheets. Multiple layers can function on top of each other (e.g., mammalian skin), but often, a single epithelial layer forms the tissue (e.g., gland ducts). The pseudostratified epithelium is a special case of such a columnar monolayered epithelium, where, due to tight tissue packing, cell nuclei seemingly arrange into multiple layers. Polarized, epithelial cells all have an apical and a basal domain differentiated, with the apical surface facing the lumen (such as the brain ventricle) and harboring the primary cilium and the basal surface laying on the afore-mentioned, basal, lamina.

The basal lamina is an epithelium-specific subtype of the extracellular matrix (ECM), a complex network of filamentous and connective proteins and polysaccharides filling the extracellular space, secreted by both the epithelial and the mesenchymal cells. The ECM can act as a scaffold, barrier and support, as well as a regulatory hub for mechanical and chemical signaling. The epithelial basal lamina (or basement membrane) is thin (40-120 nm) mostly due to the lack of hydrophilic, space-filling glycosaminoglycans (GAGs) among its components. It is mostly secreted by the epithelium and consists predominantly of laminin filaments (Alberts et al., 2014; rev. in Yurchenco, 2011). We are only beginning to understand the large extent to which such different ECM types govern both epithelial size and shape, a topic that I discuss further in several sections on extracellular cues governing growth, shape and their coordination.

The experimental advantage of studying growth in epithelia comes from the fact that they are not only versatile and important in both the developing and the adult organism, but are also often accessible to imaging or other analytical methods. This is due both to their abundance and to a stable and simple stereotypical structure, which allows quantitative characterizations and assessment of perturbations.

1.2.2 Growth regulatory mechanisms

Examples in the section on Autonomous vs. Non-autonomous growth (1.2.1) showcase how growth can be regulated differently for different tissues and in different species and that an optimal final size can be reached by employing multiple strategies. In this section, I outline some of these different, extrinsic and intrinsic growth cues and means by which tissues coordinate cellular responses to change their size and exemplify how size is regulated on a molecular level, with a focus on epithelial tissues.

1.2.2.1 *Chemical regulation of tissue growth*

Signaling pathways and nutritional constraints

In order to increase tissue size in a controlled manner, the gain of cell mass has to be coordinated to its loss. More specifically, cell number (proliferation) and mass (cell growth) increase has to be coordinated to cell loss (programmed cell death (PCD) and extrusion). Growth factors (e.g., insulin-growth factor, IGF) control cell growth, at least in part, by stimulating translation (protein synthesis), e.g., through phosphatidylinositol 3 kinase (PI-3) and the TOR kinase (see below). They often respond to nutrient availability and can, besides cell growth, also promote cell proliferation and survival and therefore act as mitogens and survival factors, as well. Mitogens are extra- or intracellular factors that are needed for cell proliferation. They act via MAP kinases and affect e.g., the production of Myc and cyclins, promoting cell cycle progression by cyclin-dependent kinases (CDKs). Cell

survival is affected by intracellular death-promoters, such as Bad in vertebrates, that trigger PCD by inhibiting death suppressors and e.g., ultimately lead to activation of caspases. Survival factors suppress PCD via inactivation of these death promoters (rev. in Conlon and Raff, 1999). However, PCD can be triggered by more than a lack of survival factors, for example by a loss of attachment to the ECM, termed anoikis (Paoli et al., 2013), or special signals that circumvent the survival pathway, such as the BMP4 in neural crest cells (Graham et al., 1994). Ill-functioning apoptotic mechanisms can lead to tumorigenesis onset, as cells that ignore signals to die can expand uncontrollably (Cory et al., 2003).

In control and coordination of organ growth, the release of hormones and growth factors (rev. in Perrimon et al., 2012) can depend on environmental conditions, such as nutrition. They can act systemically, targeting tissues whose cells express appropriate receptors to receive the signal. Signaling can act through cell-cell contact (juxtacrine), such as Notch signaling, or through secreted factors (paracrine), such as Wnt signaling. Wnt and Notch pathways have been implicated in promoting and maintaining cell proliferation, respectively (Gaiano and Fishell, 2002; Morin, 1999; Reya et al., 2003; Ross et al., 2003; van de Wetering et al., 2002), although Notch plays a more prominent role in inhibiting cell differentiation. We now know that several of such molecular signaling pathways can cross-talk to each other to control tissue size by integrating signals on multiple levels, i.e., organ and organism, or, cell and tissue level. The afore-mentioned Notch was shown to e.g., downregulate Wnt by modifying the activity of its effector, beta-catenin in *Drosophila* (rev. in Hayward et al., 2008). Locally acting signals, such as Wnts/Wingless, Bone Morphogenetic Proteins (BMPs) and Hedgehogs can be coordinated with systemic, nutrient-dependent signals such as Insulin-like peptides, transduced by the Target of Rapamycin (TOR) pathway (J. Parker and Struhl, 2015). Factors such as insulin or IGF stimulate cell growth and proliferation in response to nutrition. In *Drosophila*, they act antagonistically with another nutrient-dependent factor, the steroid hormone ecdysone that limits organism growth during juvenile development. Together, they timely regulate systemic growth in the fly (Delanoue et al., 2010).

Not all signaling pathways respond to nutritional cues. The conserved Hippo pathway regulates organ growth by responding to tissue-intrinsic cues, such as adhesion, tension and polarity. In the last 20 years, it has emerged as a central regulator of organ size (rev. in Yu et al., 2015) that controls cell proliferation and death. If Hippo signaling is active, proliferation is generally blocked. However, it was recently shown that, besides regulating and responding only to tissue-wide cues, the Hippo pathway also acts through integrating long- and short-range signals (Moeller et al., 2017). In *Drosophila*, the Hippo homolog, Warts can activate the production of ecdysone, the systemic growth regulator. In this way, Hippo/Warts can limit growth by controlling organ-scale growth (cell proliferation) in

coordination with systemic growth (Moeller et al., 2017). Besides this Hippo/ecdysone example, an example of integrating multiple cues/pathways to control tissue size is the interaction of the Hippo pathway with the mTOR pathway (Tumaneng et al., 2012). In mammalian cells, these two classical size control pathways, mTOR controlling cell growth and Hippo controlling cell proliferation, cross-talk through PTEN and miR-29 (Tumaneng et al., 2012). mTOR itself already integrates intra- and extracellular (nutrient and hormonal) signals to boost protein translation and, by this, cell growth (Kim et al., 2002). YAP, a Hippo effector, here downregulates the negative regulator of mTOR, PTEN, to coordinate cell growth and proliferation. This results in increased organ size. The mTOR-Hippo example shows that signaling pathways do not only cross-talk to each other, but that a single pathway can respond to multiple cues to deliver the same final response, such as organ growth.

Morphogen gradients

Signaling pathways discussed above act through a signal relay-mechanism and trigger other cells in an on-off manner. In order to induce variable responses in a field of cells, a non-uniform signal profile and cell response is needed (Perrimon et al., 2012). Morphogens are a type of signaling molecules that act in such a non-uniform, concentration-dependent manner, in a cell-autonomous manner, directly on the target cell receptor/ligand (rev. in Tabata and Takei, 2004). They are molecules that spread from a source point in a tissue, thus forming a gradient. The gradient (i.e., concentration of morphogen molecules) carries information that cells are sensitive and respond to, such as cues to differentiate or polarize, positional information or cell cycle information, depending on the morphogen type and its concentration (Gallet, 2011; Tabata and Takei, 2004). Therefore, the production of the morphogen at its source, the amount, distribution and sensitivity of cell receptors and morphogen progression (diffusion, degradation or cell-cell communication), all have the power to regulate tissue growth, specification and development. Identified morphogens include members of the Hedgehog (Hh), Wnt and TGF-beta families (Tabata and Takei, 2004), some of which can act cooperatively, such as decapentaplegic (Dpp) with Hh in the *Drosophila* wing disc, to pattern tissue compartments and govern growth (Zecca et al., 1995). Nodal (TGF-beta subtype) was recently shown to act in a positive feedback loop with cell-cell contacts during zebrafish gastrulation (Barone et al., 2017), in dependence of the duration of the contacts. An intercellular gradient of beta-catenin, with its highest expression at the tail, has been proposed to determine the body axis and fate (i.e., head or tail) of the cells in the regenerating flatworms. The uneven beta-catenin expression was hypothesized to originate from an upstream Wnt morphogen gradient (Gurley et al., 2008; Stückemann et al., 2017). Theoretical models explaining morphogen activities are still inconclusive,

however, partly because a consensus in the field is lacking (Bothma et al., 2010) on whether morphogen gradients progress by activating neighboring cells or by diffusion (Christian, 2011), as well as on how gradient steepness, in combination with mechanical cues affects cell proliferation and tissue growth (Lecuit and Le Goff, 2007). E.g., if morphogen gradients “flatten out” through growth, this can provide a cue to decrease proliferation and this response should be coordinated with possible proliferation halt due to increased compression, a model proposed in 2012 (Aegerter-Wilmsen et al., 2012). Therefore, despite decades of study, many questions in the morphogen gradient field remain, including the identification of candidate molecules themselves and the basic questions of how the correct gradient is established, scaled and recovered if lost, in timely coordination with other growth-regulating mechanisms.

In the past decades, we accumulated a lot of knowledge about specific signaling pathways and their function (e.g., Dpp, IGF, Hippo, TOR) and recent studies such as the ones discussed above start to reveal how multiple pathways can be integrated, mutually redundant or act cooperatively, to limit or promote growth on cell, organ and organism levels. Here, tissue-wide studies, novel experimental tools and computer simulations of signaling networks or morphogen activities have the potential to provide better understanding of the complexity that lies behind integration and coordination of the plethora of chemical cues that control tissue size.

1.2.2.2 *Growth responses to mechanical cues*

Tissue-intrinsic cues

As tissue size increases through e.g., cell proliferation, nutrient availability might become limited and growth blocked through nutrient-dependent signals such as insulin or mTOR, mentioned in the previous section. However, growth is governed by more than the abundance of nutrients. It has been proposed that mechanical cues govern growth (rev. in Paluch et al., 2015 and Lecuit and Le Goff, 2007) and many studies in the past ~10 years confirm that compression halts cell proliferation and mild stretch promotes it (Benham-Pyle et al., 2015; e.g., Mao et al., 2013). Even though nutrients might be plentiful and morphogen gradients steep, cell growth and proliferation have to slow down when e.g., tissues become too tightly packed. This might happen in case tissue growth is not well coordinated to the surrounding, e.g., stiffer, physical constraints, such as e.g., the epidermis. To result in proportional growth, the tissue has to respond to such physical constraints and slow down its growth rate and, therefore, growth has to be regulated not just by chemical (nutrition, morphogens), but also mechanical signals. This is indeed the case in most studied tissues and cells are able to sense, through “crowding” sensors (i.e., tension sensors), how densely

packed with cells the tissue is and adjust their proliferation accordingly. Here, the Hippo signaling pathway introduced above can act, as well, by responding to a plethora of mechanical cues, such as compression, ECM stiffness and cell geometry (rev. in Yu et al., 2015). In line with this, by stretching monolayers of MDCK cells, Benham-Pyle and colleagues (2015) demonstrated that they can induce cells to reenter the cell cycle as a response to lower compression (stretch-induced proliferation), in a YAP (Hippo effector)- and beta-catenin-dependent manner, to increase cell number. A similar mechanism acts in the *Drosophila* wing disc, where the YAP homolog Yorkie regulates stretch-induced proliferation at the tissue periphery (Fletcher et al., 2015; Koontz et al., 2013; Wu et al., 2008). We now know that different members of cell-adhesion complexes, such as alpha-catenin or talin, open-up their structure under tension (rev. in Han and de Rooij, 2016). This allows cytoskeletal and other elements to bind to them and transduce the tension signal into the cell, which can then respond accordingly and generate more or less cell mass for the tissue. Thus, additional to responses to nutritional signals, tissues adjust their growth by responding to mechanical compression, such as cell-cell contact, or contact inhibition.

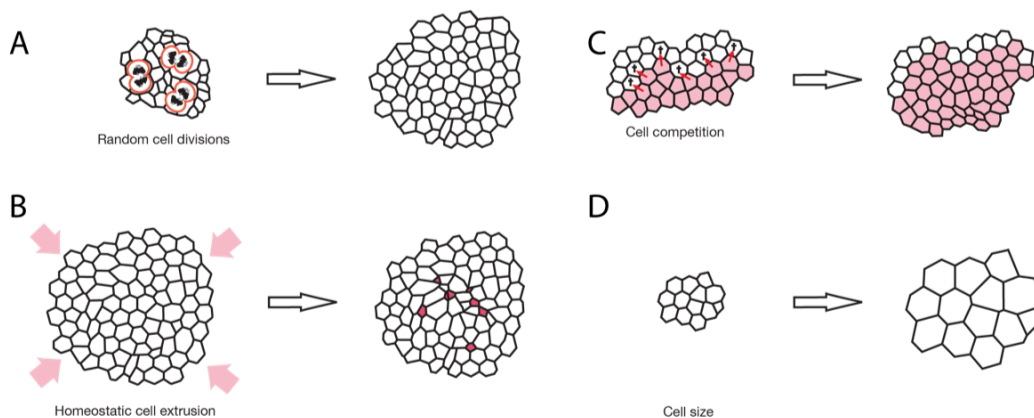


Figure 1: Cell-based modes of tissue growth.

A) Random (i.e., spatially unbiased) cell divisions will give rise to uniform tissue growth by increasing the total cell number and cell mass.

B) Mechanical constraints to growth can force the cell mass to grow slower, by, e.g., slowing down the cell cycle, or extruding dead or live cells from the tissue (small magenta cells). This allows the tissue to respond to the environment and maintain a homeostatic cell mass.

C) Cells that grow faster than others (e.g., less sensitive to growth signals) can induce cell death in slow-growing ones and spread at their expense.

D) Tissues can grow by changing cell mass not only through cell number, but also cell size. Cells can increase their size either by prolonging their cell cycle growth phase (G1, traditionally) or by growing faster as a response to nutrient availability (mTOR pathway). The control of cell growth is not well understood and varies highly depending on the system.

Figures are reused and adapted with permission from Lecuit and Le Goff, 2007.

Another way in which epithelia can actively remove cells upon too high packing (compression) is by extruding cells from the tissue (Eisenhoffer et al., 2012; Katoh and Fujita, 2012; Slattum et al., 2009). This way, cell density can be lowered in order to maintain tissue homeostasis (Figure 1B, Ninov et al., 2007). Both living (Eisenhoffer et al., 2012; Marinari et al., 2012) and dying cells (Rosenblatt et al., 2001; Slattum et al., 2009) can be extruded. Interestingly, studies have shown that this usually occurs from the basal side in *Drosophila* epithelia and from the apical surface in vertebrates (Katoh and Fujita, 2012) and we still do not know where this apparent difference between invertebrate and vertebrate mechanisms arises. Extrusion was shown to depend on the formation of contractile rings, both in the neighbors and in the extruding cell (Rosenblatt et al., 2001). The difference, however, between live and dead cell extrusion is in that live cell extrusion depends on stretch-activated channels (Eisenhoffer et al., 2012), indicating that they are, together with junctional tension-sensors, responsible for sensing tissue overcrowding and controlling homeostatic size. Similar to contact inhibition discussed in the previous paragraph (Benham-Pyle et al., 2015), cell delamination through homeostatic cell extrusion counterbalances growth upon higher tissue crowding.

Tissue-extrinsic cues

Epithelial tissues do not grow in isolation, but are surrounded by the ECM (basal lamina), as mentioned in the section on epithelia (1.2.1.1). Through cell-ECM attachments, cells can both sense and respond to the mechanical properties of the extracellular environment (rev. in Swaminathan and Waterman, 2016). Epithelial cells can produce, organize and degrade the basal lamina and attach to it by integrin ECM-receptors to form cell-matrix adhesion sites. Cell-ECM regulation does not originate just from the cellular side. Integrins transmit information about the attachment, as well as about matrix stiffness and tension, to the cell interior. ECM composition and stiffness, as well as integrin types (integrins can switch between subtypes, Meighan and Schwarzbauer, 2008) can modulate cell-ECM attachments and cellular responses. Through integrins and through modulating these attachments, the basal lamina can regulate a plethora of cell behaviors (Swaminathan and Waterman, 2016; Yurchenco, 2011), such as trigger or stop proliferation, govern differentiation and signaling. Furthermore, the ECM can act as source and modulator of e.g., growth factors, some of which also require integrins as co-receptors in order to trigger a cellular response (rev. in Brown, 2011).

If epithelial cells lose the ECM attachment, they cease the cell cycle and undergo a type of programmed cell death called anoikis (Frisch and Francis, 1994; rev. in Paoli et al., 2013), a phenomenon termed anchorage dependence and described still in the 1960s (rev. in Assoian, 1997). Cells mutant in anchorage-dependence components escape such control

and frequently develop tumors both by proliferating uncontrollably and by being able to invade other tissues after detaching from the source and delaminating basally (Slattum and Rosenblatt, 2014). In addition to acting as cell survival cue, the ECM is essential to preserve epithelial barrier function during normal growth and homeostasis. Upon altered ECM stiffness or tissue overcrowding, cell-ECM attachment can be lost. Cells that then undergo anoikis can be extruded from the apical, or basal side of the epithelium, as mentioned before (Eisenhoffer et al., 2012; Rodriguez et al., 2017 respectively), leaving the epithelial sheet intact.

Therefore, through affecting cell numbers by governing cell proliferation, death and extrusion, the ECM and cell-ECM attachments are an essential component in tissue growth regulation. As ECM and its remodeling is essential for governing tissue shape, as well, its modes of action are discussed in more detail in chapter 1.4 COORDINATING CHANGES IN SHAPE AND SIZE.

1.2.2.3 Cell size regulation

Despite gaining a lot of understanding on how tissues regulate their cell numbers, the question of how cell size (Figure 1D) is sensed and regulated is still poorly understood. Partly, this is because it is difficult to measure cell size, especially inside tissues. Studies on cell growth were so far done almost exclusively in cell culture. Additionally, studies on metazoan cells are very few compared to studies in unicellular systems such as yeast and bacteria. Cell size and even its regulation, is likely to be highly dependent on the cellular context. However, the general regulation is proposed to act through growth signals (e.g., IGF) that trigger intracellular, biosynthetic pathways (e.g. mTOR) to change cell size. Generally, it is accepted that specific cell types within a species are mostly uniform in size and that they can sense their own size (rev. in Ginzberg et al., 2015), even though the cell-intrinsic measuring tool remains elusive. By sensing their size, cells can grow in dependence of their initial size. I.e., depending on how big cells were to start with – smaller cells will add larger amounts of mass, larger cells less. This is a concept of cellular auto-regulation, similar to cells adjusting their proliferation rate depending on how compressed they are, mentioned in section 1.2.2.2 on Growth responses to mechanical . There are two main hypotheses on how different cells types can grow and each leads to a different distribution of cell size in the expanding population: *adders* and *sizers* (see Cadart et al., 2017 preprint). The growth of *adder* cells (e.g., some bacteria, cyanobacteria and budding yeast) does not depend on their initial size. They *add* a fixed amount of volume to them, resulting in a population whose variability is similar to that of the starting pool. *Sizer* cells (fission yeast, Cadart et al., 2017) have to reach a certain size threshold, that is checked at specific cell cycle point before mitosis. Only cells that have the appropriate size will proceed

into division and thus the size of the daughter cell pool is tightly regulated and variability decreased. Assuming that the cell cycle length is fixed, however, cells will grow for a fixed amount of time before division. In this situation, depending on whether cell growth is exponential or linear, size distributions will differ. With exponential growth over the cell cycle, smaller cells (right after division) will grow less than bigger ones and, therefore, their sizes will quickly diverge. If cells grow linearly, on the other hand, homeostatic variability in size will be maintained.

In addition to the mechanisms outlined above, cells can uncouple their cell cycle from cell growth, as is the case with differentiating *Drosophila* neuroblasts (Homem et al., 2014). Here, a metabolic switch from glycolysis to oxidative phosphorylation leads to slower cell growth and therefore smaller cells, irrespective of the longer cell cycles. In this case, both cell cycle and cell growth parameters, therefore, have to be analyzed to understand how cell growth is regulated. Aside from cell size governing tissue size, cells that are relatively fitter or grow faster can cause less fit or slower growing cells to undergo apoptosis, a phenomenon known as cell competition (rev. in Di Gregorio et al., 2016; Shraiman, 2005). This is a conserved mechanism where neighbor cell growth rate is registered, by as of yet unknown sensors and used to maintaining homeostatic tissue size (Figure 1C). Altogether, the question of cell size is still greatly unexplored and regulatory mechanisms might be specific to distinct cell types or organisms. As cell size is likely to highly depend on tissue- and general, environmental context, *in vivo* imaging and more biochemical studies will be necessary to better understand what the sizing mechanisms are and to what extent cell size regulates tissue growth.

1.2.3 Future challenges

The coupling and coordination of cell growth and the cell cycle is still greatly unexplored in multicellular systems. Still, these two parameters are the main contributors to increasing epithelial tissue size – cell growth by directly increasing the mass of a single cell and cell cycle by increasing total tissue mass by the generation of new cells. With respect to cell growth and the cell cycle there are, therefore, many open questions that remain. E.g., which of the two, growth or cycle, do cells change in which situation? How much does the cell growth-cell cycle coupling depend on the cell type and how much on the environment? Generation of new tissue mass through cell growth and proliferation has to be coordinated with cell loss, to fully regulate tissue size. Here, contact inhibition and cell extrusion serve the purpose of maintaining homeostasis and decreasing variability in tissue size, with the ability to respond to mechanical cues such as increased compaction. One of the big questions here is how is sensing of the cells' mechanical compaction coordinated with sensing e.g., nutrient availability, to regulate tissue size? In order to better address such

questions, methods and systems to study growth will need to be expanded. At the moment, most tissue-wide growth measurements are done by analyzing only the apical surface of an epithelium and ignoring its 3D structure. As many developing epithelia are thick and dynamic, 2D studies can be problematic because they might overlook essential changes happening away from the apical surface. Additionally, growth parameters are often assessed by clonal analysis or tracking of specific landmark structures. Such analyses, despite providing essential discoveries, need rigid validation (e.g., assessment of uniformity of growth) to prove that they are representative of the entire tissue, as they take into account only tissue subparts. Therefore, expanding the portfolio of model organs that are accessible to tissue-wide live imaging, such as the epidermis, the zebrafish retina (Icha et al., 2016; Sidhaye and Norden, 2017) or heart (Mickoleit et al., 2014) and methods that will allow direct measurements of growth by measuring tissue and cell volume or mass will be essential to understand broad problems such as coordination of cell- and tissue-wide parameters during growth.

1.3 SHAPE CONTROL

1.3.1 General introduction

In addition to maintaining correct size, tissues need to develop into a correct shape to ensure functionality. For example, if neural tube invagination and closure during the first month of human development fails or are incomplete, this will lead to congenital neural tube defects that include anencephaly and open spina bifida (Greene and Copp, 2014). These two conditions leave the neural tissue, brain or spinal cord undeveloped or exposed to the external influences, respectively and are either lethal, or cause severe neural defects, e.g., paralysis. Other examples of tissue shape changes include the process of gastrulation, *Drosophila* germband elongation, imaginal disc evaginations, vertebrate optic cup invagination, cortical folding and branching morphogenesis during gland formation. As in the examples in the topic of tissue size, e.g., mouse gland sizes (chapter 1.2.1), all of the above examples of shape changes are of epithelial tissues. The abundance and importance of these tissues, that include e.g., the mammalian central nervous system, skin or glands, as well as their complex developmental changes, motivate numerous studies, investigating how epithelial form arises or is maintained.

In general, an existing epithelial tissue can be reshaped cell-intrinsically, by changing the positions of cells within the tissue, or by changing cell shapes and cell-extrinsically, through remodeling external constraints (i.e., the ECM). Cell-intrinsic shape changes are brought about through actions of the cellular cytoskeleton. Even though other cytoskeletal elements (microtubules and intermediate filaments) can also interact with cellular junctions (Delva et al., 2009; Gomez et al., 2011), the contractile action of the actomyosin cell cortex

plays the predominant role (Lecuit and Yap, 2015). The cortex is a thin meshwork of filamentous, linker and motor proteins underlying the plasma membrane (rev. in Salbreux et al., 2012). In the cortex, filaments of the protein actin are assembled into a network by different nucleating, bundling (alfa-actinin, filamin, fimbrin) and cross-linking proteins (ezrin–radixin–moesin family, filamin) and being pulled on by the force-producing motor proteins of the myosin family (myosins, tropomyosin, tropomodulin, Salbreux et al., 2012; Winder and Ayscough, 2005). Both actin polymerization and myosin function require ATP, so cortical contractions consume cellular energy. Because actin and myosin-II are the main functional constituents of the cortex, it is often referred to as the actomyosin cortex, or actomyosin. Changes in the concentration of cortical proteins, their organization and turnover rates affect physical properties of the cortex, such as stiffness, tension or viscoelasticity (Salbreux et al., 2012) and consequently, cellular physical properties. Due to it being linked to the cell plasma membrane by anchoring proteins (e.g., alfa-catenin, vinculin, talin, Winder and Ayscough, 2005), (localized) cortical contractions are transduced into cell shape changes.

In addition to the cortex, the plasma membrane has more recently been proposed to play a role in cell shape changes, as well. By being under tension, allowing endo- and exocytosis, or harboring mechanosensitive ion channels (Cox et al., 2016), it acts as more than a passive participant in cell shape changes (rev. in Diz-Muñoz et al., 2013). However, the extent of the roles of the plasma membrane in cell shape changes is still not known and mechanisms are poorly understood. I, therefore, focus on shape changes resulting from actomyosin (cortical) activities.

In epithelia, actin-based junctional connections of cells to their neighbors, or to their external environment, allow cells to coordinate responses within the tissue (rev. in Lecuit and Yap, 2015) and can drive cell differentiation, depending on how long they persist (Barone et al., 2017). Information about cellular tension is transmitted to the neighboring cells through cadherin-based, tension-sensing junctions, triggering, e.g., increased rates of cortical assembly (Chan et al., 2017; Röper, 2015) or binding in the entire cell neighborhood (Lecuit and Yap, 2015). Recently, it was shown that not only the type and tension in the junctions, but the duration of cell-cell adhesion can play a role in cell behavior (cell fate specification) and vice-versa, as well (Barone et al., 2017). In addition to coordination through the apical junctional belt, epithelial cells are all connected to and respond to the physical properties of the ECM. Through the tension-sensor talin and integrins, actin in the cell cortex connects to the ECM (Calderwood and Ginsberg, 2003) and cells can respond to changes in ECM composition or stiffness by, e.g., increasing cortical tension on stiffer ECM (Discher, 2005). The ECM underlies the entire epithelium, which allows it to synchronize responses of epithelial cells in the whole tissue. Therefore, through

connections of epithelial cells, both to each other and to the extracellular environment, the epithelium ensures direct transduction of mechanical information and can respond as an active sheet by coordinated responses of single cells. This allows the maintenance of epithelial tissue integrity, homeostasis, as well as tissue-wide shape changes.

The shape of epithelial tissues can be changed by adding/removing cell mass in a spatially patterned way, or by reshaping the preexisting cell mass. In the following section, I explore different strategies of the latter, i.e., how existing tissue shapes are changed, irrespective of tissue growth. The topic of coordinating changes of cell number with tissue shape changes will be discussed in section 1.4.

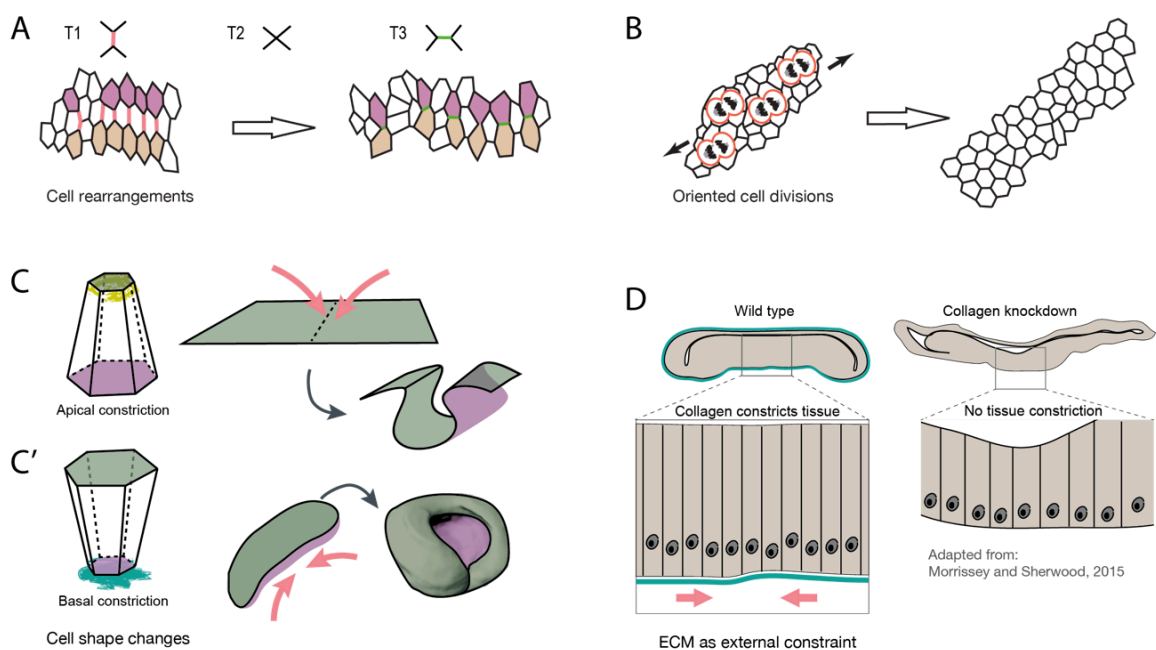


Figure 2: Representative modes of changing tissue shape.

A) Cell rearrangements (cell intercalation) through junctional remodelling (T1-2-3 transitions) result in cell neighbor exchange. Red junctions constrict, green junctions lengthen in a PCP and myosin-II dependent manner.

B) Oriented, as well as spatially non-uniform cell divisions will give rise to patterned growth that can lead to tissue shape changes. This is an example of a simultaneous tissue growth and shape change.

C) and C') Single cell shape changes are a major mode of changing tissue shape. Green: apical surface; Magenta: basal surface; Turquoise: ECM. C) Apical constriction is governed by localized contraction of the junctional belt and can cause tissue folding, such as during vertebrate primary neurulation. C') Basal constriction is not as well studied, is actomyosin- and ECM-dependent. It results in basally invaginated epithelia, such as the neuroepithelium of the optic cup.

D) The ECM is a major determinant of tissue and cell shape. It acts as an external constraint, affecting general tissue compression passively or cell shape directly through the organization of the actomyosin cortex.

A) and B) are adapted from Lecuit and Le Goff 2007. D) is adapted from a review by Morrissey and Sherwood (2015) and based on a study by Ma et al. 2017.

1.3.2 Cell-intrinsic changes of tissue shape

Reshaping the preexisting cell mass means that the relative position of existing cells, or their shape, will change. Cell rearrangement through cell intercalation (Figure 2A) is a mechanism to change tissue shape by changing relative cell positions. It is driven by myosin-dependent junctional remodeling and transient cell shape changes. One of the best-studied examples of cell intercalation is tissue elongation during germ-band extension of the developing *Drosophila* embryo, where the tissue shortens along one and elongates along the other, perpendicular axis. The cell rearranging behavior originates from a local, intrinsic tension increase on antero-posterior cell-cell boundaries (Bertet et al., 2004). This tension increase results in shrinking of these cell contacts until they disappear and new ones form perpendicularly (dorso-ventrally) through a “T1-2-3-transition”. These rearrangements effectively elongate the tissue. The junctional remodeling happens through a self-organized behavior of Myosin II (Munjal et al., 2015). The step of perpendicular-junction growth is, besides local tension changes, governed by global, tissue-scale pulling forces that help to elongate the newly forming junctions (Collinet et al., 2015). Together, this entire process of narrowing and elongation of the body axis is known as convergent extension and also occurs in other morphogenesis processes including vertebrate gastrulation, streak and notochord formation (rev. in Tada and Heisenberg, 2012).

Cells actively change their shape in a plethora of different contexts, such as cell migration, cell division or cell rearrangements. For example, the process of cell rearrangements already described above is indeed underlined by cellular shape changes, including shrinking and elongating specific junctions and results in a changed tissue shape. However, these cell shape changes are short-lived and the process itself is primarily a reordering of cell mass through intercalations. In this paragraph, I focus on shape changes that change tissue shape, but also become stabilized in the new tissue geometry, or are happening on longer timescales than cell intercalation-shape changes. Here as well, the actomyosin cortical meshwork often acts as main effector for a multitude of upstream signals that, together with the strength of cell adhesion, control cell shape through opposing effects (rev. in Paluch and Heisenberg, 2009). Cell shape results from a combination of internal mechanical properties and external physical constraints. The internal, mechanical properties of the cell can be described by surface tension, which depends on the density of the actomyosin cortex, its dynamic interactions with the cell's plasma membrane and on the ability to increase the surface of the membrane lipid bilayer (Lecuit and Lenne, 2007; Sinha et al., 2011). The contractile actomyosin can form different cortical networks, that can localize differently within the cell. Examples are apical junctional actomyosin, apicomedial actomyosin and supracellular actomyosin cables (Röper, 2013). A non-uniform cortex

density can alone lead to cell shape changes. More myosin motors in a particular region can cause a cortical contraction and a local deformation of the plasma membrane, that brings about a change in cell shape. Often, changes in cell shape result from pulsatile contractions and can get stabilized or enforced by other force-generating structures such as the stable apical myosin contractions, supracellular cables or local changes in the ECM volume (e.g., during endocardial cushion formation, Camenisch et al., 2001). Nevertheless, single cell shape changes can be sufficient to autonomously drive morphogenesis, without external stabilizing structures. The process of *Drosophila* dorsal closure for example was widely believed to be governed by pulsatile contraction of the amnioserosa cells and stabilized by a supracellular actomyosin cable. Pasakarnis and colleagues showed (2016), however, that contraction and shape change of the amnioserosa cells alone, but not the epidermal actin cable is enough to drive dorsal closure during *Drosophila* embryogenesis (Pasakarnis et al., 2016), showcasing an example of single cell shape-changes driving large-scale morphogenetic events. The supracellular cable in this scenario functions in ‘zippering’ the already closed structure.

The majority of examples of tissue shape changes driven by changes in cell shape result in buckling tissue events such as invagination or evagination, such as vertebrate primary neurulation (neural tube formation, rev. in Eom et al., 2013) or fly leg or wing imaginal disc eversion, respectively. Moreover, most changes arise from constrictions at the apical surface of the cells (Figure 2C, rev. in Martin and Goldstein, 2014), e.g., *Drosophila* mesoderm invagination or vertebrate neurulation, where autonomous changes in cell shapes lead to epithelial sheet bending (rev. in Lecuit and Lenne, 2007; Sawyer et al., 2010). In order to result in a tissue shape change, the cellular shape change (myosin contraction) has to be localized and the force has to be transmitted through junctional elements to coordinate contraction over multiple cells. Myosin-II activation is concentrated to the apical surface in fly epithelia by apical localization of RhoGEF2 pathway components, that are activated by the ligand FOG and G-protein coupled receptor Smog (Kerridge et al., 2016; Lecuit and Lenne, 2007). In vertebrate epithelia, Myosin-II is apically activated by a small GTPase Rap1 (Asha et al., 1999; Knox and Brown, 2002) and Shroom (Haigo et al., 2003). Even though junctional relaxation through cadherin downregulation can be a part of a physiological process of epithelial-to-mesenchymal transition (Chen et al., 2014; rev. in Lamouille et al., 2014), the lack of attachments can lead to tumor formation (Jeanes et al., 2008; rev. in Knights et al., 2012) through the transcription factor Twist (Onder et al., 2008), if cells delaminate from the epithelium basally (Slattum and Rosenblatt, 2014). Besides contractions of the apical surface of single cells, supracellular actin cables reshape the tissue mass as supracellular contractile structures. They form by aligning multiple actin bundles in apical junctional belts across multiple cells and act dynamically to help

invagination (neurulation), or to form and extend tubular structures during e.g., the morphogenesis of fly salivary gland and fish kidney, respectively (Röper, 2013).

Most described scenarios of shape changes are driven by changes at the apical surface, perhaps due to the apical localization of major junctional/contractile structures, such as the apical junctional belt. However, the cortex is not localized only apically, but spans the entire cell. In line with having contractile potential throughout the cell body, the basal cell surface was also shown to drive changes in tissue shape. Such basal-surface driven shape changes often result in bending of the epithelial sheet by constriction (Gutzman et al., 2008; Martinez-Morales et al., 2009), relaxation (Polyakov et al., 2014; Sai and Ladher, 2008) or protrusion formation (Sidhaye and Norden, 2017; Sun et al., 2017). For example, during zebrafish midbrain-hindbrain boundary formation, neuroepithelial cells constrict basally, while simultaneously expanding the apical surface to bend and invaginate the tissue sheet (Gutzman et al., 2008). During zebrafish optic cup morphogenesis, actomyosin-dependent basal constriction promotes invagination (Figure 2C'), as well and ensures a fast and efficient formation of a cup-shaped tissue (Sidhaye and Norden, 2017). Basal surface changes depend on the ECM (e.g., Gutzman et al., 2008; Sidhaye and Norden, 2017), indicating that intact cell-ECM connections might be required to regulate the dynamics of the basal cortical pool. Overall, basal epithelial dynamics in morphogenesis are widely spread, as well as conserved, as they occur both during vertebrate and invertebrate development (*Drosophila* gastrulation, Sun et al., 2017). However, they are still not well understood. More studies are needed to grasp the full extent to which basal epithelial dynamics govern shape changes and to elucidate the exact mechanisms behind basally-driven morphogenesis.

1.3.3 Cell-extrinsic changes of tissue shape

The above examples all showcase active changes in cell shape governed by actomyosin contractility. However, in addition to these, cell shape changes can be driven not only by intracellular components, but also the extracellular environment. The ECM has long been assumed to provide mechanical support for tissues and cues for cell survival. It becomes more and more clear however, that its mechanical properties and abundance can also shape the tissue mass by establishing a plastic surrounding (rev. in Morrissey and Sherwood, 2015). In an example of cell shape changes driven by the ECM in the *Drosophila* wing disc, the ECM maintains tissue shape by exerting compressive forces around the tissue perimeter (Figure 2D). If these are relieved by an interference with Collagen IV, a major filamentous component of epithelial basal laminas, the tissue flattens and cell height is lower due to basal surface relaxation and spreading (Pastor-Pareja and Xu, 2011). Conversely, by adding more of the cross-linker Perlecan to the same system, the

compression is higher and the cell height increased (Ma et al., 2017; Pastor-Pareja and Xu, 2011). The question still remains of what portion of these cellular changes is active, i.e., arising from the changing cell mechanical properties and what portion is passive, i.e., arising from physically constraining, external structures such as the ECM, Figure 2D) or neighboring organs.

Irrespective of whether the shape change originates apically or basally, is active or passive, it depends on cellular mechanical properties, which are chiefly governed by the cortex. Therefore, a robust control over the organization and contractility of the actomyosin meshwork, that is able to adapt to specific internal and external conditions is ultimately essential to ensure that proper tissue shape is generated and maintained.

1.3.4 Future challenges

Some of the main research in the past 10 years included the investigations of how single cell shape changes are triggered and how do they coordinate across the tissue, or how cell shape feeds back to alter gene expression and cell-cell interaction. We now have much more insight into the molecular mechanisms coordinating contractile responses throughout tissues. We know of molecular tension sensors, i.e., junctional components i.e., α -catenin or talin whose structure responds to junctional tension by recruiting more cytoskeletal and junctional elements and strengthening the cellular attachment, so the tissue can keep its integrity during changing shape. However, we still lack understanding on how particular morphogen gradients or other upstream cues form and propagate in precise, spatio-temporally controlled manners to trigger shape changes through affecting a subset of cellular actomyosin.

1.4 COORDINATING CHANGES IN SHAPE AND SIZE

Previous sections review our current knowledge on how cellular and extracellular parameters govern tissue growth and changes in tissue shape. However, these mechanisms should not be considered in isolation of each other, as we know that many tissues continue to proliferate while changing shape (e.g., the fly wing, Etournay et al., 2015). Still, we do not yet understand the cross-talk of the two. In this section, I outline our current knowledge on how growth and shape changes can be temporally coordinated in different organs.

The tissue shape changes as the tissue grows in many developing systems, for example in the developing *Drosophila* wing (Etournay et al., 2015), wing disc (Dye et al., 2017 preprint) or during zebrafish optic cup morphogenesis ((Kwan et al., 2012), During proliferative growth of the fly wing disc and maturing wing, the tissue matures and changes its shape through both cell rearrangements and cell shape changes (Dye et al., 2017; Etournay et al., 2015). In the wing disc, the tissue also changes its shape by buckling as it

grows. During optic cup morphogenesis in the zebrafish, the tissue proliferates and grows (Kwan et al., 2012) while assuming its hemispherical, basally invaginated shape (Sidhaye and Norden, 2017). A tissue can grow by receiving additional cells through their migration from a donor tissue (e.g., zebrafish optic cup). In addition to aiding growth, such a cell migration process can help change tissue shape. It can increase cell compression in the target tissue and/or lead to shape changes such as buckling, as seen during zebrafish optic cup morphogenesis (Sidhaye and Norden, 2017).

Spatially patterned growth contributes to changes of tissue shape (Nelson et al., 2005) by a localized increase in cell mass. Spatially patterned cell divisions can arise from e.g., spatially distinct morphogen gradients, such as the Dpp in *Drosophila* (rev. in Lecuit and Le Goff, 2007). Morphogen gradients provide patterning and directional information that transforms a homogenous field of cells into discrete, concentration-dependent domains (Lecuit and Lenne, 2007). For example, the Dpp morphogen gradient aids uniform overall tissue growth of the wing disc, proposed to be modulated by the direction of mechanical forces, as well as by the proportion of morphogen at the source and at the sink (Aegerter-Wilmsen et al., 2007; Hufnagel et al., 2007). Even though the resulting growth is uniform, it is ensured by non-uniform proliferation. Higher peripheral proliferation increases the compression of cells in the center of the tissue, inhibiting their proliferation in a compression-dependent negative feedback loop (Petridou et al., 2017). Moreover, the expression of the *Drosophila* homolog of Myc is modulated by the patterned activity of Wingless (Johnston et al., 1999). As Myc promotes cell size increase and cell cycle (G1/S) progression during wing disc, it results in shape changes through patterned changes in cell size in the wing disc (Dye et al., 2017). Aside from morphogen gradients, classical signaling pathways can also control cell shape, aside from their roles in orchestrating growth, patterning and cell differentiation. In another example from the developing *Drosophila* wing disc, Wnt/ Wingless signaling pathway, together with Dpp, has been shown to regulate the transition from cuboidal to columnar cell morphology (Widmann and Dahmann 2009a).

Besides patterned proliferation, regulated orientations of cell divisions are another way to change tissue shape by altering the direction of growth (Figure 2B). These are controlled by controlling mitotic spindle orientation, often by the components of the conserved planar cell polarity (PCP) pathway, which orients cells and tissues within a plane perpendicular to the apico-basal plane (Gong et al., 2004; Lawrence and Shelton, 1975; Maung and Jenny, 2011; Vinson and Adler, 1987). We now know that the process of orienting the mitotic spindle is tension-dependent (rev. in Petridou et al., 2017) and divisions will orient along the longer (higher tension) cell axis (Black and Vincent, 1988; Hertwig's rule, Hertwig, 1893). This can be viewed in its essence as similar to cell monolayers that reenter the cell cycle upon release of compression. Through such oriented cell divisions, adhesion

components Dachsous and Fat of the PCP pathway have been shown to determine the shape of the *Drosophila* wing (Baena-López et al., 2005). In vertebrate embryos, it has been shown that the spindle is oriented in dependence to the connection to the ECM through the focal-adhesion kinase (Petridou and Skourides, 2014) and in dependence to molecular motors myosin II (Campinho et al., 2013) and myosin-10 (Sandquist et al., 2016; Woolner et al., 2008), that help align the spindle according to the force distribution in the cell (Campinho et al., 2013). In the *Drosophila* wing disc, global cell non-autonomous forces in the proximal regions arise from the distal tissue proliferating and growing more (Mao et al., 2013). This stretches the proximal cells along the proximo-distal axis, so that they are exposed to higher tension. Subsequently, the tension determines the spindle orientation and results in a non-uniform proliferation pattern. This way, together with the compression-dependent decrease in proliferation mentioned above, wing disc shape is maintained through patterned growth, in the face of forces that might otherwise destroy its integrity.

The ECM, as mentioned previously, has emerged as a major determinant of tissue form. An example of such an ECM-dependent process is found in the *Drosophila* ovarian follicle, where growth through proliferation is necessary for a change in tissue shape (Aurich and Dahmann, 2016). In this situation, rather than the active cell shape changes, it is the patterned ECM constraint around the tissue perimeter that forces the growing tissue to preferentially elongate, as well as organize the actin fibers to allow elongation. The ECM seems to have a similar role in other developmental processes (rev. in Morrissey and Sherwood, 2015), such as the development of the mouse salivary gland (Harunaga et al., 2014). In the mouse gland, it also acts as a molecular corset, a patterned growth constraint similar to the follicle example, with the accumulating collagen constricting the stalk of the growing gland bud. The ECM at the tip of the bud is weaker, with microscopic perforations and this weaker constraint to growth allows an increase in size at the tip. Thus, here, a patterned ECM structure determines the “mushroom-shape” of the growing gland bud (Harunaga et al., 2014). Besides these two examples, in all other examples mentioned in this section, tissue shape was shown to depend on the ECM (Etourmay et al., 2015; Ma et al., 2017; Sidhaye and Norden, 2017). In the wing disc study by Ma et al. (2017), an intact ECM was shown not to be essential for tissue growth, but rather acted only as a regulator of cell and tissue shape, as in the previous examples. This is possibly because here a single ECM component was perturbed (Collagen IV or Perlecan) and cell attachments might have been left intact, allowing anchorage-dependent proliferation to continue. Thus, the ECM can coordinate shape and size as a passive constraint, restraining the tissue mechanically and allowing growth through proliferation if cell-ECM attachments are unperturbed, but also through organization and tension of the actin cytoskeleton, as in the example of the fly follicle.

As discussed in the sections on size (Tissue-extrinsic cues), shape (Cell-extrinsic changes of tissue shape) and here, it became clear with these and a plethora of other studies in the past 10-15 years that the ECM is much more than a passive tissue support (Brown, 2011; Loganathan et al., 2016; Morrissey and Sherwood, 2015). Besides its roles in morphogenesis (tissue compaction, swelling, cell migration), the ECM regulates signaling and morphogen concentration through secreting and binding ligands, it controls cell proliferation and survival (anchorage dependence) and is a scaffold for coordinating cell mechanotransduction, the organization of the cytoskeleton and cellular mechanics throughout the tissue. As the ECM is a tissue-wide regulator of both growth (cell proliferation, migration and survival) and shape changes, it represents an attractive candidate for a coordinator of these two processes during development.

The studies mentioned in the previous sections revealed many details about how specific cellular and extracellular parameters (e.g., cell divisions, size, shape or adhesions) bring about changes in tissue size and shape. However, methodologically, many studies of growth and especially studies of tissue shape still only take into account the apical, 2D view of cells and their apical behaviors as a proxy for relevant cell changes. While this might be a valid approach to study particularly thin tissues such as the adult fly wing, many developing epithelia and organ precursors are thick, their surfaces non-uniform and morphogenesis happening in all three dimensions (e.g., the fly wing disc). Thus, model systems that allow tissue-wide 3D, time-course studies and integrate effects of growth, cortical and ECM contributions are necessary if we want to fully understand how different cellular behaviors coordinate and contribute to morphogenesis, to give rise to optimally functioning tissues. In the next section, I introduce in detail the pseudostratified epithelium as a proliferating, growing tissue with the potential to meet these study requirements and provide insight into coordination of size and shape.

1.5 PSEUDOSTRATIFIED EPITHELIA

As discussed in the previous paragraphs, the size and shape of tissues result from an interplay of many cellular, but, importantly, also tissue-wide factors and properties. Furthermore, single-cell properties such as proliferation or shape depend greatly on the environment in which they develop. Cells will behave differently in 2D and 3D cultures (rev. in Edmondson et al., 2014), in different ECM stiffness conditions (Discher, 2005) or nutrient concentrations (Britton and Edgar, 1998; Cheng et al., 2011), to name a few. Because of this complexity, it is currently difficult to recapitulate the exact tissue conditions in an in vitro study. Therefore, in order to study complex phenotypes such as size and shape in physiological conditions, it is best to approach the question in an intact tissue environment.

With respect to this, we are in need of model systems that allow us to analyze the entire 3D structure over time and perform perturbations as tissues grow and change their shape. In this last part of the Introduction, I will present the pseudostratified epithelium, a growing, complex and widespread epithelial tissue, based on our review from 2016 (Strzyz et al., 2016) and PSE development in the zebrafish retina, as a model system to address questions of growth and shape. The pseudostratified epithelium is a tissue interesting from the tissue-growth perspective and the retina a tissue relevant because of its function, shape and neuroepithelial character, as discussed in the last part of this Introduction. Together, they form a powerful and highly relevant system that allows unprecedented imaging conditions and quantitative assessment of the development of tissue size and shape from tissue- to the subcellular-scale.

1.5.1 Main characteristics

Pseudostratified epithelia (PSE) are proliferative tissues that feature elongated cells organized into a single, tightly packed epithelial layer (Figure 3). They are widely spread and are found in diverse metazoan species from *Nematostella* to humans. PSE are especially prominent during development and give rise to many tissues and organs. In vertebrates, they form the epiblast of the gastrulating embryo (Ichikawa et al., 2013), the liver, lung and pancreas buds, gut, nasal placode epithelia, otic placode/vesicle, lens placode/vesicle and the central nervous system (CNS). They are also found building the embryonic ectoderm of the sea anemone *Nematostella* (Meyer et al., 2011), imaginal discs of fly larvae (Meyer et al., 2011), as well as the fly optic lobe neuroepithelium (Rujano et al., 2013). As these tissue arrangements are so widespread, studying their biology has the potential to generate insights origin and development of many other systems, including the CNS. PSE are real epithelial tissues, with apico-basal polarity, an apical junctional belt, centrosome and primary cilium and the basal surface resting on the basal lamina. The cells that build the PSE are slender, with a large, bulky nucleus positioned anywhere along the apico-basal axis of the cell. This egg-in-a-sock cell morphology and tight tissue packing gives the PSE tissue a stratified appearance, with seemingly multiple cell layers. However, the elongated PSE cells are attached at both the apical and the basal surface in a monolayered tissue (Sauer, 1935; Smart, 1972), (Figure 3), hence the term pseudostratified.

Interestingly, the nuclei in PSE are dynamic and perform apico-basal movements correlated with the cell cycle stage. Shortly before mitosis, in the G2 stage, nuclei migrate to the apical surface in a rapid and directed manner (Kosodo et al., 2011; Norden et al., 2009; Strzyz et al., 2015; Tsai et al., 2010), a movement termed interkinetic nuclear migration (IKNM) (Sauer, 1935). The nucleus of the progenitors is their bulkiest organelle,

protruding from the elongated cell body and undergoing actomyosin-dependent IKNM (Figure 3). IKNM is cell cycle dependent, happens during a ~20 min long G2 phase and is a directed movement, while the surrounding interphase nuclei get displaced passively and exhibit stochastic motion (Leung et al., 2011). It is still not understood what the implications of the IKNM movements on the cell cycle and packing of interphase cells are, neither is it known whether the density through which an IKNM nucleus migrates can somehow affect its migration, or even subsequent fate. All cells undergo division apically, which has been shown to be an important feature to retain tissue architecture (Strzyz et al., 2015).

1.5.2 Heterogeneity

Even though the general architecture of all PSE is similar and in all PSE nuclei exhibit IKNM, PSE occur in different forms in different organisms and especially their overall height can vary. Different PSE can span apico-basal distances from less than 30 micrometers to hundreds of micrometers and even millimeters (Figure 3C). During the development of the mammalian cortex, for example, PSE cells progressively elongate and their length is highly dependent on their developmental stage (Florio and Huttner, 2014; Huttner and Brand, 1997; Sauer, 1935; Schoenwolf and Alvarez, 1989). Furthermore, the degree of pseudostratification of a PSE, which describes how many nuclear layers are stacked within the epithelial sheet, also varies, mostly proportional to the cell length. Thus, PSE can be classified by their cell length and nuclear packing into short, intermediate and long PSE. Short PSE measure 20–30 μm in thickness (cell length) and their nuclei arrange into two to three nuclear layers (Figure 3A). These PSE make up the neural plate, optic lobes in *Drosophila* (Rujano et al., 2013), vertebrate otic vesicle (Clendenon et al., 2009; Hoijman et al., 2015) and endodermal organ buds (Bort et al., 2006). Intermediate length PSE cells (Figure 3B) span 30–60 μm and their progenitor nuclei arrange on average into four to five layers (Jeong and McMahon, 2005; Nagele and Lee, 1979). Such tissues are found in the neural tube, in retinal and hindbrain neuroepithelia of the zebrafish (Leung et al., 2011; Norden et al., 2009), the epithelium of the developing mouse intestine (Grosse et al., 2011), the fly imaginal discs (Meyer et al., 2011) and the ectoderm of the sea anemone *Nematostella* (Meyer et al., 2011). At later stages of development, intermediate length neural progenitors elongate further. For example, in the neural tube and the retina of higher vertebrates, these cells reach the final length of up to 100 μm , arranging their nuclei into eight or even more layers (Iulianella et al., 2008; Nasonkin et al., 2011; Smart, 1972). We define these as long PSE (Figure 3C).

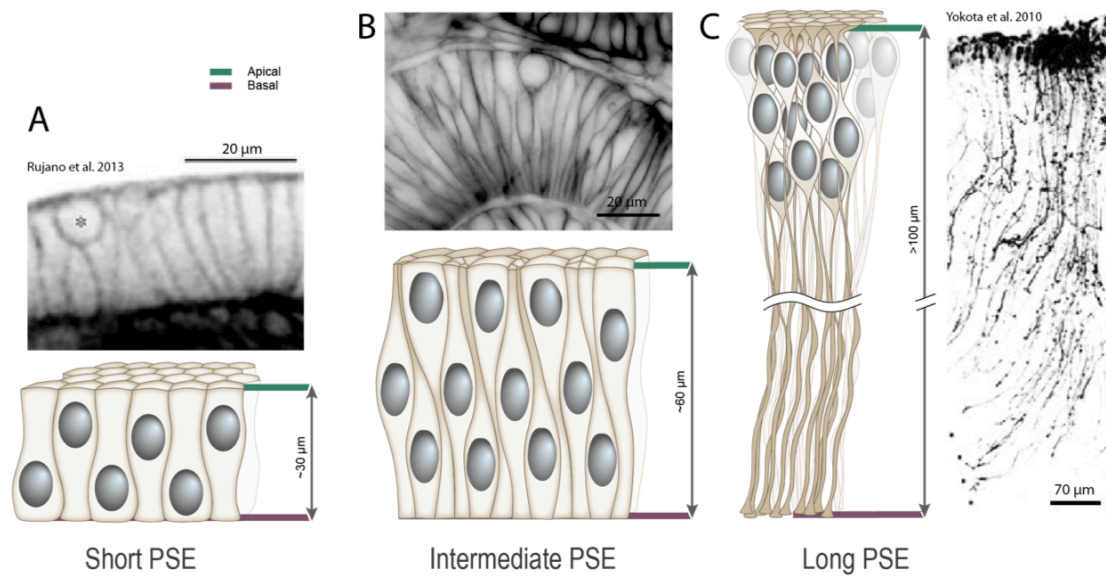


Figure 3: Heterogeneity and universality of pseudostratified epithelia.

A) Short PSE, as seen in the *Drosophila* optic lobe (Rujano et al. 2013), B) intermediate length PSE, as in the zebrafish retinal neuroepithelium (this study) and C) long E15.5 mouse cortex radial glia (Yokota et al. 2010). All cells are tightly packed, attached at both apical and basal ends. The longer the PSE, the thinner the processes and the more protruding the bulky nuclei are. In the extreme example of radial glia, this gives the cells the bead-on-a-string appearance.

Scale bars are 20 μm in A), B) and 70 μm in C). Figure is adapted from Strzyz, Matejczik and Norden, 2016.

Another feature that can vary dependent on PSE length are the cellular machineries that drive apical IKNM. These differences seem to correspond to the different length/packing classes, so the PSE could be grouped into different classes by these molecular force generators of the IKNM (Norden, 2017; rev. in Strzyz et al., 2016). In the short PSE, the mere process of actomyosin-governed cell rounding could be enough to displace the nucleus along the short distance that is 20-30 μm (Meyer et al., 2011; Rujano et al., 2013). In all of the intermediate PSE studied so far, IKNM is also actomyosin-dependent (Norden et al., 2009), but mitotic cell rounding is decoupled from it (Strzyz et al., 2015). In the long PSE, microtubules are necessary for the process (D. J.-K. Hu et al., 2013; Spear and Erickson, 2012; Tsai et al., 2010; Xie et al., 2007), indicating that forces that actomyosin can generate might not be sufficient to act during IKNM on >100 μm scales. Such classification is still hypothetical, however and awaits experimental assessment.

Despite spanning different cell sizes, organs and organisms, different PSE tissues were proposed to share a growth-related characteristic. During development, they often increase in cell length and number of nuclear layers, a topic that, together with PSE shape, I discuss in the next section.

1.5.3 Growth and shape of the PSE

The PSE are highly proliferative tissues, with their structure and cellular arrangement proposed to contribute to this proliferative capacity (Strzyz et al., 2016). All PSE cells are cycling and the number of cells in a unit of tissue volume can be maximized by changing the cell shapes and nuclear arrangement and thus maximize the proliferative potential, governed by the IKNM. However, as cells within PSE tissues are arranged in a tightly packed epithelial sheet, it has to be considered that IKNM and proliferation do not occur in isolation. On the contrary, nuclei move and divide within the dynamic tissue, which will progressively expand and increase its cell density with every round of division. Furthermore, as PSE cells proliferate, their morphology also changes. For neural PSE, it was shown that they progressively elongate and decrease their apical surface (Miyata et al., 2015; Smart, 1972), possibly due to the inability to expand the apical surface (Smart, 1972). As a consequence, proliferation in PSE tissues influences the overall tissue organization and most likely has implications for tissue maturation. In addition, by affecting cellular morphology, continued proliferation might affect cell density and tissue-scale mechanical properties, creating a regulatory loop that feeds back to control proliferation and/or differentiation rates.

When PSE cells round up at the apical side in order to undergo mitosis, they take up several times more apical surface area than their apical endfeet do during interphase (Smart, 1972). Because of this, it has been speculated that the available apical area might act as the mechanical constraint to PSE division rates (Smart, 1972). This means that the number of layers of interphase nuclei that will eventually divide apically must be coordinated with the amount of free apical surface. To understand such limitations to PSE proliferation and the maximal number of nuclear layers, it is important to know how much of the apical space a mitotic cell inhabits (relative to the interphase cell) and for how long it occupies this apical surface unit (mitosis length). Additionally, one has to identify how long interphase nuclei need to reach the apical surface (cell cycle length). As the PSE are primarily proliferative tissues, we can assume that the optimal packing will be reached when the maximal possible number of proliferative layers is packed under the apical surface of a specific PSE (Fish et al., 2008; Smart, 1972). This number of nuclear layers is thus expected to be proportional to the total cell cycle length and inversely proportional to the length of mitosis. This relation proposes a limit to growth of apically-constrained PSE, originating in all 3 dimensions, where multiple layers of nuclei “queue” to reach the apical surface for division. However, this proposed rule has been mostly speculative and we lack data analyzing changes in nuclear layering through development, to check how it applies to growing PSE.

Besides becoming thicker and packing more nuclear layers as they grow, the PSE vary in shape (Norden, 2017) and can change it as they develop. For example, the ectoderm of the cnidarian *Nematostella* is flat, while some other PSE, such as the developing zebrafish retina, hindbrain and otic vesicle (Alsina and Whitfield, 2017; Giraldez et al., 1987; Gutzman et al., 2008), or the mouse neural tube (Eom et al., 2013) are basally, or apically bent, respectively. The developing zebrafish brain (Lowery and Sive, 2005) or the fly wing disc (Sui et al., 2012), on the other hand, contains flatter regions as well as regions bent apically or basally. We now understand better how some of these PSE shapes form e.g., the zebrafish optic cup through processes of epithelial morphogenesis, such as the ECM-dependent processes of basal cell constriction and cell migration (Sidhaye and Norden, 2017). However, the variability of shapes is large and the shape of the PSE might affect the ratio of the apical to basal surface area and with this, the availability of apical space for divisions. For example, apically (inward) bent regions of the hindbrain might have to coordinate their number of nuclear layers with the degree of bending, as a smaller surface would be available for mitotic rounding if the tissue apical area is constricted. Therefore, besides being relevant to study epithelial morphogenesis in 3D, the shape of the PSE has the potential to alter the hypothetical apical constraint, or aid/interfere with nuclear migration and its coordination and possible effects on PSE growth should be considered.

The limit to PSE growth and its possible alterations by tissue shape discussed above assume that the PSE tissues are apically constrained and can therefore not arbitrarily increase their apical surface upon too high nuclear layering. In this case, the PSE cells should be able to respond to high tissue packing or a hypothetical compression of the apical surface, by altering e.g., their cell cycle parameters, size or shape. In other words, the PSE should be mechanosensitive. In the following section, I outline two studies that suggest this is indeed the case and the PSE are able to sense and respond to mechanical stimuli.

1.5.4 Mechanics of the PSE

As discussed previously, it is now well established that diverse mechanical stimuli play major roles in proliferation, tissue development and function, in many systems ((see e.g., section 1.2.2.2 Growth responses to mechanical cues, rev. in LeGoff and Lecuit, 2015; Mammoto and Ingber, 2010). Several pathways underlying the translation of mechanical stimuli into cellular responses have been unraveled during the past decade (Provenzano and Keely, 2011), such as the alfa-catenin- or talin-dependent cellular cortical changes as a response to increased tension at the cell-cell or ECM junctions (Discher, 2005), respectively. In the recent years, studies have studied upon mechanosensation in PSE tissues, as well (Mao et al., 2013; Porazinski et al., 2015; Schluck et al., 2013). For example, a study of a fish mutant in the Hippo signaling pathway demonstrated that PSE respond to

gravitational force (mechanosensation, Porazinski et al., 2015). Because of reduced actomyosin-based tissue tension, these fish mutants developed malformed (flattened) and misaligned optic cup and neural tube, both of which are PSE tissues, indicating that tissue tension is essential to maintain PSE shape. In another study, direct links between mechanical strain and PSE proliferation were investigated (Schluck et al., 2013). By mechanically stretching the explanted *Drosophila* wing disc PSE, it was confirmed that a contact inhibition-like mechanism operates in this tissue, as well. Thus, PSE seem to indeed be mechanosensitive and can respond to mechanical forces such as strain by changing their proliferation rates and possibly other cell parameters. Moreover, because of their dynamicity arising from nuclear movements and tight packing, sources of mechanical stimuli such as increased membrane tension might be plentiful in this epithelium. The PSE might, therefore, serve as new model system providing exceptional insights into the role of mechanical cues during epithelial development and function.

1.5.5 Future challenges

So far, the question of how PSE packing affects tissue maturation has been speculative. In order to understand how cell density and compaction might feed back to PSE cell numbers and size, it is important to first experimentally verify whether packing of different PSE tissues follows the previously proposed cell cycle-dependent packing limits and how they might change through PSE development. As suggested above, intricate feedback loops might be at the center of coordinating growth and cell cycle parameters, keeping proliferation of a PSE at its maximum. Furthermore, as essential processes in the PSE occur along the apico-basal axis (IKNM), tissue shape might play a role in their efficiency and it will, therefore, be important to study how growth, proliferation and shape changes coordinate during PSE development. Most of the studies of changes in epithelial size and shape still consider only two dimensions and a single tissue surface as a proxy for developmental events that happen throughout the tissue volume. The PSE, with their different shapes, stereotypical architecture and cellular dynamics provide a good model system to extend our understanding of growth, shape generation and the coordination of the two during development, to three dimensions.

Different PSE tissues still differ in their accessibility to imaging and analysis. Among them, the basally invaginated developing zebrafish retina is an exceptional system. This cup-shaped PSE combines a tissue environment of extremely three-dimensional features and simple shape, the cellular dynamics of the PSE (IKNM) and its hypothetical growth constraints, with unprecedented advantages of the zebrafish system in biological imaging, that comes from zebrafish embryo transparency and fast development, as well as from the retina position at the surface of the body. All these advantages add to the biological and

clinical relevance of the retinal tissue, due to proper retinal development being essential for vision, as well as providing possible hints to the development of the vertebrate central nervous system in general.

1.6 ZEBRAFISH RETINAL PSE

The mature vertebrate retina is a complex sensory tissue that is part of the central nervous system (CNS). As introduced above, the zebrafish is an excellent model to study its development in imaging-based studies due to its transparency, small size and fast, *ex utero* development. Moreover, many genetic tools and transgenic lines are available that allow monitoring, as well as perturbation of diverse structures. The developing zebrafish retina, a growing, hemispherical PSE located at the surface of the body, therefore, provides unprecedented access to study organ shaping, growth and differentiation using direct observation in live or fixed tissue-wide imaging approaches.

Like other CNS regions, the mature zebrafish retina develops from a PSE tissue originating in the neural tube. Its initial developmental phase involves complex morphogenetic changes to generate a hemispherical cup shape. Morphogenesis is then followed by growth of this hemispherical PSE neuroepithelium, that precedes tissue differentiation and formation of a layered, neuronal structure.

1.6.1 Optic cup morphogenesis

The zebrafish retina starts forming with the developing forebrain, when an anterior region of the neural tube becomes specified as a single eye field by the localized expression of multiple transcription factors, such as Pax6 and Rx1 (Levine and Green, 2004; Zuber, 2010). Actomyosin cables and Eph/ephrin signaling restrict the eye field cells from mixing with the rest of the neural plate cells (rev. in Bazin-Lopez et al., 2015). The field is then split along the midline (Figure 4A), forming a left and a right portion, cells of which will start evaginating to form the optic vesicles (Figure 4B). These are pouch-like structures each comprising two layers, a proximal and a distal one (green and violet in Figure 4B, respectively). Specific domains, such as the nasal and the temporal retina, are already specified as early as this optic vesicle stage (Picker et al., 2009) and have important implications for subsequent patterning and developmental processes. The proximal layer will eventually spread and thin out the typical PSE structure, forming the retinal pigment epithelium (RPE), a thin squamous layer around the apical surface of the retina. The RPE fate of the optic vesicle cells is specified around 20 hours-post-fertilization (hpf) and is Hippo-pathway (YAP/TAZ) dependent (Miesfeld et al., 2015). This epithelium will produce melanin and be essential for the survival of the photoreceptor cells in the mature retina by delivering nutrients and protecting from high light intensity. The second, distal domain of

the optic vesicle is the base for forming the retinal neuroepithelium PSE itself. It will receive cells from the thinning proximal layer through their collective migration around the rim of the structure. The neuroepithelial PSE will start invaginating from the basal side (Figure 4C), in a process dependent on the basal accumulation of actomyosin and on an intact ECM. Both cell migration into the cup and basal invagination are necessary to form a proper neuroepithelial cup in a timely manner. If cells do not migrate into the neuroepithelium in time, the final cup structure is not only flatter, indicating they aid invagination, but the delayed cells start to form stable attachments and invaginate outside of their correct target tissue (Sidhaye and Norden, 2017). If the vesicular structure invaginates properly, it will finally form the hemispherical, cup shaped PSE retinal neuroepithelium by ~20 hpf, with the thin RPE surrounding its apical surface (Figure 4D). This basally invaginated structure of the retinal PSE is the organ precursor of the entire mature neural retina (Fuhrmann, 2010) and already has its characteristic shape fully established.

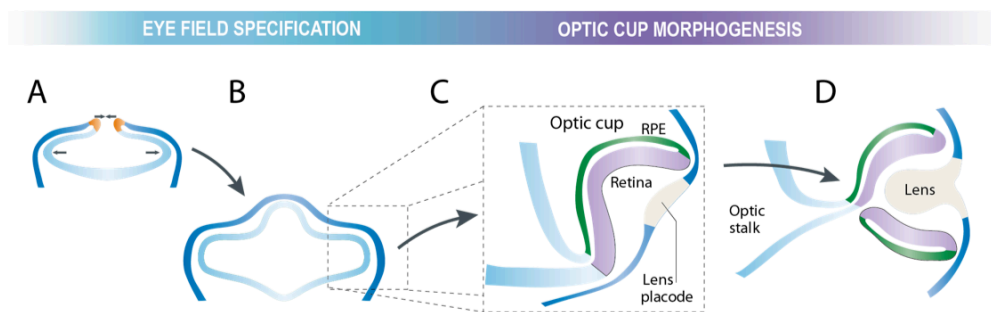


Figure 4: Early development of the vertebrate eye.

A) The eye field will become specified at the anterior part of the neural tube by expression of specific transcription factors. The single field will split into two (left and right) along the midline and B) start evaginating to form the optic vesicle.

C) Each vesicle will start invaginating basally. The RPE epithelium will spread and active collective migration of these cells into the retinal layer (green into purple) aids invagination to D) generate a proper optic cup. Adapted from Lamb et al. 2007.

1.6.2 Neuroepithelial stage

The cup shaped tissue of the prospective zebrafish retina is formed by ~20 hpf. The morphogenetic phase of invagination is followed by >15 hours of a growing PSE structure (Figure 5, He et al., 2012). Not much is known about tissue-wide properties in this developmental stage, other than that it proliferates and grows. The retinal PSE is filled with neural progenitor cells that show a typical conserved PSE morphology (Figure 5A, A'): they are slender, attached at the apical side facing the RPE, to each other at the apical junctional belts and the ECM (basal lamina). The ECM of the basal lamina contains the typical components laminin, fibronectin and chondroitin sulfate (Sidhaye and Norden, 2017). Due to it always being present in basal laminas (Kühn, 1995), even those of PSE tissues (Pastor-Pareja and Xu, 2011), collagen (type IV) is also expected to build the ECM of the zebrafish

retinal PSE. The zebrafish retinal PSE cells are of intermediate length, similar to the fly wing-disc and undergo actomyosin-dependent IKNM (Leung et al., 2011; Norden et al., 2009), with divisions consequently occurring exclusively at the apical surface. He et al. (2012) show that the number of retinal PSE cells grows from 1800 cells to 11000 cells in 24 hours (24-48 hpf), a 6-fold increase, this implies that progenitors undergo 2-3 rounds of cell division before differentiating. The S-phase of the progenitor cell cycle was shown to be the longest, followed by the G1-phase (Leung et al., 2011). G2- and M-phases are both much shorter and take ~20 minutes. Even though we have some understanding of cellular properties in the retinal PSE (IKNM, average cell cycle length), we do not know how they change during development, nor how exactly they contribute to changes in tissue size and shape.

1.6.3 Differentiation stage

Cell cycle exit and differentiation of neural progenitor cells start in the zebrafish retina around 32 hpf. Retinal neurons are not specified uniformly at the same time throughout the retina but follow a distinct temporal and spatial pattern (Almeida et al., 2014; He et al., 2012; M. Hu and Easter, 1999), conserved in most vertebrate taxa (Rapaport et al., 2004; Sernagor et al., 2009). The neuronal marker *Ath5* (Liu et al., 2001; Yang et al., 2003) is used to label the first-born retinal neuron type, the retinal ganglion cells (RGCs) and thus track the onset of differentiation (M. Hu and Easter, 1999; Icha et al., 2016; Kay et al., 2001; 2005). *Ath5* is essential for RGC development (Kay 2001) and starts being expressed in cells at a ventro-nasal patch of the tissue, to then continue spreading throughout the whole retina in a naso-temporal and central-peripheral fashion (Figure 5D', Almeida et al., 2014; He et al., 2012; M. Hu and Easter, 1999). Neuroepithelial progenitor cells start expressing *Ath5* just before their terminal division (Icha et al., 2016). 3-4 hours after the onset of *Ath5* expression, the daughter cell that has inherited the basal cell process after division will start translocating its cell body (Icha et al., 2016) and delaminating basally (Randlett et al., 2011) by detaching from the apical surface (Icha et al., 2016). After birth, the RGCs migrate to the basal-most tissue layer, where they fulfill their function and organize other retinal neuronal layers (Icha et al., 2016). RGC migration towards the basal-most side, is an ECM- and microtubule-dependent process. After reaching the basal side, RGCs will outgrow axons (Figure 5D) and form a distinct basal nuclear layer, separated from the rest of the retina with a layer occupied by a dendritic network through which RGCs eventually connect to other retinal neurons (the inner plexiform layer).

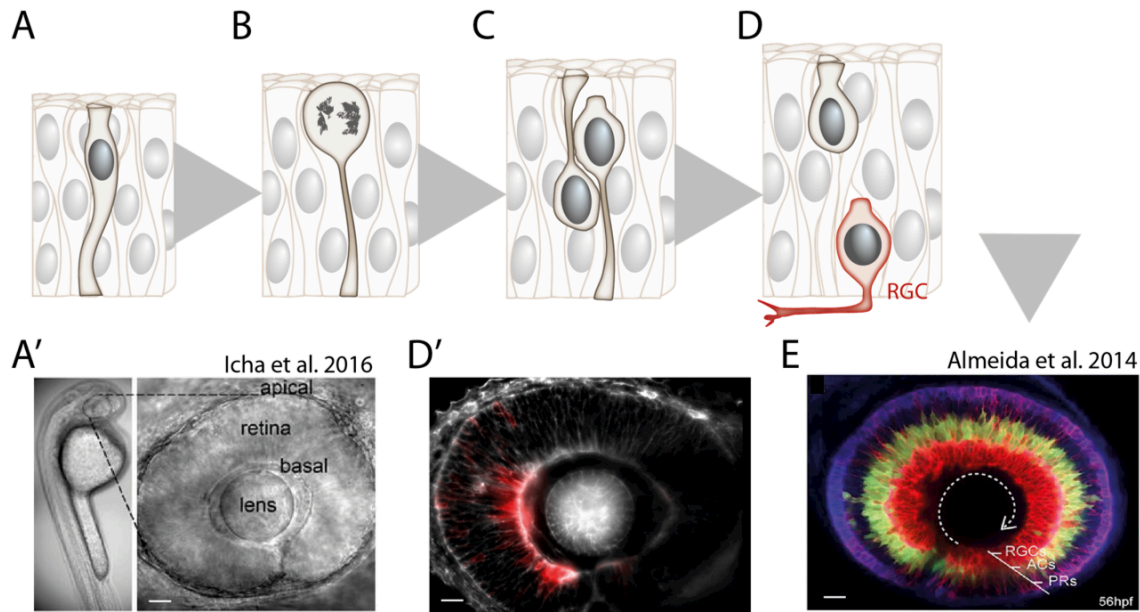


Figure 5: Development of the zebrafish retinal neuroepithelium.

A), A') After the optic cup is formed (Figure 4) ~20 hpf, the hemispherical retinal tissue grows as a PSE, with B) all mitoses occurring at the apical surface.

C) It starts differentiating ~30 hpf in a D') nasal-to-temporal manner.

D) The first cells that differentiate are the RGCs (red). They will migrate basally to form the ganglion cell layer until ~48 hpf.

E) By 56 hpf the other neuronal layers are distinguishable. By 72 hpf all the cells will be differentiated, migrate to their layer and the retinal structure fully laminated.

By ~40 hpf, the Ath5 neurogenic wave will have swept the entire tissue and other neuron-specific transcription factors, such as Ptf1a (amacrine and horizontal cells) and Crx1 (photoreceptor cells) start to be expressed in a conserved order. Eventually, all six major retinal neuronal subtypes (and one glial cell type) will be specified and, through intricate and generally unknown mechanisms migrate and delaminate through the crowded environment in a spatiotemporally conserved order, to their final position in one of the three neuronal layers (Figure 5E).

1.6.4 Variability during retinal development

As already mentioned in the section on optic cup morphogenesis, a temporal delay in cell migration into the neural retina results in migrating cells turning on neuroepithelial markers at the right time, but at a wrong place. This ectopic determination will impair retinal formation and can even result in the emergence of additional invaginating structures (Sidhaye and Norden, 2017), showcasing the importance of temporal coordination during retinal PSE development. If retinal ganglion cells do not translocate to the basal-most retinal layer during their differentiation, but stay in more apical positions, later-born retinal neurons will organize around these ectopic RGCs (Icha et al., 2016), providing an example of how

mispositioning due to faulty spatiotemporal coordination can be detrimental for retinal function. Certain cell types, such as the RGC, therefore, have an organizing function and their positioning at the right place and at the right time is a prerequisite to generate an organ of a correct form, structure and function. Not all cellular properties are equally important to be tightly coordinated and some allow a certain degree of variability. For example, if proliferative growth of the neural PSE is impaired by blocking proliferation, the optic cups will still invaginate and the cells will eventually differentiate, irrelevant of having a less cells and smaller sizes (Icha et al., 2016; Kwan et al., 2012). Moreover, if one of the retinal neuronal types is missing because its differentiation was blocked (e.g., RGC mutant *lakritz*, Kay et al., 2001) the layered structure will still form, but other neurons will inhabit the space of the missing cells (Kay et al., 2001; Randlett et al., 2013), conserving tissue structure. The main tissue function will be lost, however, as the RGCs are the cells building the axonal connection of the retina to the brain and thus ensuring transmission of visual impulse. The latter two examples again showcase that correct spatiotemporal coordination of developmental events is essential to generate a proper structure a tissue, in this case the retina, but how a certain level of error might be tolerated, as well. Therefore, a developing biological form can be robust and plastic at the same time and we need more studies to understand the mechanisms governing these properties and the extent to which developmental events, such as growth, shape change and differentiation, have to be coordinated to give rise to a functional tissue.

1.7 OBJECTIVE OF THE STUDY

In this study, my aim was to investigate the limits to growth of the retinal PSE and explain how this tissue maintains its shape while changing size.

During development, correct tissue form is ensured by a tight spatiotemporal coordination of a plethora of cellular and extracellular parameters. As evolutionary selection is proposed to act at every stage of embryogenesis (Lamb et al., 2007), developmental steps in tissues as evolutionary old as the PSE or the vertebrate retina (Lamb, 2013 respectively; both >500 million years ago, Marlow et al., 2009), likely coordinate in a near-optimal spatiotemporal order. Many examples showcase the complexity of emergence of correct tissue shape and size but we still do not know how shape and size coordinate across scales. Moreover, we do not know how much variation in this coordination is tolerated in different tissues, without compromising their function. In face of changing chemical and physical conditions during development, the coordination of parameters and constraints that regulate tissue form has to be highly dynamic. Therefore, it is not trivial to predict which cellular properties and how, give rise to the observed tissue form, nor how they change and adapt over time. To tackle this question, in this PhD thesis, I investigate how changes at the cellular scale affect tissue growth and shape and I propose a dynamic shape homeostasis in the developing retinal epithelium. My results highlight the importance of timely coordination of upstream signals and cellular responses with local, tissue form.

In the first part, I identify which cellular properties govern PSE growth and test the intrinsic constraints to tissue volume, cell number and cell cycle parameters. I then investigate how cell-scale changes enable the developing eye to maintain its shape while changing size. I propose a brake that limits changes in cell shape, that is removed tissue-wide precisely at the point where the tissue reaches its theoretical packing limit. The timely release of this brake allows maintenance of the tissue's aspect ratio and a smooth shape of the growing zebrafish retinal neuroepithelium.

2 MATERIALS AND METHODS

2.1 Zebrafish husbandry

Zebrafish were maintained and bred at 28.5 C. Zebrafish embryos were raised at 21, 28.5 or 32 C and staged in hours post fertilization (hpf) according to Kimmel et al. 1995. E3 medium was exchanged daily. 0.003% 1-phenyl-2-thiourea (PTU) was added to the embryo E3 medium from 8±1 hpf onwards and renewed daily to prevent pigment formation. Embryos were anaesthetized in 0.04% tricane methanesulfonate (MS-222; Sigma-Aldrich) directly prior to sorting for fluorescent signal (>36 hpf), imaging, intravitreal cavity injections, brain ventricle injection or retinal dissection. All animal work was performed in accordance with the European Union (EU) directive 2011/63/EU as well as the German Animal Welfare act.

2.2 Zebrafish methods

2.2.1 Transgenic and mutant lines

Transgenesis

Tg(β actin::eGFP-LAP2B) transgenic line and the Hsp70::eGFP-LAP2B and β actin::eGFP-LAP2B plasmids were generated as tools to label nuclear outlines and segment nuclear volumes through the cell cycle from live images. LAP2B-containing plasmid from Addgene (Cat. No. 21047) was used to extract the LAP2B sequence with attB primers (attB2r: 5'-GGGGACAGCTTTCTGTACAAAGTGGCTCTGTACAAGTACTCAGATCTCGAGC-3'; attB3: 5'-GGGGACAACCTTTGTATAATAAAGTTGCTCAGTTGGATATTTAGTATCTTGAAGAAAATTAGTG-3') and subclone it as the 3'-entry clone (Gateway) into the Tol2-plasmid. The Gateway cloning system (Thermo Fisher Scientific) was used. To generate the 3'-entry clone (p3ENTR(R2-L3)), LAP2B was amplified from the pmRFP-LAP2beta-IRES-puro2b plasmid using attB primers. Using the Gateway system, LAP2B 3'-entry was then combined with the β actin or Hsp70 5'-entry clones (p5ENTR(L4-R1), both (Kwan et al., 2007)) and the middle-entry clone eGFP (no stop; pENTR(L1-L2), Lawson lab) to generate the final Tol2 constructs, β actin::eGFP-LAP2B and Hsp70::eGFP-LAP2B, respectively. To generate the transgenic line, 1 nl of the plasmid Tol2- β actin::eGFP-LAP2B (20 ng/ μ l) was injected with Tol2 transposase mRNA (30 ng/ μ l) into the cell of one-cell stage embryos. Founder generation embryos were screened for with observed fluorescent signal and grown to adulthood. Germline carriers were identified by outcrossing to wild-type fish. These plasmids and line were proven to be bright and specific markers to track changes in

nuclear shape and size over time. The analysis of cell growth using LAP2B-GFP is ongoing and is not included in the Results of this Thesis. The other transgenic lines have been described previously (see table).

Table 2: Zebrafish transgenic lines and mutant used in this study.

	Line/ mutant	Labeling/ purpose	Reference
1	Wild-type WT-AB	Control studies	RRID:ZIRC_ZL1
2	Wild-type WT-TL	Control studies	RRID:ZIRC_ZL86
3	Tg(actb1::hras-GFP)	All membranes	Cooper et al., 2005
4	Tg(actb1::hras-mKate2)	All membranes	(Icha et al., 2016)
5	Tg(actb1::EGFP-utrCH)	F-actin	(Behrndt et al., 2012)
6	Tg(hsp70::h2b-RFP)	Chromatin	(Dzafic et al., 2015)
7	Tg(β actin::h2a-GFP)	Chromatin	(Geldmacher-Voss et al., 2003)
8	Tg(β actin::pcna-GFP)	Proliferating cells (nuclear/cytoplasmic)	Patricia Ramos, Norden lab
9	Tg(β actin::lap2b-GFP)	Nuclear envelope	This study
10	Tg(ath5::GFP)	Membranes of all RGCs and PRs	(Icha et al., 2016)
11	Tg(ath5::RFP)	Membranes of all RGCs and PRs	(Icha et al., 2016)
12	Tg(ptf1a::GFP)	Membranes of ACs and HCs	(Jusuf and Harris, 2009)
13	Tg(SoFa2)	Differentiated retinal cells	(Almeida et al., 2014)
14	hdac1 t24411	Inhibition of cell cycle exit and differentiation in zebrafish retina	(Stadler et al., 2005)

Mutants

Hdac1 t24411 mutants, containing a single point mutation in intron 4 of the zebrafish histone deacetylase 1 (hdac1) gene were obtained from the Zebrafish International Resource Center (ZIRC), grown to adulthood and genotyped according to a protocol established in the lab for this purpose (with Sylvia Kaufmann; see below for details). Incrossed, homozygous fish (hdac1^{-/-}) were used in experiments, as only ^{-/-} show the phenotype. Most hdac1^{-/-} fish die until 4 dpf. Before 30 hpf, mutants can be recognized by the thick optic stalk and tumbling region of the optic cup. At and after 30 hpf, the mutants are recognizable by a slight inward curl of the entire body and after 36 hpf by a lack of the pectoral fin bud and an inability to swim.

2.2.2 Hdac1 genotyping

The genotyping protocol is based on introducing a restriction enzyme cut site into the mutant sequence via specifically designed PCR primers.

Genotype of hdac1 t24411 +/- mutants was identified using DNA extracted from adult fins. hdac1 t24411 ^{-/-} embryos do not survive until adulthood, but die at 4 dpf, so the stock was kept as hdac1^{+/-}. A modified RFLP (Restriction Fragment Length Polymorphism) assay from ZIRC was used (<https://zebrafish.org/documents/protocols/pdf/Genotyping/ZIRC>

[Genotyping_A_H_Combined.pdf](#)) to introduce a cut-site for the enzyme Bfal (New England Biolabs R0568S) in the mutant sequence. Please see Appendix for a detailed protocol and electrophoresis gel example.

2.2.3 Blastomere transplantation

Donor embryos (Tg(β actin::UTR-GFP)) at stages high to sphere were dechorionated in pronase and cells from the animal pole were transplanted into the acceptor *hdac1+/-,-/-* embryos, using an agarose mold and a pulled glass injection needle. Transplanted embryos were kept on agarose for ~3-5 h and then transferred onto glass dishes. The E3 medium was supplemented with antibiotics (100 U of penicillin and streptomycin, Thermo Fisher Scientific). Homozygous mutants were identified, fixed and stained after 30 hpf.

2.2.4 mRNA and plasmid injections

To label all cells, mRNA was injected into the yolk or cell of 1-cell stage embryos (100 pg/embryo). Injection volume was 1-2 nl. mRNA was synthesized using the Ambion mMessage mMachine kit. To mosaically label cells for shorter imaging experiments (e.g., laser ablations), mRNA was injected into single cells of 32-128-cell stage embryos (50 pg/cell in 0.5 nl injection volume). To mosaically label cells for long time-lapse imaging experiments (e.g., cell cycle tracking), plasmid DNA was injected into the cell of 1-cell stage embryos (5-15 pg/embryo in 1-2 nl). Injection mixes were prepared in water, with 1:5 phenol red added to visually detect injections.

Cloning of FUCCI constructs

In addition to the PCNA cell cycle marker, the FUCCI system was used to label cells in S-G2-M (Geminin) and G1 (Cdt). The zebrafish Geminin and Cdt under the insulin promoter (*ins::mAG-zGem(1/100)* and *ins::mCherry-zCdt1(1/190)*) were obtained from the Ninov lab and subcloned into the Gateway system as the middle-entry clones (pME). Primers used for Geminin: attB1 5'-GGGGACAAGTTTGTACAAAAAAGCAGGCTGGATGGTGAGCGTATCAAGCCCG-3' and attB2 5'-GGGGACCACTTTGTACAAGAAAGCTGGGTCTTACTCATAGGCCTCTTGTGTGACCC-3'. Cdt primers: attB1 5'-GGGGACAAGTTTGTACAAAAAAGCAGGCTGGATGGTGAGCAAGGGCGAG-3' and attB2 5'-GGGGACCACTTTGTACAAGAAGCTGGGTCTTACTCTTTGCGGGCAGTTTG-3'. Each middle entry clone was then introduced into the Tol2 vector under the β actin promoter using Gateway cloning and injected into 1-cell stage as described above.

2.2.5 Morpholino injections

All morpholinos were produced by Gene Tools, LLC. Ath5 MO was used to inhibit RGC differentiation, Hdac1 MO to knock down Hdac1 mosaically, or in all cells. P53 MO was added to each morpholino injection mix to alleviate negative effects associated with injection

and knockdown. All morpholino mixes were injected into the yolk or cytoplasm from 1- to 2-cell stage.

Table 3: Morpholinos used in this study.

Morpholino (MO)	Injected amount	Sequence 5'-3'	Reference
Hdac1	0.5 ng	TTGTTCCCTTGAGAACTCAGCGCCAT	Yamaguchi 2005
Ath5	3 ng	TTCATGGCTCTTCAAAAAAGTCTCC	Pittman et al. 2008
P53	1-1.5x of main MO	GCGCCATTGCTTTGCAAGAATTG	Robu 2007

2.2.6 Intravitreal cavity injections

Tools to interfere with the ECM are still very limited, especially if one would like to target a specific component in zebrafish. Antibodies and especially function-blocking antibodies are generally mammalian and the epitope sequences are not identical to the fish ones. The mouse function blocking antibody against the cell-ECM attachment integrin-beta1 did not show a phenotype because of only ~70% epitope similarity to the fish integrin-beta1 on the protein sequence level. Morpholinos (e.g., laminin) work well in fish, but do not allow temporal control, essential in this case where I want to perturb ECM not only locally, but exactly before physiological bias disappearance.

To circumvent these issues, I injected collagenase (Liberase, Sigma Aldrich), an ECM degrading metalloprotease, into the intravitreal cavity (between the lens and the retina). I injected 36 or 42 hpf *hdac1*^{-/-} fish and 30 hpf WT fish using a pulled glass injection needle and injected 0.5 mg/ml Liberase in a volume to fill the cavity (2-3 nl). Injected fish were heatshocked in a waterbath at 37°C to activate the enzyme for 30'. They were then left to recover for 6-8 h, or fixed and stained immediately to examine the effect Liberase has on the basal actin accumulation.

2.2.7 Heatshock of embryos

Embryos injected with plasmids containing Hsp70::PCNA-GFP or Hsp70::H2B-RFP, or transgenic embryos (Tg(Hsp70::H2B-RFP)) were heat-shocked in a water bath after 24 hpf to induce the expression of the fluorescent construct. In order to obtain highly mosaic labelling in embryos injected with Hsp70::PCNA-GFP or Hsp70::H2B-RFP were heat-shocked mildly for 10' at 37°C. Tg(Hsp70::H2B-RFP) embryos were heat-shocked for 20' at 38°C.

2.2.8 Drug treatments

The minimal effective concentrations of inhibitors were determined based on previous reports and optimizations based on a series of dilutions. All inhibitors were dissolved in DMSO, except hydroxyurea, which was dissolved in water. Dechorionated embryos were

treated by incubating in the inhibitor-E3 medium at specific concentrations, either in plastic multi-well plates or directly in the chamber of the light sheet microscope (Rockout, TSA). All treatments were started after 24 hpf (Rockout always before 42 hpf) and lasted from 3 h to 2 days (TSA), with most treatments overnight (~15 h).

Table 4: Chemical inhibitors/drugs used in this study.

	Chemical	Function	Working dilution	Source/ Cat.No.
1	Trichostatin A (TSA)	Hdac1 inhibition	0.8 mM	Sigma-Aldrich; T1952
2	Rockout	Rho kinase inhibitor	150-175 μ M	Santa Cruz; sc-203237
3	Hydroxyurea (HU)	S-phase inhibitor	30 mM	Sigma-Aldrich; H8627-1G
4	Aphidicolin (A)	S-phase inhibitor	150 μ M	Sigma-Aldrich; 89458

2.2.9 Laser ablations

Laser ablation experiments were performed by an ultraviolet laser on a spinning disc system, as described previously (Etournay et al., 2015; Grill et al., 2001). An oil objective 63x/1.4 NA oil objective was used to focus the laser beam onto the lateral cell membrane, after a small (~1 μ m) linear cut region was defined. 3 repeats of the laser pulse were performed on each of the 5 points defining the region of interest. ~6 z-planes spanning 5 μ m of the tissue surrounding the cut were scanned for 1-5 minutes to record the membrane recoil after the cut.

2.2.10 Immunostaining

Wholemout immunostaining were performed on pronase-dechorionated embryos, fixed in 4% paraformaldehyde (Sigma) in PBS, at +4°C overnight. Washes were performed in PBS-T (PBS with 0.2% or 0.8% Triton X-100). Embryos were washed 3x30' and permeabilized in 1% Trypsin on ice from 15' (embryos until 36 hpf) to 25' (embryos older than 36 hpf). After washing 3x30', permeabilized embryos were blocked in 10% normal goat serum (NGS), or blocking buffer (Inoue and Wittbrodt, 2011), either for 2-3 h, shaking on room temperature, or overnight, shaking at +4°C. The blocking solution was removed and embryos incubated in primary antibodies for 64 h, shaking at +4°C. Antibodies were washed 4-5x for 1h and then incubated with primary antibodies and fluorophore-conjugated compounds overnight shaking at +4°C and then again washed 4-5x for 1h.

Table 5: Primary antibodies used in this study.

Antibody	Labelling	Working dilution	Source; Cat. No.
PH3; Anti-Histone H3 (phospho S28)	Mitotic nuclei (chromatin)	1:500	Abcam; ab10543, RRID:AB_2295065

Zn-5; neurolin	Mature RGCs	1:250	ZIRC, RRID:AB_10013770
Lam α 1; Anti-Laminin α 1	Laminin, ECM	1:100	Sigma-Aldrich; L9393, RRID:AB_477163

Secondary antibodies

Secondary antibodies were used at dilutions of 1:500 or 1:1000. Antibodies matched the species of the primary antibody. Anti-goat antibodies were avoided to diminish cross-reactivity with epitopes from the NGS blocking solution. Conjugated fluorophores included Alexa Fluor 405, Alexa Fluor 488, Alexa Fluor 568 and Alexa Fluor 647 (Thermo Fisher Scientific Inc.).

Fluorophore-conjugated compounds

To label all cell nuclei, DAPI (1:5000, or 1:2500), DRAQ5 (1:2500, Thermo Fisher Scientific Inc.; 62251) were used. Phalloidin-TRITC (1:50, Life Technologies; R415), Phalloidin-Alexa Fluor 488 (1:50, Life Technologies; A12379) were used to label F-actin in all cells.

2.2.11 Cell dissociation and flow cytometry

To obtain relative numbers of specific differentiating cells, in proportion to all retinal PSE cells, Tg(SoFa) retinas were dissected, dissociated and analyzed by FACS.

Retinal dissection and dissociation

Dissection was performed on Sylgard-coated 10 cm plastic dishes, at room temperature and in PBS. Eyes were dissected from live 36, 42 and 48 hpf Tg(SoFa) and 48 hpf wildtype anaesthetized embryos using forceps, syringe needles and/or a 5mm surgical stab knife. The pigment epithelium and the lens were removed. In total, 20 retinas/stage transferred to a glass FACS-tube using a flame-polished glass pipette. Cells were dissociated mechanically, without any enzymes, using flame-polished glass pipettes with wide and fine openings. Cells were immediately analyzed by FACS. Altogether, the time from dissection to FACS-analysis never exceeded 2 hours.

FACS-sorting

Single cell suspensions were analyzed using the FACS Aria device. Wildtype cells were used to normalize the signal to background auto-fluorescence. Populations were defined based on forward- and side-scatter signals in PE-A, FITC and DAPI channels. Data was plotted and processed using the FACSDiva software.

The resulting scatterplots were analyzed as described previously for the SoFa line (Almeida et al., 2014), in order to obtain relative values for 4 different neuronal subtypes (RGC, photoreceptors, amacrine/horizontal cells and bipolar cells, Figure 6). Total numbers of cells in the retina in different developmental stages, obtained in my initial growth analysis,

were used to calculate average absolute numbers of differentiated cells from the relative values and the total number of differentiated cells, as the sum of all subtypes.

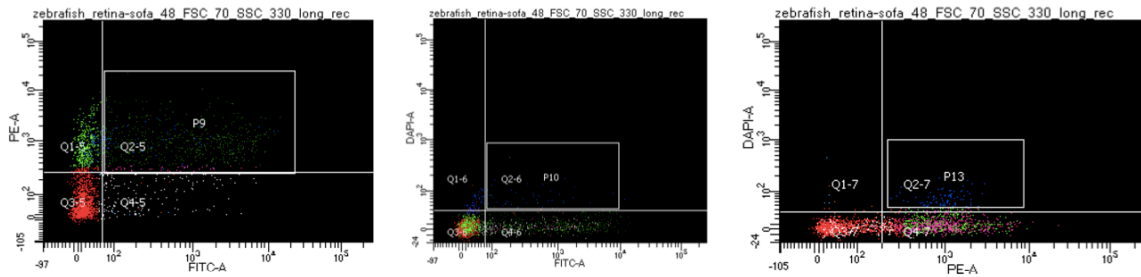


Figure 6: FACS scatterplots of cells from Tg(SoFa) retinas.

The specific combinations of signals in different channels defines the neuronal subtype (Almeida et al., 2014).

1.3 Image acquisition

Confocal laser scanning

Dechorionated, fixed and immunostained embryos were mounted in 1% low-melting-point agarose in glass-bottom dishes (35 mm, 14 mm microwell, MatTek). The agarose doem was covered with PBS or E3 to prevent drying out. Imaging was performed on Zeiss LSM 510 or 710 confocal microscopes (Carl Zeiss Microscopy) using a 40x/1.2 NA water immersion objective, at room temperature. The imaging system was operated using ZEN 2011 (black) software.

Light sheet microscopy

Dechorionated live or fixed embryos were mounted in glass capillaries in 0.6% or 1% low-melting-point agarose. Imaging was performed on a Zeiss Light sheet Z.1 microscope (Carl Zeiss Microscopy) with a Zeiss Plan-Apochromat 20x or 40x water-dipping objective (NA 1.0). Live embryos in 0.6% agarose were immersed in E3 with PTU to prevent pigmentation. and sample chamber was heated to 28.5°C. For drug treatment experiments, a separate chamber was used and filled with the drug-supplemented E3+PTU medium. Fixed embryo imaging was performed on the light sheet system as well, as it allowed for sample rotation and positioning, a feature that was important to get the most informative view of the folded retinas. For fixed sample imaging, embryos were mounted in 1% or 0.6% agarose, immersed in PBS and imaged at room temperature. z-stacks spanning the entire eye were recorded with 0.5-1 μm optical sectioning. For live imaging, z-stacks were recorded every 5-30'. The system was operated by the ZEN black software.

2.3 Image analysis

Custom MATLAB and Python scripts used for image analysis can be found at the DVD attached to the back cover and at the URL behind the QR code on the last page, together with representative data movies and animations related to specific figures.

Minimal image processing was implemented in my workflow and used only on some images, prior to image analysis. Processing consisted of image cropping, bleach correction and/or background subtraction using Fiji (Schindelin et al., 2012). After image analysis in Imaris 8 (BitPlane) or Fiji, data was analyzed and plotted using MATLAB or Microsoft Excel. Statistical analysis was performed using the Prism software.

2.3.1 Growth analysis using Imaris 8

The majority of the image analysis was done on the entire tissue in 3D, using Imaris 8 (Figure 7). This included tissue and cell volume, total tissue area, tissue height, cell and mitotic cell position and count analyses. Raw data in .tiff, .lsm and .czi formats was read into the software and segmented by manually outlining the retinal and lens tissues. 30-50 z-sections were outlined in each sample to span the retinal tissue and 10 samples/stage, in 6 stages were analyzed as part of the WT growth characterization. To analyze live images of *hdac1*^{-/-} fish, timepoints of interest were first isolated and then analyzed as fixed samples. The segmented rendered surface was used to mask the raw data and create a subset on which further measurement were performed.

2.3.2 Mitotic density distribution (Script 1)

To reproducibly assess the distribution and the density of mitoses at the apical surface in different stages, mitotic cell positions were detected and projected onto a 2D density heatmap, using a custom MATLAB tool, “PSE MitoNuc” (Benoit Lombardot, IPF, MPI-CBG). PH3+ mitotic cells in the masked retinal image were detected in Imaris using the Spot detection tool. The automatic detection was usually very accurate and only the Signal quality threshold had to be adjusted, to detect all PH3+ cells. Cartesian (x, y, z) coordinates of all these detected spots were exported from Imaris (10 samples/stage, 6 stages). In order to use the “PSE MitoNuc” tool, the user should define five points on each retinal sample to build tissue object-defining vectors: 1) center of the retinal cup (~widest point of the cup, close to the center of the lens), remaining 4 points were defined on this plane; 2) outermost point of the optic fissure; 3) point opposite to 2); 4) nasal-most point; 5) temporal-most point. It is essential here to correctly recognize nasal and temporal points. For this, it is useful to note for each sample whether it is the left, or the right eye. X, y, z coordinates of these points and respective sample names should all be collected in a single Excel file, formatted in columns as: 1x, 1y, 1z, 2x, 2y, 2z, 3x, ..., to be read-in by the MATLAB script. To run the

“PSE MitoNuc” tool, the main script “PSE_MitoNuc_mitosisDensityEstimation.m” should be started. The value of the variable `sphDataName` should be changed to the path to the file that contains the object-defining points. When prompted, the user should also choose the file containing the mitotic cell coordinates. The script “PSE_MitoNuc_convertXYZ_to_RThPh.m” will then estimate the symmetry axis of the tissue, as well as 2 perpendicular vectors, to define a new coordinate system. X, y, z nuclear coordinates will be transformed into new Cartesian and spherical (r, φ, θ) coordinates, by projecting them onto a unit sphere defined in the new system. Euclidean distance will be calculated for each such mitotic cell to a point in the defined spherical mesh and all these distances then used to calculate mitotic cell densities on each point of the mesh. The result will be plotted as a heatmap both on a sphere and on a 2D projection (Figure 8). To generate this, a MATLAB “m_map” package and its “Azimuthal Equal-area” projection is used (see: <http://www2.ocgy.ubc.ca/~rich/private/mapug.html>).

2.3.3 Division orientation

Division orientations were analyzed manually in Fiji from live images of all cells labelled with RAS-GFP (membrane). A part of the curved apical surface was imaged using the light sheet microscope. In Fiji, measurements were set to display angles and frames. Data was bleach-corrected and background was subtracted. For each observed anaphase cell, a line was drawn perpendicular to the division plane and the angle was measured. Data was processed (to be between 0° and 180°) and plotted as a rose plot in MATLAB.

2.3.4 Specific growth and shape parameters

Apical area

Apical tissue area of the retinal PSE was measured in 3D using a custom Fiji tool (Volume Manager, by Robert Haase, IPF, MPI-CBG). Areas were manually outlined, similar to the Imaris manual segmentation, except all basal tissue portions were excluded to obtain a hollow and open structure. This allowed me to extract the values for the basal tissue surface, as well, by subtracting this apical tissue area from the total tissue area measurements obtained from Imaris. Analysis and visualization were performed using Volume Manager, as well. Volume Manager is available in the Fiji SCF-MPI-CBG update site.

Cell size estimation and validation

Cell size was estimated using rounded mitotic cells. Diameters of 15-20 mitotic cells/retina were measured using the Imaris measuring tool. Under the assumption that

mitotic cells are nearly spherical, cell volumes were then calculated as sphere volumes. To check how well volumes of mitotic cells represent interphase cells, several interphase cell volumes were manually segmented from images with extremely sparse mosaic labelling of cells with RAS-GFP mRNA (cell membrane marker). This analysis indicated that mitotic cell volumes are on average 10% larger than interphase cell volumes.

PSE cells are wedge (frustum)-shaped, instead of cylindrical or spherical. To validate the cell volume analysis above, I therefore calculated cell volumes as frustum volumes, as well. I averaged apical and basal cell surface areas, obtained by dividing apical or basal tissue areas, respectively, by the total number of cells. Results on cell size from both methods were in very good agreement and I used the volumes estimated from mitotic cells for subsequent analysis.

Cell number and validation

Total cell numbers were analyzed using the Imaris spot detection tool to detect individual nuclei on the masked retinal stacks, from the DRAQ5/DAPI channel. The automatic detection was validated manually, by examining individual z-planes using the Oblique slicer tool and a combination of two Clipping plane tools to isolate and examine a specific tissue region. Automatic settings (thresholds) were manually adjusted for each sample until a satisfactory detection was obtained. Such automatic detection still produced some errors, like double counts and missed nuclei, especially in the deeper tissue layers where signal was more scattered. To validate the count, I used the cell volumes estimated from mitotic cell volumes, as described above. I divided the total tissue volume by these cell volumes, in order to obtain the average volume occupied by a single cell (i.e., cell volume). Cell volumes obtained in this way were in almost identical to the values obtained by the automatic count (Figure 9D).

Tissue thickness

Fiji was used to manually measure tissue thickness in live images of WT, *hdac1*^{-/-}, *Ath5* MO and Rockout-treated fish. The apico-basal tissue axis at the nasal region of the retina was measured at every timepoint using the line tool.

Number of nuclear layers

The number of nuclear layers along the apico-basal tissue axis was estimated in every stage by measuring the long axis of the elliptical nuclei and dividing the tissue height by this value, to get the number of layers that can fit in a tissue of that particular height. As the actin accumulation established the nuclear exclusion zone in the early stages of the WT- and the *hdac1*^{-/-} retinal PSE, the height of this zone was subtracted from the total tissue height when estimating the number of nuclear layers. In addition to this, the number of layers was counted manually and was in good agreement to the estimated values.

2.3.5 Actin and nuclear signal intensity distribution (Script 2)

The average intensity distribution of phalloidin and DRAQ5 signal along the apico-basal axis of the PSE cells was measured as described in (Sidhaye and Norden, 2017), using a custom Python script (Benoit Lombardot and Robert Haase). The region of interest was defined as a $10\ \mu\text{m} \times 10\ \mu\text{m} \times$ thickness cuboid. An average intensity value for this region was calculated for each point along the apico-basal axis. The axis length was normalized to 100. To compare different samples, the average intensities were normalized to the minimal and the maximal intensity value along the axis. This analysis was performed on 3-9 samples/stage for both WT and *hdac1*^{-/-} retinas.

2.3.6 Cell cycle analyses

Mosaically labelled cells in long (>15 h) time lapse light sheet datasets, with time resolution of 5 min were manually tracked, in 3D, in ZEN and Fiji. Cells were labeled with Hsp70::H2B-RFP, Hsp70::PCNA-GFP or β actin::PCNA-GFP. Only the points of interest were recorded: for total cell cycle analysis, time of chromosome segregation for the first, second and, in wherever possible, third division. For the analysis of specific cell cycle stages, endpoints of mitosis were recorded as limiting the phase when PCNA signal is diffused in the cytoplasm, start of G1 as the point when PCNA signal is nuclear again, start of S-phase when PCNA replication foci could be observed and start of G2-phase as the point when the foci disappear. This cell cycle data for 254 cells from 20 embryos was analyzed, binned into discreet stages and plotted in MATLAB.

2.3.7 Rate of cell division

Progenitor k_d correction

Rates of progenitor cell division (k_d) in different stages were calculated by three equivalent methods (with Guillaume Salbreux): 1) From the change in the number of cells (N) between the 6 analyzed stages: $1/N \times (\Delta N / \Delta t)$; 2) From the live measurements of total cell cycle length: $\ln(2) \times 1/T_{cc}$; 3) From a combination of live data on duration of mitosis (T_M) and fixed data on the mitotic index (MI): $MI \times 1/T_M$. The results from the last two methods k_d were initially not in good agreement with each other, indicating that there is a discrepancy between live and fixed measurements of proliferation parameters, possibly because of the different readouts of mitosis, e.g., the markers used for the quantifications. Reanalyzing the fixed images, I observed that anaphase cells were indeed not at all labelled by the PH3 antibody. This was possibly due to bad antibody penetration through the newly establishing nuclear envelope. To correct for this, I counted anaphase cells in all 6 stages. Based on this count and the difference to the initial values, I multiplied these values by an average

correction coefficient of 1.31 across all stage to the number of mitosis in mitotic index. This correction now yielded a good match between the two k_d curves.

2.3.8 Rate of differentiation

The number of differentiating cells (N) was calculated for each stage using the FACS analysis of Tg(SoFa) dissociated retinas, as described above. The rate of differentiation was the calculated as $1/N \times (\Delta N / \Delta t)$.

2.3.9 N/C ratio

To estimate the nuclear and cytoplasmic volume, I measured the long (major, a) and short (minor, b) nuclear axes, from images of nuclear stainings in different stages. Assuming the nucleus to be an ellipsoid and have two identical minor axes, I estimated nuclear volumes in the 6 developmental stages as: $V = \frac{4}{3} \times \pi \times a \times b^2$. I used these nuclear volumes to estimate cytoplasmic volumes as well, by subtracting them from the total cell volumes. The ratio of nuclear-to-cytoplasmic volume, nuclear-to-cell volume and cytoplasm-to-cell volume were calculated from this data.

3 RESULTS

3.1 Growth of the retinal neuroepithelium

The PSE is a growing, proliferative tissue. During growth, apically constrained PSE increase their thickness (apico-basal height). As the elongated, epithelial cells are attached at both the apical and the basal side, the question arises of how far they can elongate and can they limit proliferative growth. Growth constraints related to tissue thickness and nuclear packing of the PSE were proposed still in the 1970s, as mentioned in the Introduction. However, the existence of such a tissue-intrinsic constraint was never systematically tested. In order to understand the system and in order to test for the existence and propagation of a growth constraint over development, I first asked which cellular parameters contribute to tissue growth and how. In a 3D tissue-wide analysis, I decomposed growth and assessed how cell number, size and density change over ~28 hours of retinal PSE development. I then proceeded to check the tissue's proliferative parameters, such as the mitotic density, division orientation, mitotic index and cell cycle lengths, as well as tissue and cell shapes. These datasets allowed me to test the predictions on the maximal PSE packing and constraints to proliferative growth originating at the apical surface. In this section, I first explain how the retinal PSE grows, in section 3.1 and test possible constraints to its proliferative growth. I then investigate, in section 3.2, how the shape of the tissue is scaled during growth by changes of cell shape. After identifying a basal accumulation of actin as a possible brake on cell height, I examine its properties in section 3.5. I show that this brake is dependent on the ECM and its release is necessary, but not sufficient for changes in cell shape, which also depend on proliferation.

3.1.1 Growth analysis workflow

In the majority of my growth analyses, I focused on an entire developmental day (28 h), with a 4-6-hour time resolution. The developmental stages I analyzed span the time from 20 hpf until 48 hpf, from right after the optic cup shape is established, until the first neuronal layer is formed, respectively. I used a transgenic zebrafish line with ubiquitous membrane labelling (Tg(actb1::HRAS-GFP)) and a line labeling the first retinal neurons, the RGCs (Tg(Ath5::GFP) to have a readout for the differentiation wave. These samples were fixed at 6 time-points, 20, 24, 30, 36, 42 and 48 hpf, stained with a nuclear dye (DAPI or DRAQ5) and immunostained with a mitotic cell antibody, phosphohistone 3 (PH3). Imaging of these samples was done both on a laser point-scanning confocal and a Zeiss light sheet microscope (Figure 7A).

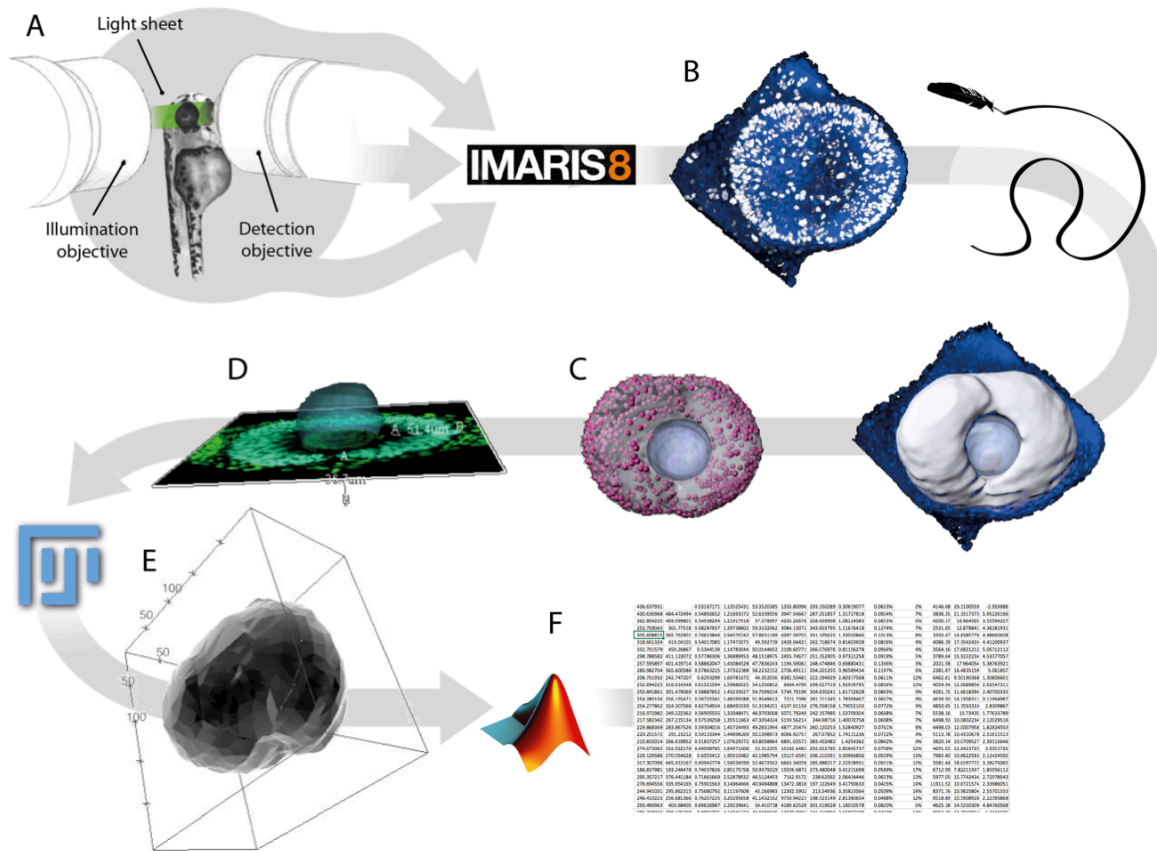


Figure 7: Retinal PSE growth and shape 3D analysis workflow.

A) Fixed or live samples were imaged at stages between 20 and 48 hpf using predominantly the light sheet microscope. For fixed samples, 10 samples per stage were analyzed for 6 stages (20, 24, 30, 36, 42, 48 hpf). Zebrafish image is from Mickoleit et al. 2014.

B) The major part of all image analysis was done in Imaris 8.3 (B-D). The analysis started by manually outlining and then rendering tissue surfaces.

C) This provided a mask to isolate the retinal tissue signal from the rest and detect and count all cells, as well as only the mitotic ones.

D) Tissue thickness was measured in multiple tissue regions, the example here showing the measurement in the proximal region, under the lens.

E) A custom plugin for Fiji was used to manually outline only the apical surface of the tissue.

F) MATLAB 2015 and 2017, as well as Microsoft Excel, was used for data analysis and plotting.

The latter allowed for sample repositioning, that proved important to obtain the signal from deep layers in older, large and more scattering tissues. Unless otherwise stated, all growth quantifications were done on the entire cup-shaped tissue in 3D, using mainly manual image analysis in Imaris (Figure 7, Movie 1) and Fiji (Figure 7).

Images of the entire retinal PSE and the lens were first manually segmented in Imaris, which resulted in the quantification of tissue-wide volumes and allowed me to create an

image mask (Figure 7B). The mask was used to isolate the retinal neuroepithelium from the surrounding tissues in the image (lens, RPE, perocular mesenchyme, brain, epidermis), in order to analyze its cell numbers. Cells were detected from the nuclear channel in the masked image automatically using the Imaris Spots tool (Figure 7C), to obtain both nuclear position and total cell number. Similarly, mitotic cell number and position was detected automatically from the PH3 channel. The total cell count in the crowded tissue was error-prone with the automatic settings, so parameters were manually adjusted for each sample and the result checked by examining individual slices. In addition to the information of how cell number increase contributes to growth, this analysis allowed me to measure cell height (Figure 7D) and assess the average single cell volumes, by simply dividing the total tissue volume with the total number of cells. The option to analyze the apical tissue surface area separately was essential in order to assess the proposed apically-originating growth PSE constraints, as well as tissue shape. Because this kind of surface analysis was not possible in Imaris, a custom-made Fiji plugin was used (by Robert Haase, MPI-CBG Image Processing Facility). Using this 3D surface segmentation tool, all open (i.e., apical and basal) surfaces were analyzed by manually outlining them in Fiji (Figure 7E).

Having this image analysis workflow established, I was able to reproducibly quantify changes in tissue size and shape, as well as the contributing cellular parameters throughout development in a 3D, tissue-wide approach.

3.1.2 Growth decomposition

3.1.2.1 *Retinal PSE growth is homogeneous and isotropic*

Using the analysis described above, I first measured by manual segmentation how the total tissue volume changes from 20 to 48 hpf. The retinal PSE grows constantly, increasing its volume ~4.5 times in the 28 hours analyzed (Figure 9A). It increases its size with an average growth rate of ~104 000 $\mu\text{m}^3/\text{hour}$. As growth can be uniform, or localized throughout the tissue, this should be taken into account to see if the analysis should focus on specific growth regions separately. In the study by He and colleagues mentioned above, it has been suggested that proliferation in the developing zebrafish retina occurs in a wave-like fashion, sweeping through the tissue and preceding the differentiation wave in a naso-temporal manner (He et al. 2012). Such a spatially inhomogeneous mitotic distribution might lead to inhomogeneous tissue growth, as discussed in the Introduction. If the retinal PSE indeed exhibits spatially patterned cell divisions, this is a parameter that might affect not only tissue size, but its shape.

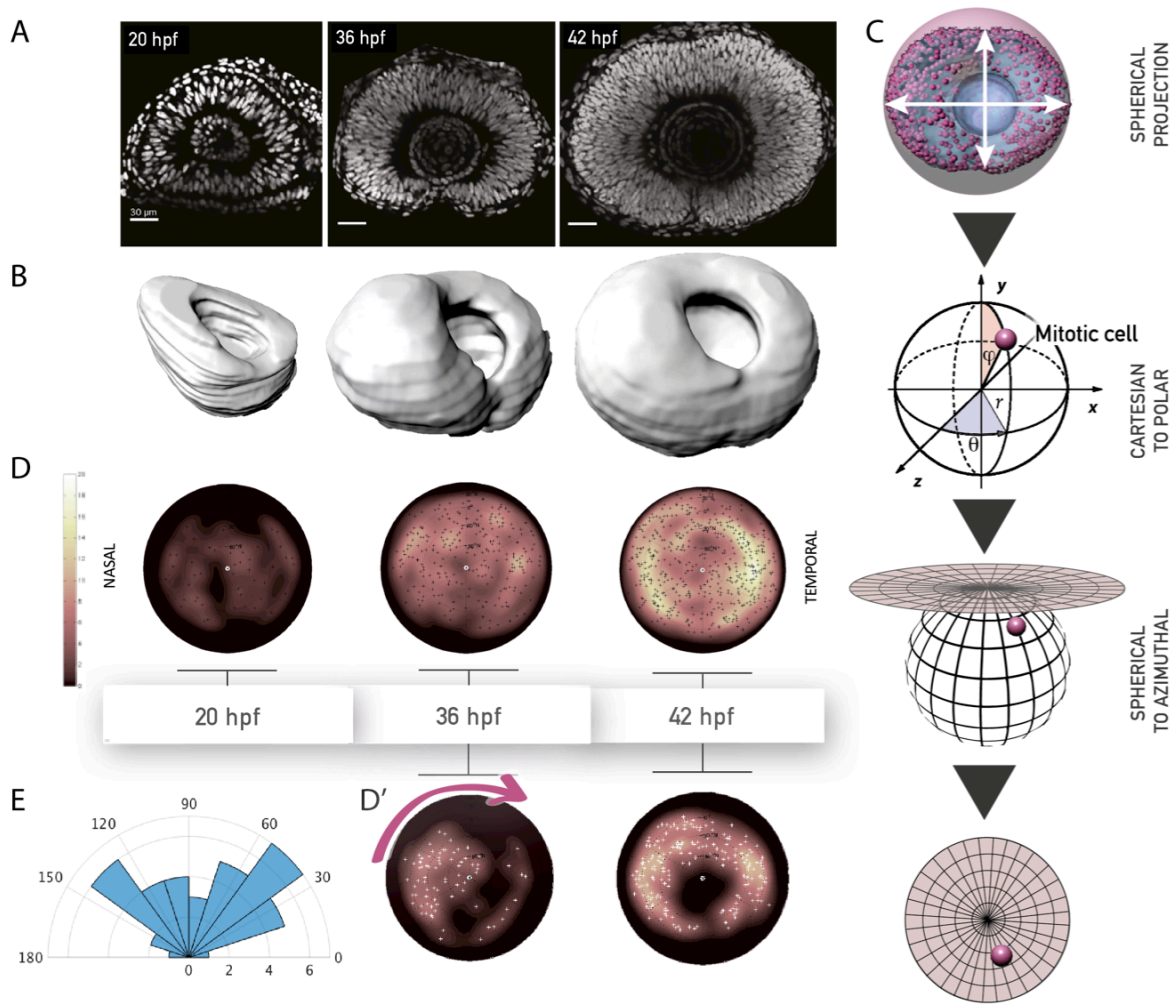


Figure 8: Retinal PSE growth is isotropic and homogeneous.

A) Images of stages from 20 to 48 hpf show tissue growth and increased cell number.

B) Exemplary Imapis-rendered tissue volumes at 20, 36 and 42 hpf, which were used as masks in further analysis of proliferation patterning ($n = 10$ samples/stage).

C) Illustration of the mitotic distribution workflow to generate 2D mitotic density heat-maps. A custom MATLAB script (see Methods) was used to transform the 3D Cartesian coordinates of every mitotic cell into polar, spherical coordinates, which were then projected into 2D using an already existing, azimuthal density-preserving projection.

D) 2D heat-maps of mitotic densities of all cells at 20, 36 and 42 hpf, results of transformations in C).

D') Same as D), but only with neurogenic divisions, revealing a naso-temporal wave (pink arrow), as expected and validating the mitotic distribution method, as a method able to detect proliferation patterns at the apical surface ($n = 10$ samples/stage).

E) An exemplary rose plot of division angles, analyzed from a movie ~ 40 hpf. Angles seem unbiased and division orientations thus random.

Therefore, in the start of my analysis of retinal PSE growth, I first analyzed the spatial distribution of mitotic events throughout the 20-48 hpf developmental time-course (Figure 8). This was done by transforming the positions of all mitotic cells on the tissue's apical surface, into 2D density projections using a custom MATLAB script (with Benoit Lombardot,

MPI-CBG Image Processing Facility, Figure 8). More specifically, 3D coordinates of apical, mitotic cells were obtained from 10 samples in 6 developmental stages through the growth analysis workflow. 5 points describing each retinal tissue were defined and used in the script to transform the mitotic coordinates, by projecting them from an uneven tissue surface onto a sphere. Cartesian mitotic coordinates (x, y, z) were transformed into polar coordinates (r, φ, θ) and then plot onto a 2D density map (Figure 8C), using a density-preserving map projection (azimuthal) in MATLAB (see Materials and Methods and Script 1 for more details). 2D maps allowed us to more easily assess the mitotic distribution, which, despite an increasing density through the stages, did not reveal any spatial bias (Figure 8D). This indicated that retinal PSE proliferation is uniform and the growth homogenous. Still, I wanted to validate our mitotic distribution method to make sure that I could detect a proliferative wave pattern if there was one. To do this, I analyzed the densities of the terminal, neurogenic divisions in the same way. Neurogenic divisions are known to occur in a wave and in this case, our method indeed revealed a wave originating at the ventro-nasal region and spreading throughout the tissue in the naso-temporal direction (Figure 8D'). This clear visualization of a neurogenic proliferative wave using our method suggested that the observed mitotic density distributions are genuine. Thus, I concluded that proliferation in the developing retinal PSE is indeed spatially uniform and proliferative growth homogeneous.

The above analysis resulted in snapshots of mitotic distribution. However, as also discussed in the Introduction, growth can be biased in one direction or another not just by spatially patterned mitotic distribution, but also by changing the orientations of cell divisions. A biased distribution of division orientations can result in a changed tissue shape by making growth anisotropic. To check how division orientation contributes to the growth of the retinal PSE, I imaged the nasal portion of the apical surface live using the light sheet microscope. Measurements of division angles in Fiji revealed that division angles have an unbiased distribution from 0° to 180° (Figure 8E). Thus, division orientations are random and they, together with uniform proliferation, contribute to a homogeneous and isotropic growth of the retinal PSE.

3.1.2.2 *Cellular contributions to retinal PSE growth*

Cell number

After describing how the retinal PSE grows from the tissue-wide perspective, I moved on to identify the cellular parameters that increase tissue size. Cells can change tissue size by contributing in number and in cell size. I, therefore, started by measuring these two parameters. Cells in the entire tissue were counted in Imaris from the masked nuclear

channel (Figure 9C) and the count was validated as described in the workflow section (Figure 9D) and Methods. As the tissue grows from 20 to 48 hpf, the total number of cells increases more than 8 times, from ~2000 to ~18000 (Figure 9B), with an average ~550 new cells being added each hour.

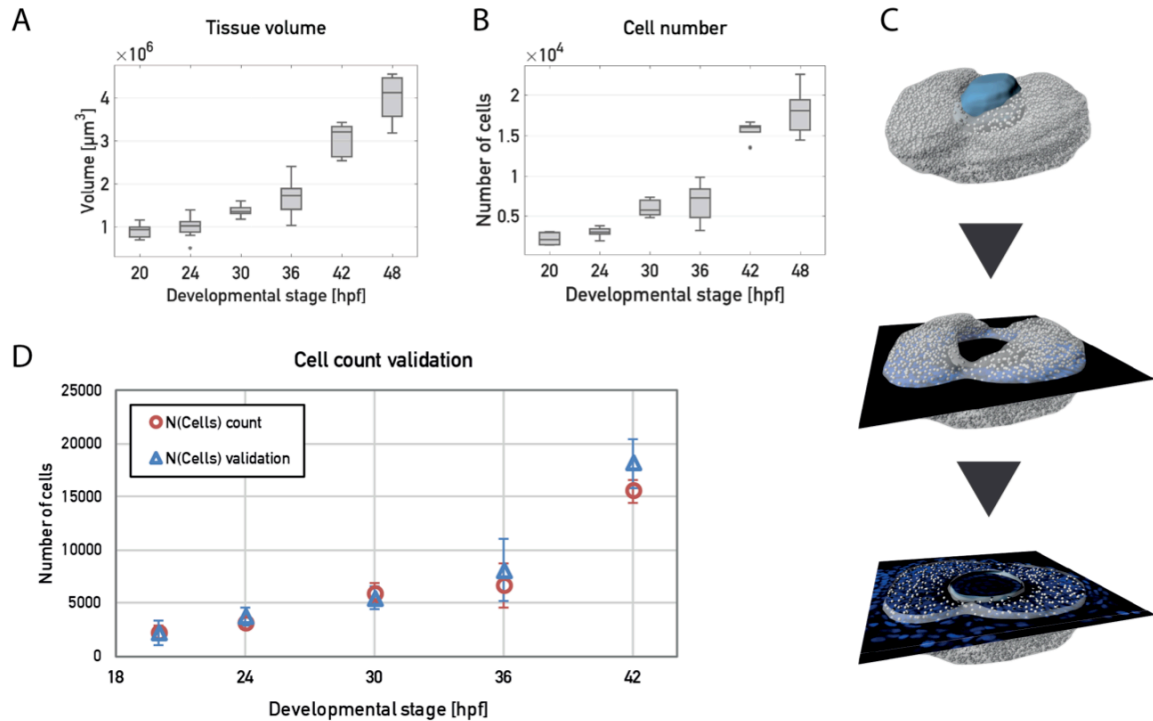


Figure 9: Cell number increase during retinal PSE growth.

A) The retinal PSE grows constantly during development, as analyzed by Imaris segmentation in different stages (20-48 hpf).

B) Total cell number increases from ~2000 to 18000, as analyzed by detecting all single cell nuclei in Imaris.

C) In Imaris, cells were first automatically detected (white points) in the generated tissue mask (transparent grey). The detection quality was then manually checked on single optical slices. ~5-10% of cells were sometimes undetected, depending on the image quality and developmental stage. No manual correction was done to the detection, except adjustment of automatic parameters. Segmented lens tissue is shown in blue for orientation.

D) The cell count (red) was validated using mitotic cell volumes (blue). Single volumes of ~spherical mitotic cells were estimated independently of the automatic cell count. The number of mitotic cells that fits in the total tissue volume was calculated and showed a very good fit to the automatic count. Data is plotted as stage mean \pm SD. n=10 samples/stage for all.

General remark on boxplots: on each box of the boxplots, the central line indicates the median, box edges the 25th and the 75th percentile and the whiskers the most extreme non-outlier data points.

As mentioned before, after 30 hpf, first neuronal differentiation starts in the retinal PSE. To know how many cells exited the cell cycle and are thus not contributing to proliferative growth, I analyzed the increase in the number of neurons over time (Figure 10). This was done by FACS analysis of the transgenic SoFa fish line that labels all the different neuronal subtypes in the retina (Almeida 2014, Figure 10A'). More specifically, retinas were dissected and dissociated from live SoFa fish sorted for all three transgenes, at 36, 42 and 48 hpf (Figure 10A). FACS analysis resulted in relative numbers of different positive and double positive cells (Figure 10B), that were then identified as one of 4 neuronal groups, as in the original SoFa publication. For more details on this analysis, please see the Materials and Methods section.

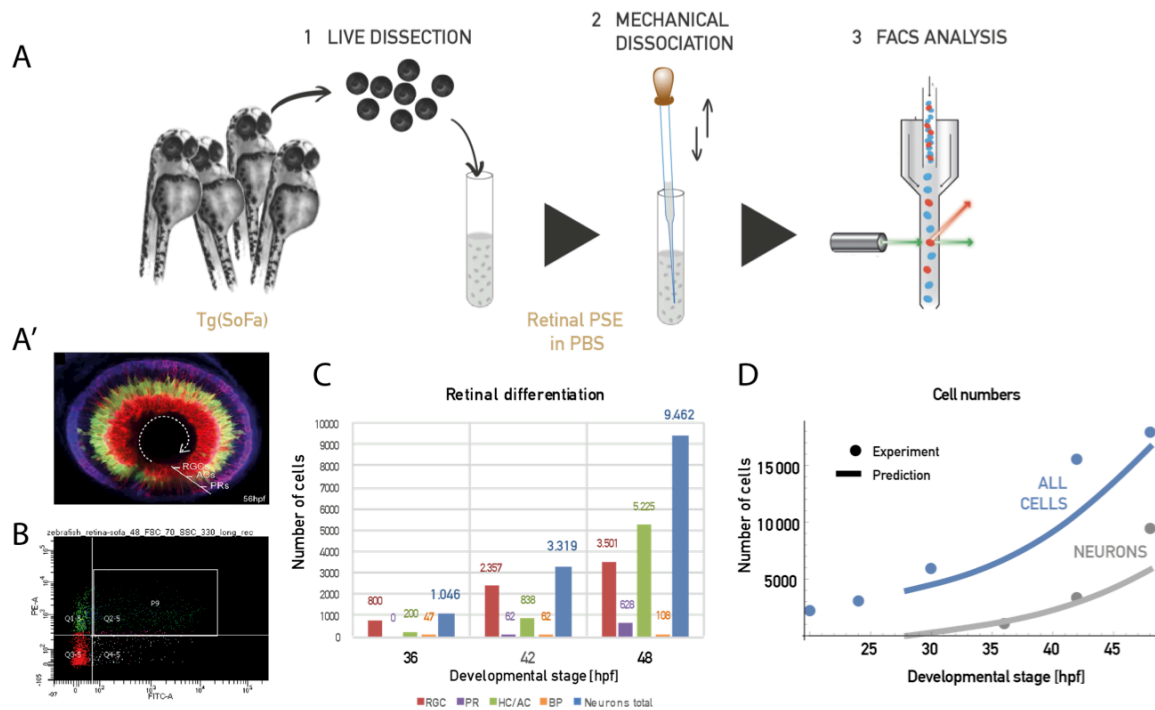


Figure 10: Retinal neuronal number increases exponentially, as assessed by live FACS analysis.

A) Retinas were dissected from anesthetized live A') Tg(SoFa) and wildtype control fish at 36, 42 and 48 hpf, 20 in each stage. The RPE and the lens were removed and retinas mechanically dissociated using different gradation glass pipettes. Samples were FACS sorted an hour after dissection. Zebrafish illustration is from Mickoleit et al. 2015.

B) Populations of the three single transgenes and their combinations were defined after normalizing for wildtype auto-fluorescence.

C) Neuronal subtypes were defined from the FACS populations as in the original SoFa publication (Almeida et al. 2014). See Methods for a more detailed explanation.

D) A change in total cell numbers (Figure 9B) and neuronal numbers through time allowed us to estimate the rate of cell division and rate of differentiation, respectively. Predictions of cell numbers using these rates fits quite well with the experimental values and the rates can be further used in a growth simulation of this tissue.

Absolute numbers of all neurons were then calculated from the FACS-based neuronal fractions and the previously obtained total cell number. This analysis revealed that the number of neurons increases exponentially over time (Figure 10C), from ~1000 at 36 hpf to ~9500 at 48 hpf.

Cell cycle

Even though the spatial distribution of mitoses in the retinal PSE seems uniform in all stages, the increasing mitotic density on our 2D projections suggested the mitotic temporal distribution not to be uniform. To assess the temporal distribution of mitotic events, I analyzed the mitotic index, the fraction of cells in mitoses, or the ratio of mitotic cells to all cells (Figure 11A). The mitotic index in this tissue is not constant, but peaks to 3.5% at 36 hpf and decreases again (Figure 11C). This tissue is composed of proliferative progenitors that all divide and contribute to the analyzed mitotic index. Thus, a peak in mitotic index suggests a change in the cell cycle, rather than in the number of cells that are cycling. Progenitor cells could have a longer mitosis, resulting in cells remaining at the apical surface for longer and consequently, more mitotic cells being detected per time point. However, I have analyzed the length of the mitotic phase (from nuclear envelope (NE) breakdown, to NE rebuilding) and have not observed an increase in mitotic length (~18 min at both 30 and 36 hpf, plot not shown). An increase in mitotic index could, therefore, mean that the cells are cycling faster. Moreover, as just presented in the previous paragraphs, retinal PSE cells become smaller and smaller as the tissue grows. This also might result, at least in part, from shorter cell cycles, as cells might not have as much time to increase their mass before division.

As the peak in the mitotic index pointed to a possible change in the duration of the cell cycle, I decided to analyze the PSE cell cycles directly, using live imaging and manual cell tracking. I used a transgenic fish line labeling the first-born neurons (Tg(Ath5::GFP)), with mosaically labelled nuclei (Hsp70::H2B-RFP injection), in order to be able to track single cells (Figure 11B, Movie 3), but also to make sure I am tracking only progenitors (GFP⁺ cells), as well as to have a readout of any possible developmental delay in neurogenesis. From 20 such overnight light-sheet movies, I was able to track 254 cells and defined their cell cycle duration as the time between two mitotic events (anaphase). This cell cycle analysis revealed that, interestingly, cell cycles span lengths to minimal 4 h, with the entire cycle length distribution skewed to these short durations (Figure 11E). Moreover, the overall cell cycle variability decreased over development (Figure 11D). Around 30 hpf, the cell cycles were highly variable, with cells taking from 18 to 4 hours to complete their cycle and divide. After 30 hpf, however, this variability decreased and the overall cell cycles shorten, with the majority being around 5 h long. This period of shortest cell cycles coincides with

the highest mitotic index. Therefore, increased mitotic index at 36 hpf and 42 hpf is likely the result of cell cycle shortening and more cells consequently dividing in a time unit.

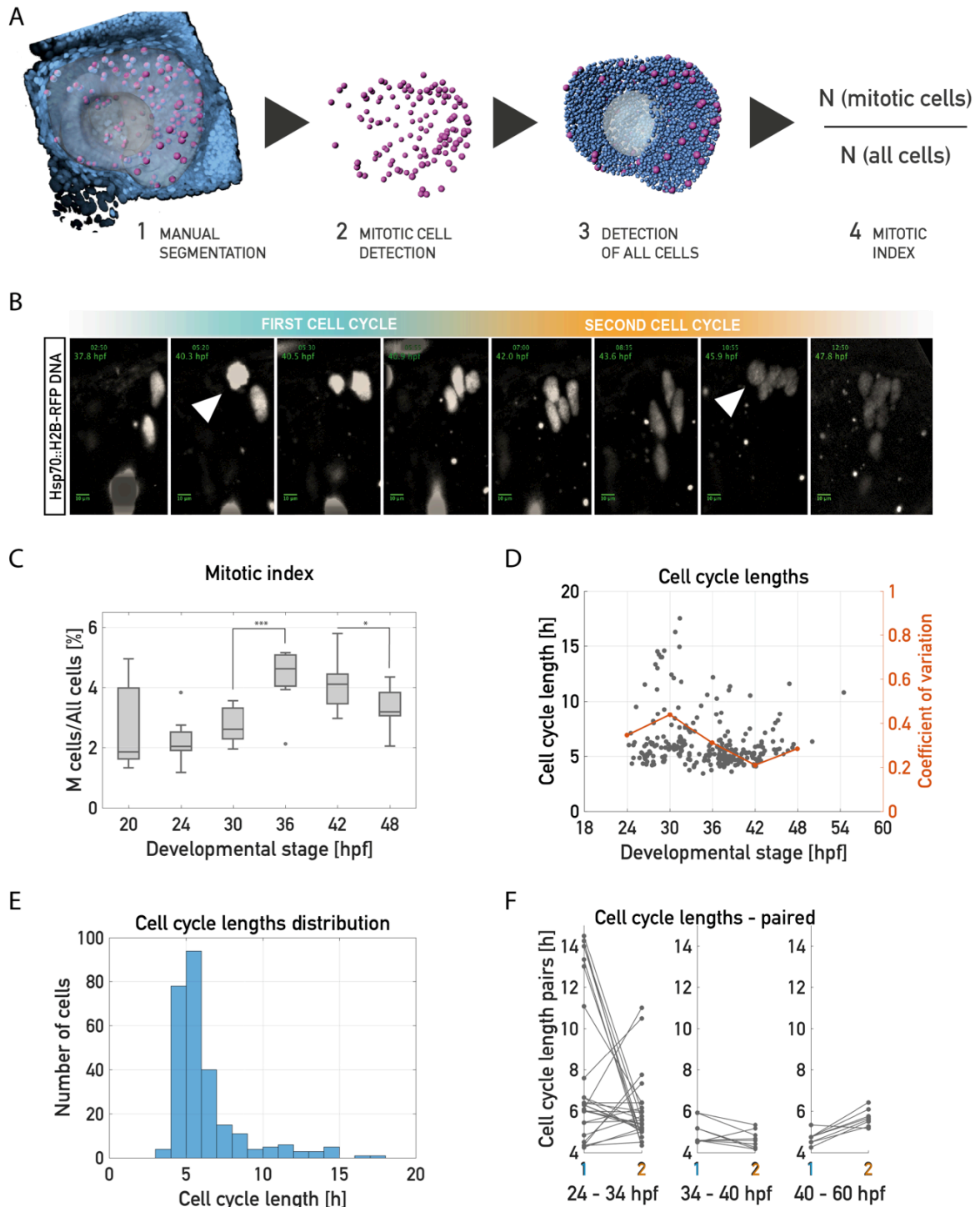


Figure 11: Proliferative peak might result from an overall shortening of cell cycles.

A) Mitotic index was calculated as the ratio of the tissue-wide number of mitotic cells to all cells, using numbers obtained from the Imaris 3D analysis.

- B) Cell cycle analysis was done on live light sheet timelapses, by manually tracking mosaically labelled cells. Cells were labelled by a mosaically distributed injected DNA construct, Hsp70::H2B-RFP, to label cell nuclei. Only progenitor cells were tracked and a neuronal marker was used to select out the differentiating cells, which might have a different (longer) cell cycle. A cell cycle was defined from cell rounding to the next cell rounding (white arrowheads). 2, to maximally 3 cell cycles could be tracked from overnight movies. The developmental stage of the cycle was taken as a middle point, the time in the middle of the 2 mitoses.
- C) Mitotic index remains between 2 and 5%, with a peak at 36 hpf. $n=10/\text{stage}$.
- D) Cell cycle lengths of progenitor cells are variable ~ 30 hpf and become less variable and overall shorter ten hours later, ~ 40 hpf. $N=254$ cell from 20 embryos.
- E) Histogram of all tracked cell cycle lengths. Cell cycle distribution is biased to the shorter cell cycles.
- F) For most cells, I was able to track their 2 cell cycles, plotted in the parallel coordinates plot. Each line connects a mother and a daughter cell cycle. In the earlier stages, cell cycles generally shorten from one division to the next (ratio of lengths $\text{division1}:\text{division2}$ is > 1) and after reaching the least variable and shortest state, cell cycles lengthen again (ratio is < 1).

I further wanted to check the changes in the cell cycles themselves that result in the observed shortening (Figure 12). To pinpoint in which stage of the cell cycle major changes occur, I again performed manual cell tracking, this time using the cell cycle marker PCNA or the FUCCI plasmids. Fluorescent PCNA was preferred, as it is a single construct that allows distinguishing all four cell cycle stages based on the differently distributed fluorescence (Figure 12A, Leung et al., 2012) and it thus allowed me to use it in combination with another marker, such as the neuronal marker, Ath5 that I used in the total cell cycle analysis. Again, just the self-renewing progenitor cells were tracked and the results, after tracking 132 cells and their cell cycle phases, suggest that S-phase might be the target of cell cycle regulation, as this is the phase changing the most and in accordance with the total cell cycle length (Figure 12B). G1 is rather short, taking 38 min on average and S phase is the longest cycle phase, taking on average 3.3 h (Figure 12C, Icha et al., 2017). A long S-phase might allow for more variability in its duration, which could be one of the advantages to center cell cycle length regulation on the S-phase, rather than on any other shorter phase.

The G1-phase is traditionally thought to be the growth phase of the cytoplasm. As I observed G1 shortening through my analysis of cell cycle phases, I reasoned that it might reflect the observed decrease in cytoplasmic volume. To check whether cells indeed grow the most during G1-phase, I have also started to manually segment nuclei and cells in 3D, through the entire cell cycle. Here, preliminary data on 5 cell cycles (data not shown) suggests that retinal progenitor cells grow most in S-, instead of in G1-phase of the cycle. This is an interesting possibility and I plan to continue this analysis to relate the analyzed changes in specific phases of the cell cycle, to cell size over development.

By dividing the total tissue volume by cell numbers, I estimated the average volume of single cells (Figure 13A). To validate both my cell count and this cell volume estimation, I asked how many cells of a certain size could maximally fit into this tissue. For this, I needed a measure of single cell volume. As the PSE cells are very slender and close to each other, their manual segmentation was imprecise and an automated approach very difficult with the available tools. To circumvent this problem, I used the volume of apical, rounded mitotic cells as a proxy for all PSE cell volumes, as for the cell count validation (Figure 9D).

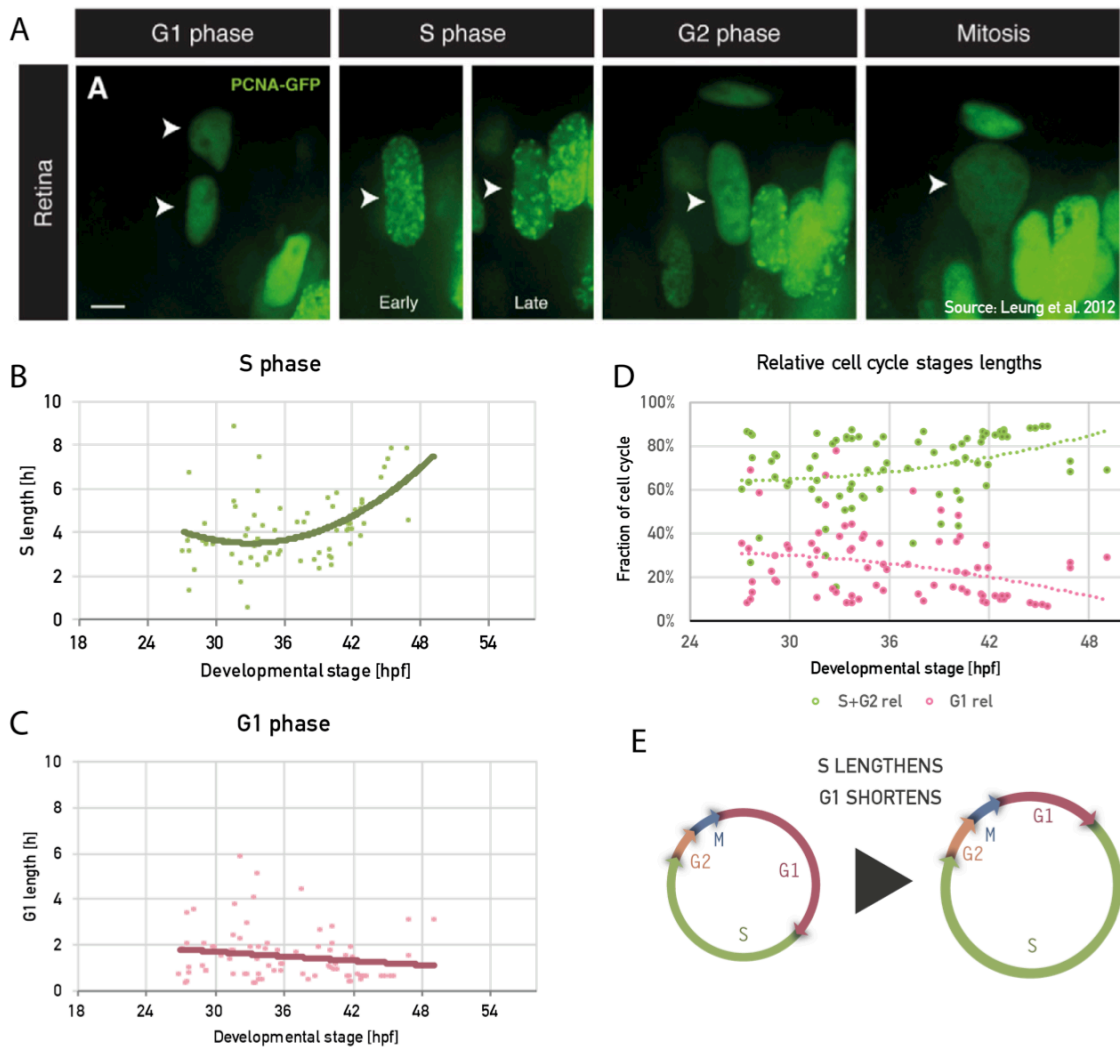


Figure 12: Possible differential regulation of S- and G1-stage throughout development.

A) PCNA was used as a cell cycle phase marker to track lengths of specific cell cycle stages. It allows identification of all 4 cell cycle phases by a different distribution of the marker. At mitosis, after nuclear envelope breakdown, PCNA is cytoplasmic. At G1 and G2 it is diffused nuclear, but stages are distinguishable in live movies by the IKNM at G2 and a smaller relative nuclear size in G1. S-phase is distinguishable by PCNA at replication foci. Image is reused from the Norden lab study by Leung et al. 2012, for clarity.

B) S-phase is the longest cell cycle phase, as shown before by Leung et al. 2012 and Icha et al. 2017. It is shortest ~36 hpf and then lengthens again. Line is a 2nd order polynomial fit in B), C) and D).

C) G1 was confirmed to be shorter than S-phase, as already shown also by Leung et al. 2012 and Icha et al. 2017. It shortens after 36 hpf, becoming as short as 30 min, which is similar to the short M- and G2-phases.

D) In the earlier stages, the ratio of S- and G1-phase in the total cell cycle is roughly 2:1, respectively. In the later stages (after 42 hpf), total cell cycle length is determined almost exclusively by the S-phase length, which takes more than 80% of the cell cycle.

E) Summary illustration of changes to the cell cycle: ~40 hpf, when cycles are overall shortest, S-phase is also at its short period. As cycles become longer (right diagram), their S-phase lengthens and G1 shortens. S-phase seems to be the major contributor to the cell cycle lengthening in the retinal PSE post-40 hpf.

Assuming that the mitotic cells are spherical, I measured their diameters and calculated the volumes for spheres, in each of the 6 developmental stages. Mitotic cells, however, might have a different volume than interphase cells. To calculate the difference between average mitotic and interphase cell volumes, I segmented 5 single cells in 3D from live movies, at the time of rounding and before and after division. This revealed that mitotic cells are on average 10% larger in volume than interphase cells, so I subtracted these 10% from all mitotic cell volumes in my analysis, to better represent the whole cell population. This estimation of single cell volumes fit extremely well to my initial estimations of cell size. I proceeded to use these cellular parameters in the remainder of the growth analysis. Overall, this analysis of cell size revealed that, as the cell number increases by >8-fold, cells become smaller and smaller, decreasing their volume by more than half (2.3-fold) during growth.

The decrease in cell volume, together with an increase in cell number hinted to an increasing density of cells within the tissue. Indeed, when I calculated the number of cells-per- μm^3 of tissue volume, I saw that the tissue does get more densely packed with cells while growing (Figure 13C). Looking at the images of the tissue in e.g., 24 and 42 hpf, it seemed that nuclei are not only smaller, but also much closer together. To check if this might be due to the volume of the cytoplasm becoming smaller, I measured the nuclear volume, that would allow me to estimate cytoplasmic volume, as well. Interestingly, 30 hpf is the time at which the nucleus-to-cytoplasm ratio (N/C ratio) of these cells seems to be the highest and the absolute cytoplasmic volume the lowest (Figure 13B, C), with the cytoplasm taking up only $100 \mu\text{m}^3$ in a $230 \mu\text{m}^3$ cell (43%). In the 6 hours from 24 to 30 hpf, average cell volume decreases by 30%, but seems to be due just to cytoplasm shrinking, as the nuclei do not become smaller at this time. Therefore, the N/C ratio in these cells changes and might contribute to the changes in the nuclear and cell packing. As the N/C ratio is traditionally considered constant in a particular cell type, it would be interesting to investigate this in more detail, as a possible response to putative tissue compression resulting from increased cell density.

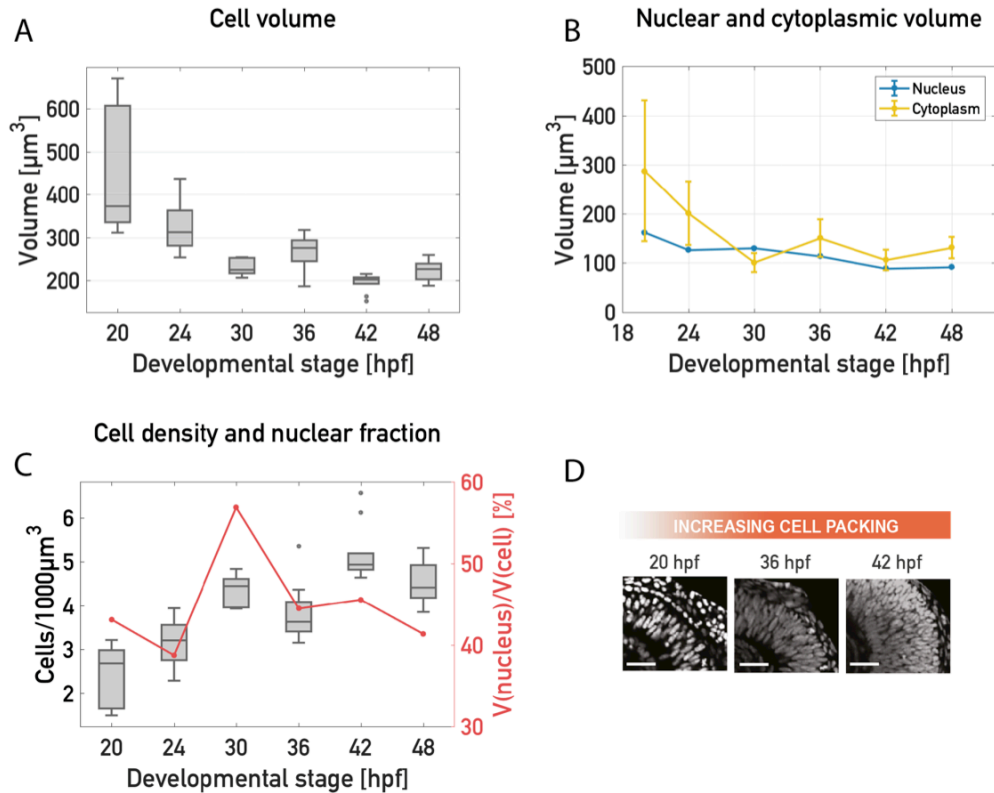


Figure 13: Decrease in cell size contributes to increasing cell density

A) Single cell volumes were estimated by dividing the total tissue volume by the total number of cells. Cells decrease their volume by more than half throughout development. This volume estimation was validated by calculating mitotic cell volumes, as well as frustum volumes (see Methods for more details). All 3 methods showed a more than 2-fold decrease in cell volume.

B) Both the nucleus (blue) and the cytoplasm (yellow) become smaller over time, taking up 40:60% of total cell volume, respectively. Nuclear volumes were estimated by measuring nuclear major and minor axes and calculating ellipsoid volumes. These were then subtracted from cell volumes to estimate the cytoplasmic volumes. Data points shown as means \pm SD.

C) Cell density increases and was measured by dividing the total cell number by the tissue volume.

D) Tissue nuclei images illustrating increasing cell density from C).

N=10/stage for all.

Altogether, in this part of the project, I decomposed retinal PSE growth into its cellular contributions, in a tissue-wide, 3D analysis through 28 hours of development. I quantified how cell number and size (Figure 9B and Figure 13B, respectively) contribute to the constantly increasing retinal PSE tissue volume (Figure 9A), that, due to random cell division orientation and uniform proliferation (Figure 8), grows in an isotropic and homogeneous way. I am now working on theoretically confirming this decomposition and modelling PSE growth (with Guillaume Salbreux).

3.2 Constant tissue shape is ensured by changes in cell shape

Considering growth is isotropic and homogeneous, it is possible that the retinal PSE tissue keeps its shape unchanged while changing size. To check if this might be the case, I first wanted to get a quantitative description of how tissue shape develops with ongoing growth. To measure how the shape of the retinal PSE changes as the tissue grows, I used the aspect ratio as a proxy for tissue shape. The aspect ratio measures the relation of different dimensions of a geometrical object, e.g., the shape's width to its height and is typically used to describe shapes of 2D-objects. As the retinal PSE tissue is three-dimensional, but has a simple, hemispherical geometry, I used the square root of the apical surface area, to relate it to the height of the tissue (Figure 14D) and obtain the tissue's aspect ratio as $\text{height}/\sqrt{\text{area}}$. As all PSE cells are attached at both the apical and the basal surface of the tissue, the thickness of the tissue is simultaneously a measurement of cell height. Height measurements were done in 3D on segmented tissue volumes, in multiple regions: the lateral, as well as in the deep domain of the tissue (behind the lens; Figure 14A'), to obtain average heights for each optic cup (10 samples/stage). At 20 hpf, cells were $\sim 40 \mu\text{m}$ long and increased their length by more than 50%, to $\sim 67 \mu\text{m}$, over the next 28 hours (Figure 14A).

Next, tissue apical areas were segmented manually and separately from tissue volumes and showed that the apical surface increases 2.5-fold, from ~ 53000 to $\sim 132700 \mu\text{m}^2$ (Figure 14B, B'). The aspect ratio for the tissue, calculated from these values as $\text{height}/\sqrt{\text{area}}$, indeed showed no significant change, staying at ~ 0.18 (Figure 14E, E'') and confirmed that the retinal PSE shape is indeed maintained during development. I next analyzed how single cell shape changes might contribute to this maintenance of tissue shape. Single cell apical areas were first estimated by dividing the apical surface area of the tissue with the total number of cells (Figure 14C).

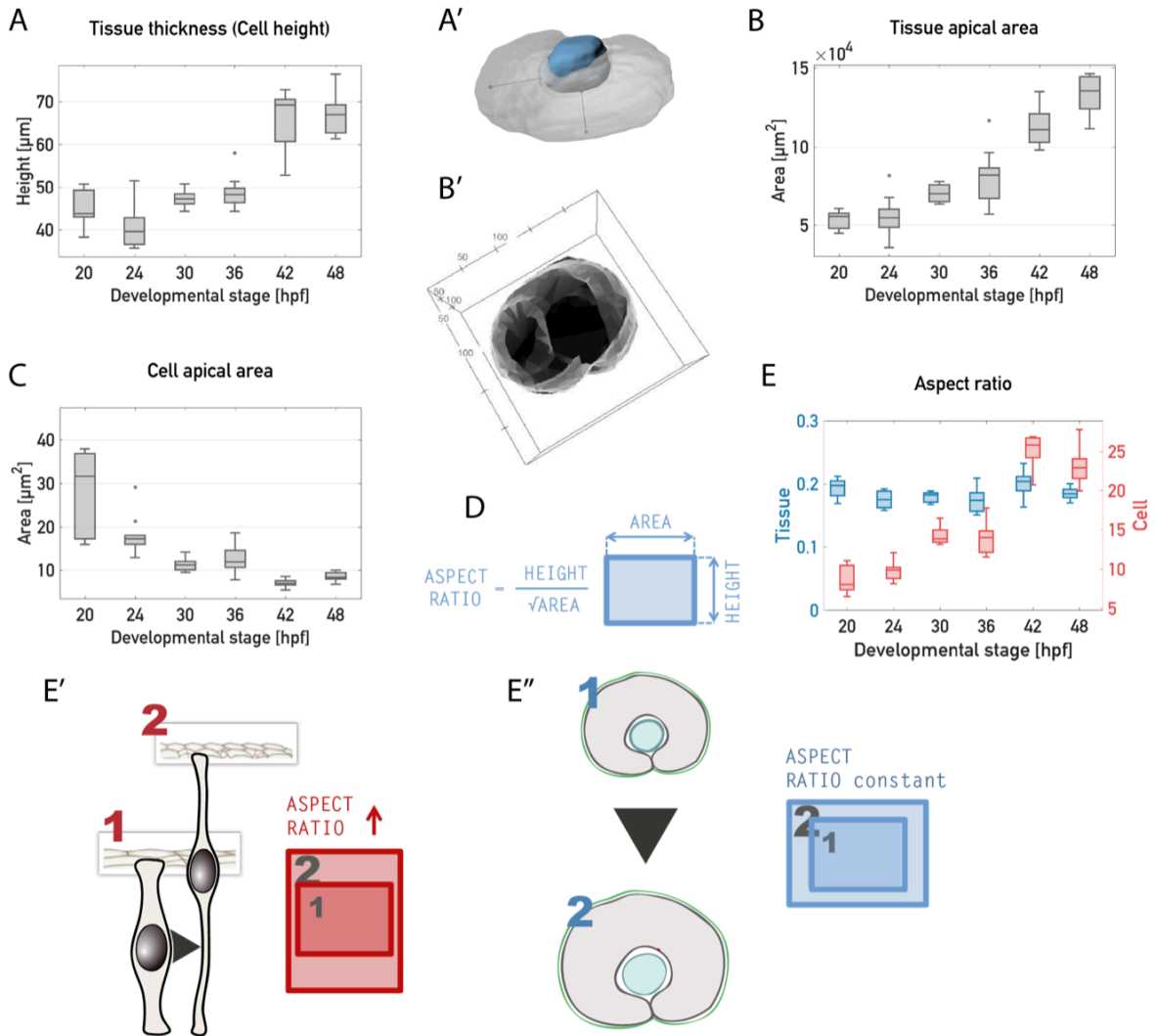


Figure 14: Cell shape changes ensure maintenance of tissue shape.

A) Tissue thickness (cell height) increases through development by ~50%, from 40 to 67 μm .

A') An exemplary sample of tissue thickness measurement in Imaris. Faint grey lines represent the apico-basal length. As all other analyses, it was done in 3D.

B) Tissue apical area constantly increases during growth 2.5-fold.

B') Visualization of the segmentation of the retinal apical surface using a custom Fiji plugin.

C) Cell apical areas were estimated by dividing the total apical tissue area by the total number of cells. The number of RGCs obtained by the FACS analysis was subtracted from this total cell number, assuming that all RGCs have delaminated to the basal side and do not have an apical process any longer.

D) The equation used to calculate the aspect ratio, used from now on as a measure of shape. The aspect ratio is equal to the tissue thickness (cell height) divided by the square-root of tissue (cell) area.

E) Cell aspect ratio increases, reflecting the fact that E') the cells become longer and thinner. At the same time, tissue aspect ratio (shape) stays constant during development, with E'') the retinal PSE maintaining its typical hemispherical shape.

The area covered in rounded, mitotic cells was excluded, to only estimate the apical endfeet areas of elongated, interphase cells. While cell length increases with tissue growth, cell areas decrease, with their apical endfeet being ~3.5 times smaller at 48 hpf than they were

at 20 hpf. This increase in height and decrease cell area, with the increasing aspect ratio show that the already slender PSE cells change their shape and become thinner and longer over development (Figure 14E, E').

PSE cells not only change their shape as development progresses, but also become smaller, ultimately halvening their size as mentioned before (Figure 13A). Surprisingly, preliminary analysis indicated that these cells grow most in S-phase of the cycle, as shown by manual segmentation of cells and nuclei through specific cell cycle stages. As S-phase seemed to be shortest ~42 hpf, I hypothesize that the period of shortest S-phase might, therefore, participate in the overall cell size decrease and in increasing cell density in the growing tissue. This remains to be tested by already mentioned manual segmentation of cells and cell nuclei through the cell cycle.

Altogether, this 3D analysis provided me with a detailed description of how cell shape, increase in cell number and decrease in cell size maintain retinal PSE shape during tissue growth. I next used this dataset to investigate the potential limits to proliferative growth.

3.3 Growth limits in apically constrained PSE

Having at hand detailed data on how the retinal PSE size increases and shape remains constant during development, I asked whether there are limits to PSE growth. During development, PSE cells elongate and the number of nuclear layers increases (Figure 15A). In relation to this number of layers, still in the 1970s IHM Smart proposed that growth of PSE tissues is limited by a packing maximum (Smart 1972), which arises from the inability of their apical surface to accommodate the growing number of rounded, mitotic cells. These problems of progressive pseudostratification could arise over development, in PSE that are constrained from spreading their apical surface, as briefly presented in the Introduction. Therefore, an apically constrained PSE tissue would block its own growth if it reached this packing maximum. If the number of divisions is poorly coordinated with the amount of free apical surface, the PSE can enter a self-inflicted, “proliferative trap” (Smart 1972), that will force it to e.g., decrease its proliferation rate and limit its growth.

Three main ways of how a PSE can enter a proliferative trap were proposed: i) The constant subdivisions of the cell's apical endfoot might render the apex too small to function as an anchor point, or signaling receptor base; ii) apical surface might be completely filled with rounded mitotic cells, inhibiting any further divisions; iii) the “queuing” problem: the ratio of the number of nuclear layers to the available apical space might be too high (type III trap was outlined in the Introduction). To check if proliferation-based limits to PSE growth might exist and whether cell packing and cell cycle might indeed block further growth, I set out to test the zebrafish retinal PSE for such constraints. After obtaining the growth and cellular

parameters from the previous analyses, I was able not only to check for the proliferative traps, but also see how they might evolve through development.

3.3.1 Availability of apical surface is not a growth constraint to the retinal PSE

3.3.1.1 *Type I proliferative trap*

From the already existing data, we know that the cell's average apical attachment decreases in surface area from ~ 28 to $8 \mu\text{m}^2$, staying at $8 \mu\text{m}^2$ over the last two analyzed developmental stages (Figure 14C). So, the apex does indeed become smaller, not decreasing after it has reached $8 \mu\text{m}^2$. However, I cannot say if this is the constraint to growth, or a cue for cells to delaminate. Most likely it is not, as neuronal delamination occurs irrespective of this. If proliferation is blocked, retinal PSE has fewer, bigger cells, but they still delaminate.

3.3.1.2 *Type II proliferative trap*

The apical surface might get filled with rounded, mitotic cells in the retinal PSE, so it cannot fit any more divisions. Looking at some of the images with mitotic cells detected, it might seem so (Figure 7C). Therefore, I analyzed how the total area under mitotic cells changes over time with respect to the total tissue apical surface. This revealed that the mitotic cells never occupy more than 20% of the apical surface (Figure 15B), which is far from a completely filled surface (100%). Looking at the round mitotic cells as rigid circles on the apical surface, one can assess their maximal packing with the approach of circle packing. Circle packing examines the most efficient way to pack circles onto a given surface, without overlaps. Packing circles onto a 3D, spherical object is not trivial (Tammes problem, or general Thompson problem). I therefore used a freely available tool (http://www.engineeringtoolbox.com/smaller-circles-in-larger-circle-d_1849.html) to calculate the maximal packing density in 2D, on a circle, instead of a sphere. The circle had the same total area as the apical surface of the retinal PSE and I assumed that all mitotic cells have the same cross-sectional area (average of a stage). This approach also showed that mitotic cells do not fill up the apical surface, as in every stage a several fold-increase in mitotic cell number would theoretically be allowed (Figure 15C, C'). The apical surface does not get filled with mitotic cells in any of the developmental stages and no more rounded cells could theoretically fit. This also indicates that the total availability of the apical surface is not a constraint to further proliferative growth of the retinal PSE.

I checked this result by rephrasing the total mitotic occupancy as the cell area density (number of cells-per- μm^2 , Eq. (2), with Guillaume Salbreux). This is essentially the same as the previous measures of apical occupancy but takes more of our measured cell cycle parameters into account to describe the system better. The ratio of the duration of mitosis and the total cell cycle time, T_M / T_{CC} , is equivalent to the mitotic index and denotes the fraction of total cells that are mitotic (\sim rounded). The number of mitotic cells is the product

of this mitotic fraction and the total cell number, N_{tot} and the total area covered under mitotic cells the product of the number of mitotic cells, N_M and their cross-sectional area, A_M (left expression of Eq. (1)). This total area covered by mitoses has to be smaller or equal to the total available apical tissue area, A_{tot} :

$$\frac{T_M}{T_{CC}} \times N_{tot} \times A_M \leq A_{tot} \quad (1)$$

T_{CC} is the time period a cell takes to cycle, so $1/T_{CC}$ is equivalent to the rate (frequency) of cell division, k_d . Using the k_d , the number of cells-per- μm^2 (cell area density) has to respect the constraint given on the right of Eq. (2):

$$\frac{N_{tot}}{A_{tot}} \leq \frac{1}{k_d \times T_M \times A_M} \quad (2)$$

The constraint (right expression, Eq. (2)) here was as well far from the measured cell area density (Figure 15D) and I suggest that the total availability of the apical surface to mitoses indeed does not pose a constraint to proliferation of the retinal PSE.

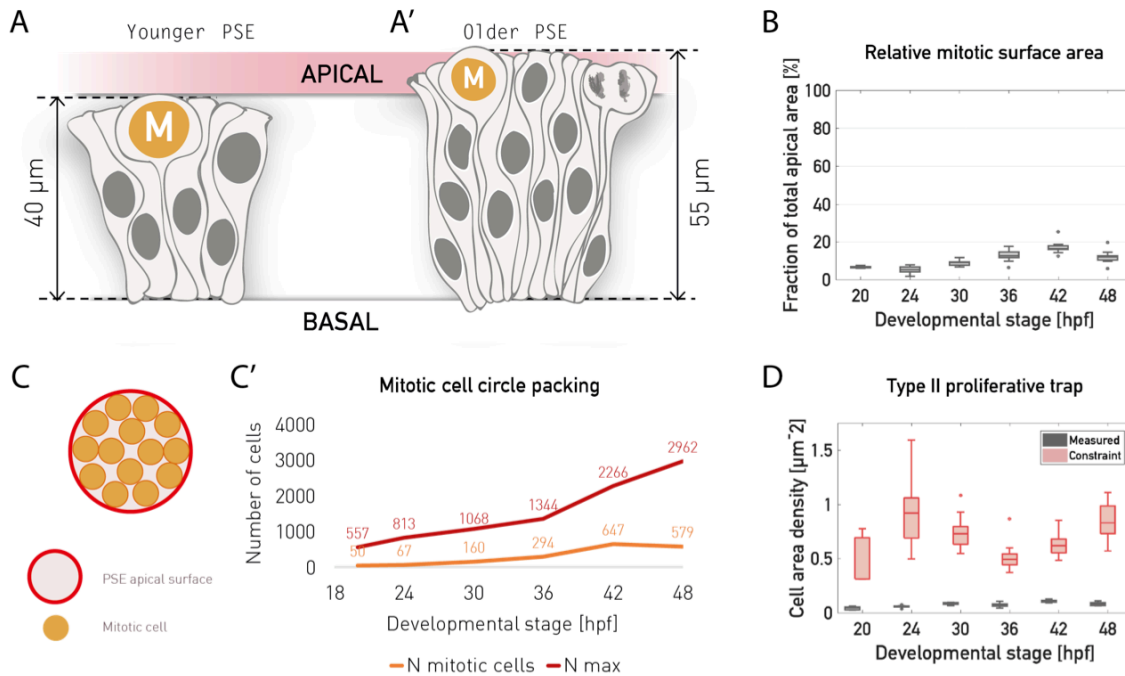


Figure 15: Availability of apical surface for mitosis is not the growth constraint to the retinal PSE.

A) In a growing, apically constrained PSE, cell density increases, cell cycles shorten and more cells will divide at the apical surface, making it possible that the tissue enters one of the proliferative traps and restricts its own proliferative growth, because of lack of space at the apical surface (type II proliferative trap).

B) Mitotic cells never occupy more than 20% of the total apical surface available for divisions.

C) Even if circle packing of mitotic cells is taken into account, C') the number of cells rounded apically does not reach the maximal number. Data points shown as means.

D) To test our other cell cycle parameters, I retested (with Guillaume Salbreux) the availability of the apical surface as the cell area density, that has to be lower than the proposed constraint. Again, the measured apical surface packing does not reach the proposed constraint. Therefore, the availability of the apical surface seems not to constraint growth.

3.3.1.3 Type III proliferative trap

As the availability of the apical surface did not seem to pose a constraint to proliferation, I tested the last of the proposed PSE growth constraints. The above (type II) proliferative trap poses the availability of the apical surface as a 2D problem. The constraint could be defined in the same way for a typical monolayered, non-pseudostratified epithelium. However, in the PSE multiple layers of nuclei all participate in the “queuing” to reach the apical surface (Figure 16A). This requires the putative constraint to be treated as a 3D problem, instead. Smart’s type III proliferative trap is exactly that and it was the one briefly presented in the Introduction. I should note at this point it does not seem that the interphase nuclei are indeed queuing to reach the apical surface. Their apical migration (IKNM) is cell cycle dependent and it is unlikely that entry into G2 phase is awaiting some queuing cue,

as its length is always ~20 minutes. That being said, the limit to growth in Smart's type III trap arises from the disproportion of the time the PSE cells need to complete their cell cycle, during which they are absent from the apical surface and the time and relative space they occupy once rounded apically (T_M and $A_{M(relative)}$), so one might use "queuing" as an intuitive description. The relative space occupied by a mitotic cell is the relative size of the mitotic cell, or the measure of how much more surface area a mitotic cell occupies in comparison to an interphase cell (Figure 16A'). Perhaps more intuitively, one could first imagine a rounded mitotic cell on the apical surface, with the PSE nuclear layers under it. One would then have to think how many cells will eventually "want" to reach the same apical surface, i.e., how many interphase nuclei are stacked under this one rounded cell, "waiting" to reach the surface and round up. This number of cells will be the relative size of the round cell (how many interphase cross-sections fit into the round cell cross section, e.g., 4) multiplied by the number of nuclear layers in which the interphase nuclei are stacked (e.g., 5). The cycling time of each cell has to be longer than the time the apical surface above it is occupied by cells other than itself. This occupancy time is the number of cells that will eventually occupy it (our N_L , $A_{M(relative)}$ from above, 4 x 5), multiplied by the amount of time each of them will remain rounded apically (length of mitosis, T_M ; Eq. (3)).

$$T_{CC} \geq T_M \times N_L \times A_{M(relative)} \quad (3)$$

In other words, the number of PSE layers, N_L , cannot exceed the maximum:

$$N_L \leq \frac{T_{CC} [h]}{T_M [h] \times A_{M(relative)}} \quad (4)$$

For the PSE to proliferate further upon reaching the maximal number of nuclear layers given by Eq. (4), it would need to adjust its cell cycle or cell size parameters, e.g., lengthen its cell cycle. Eq. (4) is the final expression of the Smart's type III trap, that I used to test for PSE growth constraints originating in all three dimensions, i.e., in the apical surface from the relative size of the mitotic cell and in tissue depth from the "queuing" nuclei. I checked for the existence and evolution of such a constraint throughout development by comparing the measured (experimental) number of layers to the values predicted by Eq. (4), from our cell cycle and cell size data. The experimental number of nuclear layers comes from dividing the average total cell length by the average nuclear length, saying how many nuclear layers can fit into the cells at every given stage. The 3D aspect is contained in the relative size of the mitotic cell, $A_{M(relative)}$, that relates the apical mitotic cell to the more basal interphase nuclei under it. $A_{M(relative)}$ is, therefore, the major difference to the 2D, type II trap. The relative

size of the mitotic cell is the ratio of the cross-sectional area of the mitotic cell, to the cross-sectional area of the interphase cells (Figure 16A'). As the nucleus is the bulkiest organelle of the interphase cells, I measured the nuclear minor axis to calculate the average cross-sectional area of the interphase cells, thus using nuclear width as a proxy for cell width.

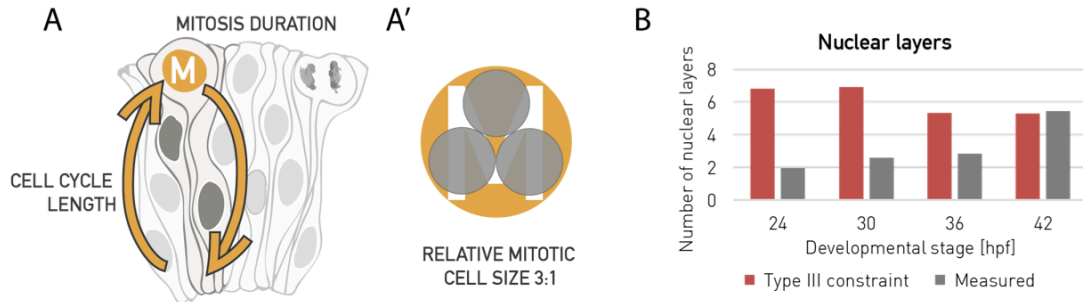


Figure 16: Retinal PSE grows in accordance to 3D packing constraint.

A) Proliferation and cell size during progressive pseudostratification has to be coordinated with the number of nuclear layers. I.e., the time for which nuclei are absent from the apical surface (cell cycle length) has to be coordinated with how long a mitotic cell occupies the apical surface and A') how many nuclei are “queuing” under it to reach the surface and divide. Illustration depicts apical view.

B) The retinal PSE operates below (early stages) or at (42 hpf) the type III constraint. Because of the nuclear layering and apical mitoses, proliferation in the retinal PSE has to be considered as a 3D, not a 2D problem. Bars show mean values.

Comparing the theoretical maximal number of layers, given the cellular parameters, to the measured number of layers revealed that the retinal PSE operates below the maximal layering level in earlier stages, even at its most proliferative stage of 36 hpf. At 42 hpf, however, the actual measured number reaches the prediction based on Eq. (4) (Figure 16B). This result suggests that the retinal PSE indeed grows in accord with the proposed Smart’s law for PSE tissues, with the actual number of nuclear layers staying at or below the theoretical maximum throughout development. The point when the tissue reaches its layering maximum (42 hpf) coincides with the point when other cellular parameters change the most, as well: cell height increases the most and overall cell shape changes the most at 42 hpf. Additionally, reaching the maximal layering coincides with the time when the first neurogenesis wave has swept over the entire retina (Figure 8D') and major neuronal differentiation starts taking place (Figure 10C). Because changes in cell shape coincide with major cell cycle exit and delamination across the tissue, I next asked whether there might be a link between the two. In addition, cell cycle exit might be necessary to slow down the tissue growth rate and keep it in accordance with the layering maximum. To test how far can such purely proliferative growth continue and how far tissue thickness can increase, I blocked cell cycle exit and differentiation.

3.4 A brake on tissue thickness in differentiation mutants

3.4.1 PSE characteristics are maintained in *hdac1*^{-/-} retinas

To test the limits to tissue proliferative growth, I needed a tool to inhibit differentiation in the retinal PSE. It has previously been shown that the retinas in zebrafish mutants in histone deacetylase 1 (*hdac1*^{-/-}) do not differentiate (Yamaguchi et al. 2005, Stadler et al. 2005). Hdac1 is an upstream regulator of Wnt and Notch signaling in the zebrafish retina (Yamaguchi et al. 2005). Timely Wnt inhibition by Hdac1^{-/-} ensures cell cycle exit and Notch inhibition cell differentiation, resulting in these pathways remaining active in the *hdac1*^{-/-} fish.

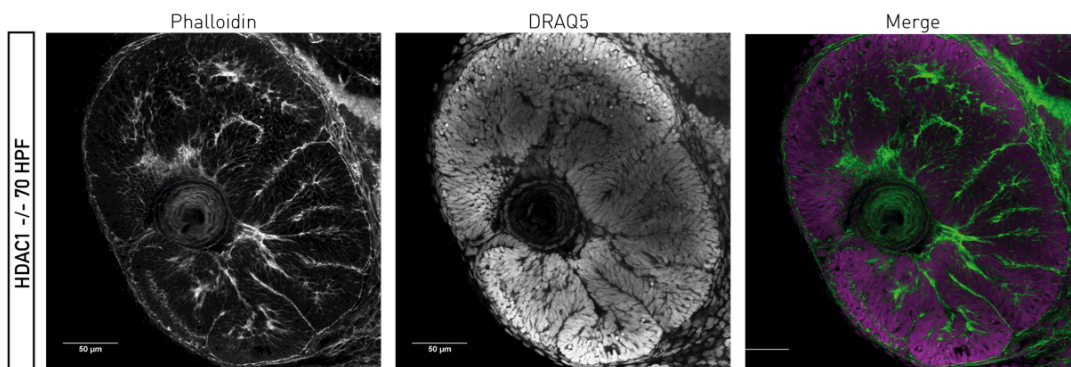


Figure 17: Differentiation mutants have perturbed retinal PSE shape.

From 60 hpf onwards, the *hdac1*^{-/-} retinal PSE exhibit the heavily folded phenotype.

I first confirmed the reported mutant phenotype: the *hdac1*^{-/-} retinal PSE loses its typical smooth shape and folds upon itself around 2 dpf and leading to a highly folded structure by 60 hpf (Figure 17). To identify the mutants, we developed a genotyping protocol in the lab. For more details on this, please see Appendix X. I first checked whether differentiation is blocked in the *hdac1*^{-/-} mutants. Indeed, I could never observe any distinct layering in the mutant, indicating that neuronal delamination and migration do not occur. The Zn5 antibody, that marks mature RGCs, also did not recognize any epitope in the *hdac1*^{-/-} tissue (Figure 18A), confirming that the differentiation phenomenon is indeed absent in these retinas. The *hdac1*^{-/-} fish have a slight defect in the optic stalk region in the retinal periphery, which seems buckled and thicker than in the wildtype (Figure 18B, right upper panel). As this cell accumulation might, in theory, exert compression on the retina, it might also cause the folding phenotype. The optic stalk defect arose during early optic cup morphogenesis (<20 hpf), so to check whether this, instead of an intrinsic, retinal parameter, causes the folding, I wanted to have temporal control over the *hdac1*^{-/-} phenotype, to induce *hdac1*^{-/-} knockdown just after the optic stalk has formed correctly. To have such temporal control, I used the *hdac1*^{-/-} inhibitor drug, Trichostatin-A (TSA). At constant incubation at

concentrations of 0.2-0.8 μM , 100% wildtype fish in TSA still developed the *hdac1*^{-/-} phenotype, with heavily folded retinas by 60hpf, confirming that the drug recapitulates the mutant phenotype. If TSA was added to wildtype fish just between 24 and 30 hpf, after their optic stalk formed correctly, by 60 hpf the retinal tissue was folded as well (Figure 18B). This suggested that the defect in the optic stalk is not the cause for retinal folding in the *hdac1*^{-/-} mutants.

If the TSA drug medium was not renewed every 24 hours, the drug effect declined. Interestingly, in this case, differentiation recovered and neuronal layers formed, in parallel with the existing PSE folds (Figure 18C). This suggests that differentiation might be able to continue “where it left off” if it is blocked only transiently. Moreover, this suggests that the folds in the retinal PSE tissue do not inhibit differentiation and that neurons do not have a read-out for an intact tissue shape before they start differentiating. These ideas would be interesting to test in the frame of a cell cycle exit and differentiation study in the PSE.

To characterize the tissue in *hdac1*^{-/-} mutant retinas, I checked whether they preserve the epithelial character and a monolayered PSE architecture. Immunostaining samples fixed at ~60 hpf with the mitotic antibody PH3 revealed that all divisions in *hdac1*^{-/-} retinas take place at the apical surface (Figure 19A), as they do in all intact PSE tissues. Moreover, anti-laminin β 1 antibody showed a smooth basal lamina signal that underlined the cells' basal endfeet (Figure 19B). Live imaging revealed intact nuclear migratory movements in the mutant retinas, ensuring that IKNM still occurs normally and the apical divisions previously observed by PH3 staining are not e.g., accumulated, incomplete divisions. Therefore, the *hdac1*^{-/-} retinas retain an intact PSE character irrespective of the shape perturbation.

By long light sheet time-lapses (>15 h), I was able to observe for the first time the retinal buckling event live (Movie 5). Buckling was always initiated at the apical surface, possibly because of an instability that mitotic events might introduce there. To test whether an increase in cell number is the driver of retinal folding, I inhibited proliferation in *hdac1*^{-/-} using hydroxyurea (HU) and aphidicolin (A), combined pharmacological inhibitors of progression through the S-phase of the cell cycle (Harris and Hartenstein, 1991). This experiment showed that the *hdac1*^{-/-} folded retinal phenotype depends on proliferation, as the tissue did not buckle when proliferation was blocked (Figure 20).

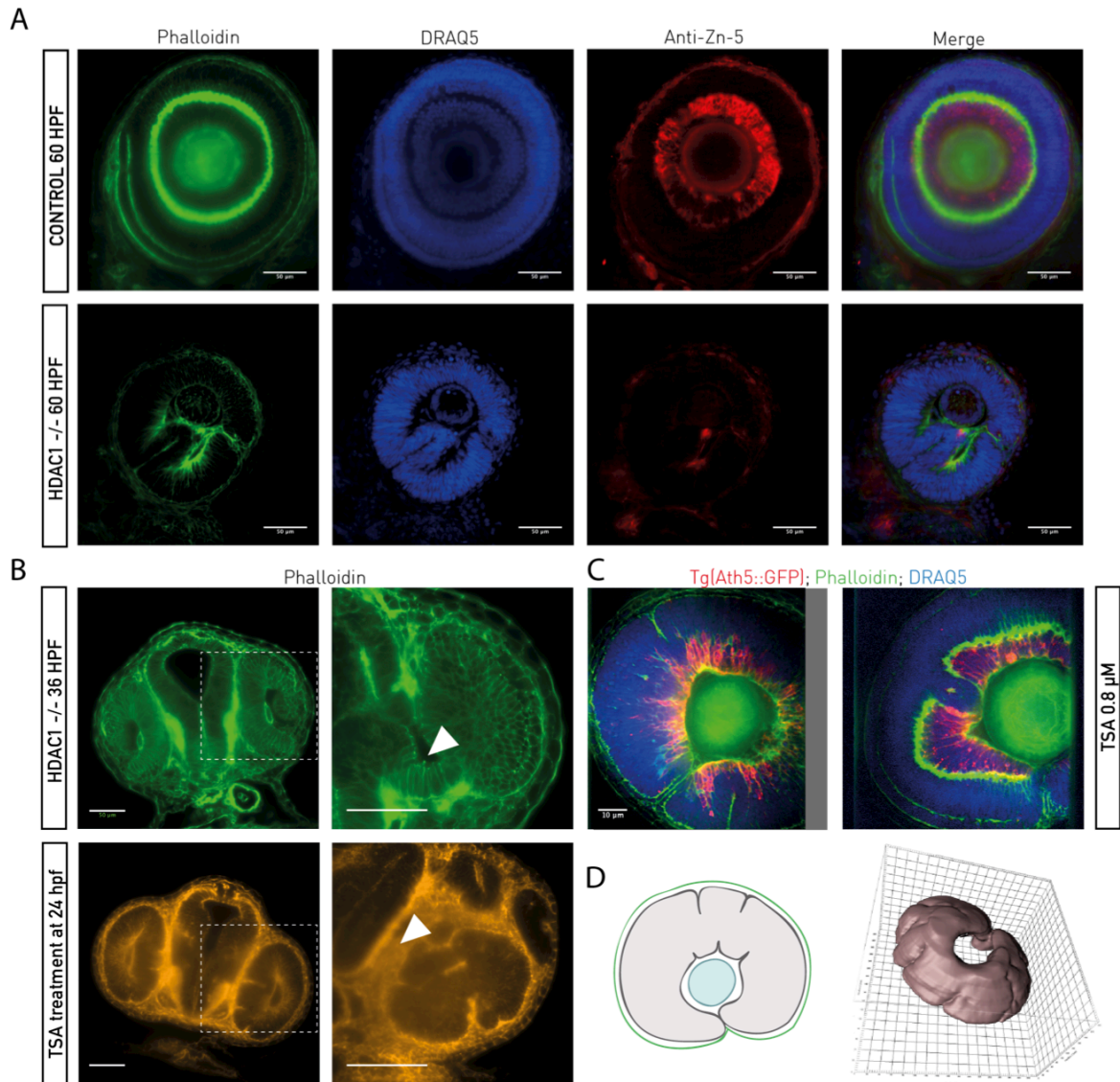


Figure 18: Retinal cells do not differentiate in the *Hdac1*^{-/-} mutant.

A) By 60 hpf, the wildtype tissue is layered and almost fully differentiated. Zn-5, a readout for the maturity of the RGC layer, is fully present (upper panels). In the *hdca1* retinas (lower panels) at the 60 hpf and later, no retinal lamination or Zn-5 staining could be observed, indicating that differentiation is indeed blocked in these mutants. Scale bars are 50 μm.

B) Upper panels: *hdac1*^{-/-} fish typically exhibit a thickened optic stalk phenotype (white arrowhead, upper panel), that might cause the observed folding. However, if the phenotype was induced only later, using Trichostatin-A treatment after the optic stalk already developed properly (at 24 hpf), retinal folding still occurred (lower panels). Right panels are enlargements of the deeper layers of the dashed region on the left. Scale bars are 50 μm.

C) If TSA medium was not renewed, the *hdac1*^{-/-} phenotype diminished and differentiation started in a folded tissue (RGCs in red). Scale bar is 10 μm.

D) A schematic of the buckled and folded retinal tissue and an example of its apical surface rendering after manual segmentation (right) to visualize folds in 3D.

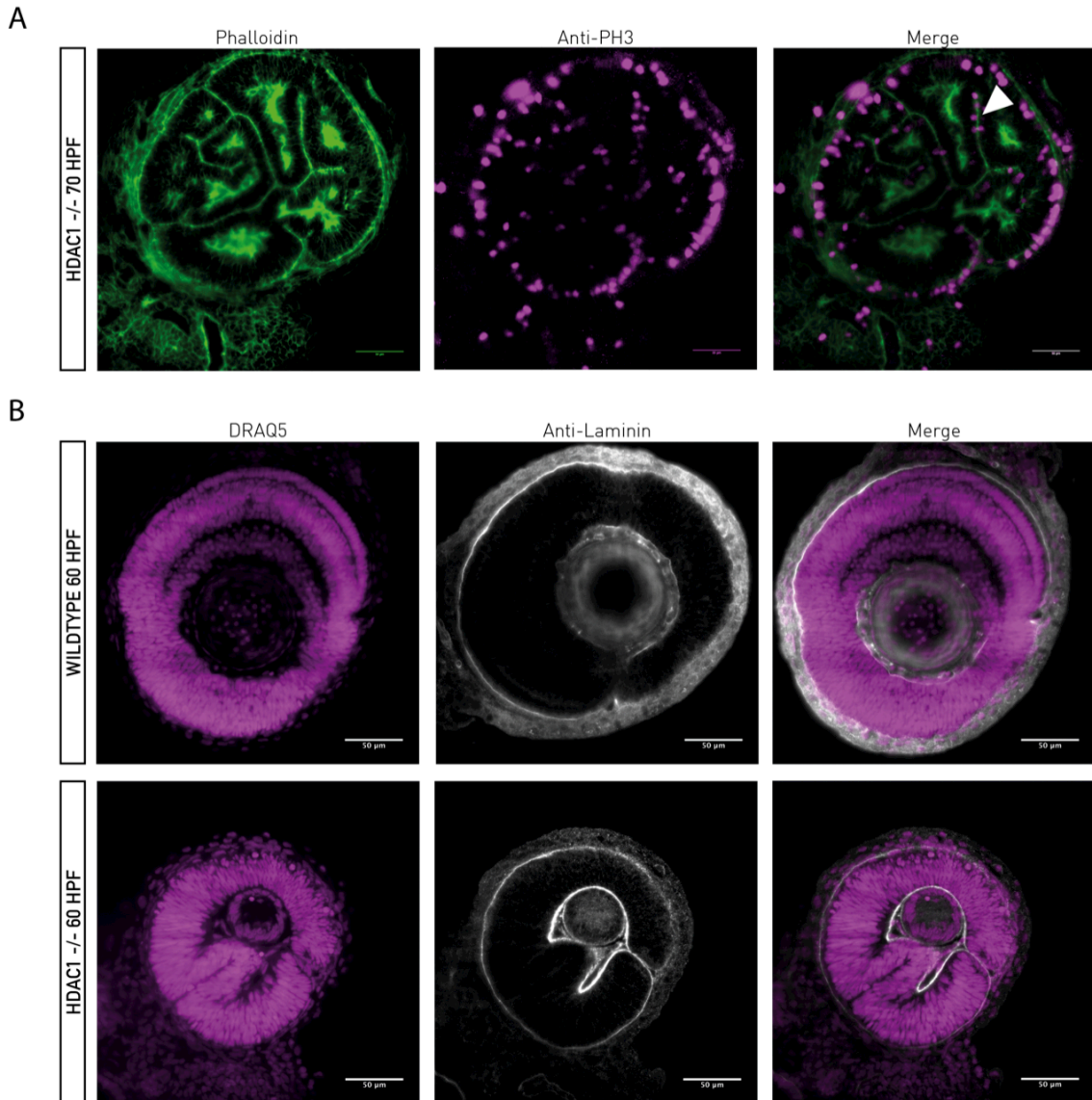


Figure 19: PSE tissue structure and characteristics are preserved in *Hdac1*^{-/-} mutants.

A) Proliferation in the folded retina still occurs only at the apical surface, as shown by the PH3 staining.

B) The *hdac1*^{-/-} tissue is, as the wildtype one, surrounded by a basal lamina, as shown by the laminin antibody staining.

Scale bars are 50 µm in all cases.

Together, the mutant characterization outlined above confirmed that in the *hdac1*^{-/-} condition, lack of differentiation leaves the retinal PSE structure intact, with all characteristics of a PSE tissue present: IKNM and apical divisions, multiple nuclear layers and a basal lamina. Therefore, the *hdac1*^{-/-} retinal tissue was a proliferative retinal PSE system, but with its growth unbound by the timing of differentiation. With this powerful tool at hand, I proceeded to use the *hdac1*^{-/-} mutants to investigate the limits to retinal PSE size, packing and shape and the factors affecting them.

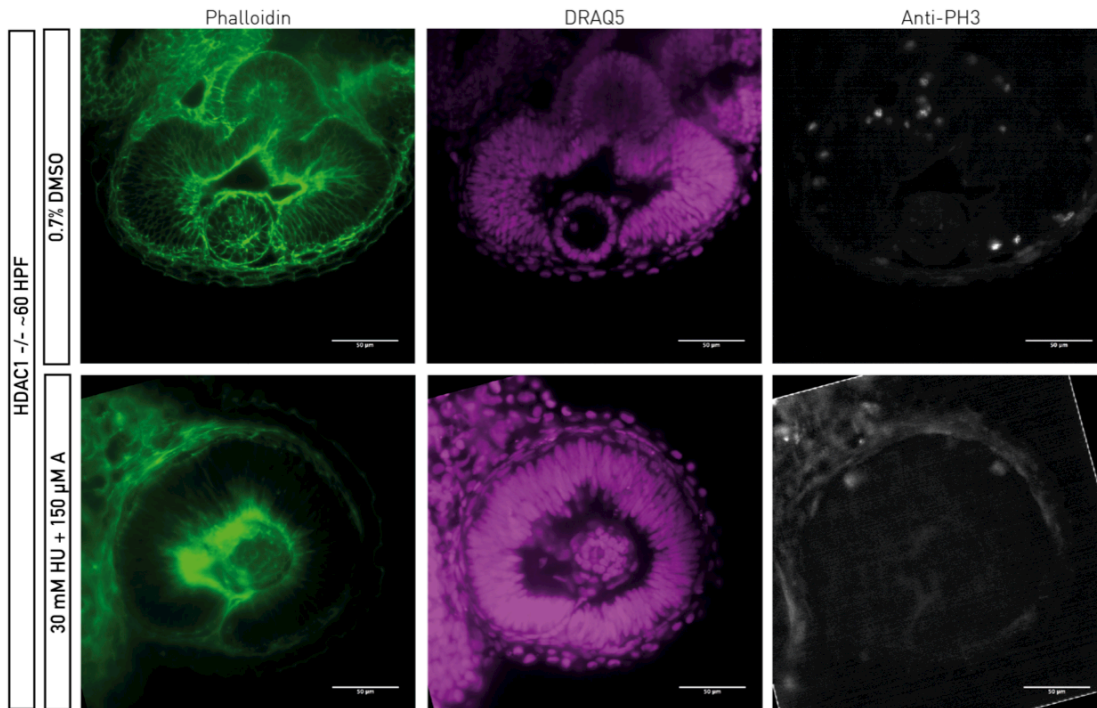


Figure 20: Proliferation is necessary for the folding of the *hdac1*^{-/-} retinal PSE.

Top panels: Mutant fish treated with DMSO fold their retinas and proliferate normally (PH3 staining). Bottom panels: Mutant retinas treated with a combination of cell cycle inhibitors hydroxyurea (HU) and aphidicolin (A) do not fold when their proliferation is inhibited.

3.4.2 Cell height is the major shape constraint in *hdac1*^{-/-} mutants

The *hdac1*^{-/-} PSE tissue changes its shape from smooth, to a tissue folded onto itself. In order to know what perturbs the development of a normal shape, one has to understand how the folded phenotype arises in the first place. Therefore, to check how the *hdac1*^{-/-} PSE at the point of buckling differs from the WT, I first started to investigate how the folded *hdac1*^{-/-} phenotype develops from a smooth WT-like PSE tissue. Initial movies showed that the events of the folded phenotype, such as a buckling event, happen fast, within less than an hour. Live, light sheet imaging proved to be the most adequate method to get a complete sequence of events during the development of *hdac1*^{-/-} retinas. Because of its low phototoxicity (Icha 2017) and high speed, light sheet microscopy allows long time-lapses at high temporal resolution. The downside of such imaging experiments is their extremely low throughput, though and this remains one of the biggest weaknesses of the approach. However, such experiments allowed direct observation of *hdac1*^{-/-} development at much higher temporal resolution than fixing the samples could and I used it for all further analysis on *hdac1*^{-/-} fish.

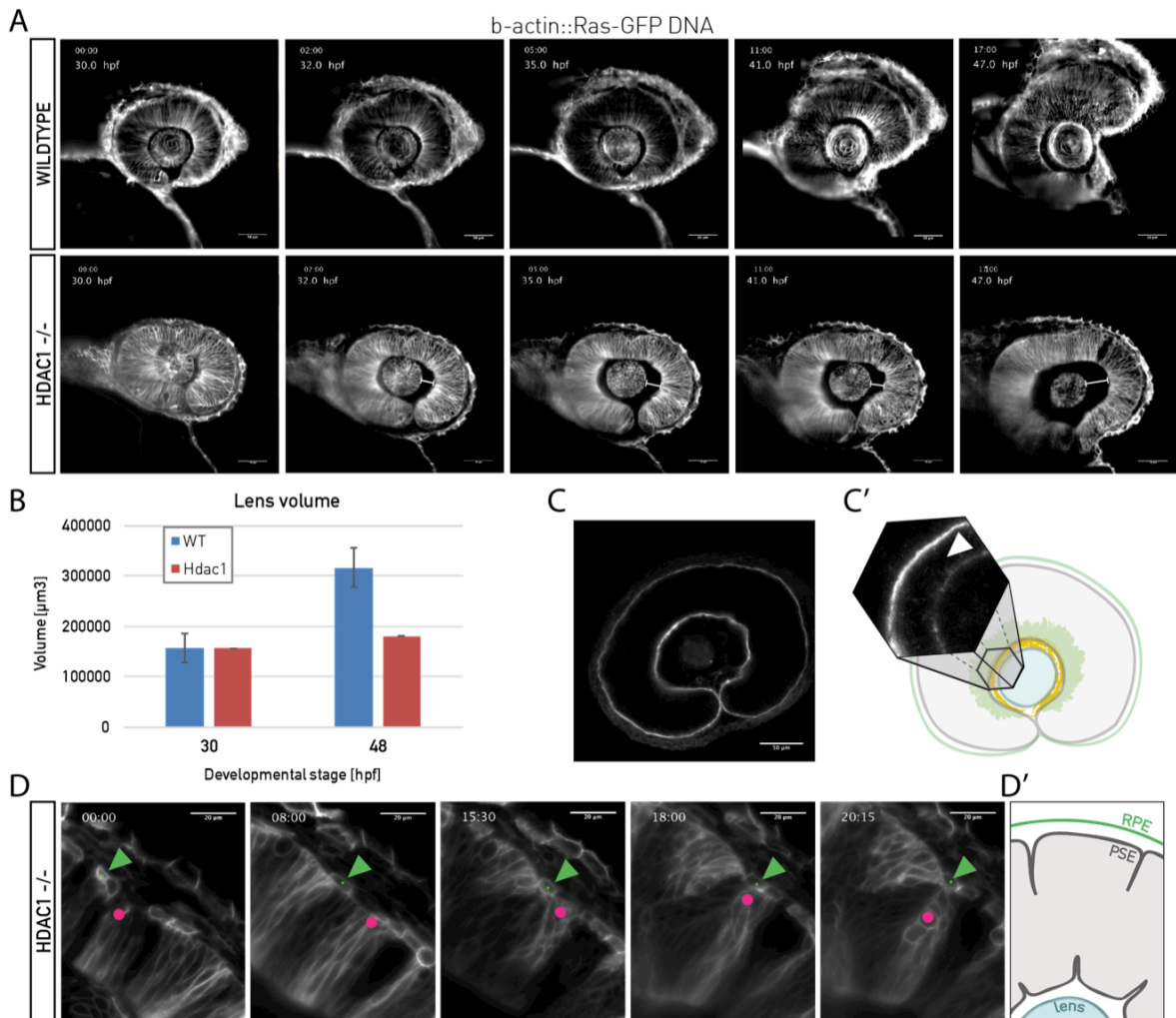


Figure 21: Characterization of *hdac1*^{-/-} development.

A) Live light sheet imaging revealed that retinal PSE detachment from the lens precedes tissue buckling (lower panels). The WT tissue, conversely, remains close to the lens throughout development (upper panels).

B) The lens tissue in the WT grows as the retinal PSE grows (blue). In the *hdac1*^{-/-}, lens growth ceases. Data bars show mean \pm SD.

C) Anti-laminin staining of the basal lamina in *hdac1*^{-/-} revealed that, with PSE detachment, the ECM remains closely associated to the PSE tissue. C') Thin ECM tether-like structures (white arrowhead) still span the cavity between the retinal PSE and the lens.

D) The RPE does not fold with the retinal PSE, but remains to smoothly surround it. Green arrowhead: RPE cell, magenta dot: bright PSE clone that buckles apically. D') Schematic representation of the last panel in D).

At 30 hpf, all the necessary body features to stage *hdac1*^{-/-} embryos were present, but after this stage, it became increasingly difficult to determine the age, because hallmark staging structures, the pectoral fin, or characteristic swimming patterns, did not develop. Analyses were therefore started at 30hpf. At this stage, before any differentiation starts taking place in the control, the *hdac1*^{-/-} PSE tissue looks almost indistinguishable from the WT. It then continues to proliferate and grow from 30 hpf onwards. Around 35–40 hpf, a change in retinal shape is onset. The basal surface of the PSE, otherwise very close to the

lens, starts to separate and spread away from the lens (Figure 21A). This spreading continues to extremes (Figure 21, Movie 4) over the next ~10 hours. First buckling events following this tissue spread happen between 42 and 48 hpf (Movie 6). The PSE continues to proliferate after the first buckling and by ~60 hpf, a heavily folded PSE structure will have formed (Figure 19, Movie 5). Staining the folded *hdac1*^{-/-} samples for the ECM component laminin revealed that the basal lamina remains at the basal surface of the retinal epithelial cells as the gap between the retinal PSE and the lens increases (Figure 21C). Few dim ECM tether-like structures seem to span the space between the two ECM domains, the retinal and the lens ECM (Figure 21C'). The retinal tissue is not the only eye component affected by the *hdac1* mutation. In the WT condition, the lens continues to grow along with the retinal neuroepithelium. Conversely, the lens in the *hdac1*^{-/-} condition, once separated from the retinal tissue, ceases to increase its size (Figure 21B). The squamous RPE tissue surrounding the retinal PSE does not fold with it, but instead remains smoothly surrounding the buckling tissue (Figure 21D).

Live imaging allowed me to describe the sequence of events leading to the folded *hdac1*^{-/-} phenotype. The *hdac1*^{-/-} retinal PSE proliferates at a slightly lower rate than the WT and keeps its PSE properties throughout development. After 36 hpf, significant shape changes occur, including a spread from the lens and buckling. The first buckling event usually occurs in the proximal domains, i.e., in the regions behind the lens. Shortly after, other buckles follow throughout the tissue, in a non-stereotypical manner. The resulting folds do always start from the apical surface, but in the end, the basal surface is buckled as well and the whole apico-basal tissue axis affected by the folding. By ~60 hpf, the retinal PSE is severely folded, but it continues to proliferate, with many divisions still taking place at the apical surface (Figure 19A PH3 panel).

The spread of the tissue is the first event where the *hdac1*^{-/-} PSE looks clearly distinguishable from the WT. This indicates that, at the stage when the spreading initiates, an unknown parameter starts differing from the WT tissue. A hypothetical change on the cellular level might alter the force balance in the tissue, resulting in a perturbed shape. To first quantify how the shape of the *hdac1*^{-/-} tissue changes with respect to the WT, I analyzed the aspect ratio, in the same 3D analysis workflow as I employed for the WT, by segmenting the apical tissue surface and measuring the tissue thickness in multiple regions. While in the WT the aspect ratio stays constant during growth, the aspect ratio of the *hdac1*^{-/-} tissue decreases (Figure 22A), quantitatively confirming a shape change. The aspect ratio of cells showed that, contrary to the WT and to the *hdac1*^{-/-} tissue aspect ratio, these cells do not change their shape (Figure 22B). So, the very prominent thinning of cells shown in the WT is absent in the *hdac1*^{-/-} condition.

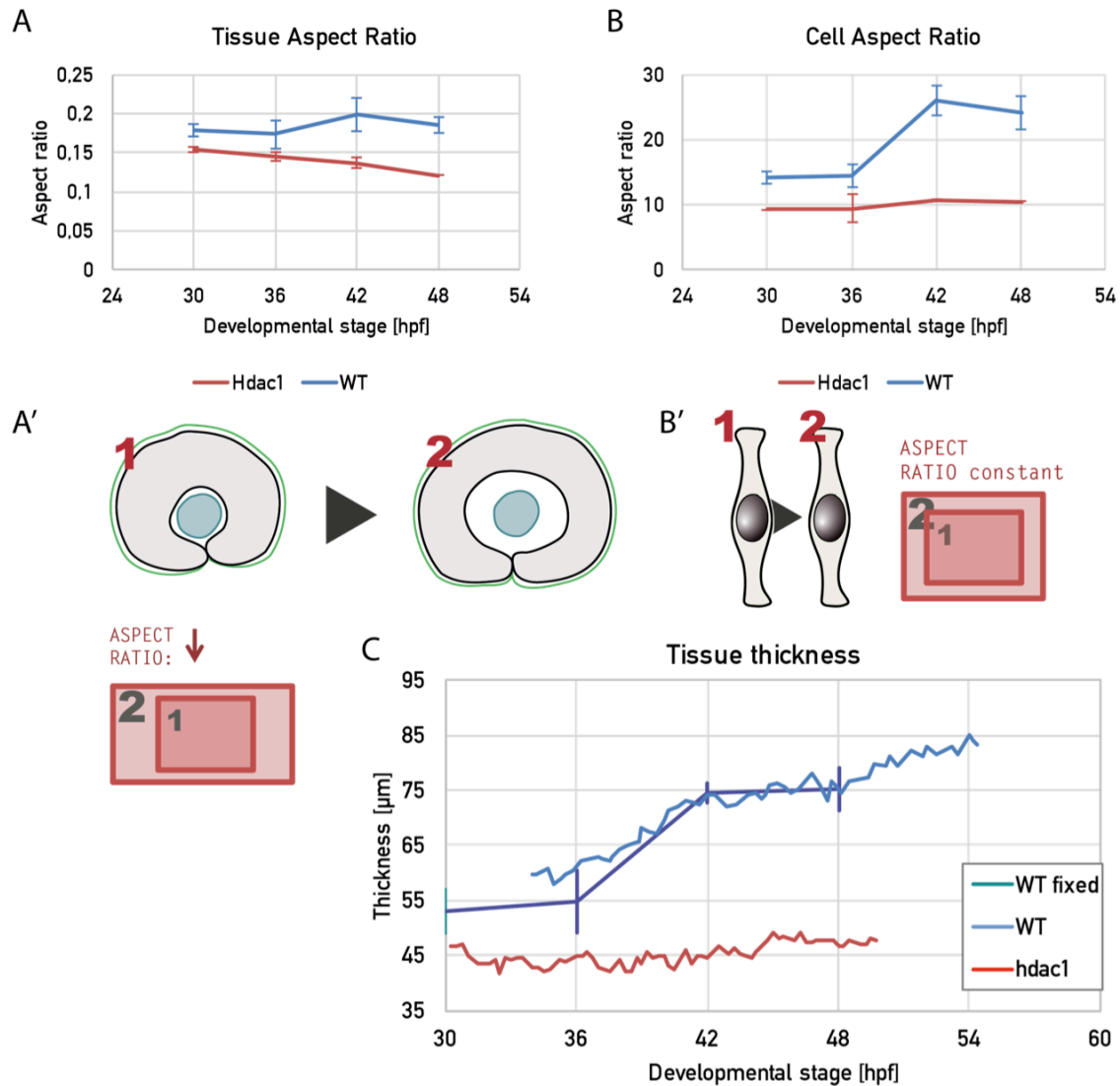


Figure 22: Hdac1^{-/-} retinal PSE changes its shape due to a lack of cell height increase.

A) Tissue aspect ratio of the retinal PSE decreases in *hdac1^{-/-}* fish, pointing to change in shape A') evident from the spread phenotype and detachment from the lens.

B) Tissue shape change in the *hdac1^{-/-}* arises from cells not changing their shape during development. Cell shape in the *hdac1^{-/-}* does not change, unlike the shape of WT cells, which become longer and thinner. B') This aspect ratio conservation in the *hdac1^{-/-}* might be due to the cells increasing their apical surface area more than the WT, or due to the cells not increasing their height. Data points are mean \pm SD.

C) Tissue shape in *hdac1^{-/-}* arises from cells not increasing their height. Cell height in *hdac1^{-/-}* remains at constant 45-50 μm throughout development (red), as revealed by height measurement from live imaging. Such measurements recapitulate cell height measurements from fixed images (blue).

Altogether, shape changes are opposite in the WT and *hdac1^{-/-}* : in the WT, cells change their shape and this allows the tissue to keep its shape. In the *hdac1^{-/-}* , cells do not change their shape and consequently, tissue shape is perturbed. This showcases how cells, by not adjusting their shape as the tissue grows, can affect the final shape of the entire tissue. The decrease in the aspect ratio (height/ $\sqrt{\text{area}}$) of the *hdac1^{-/-}* tissue points to two

extreme possible causes. Either, i) the apical tissue area increases more than in the WT, or ii) cell height does not increase/ it decreases. Comparing the cell height and tissue area parameters in the *hdac1*^{-/-} condition to the WT revealed that cell height (tissue thickness) does not at all change during *hdac1*^{-/-} development (Figure 22C), while the apical tissue surface grows indistinguishable from the WT values (not shown). This indicates that, in the *hdac1*^{-/-} condition, the perturbed tissue shape is caused by a putative brake on cell height increase. As the tissue's apical area ultimately increases greatly with folding, but cell height does not, this indicates that cell height is a stronger constraint than tissue apical area. Therefore, seemingly apically constrained PSE such as the retinal neuroepithelium can increase their apical surface if needed, showcasing how cellular constraints can alter tissue-level constraints. I next proceeded to search for the factors that might be responsible for the "freeze" of cell height in the *hdac1*^{-/-} and for the nature of such a hypothetical brake on height.

3.5 Basal actin accumulation is preserved in *hdac1*^{-/-} cells

Cell shape does not change in the *hdac1*^{-/-} condition, leading to a perturbation of tissue shape during growth. As discussed in the Introduction, cell shape is very often governed by localized contraction, stabilization or reorganization of the cortical actomyosin meshwork. Therefore, it might also be responsible for the shape changes, or lack of, that I see during retinal PSE development. To check whether actin might be differently distributed in the *hdac1*^{-/-} and WT cells, I labelled the polymerized, F-actin pool in the cells using a GFP-fused utrophin, which is an F-actin-binding protein (Burkel et al., 2007). I used RNA-injection of the EGFP-UtrophinCH or the transgenic line (Tg(*actb1::EGFP-UtrCH*)) to visualize F-actin distribution within living cells without affecting it. For staining F-actin in fixed samples, I used phalloidin, an F-actin binding mushroom toxin and a well-established actin marker for fixed cells.

3.5.1 Basal actin accumulation persists in *hdac1*^{-/-} mutants

To examine the distribution and dynamics of F-actin, I imaged both WT and *hdac1*^{-/-} fish with nuclei and F-actin labelled live for ~20 h using a light sheet microscope. At the basal portion of the tissues until ~42 hpf, F-actin distribution was strongly biased towards the basal region in all cells, both in WT and the *hdac1*^{-/-} (Figure 23A, D).

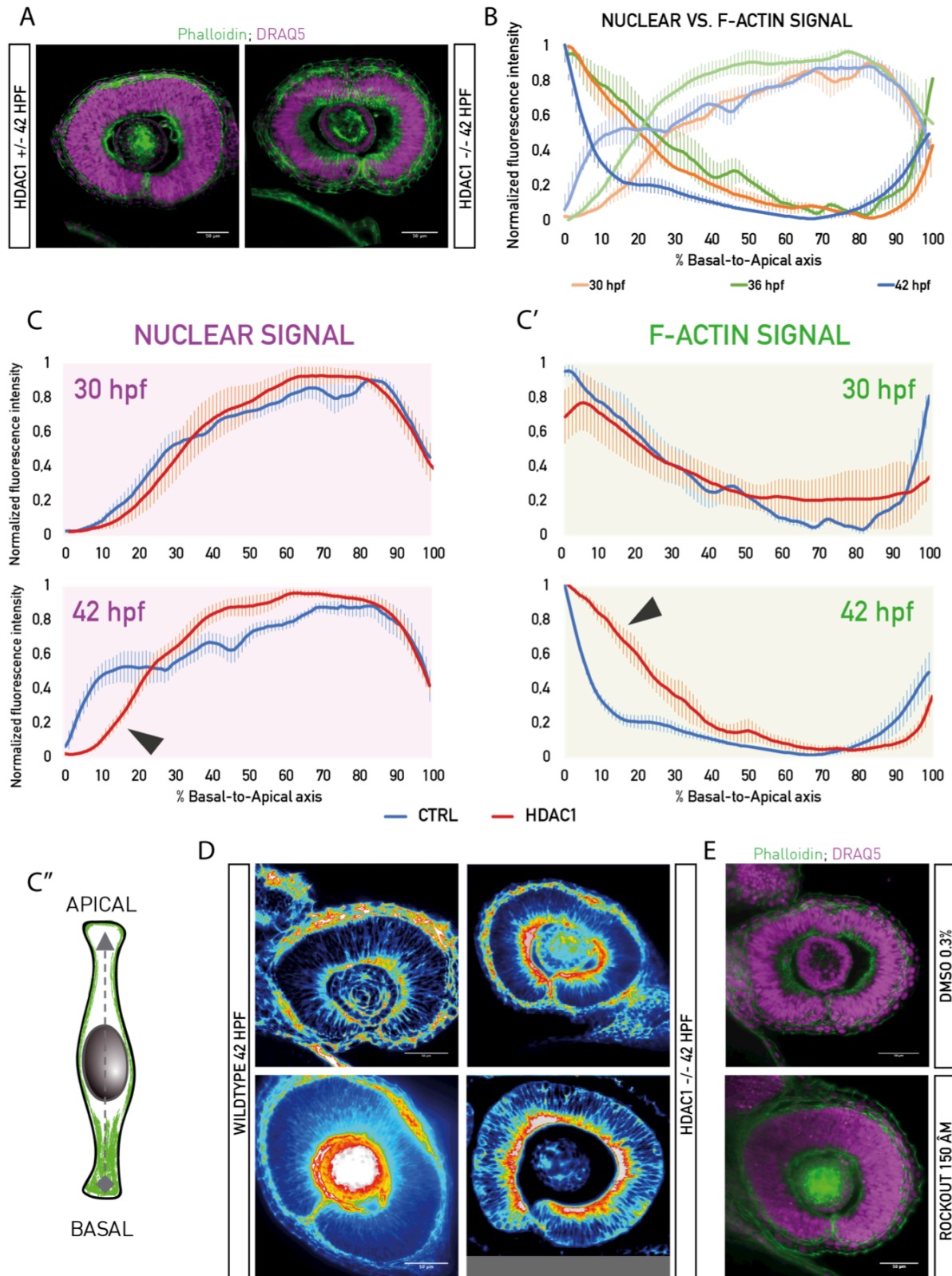


Figure 23: Basal actin accumulation persists throughout *hdac1*^{-/-} development.

A) Phalloidin staining revealed a prominent basal accumulation of actin in *hdac1*^{-/-}, spanning the entire basal region of the tissue. This accumulation is not present in the WT at the same stage (42 hpf).

B) Phalloidin and nuclear (lighter color shades) signal intensity were measured in the WT at 30, 36 and 42 hpf. Data normalized to min and max values and shown as mean \pm SEM. N=3-9/stage.

C) Signal intensity profiles for phalloidin in young (30 hpf) and older (42 hpf) embryos. At 30 hpf, both WT and *hdac1*^{-/-} tissues show a prominent basal accumulation. At 42 hpf the accumulation disappears in the WT, but persists in the *hdac1*^{-/-} tissue (arrowhead). Data normalized to min and max values and shown as mean \pm SEM. N=3-9/stage.

C') Signal intensity profiles for nuclear signal in young and older embryos. At 30 hpf, both WT and *hdac1*^{-/-} tissues have a basal zone devoid of nuclei. At 42 hpf, this zone disappears in the WT, in correlation to the disappearance of the basal actin accumulation. In the *hdac1*^{-/-}, the basal nuclear exclusion zone persists also at 42 hpf. C'') An illustration depicting the approach to measure the apico-basal intensity profiles. Data normalized to min and max values and shown as mean \pm SEM. N=3-9/stage.

D) Heatmaps showing the persistence of the basal actin accumulation in the *hdac1*^{-/-}. Blue: low signal intensity, white: high signal intensity.

E) The basal actin accumulation establishes the nuclear exclusion zone. In Rockout-treated *hdac1*^{-/-} embryos, the otherwise persistent basal actin is removed, as well as the nuclear exclusion zone.

The distribution of the actin signal was analyzed by plotting a normalized signal intensity along the apico-basal axis of the cell (see section 2.3.5 for more details). The actin-rich cell region was completely devoid of nuclei, creating a distinct nuclear- and a nuclear-exclusion zone in the tissue (Figure 23B). As seen from the movies, this separation seems extremely robust, as nuclei never crossed into the basal, actin-rich region and all nuclear migration typical of the PSE was confined to the more apical, nuclear region. At ~42 hpf, however, this basal accumulation disappeared in the WT and the nuclei filled up the basal tissue zone, as well (Figure 23B). In the *hdac1*^{-/-}, however, the basal bias did not disappear at 42 hpf, but persisted indefinitely (Figure 23C'). The *hdac1*^{-/-} tissue also maintained the nuclear zone sharply separated from the basal actin-rich zone throughout growth, suggesting a causal relationship.

To target actin and see if this perturbation changes nuclear distribution, I used the Rho kinase (Rock) inhibitor Rockout. At 150 and 175 μ M and ~3-5 hours after start of treatment, Rockout perturbed actin and, consequently, the nuclei indeed occupied the basal zone of the tissue (Figure 23E, Movie 8 and 9). This effect could be reproduced both in the WT before 42 hpf and in the *hdac1*^{-/-} after 42 hpf, removing the otherwise persistent basal accumulations. This result indicated that the basal actin bias establishes the nuclear exclusion zone in both *hdac1*^{-/-} and WT.

3.5.2 Basal actin accumulation disappearance is cell non-autonomous

The disappearance of the basal actin accumulation in the WT disappears synchronously, tissue-wide ~40 hpf (Movie 7). However, we do not know whether this is a concerted action of cells governed by intrinsic, cellular signals, or a response to a tissue-wide, cell-extrinsic cue. To check whether the basal bias disappearance is a cell-autonomous event, cells from the accumulation-losing, WT cells, were transplanted into the bias-maintaining *hdac1*^{-/-} environment and vice versa. To first introduce WT cells into the *hdac1*^{-/-} tissue, the method of blastomere transplantation was utilized (Figure 24A). In this

technique, cells are taken up from a donor embryo between the "high" and "oblong" developmental stage, (~3.5 hpf). They are then transplanted to an acceptor embryo of the same stage, where they integrate into the tissue and develop with the acceptor. To have a readout of the transplanted cells and the actin in the older embryo, cells were taken from the donor transgenic line and transplanted into the *hdac1*^{-/-} or +/- acceptors. Homozygous mutant acceptor fish were identified after 42 hpf, fixed and stained for nuclei (DRAQ5) and F-actin (phalloidin). This allowed me to have a readout of i) which cells were transplanted and their actin distribution (EGFP-UtrCH⁺ donor cells) and ii) of the actin distribution (phalloidin signal) and the nuclear zone (DRAQ5 signal) in the acceptor mutant fish. The results were strikingly uniform in all transplanted cells in all imaged mutants and showed that WT cells maintain both their actin bias and nuclear exclusion zone at 42 hpf in the mutant tissue, indicating that bias disappearance is cell non-autonomous (Figure 24A'). In the opposite experiment, I tested if the *hdac1*^{-/-} cells maintain their bias in the WT environment. To check this, I introduced *hdac1*^{-/-} cells into the WT tissue in a mosaic fashion, by injecting the previously published *hdac1*^{-/-} morpholino (Stadler 2005) into single cells at the 64- to 128-cell stage. This delivered the morpholino only to a subset of cells. To make sure the morpholino was functional, I injected it into 1-cell stage embryos. In this case, 100% of fish indeed showed the typical *hdac1*^{-/-} overall phenotype, as well as the heavily folded retinal phenotype by 60 hpf. To detect injected cells, I co-injected the morpholino with RNA of a fluorescently tagged nuclear marker, H2B-RFP and fixed the fish at 42 hpf (Figure 24B). In these retinal tissues, all WT cells showed the loss of the nuclear exclusion zone, in line with their developmental stage (Figure 24B). The *hdac1*^{-/-} morpholino-knockdown cells followed the WT morphology, increasing their height at 42 hpf and removing the nuclear exclusion zone, something they never exhibit in the full *hdac1*^{-/-} tissue (Figure 24B). Together, these results suggest that the basal bias disappearance and cell height increase in the WT, as well as the basal bias and nuclear zone exclusion maintenance are cell non-autonomous phenomena.

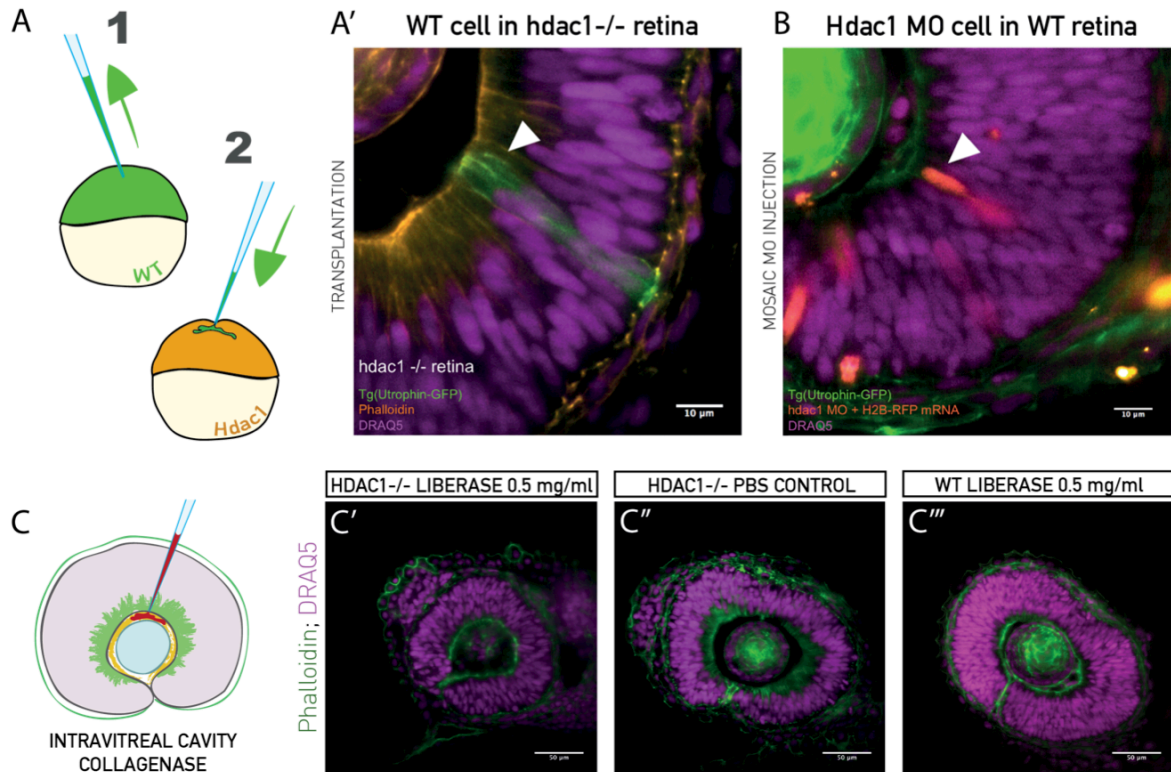


Figure 24: Basal actin accumulation disappears cell non-autonomously and is ECM-dependent.

A) Schematic of the transplantation experiment. Blastomeres from Tg(*actb1*::EGFP-UtrCH) embryos were transplanted into acceptor *hdac1*^{-/-} embryos between high and sphere stage. A') WT cells in *hdac1*^{-/-} tissues do not lose their basal actin accumulation at 42 hpf (green cells, arrowhead), when it would otherwise be lost in WT environment.

B) Mosaic injection of *hdac1* morpholino (MO) into Tg(*actb1*::EGFP-UtrCH). Cells with *hdac1* MO were co-injected with H2B-RFP mRNA for visualisation. Their basal actin zone disappears at the same time as in the WT (orange cells, arrowhead).

C) ECM integrity was perturbed by injecting collagenase (Liberase) into the intravitreal cavity. C') After enzyme activation, the basal actin accumulation disappears in 42 hpf *hdac1*^{-/-} tissues and C'') remains intact when PBS is injected as control. C''') Collagenase injection abolishes the basal accumulation in young WT embryos, as well.

3.5.2.1 Nuclear exclusion zone is ECM-dependent

Actin organization in cells is known to depend on the ECM and cell-ECM connections, as described in the Introduction (e.g., in section 1.4). In order to check if the ECM might be the external cue coordinating actin reorganization throughout the tissue, I degraded it using matrix-degrading metalloproteases. As collagen IV is one of the main structural components of epithelial basal laminas, I injected collagenase into the intravitreal cavity (between the lens and the retina) of the fish eye using a glass needle (Figure 24C). More specifically, I injected highly functional collagenase (Liberase, Sigma-Aldrich) into the eye cavity at 30 or 36 hpf (when bias is present) in both WT and *hdac1*^{-/-} fish. I activated the enzyme on 37 C for 30 minutes and then either fixed the fish immediately, to see if collagenase disturbed

the actin accumulation, or allowed them to recover several hours (*hdac1*^{-/-}) to see if the bias will regenerate. In ~40% of both WT (Figure 24C''') and *hdac1*^{-/-} (Figure 24C') of the injected fish, the bias was gone after the collagenase treatment and remained intact in the PBS-injected control (Figure 24C''). This experiment indicated that the basal actin accumulation in WT and *Hdac1*^{-/-} is the same, ECM (collagen)-dependent structure.

3.6 Actin reorganization and proliferation allow cell height increase

3.6.1 Cell height increase does not depend on neuronal delamination

The delamination of differentiating cells in the retinal PSE disturbs the homogeneous tissue structure by starting to introduce distinct cell layers into the otherwise monolayered epithelium. Moreover, the first-born retinal neurons, the retinal ganglion cells (RGCs) actively migrate towards the basal portion of the tissue. To check if such movements and structural change might contribute to the progenitor-cell height increase, I inhibited the production of the RGCs using the *Ath5* morpholino (Icha et al., 2016; Pittman et al., 2008; Randlett et al., 2013; Weber et al., 2014). Using live imaging (Movie 10), I measured cell height in *Ath5* morphant retinas from 42 hpf onwards, as the apico-basal tissue axis, as in other cell height analyses. However, RGC absence did not result in any significant change in tissue size or shape, as the tissue still grew and kept its shape as the WT, indicating that RGC delamination does not affect overall tissue form. Cell height was already increases at 42 hpf when imaging started, irrespective of the lack of delamination (Figure 25A), showing that cell height increase does not depend on neuronal migration or differentiation.

3.6.2 Cell height increase is proliferation-dependent

After 40 hpf, the basal actin accumulation in WT disappears tissue-wide (Movie 7) and the nuclei move and inhabit the basal zone. I was able to reproduce the removal of the nuclear exclusion zone by actin (Rockout) or ECM perturbations (collagenase). These experiments showed that the basal actin accumulation is indeed responsible for the maintenance of the nuclear exclusion zone. However, they failed to reproduce the WT cell height increase, indicating that a disturbance of the basal actin is not sufficient to trigger cell elongation. The perturbations of actin or the ECM were also lowering or inhibiting proliferation, as these structures are necessary for cell division. Mitosis requires unperturbed actin assembly and reorganization processes to drive cell rounding and cytokinesis and cell-ECM attachments are known to be essential for cell proliferation (anchorage dependence). My perturbations of the basal bias, therefore, possibly failed to reproduce the cell height increase because they interfered with proliferation.

To check whether cell height increase is proliferation-dependent, I blocked proliferation in the WT. From 30 to 48 hpf, I treated the WT fish with a combination of hydroxyurea (HU) and aphidicolin (A), the already mentioned inhibitors of S-phase progression (Harris and

Hartenstein, 1991). In the HU+A condition, the basal bias was physiologically gone at 48 hpf in the WT and the nuclear exclusion zone disappeared, but cell height did not increase past 50 μm (Figure 25B). This indicated that cell height increase in the WT is indeed proliferation-dependent.

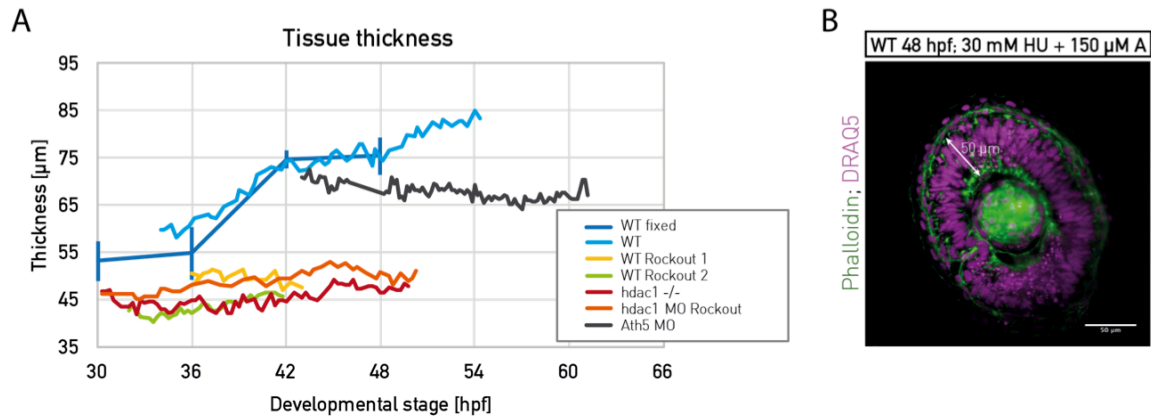


Figure 25: Cell height increase depends on proliferation.

A) Live measurements of cell height. Treatment of hdac1 MO tissues with Rockout did not induce an increase in cell height. The same effect was observed in the WT tissues where height physiologically increases, indicating that Rockout treatment inhibits height increase. Height increase does not depend on neuronal delamination (grey line), as it increases normally in WT tissues injected with Ath5 MO to inhibit RGC differentiation.

B) Cell height increase in the WT is proliferation-dependent. In older HU+A-treated embryos height does not increase despite the disappearance of the basal accumulation.

3.6.3 Actin reorganization is necessary for cell height increase

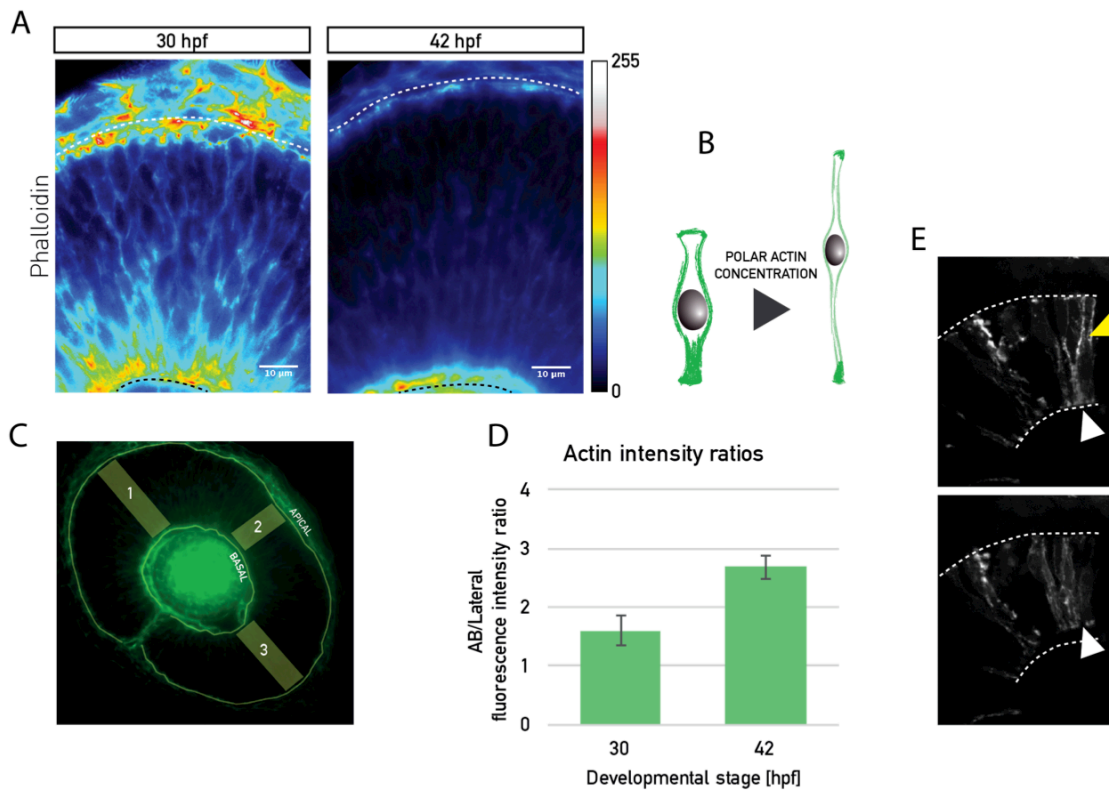
To understand how actin reorganization occurs and how it relieves the brake on cell height, I investigated the changes in actin distribution in more detail. The actin signal seems to get depleted from the lateral plasma membranes as the basal accumulation disappears and cell height increases (Figure 26A). To analyze this change in actin distribution at the apical and basal cell poles and the lateral membranes, I measured phalloidin intensities at the apical and basal surfaces, as well as the lateral, cell-cell interfaces (Figure 26C).

Table 6: Summary of basal actin experiments.

Cell height increases only if basal bias is reorganized and if proliferation persists, suggesting that both are necessary and together sufficient to increase cell height.

Basal actin	Proliferation	Height increase	Condition
+	+	NO	hdac1 ^{-/-}
+	-	NO	HUA hdac1 ^{-/-}
-	+	YES	WT
-	-	NO	Rockout WT or hdac1 ^{-/-} ; HUA WT

I plotted the ratios of this apical or basal signal, to the lateral signal at 30 hpf and 42 hpf. At 42, the ratios increased compared to the 30 hpf (Figure 26D). This revealed that the actin

**Figure 26: Actin concentration at the cell poles might be permissive for cell height increase.**

A) Heatmap of phalloidin signal in WT tissue at 30 and 42 hpf.

B) Model of actin reorganization at 42 hpf. Actin concentrates at the poles and/or gets depleted from lateral cell membranes.

C) Analysis of actin intensity ratios. Actin intensities were measured along apical, basal and lateral membranes in Fiji. Measurement was done on a z-plane at the central region of the tissue. Signal intensities were measured along the entire apical and basal surfaces and at 3 lateral regions (nasal, central and temporal).

D) Ratio of average apico-basal actin signal intensity, to the average lateral intensity. Higher ratios with cell height increase, at 42 hpf, indicate a polar concentration/lateral depletion of actin.

E) Laser ablation in WT tissue. Cell cortex is labelled mosaically by Utr-GFP mRNA. Upon a lateral cut (yellow arrowhead), cells collapse along the apico-basal axis. White arrowheads denote current tissue position and dashed line initial tissue position.

meshwork undergoes a cell-wide reorganization, that can be due to two reasons: either the lateral actin pool is depleted even more than the disappearing bias, or, polar pools concentrate more actin than the lateral pool.

I can at the moment not distinguish between these two possibilities, but the change in the ratio itself might be enough to act permissive on cell height change, by altering the force balance along the plasma membranes. Such a change in cortical organization might induce a tension redistribution within the cells and play a role in cell height increase (Figure 26B). A similar reorganization of concentrating actin at the poles is predicted by a 3D vertex model (see section 4.2.7.1). In this model, the change of the ratio of contractile actin pools in a cylindrical cell changes the tension distribution along the membranes. The tension ratios between apico-basal and lateral actin pools can then drive cell height increase.

To examine how tension is distributed along the apico-basal axis and whether it might indeed restrict cell height, I probed for cell contractility along the axis. Here, preliminary data from laser ablations of these lateral membranes showed that PSE cells are under apico-basal tension, as they collapse towards the cell center upon the cut (Figure 26E, Movie 11 and 12). More analysis will be necessary in order to have a map of cell tension at the apical, basal and lateral interfaces and to know how it changes as cells become longer.

In summary, my findings explain how specific cellular parameters contribute to proper growth and correct shape of the retinal neuroepithelium. I highlight a dynamic homeostasis of cell shape, showing that timely cell height increase is essential to maintain retinal tissue shape during growth. This height increase depends both on proliferation and on timely actin reorganization, which is possibly driven by a change in cell-ECM attachments. My data points to the basal accumulation of actin imposing a brake on cell height increase, thus defining height as the greater constraint during tissue growth than the previously proposed apical surface. With the release of such a brake, cell height is allowed to increase and is not the major constraint any longer. Taken together, my data showcases the importance of precise coordination of proliferative growth to tissue-wide cell shape changes and reveals that tissue-wide constraints need to be dynamic in order to maintain shape while changing size of the retinal neuroepithelium.

4 DISCUSSION

In this thesis, I identified changes in tissue size and tissue shape and explained how their coordination occurs at the cellular level in the developing zebrafish retinal neuroepithelium. From my findings I propose that, as the tissue grows, mechanical conditions at the cellular level change and cell height becomes the major physical constraint governing development of tissue shape. At that point, cells release an ECM-dependent actin brake that previously inhibited cell height increase. By this cortical reorganization, cells redefine the major constraint, by distributing it between height and area increase. This timely coordination of shape changes to tissue size allows tissue shape to be maintained throughout development and might be essential to maintain retinal function as well.

The retina is a part of the central nervous system and functions in the optical path of the eye to deliver unperturbed visual impulses to the brain. Even a minor perturbation of its shape in the human eye (macular pucker) leads to distorted vision, so one can argue that a smooth hemispherical shape is essential for retinal function. My results showcase the severe consequences on tissue shape if timely coordination of tissue-wide cellular responses is perturbed. By this, I demonstrate a dynamic cell shape homeostasis during tissue growth, necessary in order to maintain the shape and function of the zebrafish retinal neuroepithelium.

In this chapter, I discuss my findings on how cellular contributions contribute to growth of retinal PSE and the reason cell height increase is essential to maintain retinal shape. I relate these findings to other PSE systems, state the open questions and propose future studies that should help answer these questions.

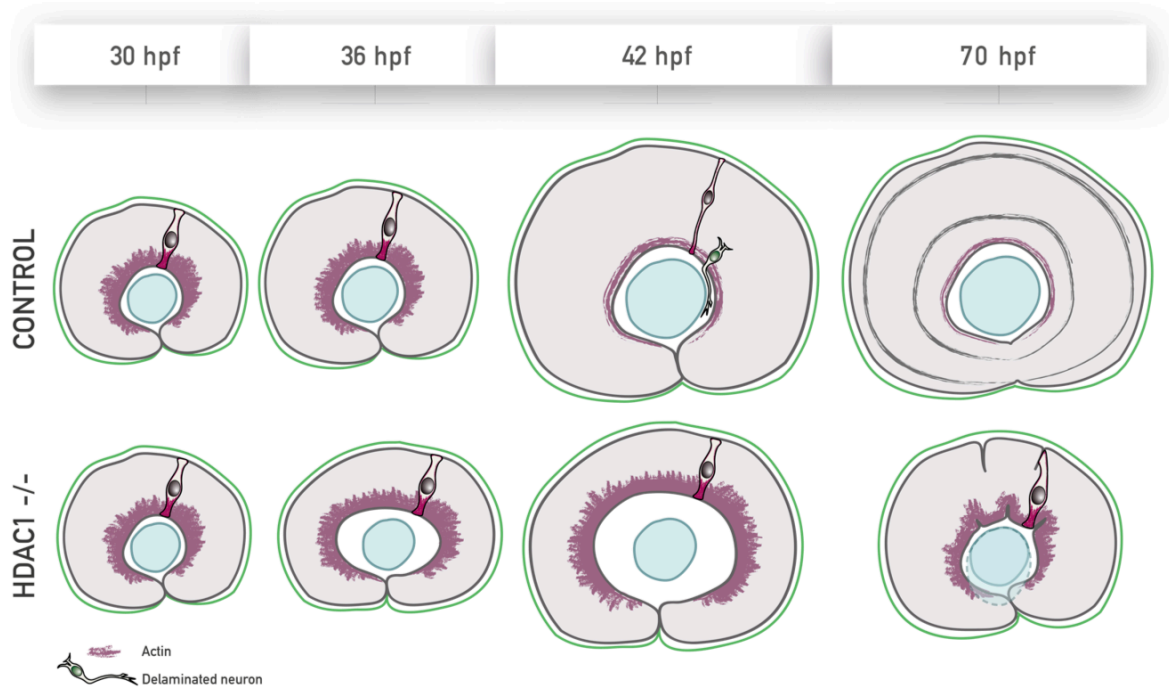


Figure 27: Graphical summary.

Actin reorganization releases a brake on cell height and allows maintenance of tissue shape during growth of the retinal PSE.

CONTROL: In wildtype fish, an ECM-dependent basal accumulation of actin (purple) disappears ~40 hpf. Actin signal gets concentrated at the apical and basal cell poles and depleted from the lateral membrane. Actin reorganization occurs synchronously throughout the tissue. An increase in cell height depends on this reorganization, as well as on cell proliferation and is necessary to maintain tissue shape.

HDAC1 -/-: In the *hdac1* mutant fish, that do not differentiate, basal actin accumulation persists throughout development, cell height does not increase and tissue shape is perturbed. The perturbation is detectable from ~36 hpf, when the tissue starts spreading away from the lens while keeping its thickness constant. Eventually, growth promotes apical buckling and with progression of this condition, the mutant retina will be heavily folded by ~60 hpf.

4.1 GROWTH OF THE ZEBRAFISH RETINAL PSE

4.1.1 Two phases of growth in the retinal PSE

Based on my growth analysis, I distinguish two phases of retinal PSE growth, the first one before and the second one after 40 hpf. The zebrafish retinal neuroepithelium is a cup-shaped PSE that proliferates and grows during ~20 hours of development, between 20 hpf and 42 hpf. Between the two proposed growth phases, major changes occur in the growing tissue. Differentiation starts in all tissue regions; cell number and cell height increase the most (Figure 9 and Figure 14, respectively); and overall cell cycles shorten and decrease their variability (Figure 11), mainly through changes in S-phase. The cell height increase from ~50 to ~68 μm in the WT between the two phases is essential to maintain tissue shape and is dependent on proliferation, but not on neuronal differentiation or delamination (Figure

25). The distinct growth characteristics in the two phases might reflect, for example, an underlying change in mechanical constraints that arises with changing size. Alternatively, they might reflect changes in upstream signaling cues. Based on my analyses, I suggest that a combination of the two, mechanical changes triggered upstream signaling cues, is most likely responsible for distinct cell and tissue characteristics in the two growth phases.

In a study from 2012, He and colleagues analyzed zebrafish retinal neuroepithelial growth, but with a focus on later developmental stages and differentiation (He et al., 2012), rather than tissue shape. The initial analysis of He et al. included an Imaris-based tissue-wide volume measurements and cell counts, similar to my analysis. The resulting data on growth differs somewhat between our two studies. E.g., in He et al. the number of cells at 48 hpf is 11000, which is ~7000 cell less than in my analysis and even ~4000 cells lower than in the previous stage of 42 hpf. This discrepancy is most likely due to differences in the way fish embryos were staged, as both of our analyses included a validation of the cell count. The major difference between the study of He and colleagues and this one, however, is in their result that retinal PSE proliferation is not uniform, but occurs in a proliferative wave preceding the differentiation wave. This finding is in contradiction to my analysis. The analysis of He et al. was based on Geminin-GFP, a marker of the FUCCI toolkit that labels cells in G2 and M phase of the cycle. Using the same marker, I was not able to observe such a wave (data not shown). They demonstrated a clear contrast in the proliferative regions of the tissue to the regions where the wave has not reached yet, which seemed completely devoid of dividing cells. I analyzed the distribution of progenitor cell mitoses on the apical surface (Figure 8) and could still not observe such a proliferative wave. After validating our method and confirming that I am indeed able to detect a wave if there is one, such as in the terminal dividing cells (Figure 8D'), I concluded that proliferation in the retinal PSE is homogeneous and indeed does not occur in a wave.

Besides studies on the zebrafish retinal PSE, studies of growth and shape of PSE tissues focus almost exclusively on the *Drosophila* wing disc. This tissue is an intermediate length PSE, as the retinal PSE, but is not a neuroepithelium and will not generate a laminated structure later in development. Rather, it will thin out and spread into the adult wing epithelium, maintaining a single cell layer. In the wing disc, cells transition from columnar into a cuboidal morphology, while in the retinal PSE they become increasingly pseudostratified. Therefore, the mechanisms underlying growth and shape changes in these two tissues most likely differ as they lead to the generation of different structures. In the zebrafish retinal PSE, uniform proliferation gives rise to homogeneous and isotropic growth. In the *Drosophila* wing disc PSE, non-uniform proliferation gives rise to uniform

growth (Mao et al., 2013). The interaction of multiple morphogen gradients across the wing disc tissue, such as the Wingless and Dpp, for example, affect and localize proliferation. This localized proliferation then affects cell density and in turn, compression and force distribution within the tissue, as presented in the Introduction. As cell divisions (mitotic spindle) orient along on the higher tension axis, division orientations in the wing disc are not random, but orient to relieve the tension. In the retinal PSE, conversely, division orientation is random.

Comparison of the growth in these two PSE systems, the zebrafish retinal neuroepithelium and the wing disc, indicates that it is not completely defined by the PSE architecture, but also depends highly on the molecular and physical parameters. It would be interesting to investigate to what extent PSE architecture governs growth in different systems, a topic I touch upon in section 4.2.2.

4.1.2 Cell cycle duration as a putative target of mechanoregulation in the retinal PSE

Using single cell live tracking, I showed that cell cycles are highly variable in the first growth phase (specifically, ~30 hpf), to then start decreasing their variability towards overall shorter lengths. ~40 hpf, overall cell cycles are shortest, taking ~5h. This overall shortening might influence tissue packing, by producing more cells in a given time and the variability in cycle lengths might affect the distribution of cell sizes in the tissue, to possibly make them more uniform prior to differentiation.

If cell growth and cell cycle are coupled in this tissue, the observed early variability in cell cycle lengths might be due to a variable concentration of a putative cell size regulator (rev. in Amoddeo and Skotheim, 2016), or reflecting a lower sensitivity to such a regulator. Furthermore, it might reflect underlying differences in the cell population, such as the elapsed time since attaining neuroepithelial character, or cells already poised for neuronal differentiation. Finally, variable cell cycles might change the variability of cell sizes (Di Talia et al., 2007), to e.g., decrease this variability through the first growth phase. A variable cell cycle, that makes the size of the cell population more uniform, would suggest that these cells act as sizers, (section 1.2.2.3), that add a specific amount of volume through the cycle, in dependence of the cell's initial volume (Cadart et al., 2017 preprint). However, the relation of cell cycle to cell growth in the retinal PSE is highly speculative and we need more data on the growth of single cells to start exploring this topic. At the moment, such an analysis can be done by manually segmenting single cells in 3D, live imaging datasets. Here, increased resolution, brighter markers and novel image analysis tools would help increasing the throughput and reproducibility of single cell segmentation. Follow-up studies should focus on how cell cycle length relates to cell growth and how the two might coordinate to affect tissue size in the retinal PSE.

After the initial overall shortening, in the second growth phase, cell cycles start lengthening again. Cell cycle lengthening was proposed to occur in differentiating mammalian brain neuroepithelium (Calegari, 2005; Lange et al., 2009). However, as in my analysis I tracked only progenitor cells, that have not turned on the neuronal marker (Ath5), the changes in cell cycle are not attributed to terminally differentiating cells. Lengthening might, therefore, indicate that the tracked progenitor cells are somehow already poised for differentiation after 40 hpf. This hypothesis should be investigated, possibly by a transcriptomic analysis of progenitor cells before and after 40 hpf. This would reveal which genes are differentially expressed between the younger and the older progenitor cell pool and whether they act in known differentiation-related pathways.

In addition to the total cell cycle length analysis, I tracked single cells through specific phases of the cell cycle. By this, I saw that the observed cycle lengthening after 40 hpf is due to a lengthening of S-phase, conversely to G1 lengthening (Lange et al., 2009) and S-phase shortening (García et al., 2016) as reported for the ventricular zone of the differentiating mammalian brain. This might be due to the fact that the retinal PSE tissue is at 40 hpf still predominantly composed of self-renewing progenitors, but it also might reflect fundamental differences in the development of the zebrafish retina and the mammalian brain, despite the fact that they both originate from a PSE neuroepithelium. The importance of regulating S-phase length was reported for the neural stem cell niche in the adult *Xenopus* retina (Cabochette et al., 2015). Here, S-phase was regulated by the Hippo pathway and its main effector, YAP. In absence of YAP, S-phase was too short, leading to an accumulation of DNA damage. YAP was also shown to affect the cell cycle in response to cell compression (Benham-Pyle et al., 2015) and to be expressed in the zebrafish retina (Joel B Miesfeld, 2014). These findings make it an attractive candidate to test in mentioned speed-up or slow-down of cell cycles and S-phase duration in the zebrafish retinal PSE. It would be interesting to check if YAP might mediate a putative response to tissue compression upon increased packing ~40 hpf, by inducing cell cycle lengthening. To test this possibility, experiments investigating YAP effects on cell cycle in the retinal PSE are first needed. Such experiments should focus on analyzing the cell cycle and cycle phases in the YAP mutant condition, in order to see if YAP might affect S-phase length in the retinal progenitor cells.

4.2 COORDINATING GROWTH CONSTRAINTS AND TISSUE SHAPE

4.2.1 Apical surface availability is not a constraint to retinal PSE growth

My growth analysis resulted in the quantification of how cellular contributions to growth, such as cell number, size, cell cycle or cell shape, change during retinal PSE development. With these parameters at hand, I was able to for the first time systematically test for previously proposed PSE growth constraints and their effect during development. In the 1970s, IHM Smart reported, based on his studies on the mouse spinal cord (Smart, 1972) and cortex (Smart, 1973), that neuroepithelial PSE increase their thickness as development progresses. In addition, he noted that the number of nuclear “layers” that they harbor under the apical surface increases, as well. Based on these observations and the fact that in the PSE all mitoses occur at the apical surface, Smart proposed the three possible constraints to further proliferation of an apically constrained PSE tissue: i) the cell apical endfoot might become too small for further subdivisions, ii) the tissue apical surface might become completely filled with rounded mitotic cells and unable to accommodate more, or iii) the amount of free apical surface is too small in relation to the number of nuclear layers under it that will reach apically by IKNM (Figure 16).

By estimating the surface area of the cell apical endfoot (type I proliferative trap), I showed that the average apical cell attachment decreases in surface area from ~28 to 8 μm^2 , staying at 8 μm^2 over the last two analyzed developmental stages (Figure 14C). This saturation might mean that the apical attachment reaches its minimal surface area and cannot decrease below 8 μm^2 . However, as the basal attachment becomes even smaller than the apical one, it might be physically possible to decrease the apical attachment further, as well. Basal cell attachments in epithelia differ significantly from the apical ones, though. They usually attach to the ECM components through integrins and do not harbor elaborate junctional belts, nor cilia, as the apical endfeet do. Because of these structural and functional differences, a comparison of minimal functional sizes of apical and basal attachments is misleading and I cannot say whether an apical endfoot smaller than our measured 8 μm^2 (1.8 μm^2 diameter) would be functional or not. Thus, I also cannot conclude whether apical endfoot size in the retinal PSE poses a limit to further increase in PSE packing, nor whether it might feedback to proliferation mechanisms to, e.g., lower the division rate to stop the apex from shrinking further. To test this possibility, the putative endfoot-constraint should be tested, e.g., by inhibiting neuronal delamination, so all cells remain attached apically and continue proliferating, to see if proliferation would stop. Analyzing apices of longer PSE cells, such as the radial glia and measure how their apical attachments change over time and how small they can be, could also provide insight into what the minimal area of the endfoot might be and whether it might limit proliferative growth in the PSE.

Retinal PSE grows in accordance with a proposed 3D constraint

The availability of the apical surface to accommodate more mitoses is another constraint proposed by Smart as a possible limit to PSE proliferative growth. It was, however, never tested over development of a PSE tissue. My analysis 3D analysis of how cellular parameters such as cell size and the cell cycle length contribute to tissue growth, allowed me to for the first time test this hypothesis, throughout the development. I showed that the total apical surface does not get saturated with mitoses at any point in development (Figure 15). By this, I showed that the constraint to PSE growth does not lie in the total availability of the apical surface (type II proliferative trap). Instead, the proliferative trap arises from the 3D architecture and nuclear movements of the PSE, i.e., from the ratio of free apical surface to the number of nuclei below it (Figure 16). This theoretical maximum is reached at ~42 hpf, coinciding with major neuronal delamination across the tissue.

In a continuation of this study, it would be interesting to confirm this finding, by analyzing whether the tissue adjusts its proliferation rate in a condition where the number of nuclear layers might cross the theoretical maximum, e.g., if delamination and cell cycle exit do not occur. This could include a condition where actin is reorganized and the actin brake on cell height, which I propose to act, removed while the tissue continues to proliferate. Using a combination of morpholinos, inhibiting differentiation by directly targeting specific neuronal subtypes in the WT might provide such a condition. Neuronal differentiation would be inhibited, cell cycle exit and delamination would not occur, but an increase in cell height and number of nuclear layers should still occur due to the tissue-wide release of the actin brake.

Growth in accordance with the proposed 3D constraint assumes that the PSE is apically constrained. If it was not apically constrained, the tissue could increase its apical surface upon reaching the packing maximum and escape the proliferative trap. My analysis of the apically folded *hdac1* condition revealed that the retinal PSE can increase its apical surface, if the constraint on cell height is greater. Here, my results stress that an apical constraint in an epithelium should not be viewed as a fixed constraint, but as dynamic and in relation to other constraints acting on the tissue, such as cell height. A study on the formation of the mouse neural tube also confirms this notion (Grego-Bessa et al., 2016). Here, the tissue has to remodel from a cuboidal epithelial sheet to columnar PSE cells to attain the PSE architecture. This elongation was shown to depend on stabilizing apical junctions via PDK1 kinase and PTEN. Stable apical junctions promote the formation of apico-basal microtubule arrays that help cell elongation (Grego-Bessa et al., 2016). Once the PSE architecture is formed, the tissue will elongate further as it grows, packing more nuclear layers under the apical surface. If cells cannot elongate and they continue to proliferate, as the tissue grows it will increase its apical surface, instead of thickness, as the *hdac1*^{-/-}. Ultimately, this will lead to a folded neural tube, a phenotype similar to the *hdac1* retina. This example from the

mouse neural tube, together with my study, suggests that apical surface indeed does not pose a constraint to further PSE growth if cell height increase is inhibited.

Altogether, these analyses of putative constraints to proliferation and growth limits in a PSE tissue suggest that in epithelia that are not thin, proliferative growth should be considered as a 3D problem. It would be interesting to investigate if cell cycle parameters, such as the observed lengthening of the S-phase after 40 hpf and progenitor cell cycle lengths in general, might be responding to a proliferative trap and the need for the tissue to lower its proliferation rate. Here, YAP represents an attractive candidate that might coordinate mechanosensation arising from the apical surface, with changes in S-phase. It would be fascinating if such mechanisms would indeed be identified and the upstream cues and downstream molecular cascades involved in their regulation dissected. This would provide insights into how proliferative growth of complex epithelial tissues such as the widespread PSE might be orchestrated with mechanosensation.

4.2.2 PSE shape in relation to tissue growth

PSE growth might be influenced by shapes of, elongated, PSE cells. My analyses revealed that the retinal PSE grows in accordance to the proposed 3D constraint. This constraint arises from the ratio of cells in the depth of the epithelium, i.e., the cycling nuclei that will occasionally reach the apical surface, to the availability of the apical surface. In the retinal PSE, the longer the cells are, the more nuclear layers are packed under the apical surface, affecting this constraint ratio. Therefore, the aspect ratio (thickness-to-area, i.e., shape) of the retinal PSE is related to its proliferative growth through the shape of the cells. Based on the proposed constraint, the shortest cell cycle length (proliferation) is defined as a product of 3 parameters: the number of nuclear layers (\sim cell length), cell size and the length of their mitoses

$$T_{CC}[h] \geq N_L \times T_M[h] \times A_M(\text{relative}) \quad (5)$$

Such a shape-to-growth relationship might govern the form of PSE tissues, where cell height is not the major constraint and is increasing during development. We know that neuroepithelia other than the retinal PSE, for example the neural plate and the neural tube, are such PSE and increase their height during growth (Fish et al., 2008). The number of nuclear layers here increases proportionally to cell height during growth, most likely reaching the maximal predicted values (Fish et al., 2008; Smart, 1972). However, as mentioned before, such ideas on a direct relationship of PSE cell shape to tissue growth

have not been experimentally tested and we do not know how this possible constraint would develop over time, nor whether it defines, e.g., spinal cord growth and shape.

Several studies (Ma et al., 2017; Pastor-Pareja and Xu, 2011; Sui et al., 2012; Widmann and Dahmann, 2009a) analyzed cell shape in the wing disc PSE tissue and concluded that maintaining elongated, columnar cells is essential for tissue shape and function. However, these studies have not touched upon the limits to wing disc nuclear layering, nor on how cell height develops over time. Based on the 3D growth constraint for the PSE, the theoretical maximum of nuclear layers that the wing disc could accommodate is ~6, if the mitotic index is 4% [from time of mitosis is 20 min (Handke 2014) and cell cycle length 7 h (Dubatolova et al., 2011)] and relative size of a mitotic cell 4 (estimated from (Widmann and Dahmann, 2009a)). The wing disc thickness, however, accommodates 2-3 nuclear layers, similar to the retinal PSE in early stages and is, therefore, not growing at its maximum. This difference suggests that the 3D growth constraint might not be limiting growth in the wing disc. Even though this tissue and the retinal PSE are both intermediate length PSE and their cells are ~50 μm thick, the wing disc does not seem to thicken as much as the retinal PSE during growth, perhaps because it will transition into a squamous epithelium of the wing as it develops. Therefore, cell height might be a major constraint for wing disc PSE growth and the 3D constraint thus not governing its development. As mentioned in the Introduction, growth analyses of PSE tissues are few and most of the ones that do exist take into account only planar growth from the apical surface, making it hard to compare different tissues and propose more unifying growth principles. Therefore, I cannot speculate further on whether the above cell shape-tissue growth relationship might be applicable in other PSE tissues because their thickness (cell height) was not measured during growth.

Changes in PSE tissue thickness and cell shape are related to its growth and studying growth of PSE in all three dimensions is a prerequisite in order to gain full understanding of the events that determine the shape and size and, with this, the function of these abundant tissues. Although studies in the *Drosophila* wing disc revealed essential mechanisms of how signaling pathways, morphogens and planar forces govern PSE growth, 3D studies are absent (reviewed in Diaz de la Loza and B. J. Thompson, 2017), partly due to the limitations to imaging all three dimensions. With respect to studying PSE growth in 3D, the zebrafish provides a more adequate system, allowing new insights as showcased by this study.

4.2.3 Tissue and cell characteristics in the *Hdac1*^{-/-} retinal PSE

In order to test the limits to proliferative growth in the retinal PSE, I took advantage of the previously described *hdac1* mutant condition (Yamaguchi et al., 2005). Here, histone deacetylase 1 is knocked down by a nonsense mutation and this results in the lack of inhibition of Wnt and Notch signaling pathways. As Wnt promotes cell cycle exit and Notch

promotes cell differentiation in the zebrafish retina, the *hdac1* knockdown causes a complete lack of retinal differentiation and a continuous proliferation in *hdac1*^{-/-} fish. In my analysis, I show that in the *hdac1*^{-/-} growth scenario, a cell shape change, necessary to maintain tissue shape in the WT, is inhibited. Specifically, in *hdac1*^{-/-} fish, cell height does not increase between 36 and 42 hpf as in the WT and this leads to height conservation, tissue buckling and the previously observed folded, perturbed tissue shape. Such a severe perturbation of the otherwise smooth retinal surface would most likely perturb its function in the optical path of the eye.

Throughout the shape changes and folding of the *hdac1*^{-/-} retinal PSE, its “external” shape remains the same. I.e., a smooth ellipse can always be circumscribed to the tissue, raising the possibility that external constraints, that help maintain the shape, do not adapt to these perturbations in tissue shape. In accordance with this hypothesis, the RPE, the thin surrounding epithelium and a possible external shape determinant, remains to smoothly surround the retinal PSE surface in the *hdac1*^{-/-} fish, instead of folding with it (Figure 21D).

The effects of the *hdac1* knockdown in the eye are not restricted to the retina. I showed that the lens in the *hdac1*^{-/-} condition, once separated from the retinal tissue, ceases to increase its size, conversely to the lens in the WT, that continues to grow with the retina (Figure 21B). It would be interesting to investigate whether this difference might be due to the retinal tissue, its ECM, or other secreted factors providing instructive cues for the growth of the lens tissue. Such an effect, causing lens size that is disproportional to the retinal size might be another loss for eye function in the *hdac1*^{-/-} fish.

4.2.3.1 *Buckling in PSE tissues*

Folding of the zebrafish retinal PSE in the *hdac1*^{-/-} fish is a perturbation of tissue shape that is most likely incompatible with retinal function. Initial buckling always happens at the apical surface, but the position of the folds in the tissue seems random and the resulting folding pattern is not stereotypical. However, in other PSE tissues, buckling instability and tissue folding are regulated developmental processes and the function of these tissues depends on reproducibly generating the folded pattern (Pilot and Lecuit, 2005; Razavi et al., 2015).

In the gyrencephalic mammalian brains, folding during growth in early development generates a characteristic pattern of convex gyri (ridges) and concave sulci (grooves; (Razavi et al., 2015)). Even though the final adult patterns differ, main landmark grooves and their origin during development, are stereotypical. Multiple hypotheses exist to explain brain folding, including increasing cell numbers towards the basal, cortical plate, brought about by proliferation and cell migration and mechanical buckling. However, there is still no consensus on the overall mechanism, nor on how the typical positions of the early folds are

determined. Diseases that perturb brain folding, like lissencephaly (smooth brain) or polymicrogyria (miniature gyri), can have severe consequences on brain function and cause developmental defects, seizures or impaired muscle function, depending on the position and size of the affected folds (Jansen, 2005).

However, folding of the gyrencephalic brain differs greatly from the extensive folding in the *hdac1*^{-/-} tissue investigated in my study. Unlike folding in the fish *hdac1*^{-/-} retinal neuroepithelium, cortical folding occurs at the basal tissue surface. In addition, folds do not form in the purely PSE tissue architecture, but once specific layers of, e.g., apical, basal radial glia and neurons already start differentiating. Thus, folding of the cortical neuroepithelium is a tissue folding phenomenon fundamentally different than folding in the retinal neuroepithelium, despite generating a seemingly similar final structure.

In the *Drosophila* wing disc, three main folds divide the PSE tissue into regions (notum, hinge, blade, Diaz-Benjumea and Cohen, 1993; Sui et al., 2012) that will have specific functions during wing development and generate distinct structures of the adult wing. Folds form by apical shortening (Sui et al., 2012) at three points, giving rise to the hinge/notum, hinge/hinge and blade/hinge fold. Narrow stripes of specific molecular determinants define the position and cell identity of distinct folds. For example, the Iroquois complex (Iro-C) homeodomain proteins are expressed in the prospective notum wing disc fold. They specify body wall identity and cells lacking these proteins switch their fate from notum to hinge cells (Diez del Corral et al., 1999). Apposition of Iro-C expressing and non-expressing cells induces invagination and apico-basal shortening of the Iro-C- cells (Villa-Cuesta et al., 2007), aiding invagination and formation of the hinge/notum fold.

In summary, epithelial folding is a wide-spread mechanism to generate 3D shapes during morphogenesis (LeGoff and Lecuit, 2015; Pilot and Lecuit, 2005) and drives diverse processes such as invagination (*Drosophila* mesoderm invagination, zebrafish optic cup), functional determination (wing disc) and surface expansion (neocortex). Although the mechanisms driving buckling and folding might differ greatly between the retinal PSE and other epithelia, a putative constraint on cell height might act in other folding systems, as well, aiding morphogenetic changes by allowing preferential expansion of apical or basal surfaces. Future studies examining changes in cell shape during buckling of diverse tissues will be essential in order to investigate this possibility.

4.2.4 Nature of the brake on cell height

Based on my analysis of the shape perturbation in the *hdac1*^{-/-} condition and comparison to the WT shape development, I suggest that a brake acts on cell height increase in young (until 40 hpf) WT retinal PSE. This brake has to be released in order to allow cell elongation and maintenance of WT tissue shape. In the *hdac1*^{-/-} retinal PSE, this

brake persists throughout development, resulting in PSE cells never becoming longer than 50 μm . The brake on cell height takes the form of a prominent basolateral actin accumulation that spans the entire basal domain of the tissue (Figure 26A).

This actin accumulation is established early in retinal development, during the process of optic cup morphogenesis, where it is essential for basal cell constriction and the formation of the hemispherical tissue shape (Sidhaye and Norden, 2017). Therefore, the basal actin accumulation is a “morphogenetic relict” that persists indefinitely in the *hdac1*^{-/-}, while in the WT it gets removed at the end of the first growth phase, i.e., ~40 hpf. The actin accumulation is most likely a cortical, not medial cytoskeletal structure, as the basal view on the cells shows a membrane-bound, ring-like signal, with cytoplasm almost devoid of actin (Sidhaye and Norden, 2017). Myosin motors co-localize with this actin accumulation (Sidhaye and Norden, 2017), suggesting, together with the structure’s role in invagination, that it is contractile. Furthermore, I show that the basal actin establishes a tissue-wide zone devoid of nuclei (nuclear exclusion zone), a feature that can be used as a readout for the basal actin accumulation, even without an actin marker. Treatment with the Rho-kinase inhibitor Rockout perturbs actin accumulation and abolishes the nuclear exclusion zone in *hdac1*^{-/-}, as well as in the WT in the first growth phase, when the accumulation is still present.

In addition, I show that cell height increase in the WT depends not only on actin reorganization, but also on proliferation, as cells did not increase their height past 50 μm when proliferation was blocked by hydroxyurea and aphidicolin (HU+A) (Table 6). Therefore, both actin reorganization and proliferation are necessary to increase cell height. Direct testing of how the actin accumulation and proliferation affect cell height is difficult, as tools that interfere with actin organization interfere with proliferation as well. We would first need to develop tools that target specific actin pools in the cell, to perturb only the basal region. The first step towards such tools would have to identify the exact nature of the actin accumulation (e.g., actin bundles, stress fibers, meshwork, ...), as well as the molecular players organizing the actin in the basal portion of the retinal PSE, such as specific formins, capping or bundling proteins. Identifying the exact molecular players organizing actin in the basal portion of the retinal PSE is essential in order to be able to interfere with it specifically, without disturbing overall cortical activity, intracellular transport, or cell divisions (cell cycle).

Cell height changes in many systems during development, for example during initial formation of the PSE tissue architecture from cuboidal cells in the mouse neural tube (Grego-Bessa et al., 2016) or the wing disc (Widmann and Dahmann, 2009a). It would be interesting to see if a brake on cell height might limit cell elongation in such processes, as well.

4.2.5 ECM-dependence of actin brake

As the actin accumulation and its disappearance takes place in the basal tissue region, I investigated the effect that the underlying ECM (basal lamina) has on the actin bias and nuclear exclusion zone. It is already known that changes in the ECM composition and increased tension to the cell-ECM attachments can cause major cytoskeletal rearrangements, such as actin stress fiber formation (rev. in Burridge and Guilluy, 2016). In addition, as mentioned before, the basal actin accumulation, necessary for invagination during zebrafish optic cup morphogenesis depends on the ECM integrity (Sidhaye and Norden, 2017). Therefore, changes originating at the ECM are highly relevant candidates as external cues for basal actin removal. To test this, I have perturbed ECM organization using the collagen-degrading enzyme, collagenase, by injecting it into the intravitreal cavity of the eye. This treatment indeed removed the basal actin accumulation and the nuclear exclusion zone, suggesting that these features depend on an intact basal lamina. Proliferation, aside from many other epithelial features, depends on cell-ECM attachments so my perturbing of this connection probably inhibited proliferation, as well. While this effect should still be analyzed in more depth, severing of cell-ECM attachments is most likely the reason why collagenase treatment, even though it perturbed the basal actin, did not induce an increase in cell height as I showed this depends on proliferation as well as actin reorganization.

If the brake on cell height depends on the ECM and my data indicates that this is the case, a putative change in the ECM is possibly absent in the *hdac1* condition, causing the actin accumulation to persist and restrict cell height. The question remains of what exact change in the ECM might trigger actin reorganization and why exactly it is absent in *hdac1* retinas. Follow-up studies focusing on the mechanism of ECM-dependent actin reorganization should identify the ECM component or structural feature that changes with actin reorganization in the WT. Such studies could analyze the transcriptome for ECM genes, in different developmental stages of the WT and *hdac1*^{-/-} retinas, to investigate how their expression changes before and after brake release (~40 hpf).

4.2.5.1 *ECM in maintaining PSE shape*

My study points to a critical role of the ECM and/or cell-ECM attachments in maintaining tissue shape during retinal PSE development. This effect is most likely achieved through ECM-dependent timely tissue-wide cytoskeletal reorganization that allows cell height increase. Besides my data, several studies on the *Drosophila* wing disc showcase such a prominent role of the ECM in regulating the shape of PSE cells and tissues (Domínguez-Giménez et al., 2007; Ma et al., 2017; Sui et al., 2012).

Dominguez-Gimenez et al. (2007) showed that cell-ECM adhesions are essential for the formation of PSE architecture. During fly embryonic development, the wing disc PSE arises from a cuboidal epithelial sheet. Transition from cuboidal to pseudostratified columnar in wing disc depends on TGF-beta/Dpp (Gibson, 2005; Shen and Dahmann, 2005; Widmann and Dahmann, 2009a) and Wnt/Wingless signaling (Widmann and Dahmann, 2009b), as well as integrins (Domínguez-Giménez et al., 2007). This cell elongation into a cuboidal shape is necessary for the development of wing disc folds, that allow specific tissue regions to come in contact, a feature essential for future developmental steps and tissue patterning (Domínguez-Giménez et al., 2007). Cell-ECM attachments through integrins here provide an instructive, rather than a structural role for cells to become longer. The authors also propose that the maintenance of this developed columnar cell shape is ensured by lateral, not only basal, integrin-mediated cell-ECM attachments.

In the wing disc of a Dorsocross (Doc) mutant fly, (Sui et al., 2012) ECM degradation by metalloproteases and loss of cell-ECM attachments promotes tissue bending and perturbs the stereotypical wing disc fold formation, similar to the example above. Here, the degradation of the ECM inhibited proper organization of the microtubule cytoskeleton, which led to the cells changing their shape by shortening the apico-basal cell axis. Sui et al. present T-box Doc genes as novel regulators of ECM integrity and degradation and the ECM as an essential structural support that ensures proper cell shape changes, as well as tissue-wide shape remodeling of the wing disc PSE.

In the 2011 study by Pastor-Pareja and Xu and a follow-up study from 2017 (Ma et al., 2017), the authors also point to the major role that the ECM has in cell shape of the growing wing disc PSE. They confirm that ECM degradation induces shortening of PSE cells. In addition, the authors suggest that specific effects on cell shape depend on ECM composition, by affecting ECM and cellular mechanics. Knockdown of the ECM cross-linker Perlecan increased cell compression and changed cell shape by making cells longer and thinner, but had no effect on tissue size. Collagen IV loss, as well as ECM degradation by metalloproteases had the opposite effect, making cells shorter and wider. The authors suggest that this is due to lower compression being exerted by the ECM onto the wing disc, promoting cell relaxation. Additionally, Ma et al. suggest that ECM controls the escape of the morphogen Dpp from the tissue. As Dpp, a BMP/TGF-beta pathway ligand, promotes wing disc growth, this conclusion implies a role of the ECM in tissue growth not just through mechanisms of anchorage-dependent cell proliferations, but through retention of proliferation cues inside the tissue.

Aside from my study on the zebrafish retinal PSE and studies on the wing disc, the shape of the PSE in human retinal organoids was shown to depend on an intact ECM and cell-matrix adhesions, as well (Nakano et al., 2012). Here, ECM perturbation by integrin-

blocking antibodies abolished a basal nuclear exclusion zone, very similar to my results from the retinal PSE. The PSE structure and development of human organoids bares striking similarities to the zebrafish retinal PSE, more so than the mouse retinal organoids. This might suggest that, when it comes to retinal PSE tissue shape maintenance, the mechanisms behind human retinal PSE are more similar to zebrafish than to mouse. It would be very interesting to investigate these similarities and differences in more detail in a continuation of this study, to check for a brake on cell height in human retinal organoids and investigate how changes in cell height in this system might have to coordinate with overall tissue size, shape and differentiation to generate a functional retina-like tissue.

Regulating cell height might be an important developmental task for PSE tissues in general, possibly because of the necessity to coordinate their cell shape and proliferation (section 4.2.2) to regulate tissue shape. Here, the regulation of cell shape through the ECM might be a conserved mechanism. Based on the essential role that the ECM has in regulating cell shape in various PSE, I suggest that an intact ECM and cell-matrix attachments might be conserved regulators of cell and tissue shape during PSE development. Additional to the previous studies and based on my findings, I also propose that in the zebrafish retinal PSE, ECM composition and adhesions have to not only be intact, but also actively changed at a precise developmental time point in order to allow acute cell elongation and tissue shape maintenance during growth.

Although we now have many insights into the different roles and the importance of ECM and cell-ECM attachments in development of PSE tissues, the exact upstream mechanisms by which such regulation is achieved remain elusive. In the following section, I propose a putative mechanism by which timely cell-ECM regulation might act in the zebrafish retinal PSE. This mechanism might be suggestive of the possible molecular players regulating cell height in other PSE systems, as well.

4.2.6 Putative regulatory mechanisms for actin brake release

Upstream signaling cues most likely affect ECM and cytoskeletal organization during retinal PSE growth and play a role in coordinating tissue size and shape with, e.g., cell differentiation. Although I have not identified such cues, I can hypothesize what they might be based on previous studies.

Wnt and Notch signaling pathways are active in the zebrafish retinal PSE and become inhibited by Hdac1 in the WT, to allow cell differentiation (Yamaguchi et al., 2005). As this inhibition is absent in the *hdac1*^{-/-} retinas, Wnt and Notch signaling remain active and result in the folded retinal phenotype. As I showed that cell height conservation and a basal actin

accumulation in the *hdac1*^{-/-} underlies this tissue buckling and folding, I assume that lack of Wnt and Notch inhibition by Hdac1 might also govern the stability of the basal actin accumulation. The basal accumulation, in turn, depends on the ECM. We know that actin polymerization inside cells can be affected by the components of cell-ECM attachments (integrins, talins, kindlins, focal adhesion kinases), the components of the ECM itself, as well as tensions exerted on the attachments (Burrige and Guilly, 2016). All these parameters can trigger the formation (high tension) or disassembly (low tension) of actin fibers and bundles (rev. in Swaminathan and Waterman, 2016). This relationship suggests that Wnt and/or Notch might be involved in upstream regulation of the cell-ECM adhesion, or ECM composition or structure and through them regulate actin organization. In the WT, this would imply that timely physiological inhibition of Wnt and Notch by Hdac1 triggers an ECM change that reorganizes actin and releases the brake on cell height.

We are only beginning to understand how Wnt and Notch signaling pathways integrate with cell-ECM adhesion regulation (rev. in Astudillo and Larraín, 2014; LaFoya et al., 2016 respectively). A lot of evidence now exists that ECM components regulate Wnt and Notch. However, several studies also show the reciprocal relationship. For example, Notch signaling can increase the affinity of integrin cell-ECM receptors to collagen (Hodkinson et al., 2007; Leong et al., 2002), thus strengthening cell-ECM attachments. Non-canonical Wnt signaling can modulate dynamics of focal adhesions and regulate ECM assembly. The canonical, Wnt/ β -catenin signaling pathway, on the other hand, regulates the expression of genes encoding ECM proteins (rev. in Astudillo and Larraín, 2014). Therefore, by modulating integrin connections to the ECM, focal adhesions and ECM assembly, Wnt and Notch signaling indeed have the ability to modulate both cell-ECM force transmission and ECM composition and structure. Wnt and Notch inhibition by Hdac1 in the WT could, thus, trigger actin depolymerization inside the cell and result in the depletion of the basal actin pool. In the *hdac1*^{-/-} fish, Wnt and Notch are not inhibited, so in the previous scenario, the cell-ECM attachments, as well as ECM itself, would also be unaffected, basal actin pool preserved and cell height increase inhibited.

Another putative pathway by which Hdac1 might affect cell-ECM attachments and actin organization, is via Numb. During zebrafish optic cup morphogenesis, the Notch signaling antagonist Numb has been shown to affect basal cell constriction by inhibiting cell-ECM force transmission (Bogdanović et al., 2012). By promoting integrin endocytosis and depletion of focal adhesion kinase from the basal side of the cell, Numb depletes the basal actin pool. If Hdac1 would inhibit Notch via Numb activation, such an Hdac1-Numb pathway would constitute one more way by which Hdac1 might interfere with actin organization and cell height. However, a link between Hdac1 and Numb remains to be investigated.

In order to understand how exactly Hdac1 knockdown preserves the basal actin and cell height, follow-up studies should focus on investigating this molecular mechanism and upstream cues that trigger the ECM change. They should examine the role of Wnt/Notch signaling in the putative physiological change in the ECM ~40 hpf and how exactly this change might affect actin distribution, i.e., induces actin concentration at the apico-basal cell poles. The effect of Wnt/Notch on ECM composition could in the future be tested by transcriptomic analyses of ECM genes in different developmental stages of WT and *hdac1*^{-/-} retinas, to check how their expression might differ and whether *hdac1*^{-/-} transcriptomic profiles mimic young WT profiles with respect to these genes. The effect of Wnt and Notch on cell-ECM adhesion and force transmission will be difficult to test directly in the tissue and could be inferred from laser ablation experiments and quantitative image analysis (Goodwin et al., 2016) using high resolution imaging systems.

Overall, the molecular mechanism behind the developmental cell height increase in the zebrafish retinal PSE might include the interplay of Hdac1, Wnt/Notch and their effect on cell-ECM force transmission. Its elucidation could provide hints to how coordination of tissue shape and size might work in other PSE systems and could be tested for effect in the human retinal organoids mentioned above.

4.2.7 Physical models for tissue-wide cell height increase

4.2.7.1 3D vertex model predictions of cell height increase

Experimentally, it is difficult to directly show that the basal actin accumulation acts as a brake on cell height increase. To test this, I would have to not only generally perturb actin organization in the *hdac1*^{-/-} tissue, but induce the exact reorganization that occurs in the WT condition. I think (with Guillaume Salbreux) that the actin effect on cell height arises not just from removing the basal accumulation, but reorganizing it, by concentrating at the poles and depleting from lateral membranes. A 3D vertex model (Alt, 2016; Alt et al., 2017) predicts that such a redistribution would cause a change in the force balance of epithelial cells through redistributing tension, which could be sufficient to generate an increase in cell height. Unlike the more generally applied 2D vertex models, the 3D vertex model takes into account stresses not generated only at the apical cell surfaces and allows the study of complex 3D deformations of epithelia. It bridges the scales between vertex models and continuum models, to predict tissue wide cell behaviors, such as cell height and density changes, that originate from cell-intrinsic, as well as extrinsic, tissue-wide tensions and pressures. This model was successfully applied to describe shapes and stability of epithelial during 3D morphogenetic processes of *Drosophila* tissues {Alt:2016wn} and we plan to use it to predict the behaviors of the retinal PSE cells, given my measured parameters.

4.2.7.2 *IKNM as a mechanism to lower tissue viscosity*

Despite the actin reorganization being sufficient to predict the cell height increase from the 3D vertex model, my data shows that height increase does not happen without proliferation, even if basal actin accumulation is perturbed. Therefore, actin reorganization is not sufficient to increase cell height in the retinal PSE and the mechanism proposed above has to be modified to correctly predict the observed cell behaviors.

Proliferation in the PSE is underlined by the cell cycle-dependent phenomenon of IKNM, where nuclei actively migrate apically in the G2 phase of the cycle. It was previously shown (Leung et al., 2012) that these active apical movements trigger passive motion of the surrounding nuclei. When cells are blocked in S-phase by HU+A, apical migration is blocked and this, in turn, results in the cessation of the passive movements as well. Therefore, inhibition of proliferation abolishes all nuclear movement in the retinal PSE and we reasoned (with Guillaume Salbreux), that proliferation is necessary to increase cell height due to its effect on tissue dynamicity, rather than by increasing overall tissue size. Nuclear movements in an intact proliferating tissue might lower its viscosity and we hypothesize that such a material property of the tissue is required to allow changes of cell shape.

To reproduce the above condition of “freezing” nuclei, I plan to block proliferation by applying a ~6-10 h HU+A pulse to only transiently inhibit nuclear motion. In this experiment, WT fish would be treated with HU+A until the actin accumulation physiologically disappears. If cell height increase depends on IKNM, height should not increase in this time, irrespective of the basal actin disappearance. After the HU+A pulse, the tissue should resume IKNM and proliferation. If cell height increase depends on nuclear movements, cell height should in theory increase, with a fixed delay compared to the control tissue. Cell height would be analyzed at specific time-points after HU+A washout in fixed tissues. The HU+A experiment should allow me to obtain estimations of the tissue’s material properties and measurements of how cell height relates to proliferation. These could then be used as parameter values of a model based on our theory that nuclear dynamics and actin reorganization are both necessary to drive cell height increase. The predictions of the model would be compared to our initial experimental data on cell height in different conditions, to see how well our theory might explain experimental observations.

4.3 PERSPECTIVES

4.3.1 3D in vivo analyses of growth and shape as essential datasets for systems and synthetic biology

With respect to integrating complex biological findings across scales, we are today seeing the dawn of the systems biology era of biology. It aims to understand entire biological systems on multiple functional scales well enough to be able to rebuild them

computationally. At the moment, however, we still have mostly fragmented data from multiple sources and systems. Several groups tried to simulate large biological systems for which quantitative data on single cells and cellular dynamics is available. See e.g., virtual worm (Palyanov et al., 2016; <http://www.openworm.org/>, Szigeti et al., 2014), virtual liver network (<http://www.virtual-liver.de/>) or digital mouse embryo (Guignard et al., 2017). Arthur Lander reviewed such system-biology approaches and interpretations of how cellular machinery controls tissue patterning and growth (Lander, 2011).

3D tissue-wide analyses with cellular and subcellular resolution are important for the aims of organoid and synthetic biology, as well. Here, they provide a ground truth of the cellular-level events that build a healthy tissue. With this, 3D tissue-wide datasets might provide possibilities to troubleshoot, e.g., organoid development, where an organoid system does not grow into a correct shape. My study, with others, raises the possibility that ECM composition might have to be changed during organoid development to control cytoskeletal reorganization and correct cell shape changes. Without this change, the organoid might not have an optimal shape and, in turn, its function might be compromised, as well. Studies such as mine would have to be combined with data about chemical conditions and external constraints that affect tissue development, in order to come closer to reproducing *in vivo* conditions. Altogether, findings obtained in such interdisciplinary studies allow insights into development at multiple scales. 3D tissue-wide studies on how size and shape is generated, maintained and coordinated might be instrumental to reach new goals of biology.

4.3.2 Apico-basal support in thick epithelia

My laser ablation experiments indicated that PSE cells act like springs, as they recoiled towards center of the cell upon the cut. Because of this centripetal tension, these cells perhaps cannot, with a given volume, be longer than the $\sim 70 \mu\text{m}$ I measure after the brake on height is released. In theory, these cells could increase their volumes to perhaps allow further elongation. However, the retinal PSE grows by an increase in cell numbers, rather than by cell growth. As the zebrafish retina grows throughout the life of the fish, in order for the tissue to grow in thickness more than $70 \mu\text{m}$, a break in PSE structure might be necessary. Neuronal delamination and layering might provide such a structural dissipation.

Interestingly, not all cells delaminate from the retinal tissue surface as they differentiate. The retinal glial cell type, the Müller glia, are the only cells that continue spanning the entire retina after the monolayered PSE architecture is broken by delamination. Even though they function in more processes, Müller glia connect the apical-most to the basal-most surface, similar to the PSE cells in earlier developmental stages and have a role in mechanical support (MacDonald et al., 2015). Without them, the soft neuronal retinal tissue was shown to more easily rip and tear at the layer boundaries (MacDonald et al., 2015). With intact

Müller glia, the retina was able to resist tear. The progenitor PSE tissue, with all its cells attached apico-basally, also resisted tear, similar to the laminated tissue with Müller glia. It was thus proposed that the thick PSE and retinal tissues need the tensile strength provided by spring-like cells that connect the apical and basal surfaces, in order to resist external forces (MacDonald et al., 2015). This model has possible implications on PSE growth studies, as a maximal cell length could exist for PSE progenitor cells due to such spring-like properties.

With respect to my study, this putative intrinsic length maximum might depend on cell volume and could be incorporated into the model of limits on PSE proliferative growth, if one would like to account for all constraints that might act on this tissue's form.

4.3.3 Timing in retinal PSE development

Whatever the upstream coordinator and the physical mechanism of changes in tissue size and shape might be, timing is essential during retinal PSE development. My results show that mechanical constraints that govern tissue development have to be precisely coordinated in time. If the actin brake on cell height is released too late (i.e., when the tissue is too large), the retinal shape will be perturbed, as in the *hdac1*^{-/-} phenotype, causing irreparable structural and most probably functional damage to the eye.

Timing of developmental events is similarly important in the earlier stages of development. During zebrafish optic cup morphogenesis, cell migration has to be coordinated with acquisition of neuroepithelial character. If migration is too slow, cells will start invaginating outside of their target tissue, leading to a perturbed tissue shape (Sidhaye and Norden, 2017). Therefore, migrating cells have to reach their target tissue in time in order to properly form the optic cup. Among the events of later retinal developmental stages, the timing of neuronal differentiation does not depend on reaching an optimal tissue size. If proliferation is blocked with HU+A, retinal tissue will be smaller and have fewer cells (Kwan et al., 2012), but will still differentiate (Icha et al., 2016). Such differentiation inside a smaller tissue might result in fewer neurons and a less elaborate synaptic network, creating a sub-optimally functioning retina. My data suggests that differentiation does not depend on retinal shape, either, because PSE cells differentiate in the tissue that buckled and developed folds (Figure 18C). In this case, neuronal layers form and cell numbers might be similar to the WT condition, but the folds in the retina will most likely affect light propagation and detection, i.e., retinal function.

These examples from the retinal PSE demonstrate that processes that regulate tissue size, shape and differentiation have to be extremely well coordinated in time, as one does not necessarily rely on the successful completion of the other. We still do not know what

level of developmental error (variability) is tolerated in cases where this coordination is faulty, to still reproducibly generate an optimally functioning tissue.

The question of how tissue size, shape and differentiation are coordinated remains a major open question in developmental biology. Overall, deciphering how tissue growth, governed by nutrition and signaling pathways, is spatiotemporally integrated with cellular- and organ-scale mechanics and dynamics, will be necessary future goals towards an understanding of how emergent properties coordinate across multiple scales (Dumont and Prakash, 2014; Lecuit and Le Goff, 2007).

4.4 CONCLUSION AND OUTLOOK

In this thesis, I analyzed the cellular contributions to growth and shape of the retinal PSE through development, in a 3D tissue-wide study. I tested proposed limits to PSE growth and suggest that this tissue grows and maintains its shape in accordance with a three-dimensional constraint specific to the PSE architecture. I revealed that a brake on cell height increase exists in earlier stages of development and prevents premature cell shape change during growth. Based on my analyses, I propose that a timely release of this ECM-dependent brake is necessary to maintain the shape and function of the retinal tissue.

Findings obtained in this study highlight the cytoskeleton and the ECM as the main players that directly orchestrate changes in size and shape. Furthermore, cell height and its precise temporal regulation might be a key cellular parameter in generation of functional epithelial tissues. This might be a more general mechanism, in which thick epithelial tissues alter their cellular mechanics and by this redefine the major physical constraints that govern their development. Overall, this work contributes to our understanding of how cell-scale parameters such as size, cycle length and shape, change during development, to generate a zebrafish retinal tissue of correct size and shape. It showcases that maintenance of uniform tissue growth during development is not a default state, but one that requires active maintenance at the cell level (Shraiman, 2005).

As a model to study developmental shape and size disturbances, the zebrafish retina provides unprecedented study conditions. It is a transparent tissue that is situated at the surface of the animal, allowing direct observation and analysis of growth and shape by live and fixed imaging. This makes it an exceptional system to study size and shape of developing epithelia on the cellular level and in a tissue-wide, 3D, quantitative manner, a feature that was extensively employed throughout this study. Such 3D tissue-wide studies

of long developmental courses have the potential to provide us with unprecedented understanding of coordination of developmental events across scales.

Future experiments should aim at identifying the exact molecular players that trigger actin reorganization, e.g., investigate the effect of premature Wnt and Notch inhibition on cell height in the WT. Biophysical modeling using the measured cellular parameters can help us understand the necessary distribution, scale and effect of mechanical forces on PSE cell height increase. Finally, it would be interesting to study growth of the human retinal organoids in comparison to the zebrafish retinal tissue, to check if the model of cell height-based coordination of growth and shape, proposed in this study, might be applied to drive *in vivo*-like development of the organoid.

REFERENCES

- Aegerter-Wilmsen, T., Aegerter, C.M., Hafen, E., Basler, K., 2007. Model for the regulation of size in the wing imaginal disc of *Drosophila*. *Mechanisms of Development* 124, 318–326. doi:10.1016/j.mod.2006.12.005
- Aegerter-Wilmsen, T., Heimlicher, M.B., Smith, A.C., de Reuille, P.B., Smith, R.S., Aegerter, C.M., Basler, K., 2012. Integrating force-sensing and signaling pathways in a model for the regulation of wing imaginal disc size. *Development* 139, 3221–3231. doi:10.1242/dev.082800
- Alberts, B., Johnson, A., Lewis, J., Raff, M., Roberts, K., Walter, P., 2014. *Molecular Biology of the Cell*, in: Garland Science.
- Almeida, A.D., Boije, H., Chow, R.W., He, J., Tham, J., Suzuki, S.C., Harris, W.A., 2014. Spectrum of Fates: a new approach to the study of the developing zebrafish retina. *Development* 141, 1971–1980. doi:10.1242/dev.104760
- Alsina, B., Whitfield, T.T., 2017. Sculpting the labyrinth: Morphogenesis of the developing inner ear. *Seminars in Cell & Developmental Biology* 65, 47–59. doi:10.1016/j.semcd.2016.09.015
- Alt, S., 2016. *Epithelial Mechanics in 3D*. PhD thesis. TUD, Dresden.
- Alt, S., Ganguly, P., Salbreux, G., 2017. Vertex models: from cell mechanics to tissue morphogenesis. *Phil. Trans. R. Soc. B* 372, 20150520. doi:10.1098/rstb.2015.0520
- Amodeo, A.A., Skotheim, J.M., 2016. Cell-Size Control. *Cold Spring Harb Perspect Biol* 8, a019083. doi:10.1101/cshperspect.a019083
- Andersen, D.S., Colombani, J., Léopold, P., 2013. Coordination of organ growth: principles and outstanding questions from the world of insects. *Trends in Cell Biology* 23, 336–344. doi:10.1016/j.tcb.2013.03.005
- Asha, H., de Ruyter, N.D., Wang, M.G., Hariharan, I.K., 1999. The Rap1 GTPase functions as a regulator of morphogenesis in vivo. *The EMBO Journal* 18, 605–615. doi:10.1093/emboj/18.3.605
- Assoian, R.K., 1997. Anchorage-dependent Cell Cycle Progression. *J Cell Biol* 136, 1–4. doi:10.1083/jcb.136.1.1
- Astudillo, P., Larraín, J., 2014. Wnt signaling and cell-matrix adhesion. *Curr. Mol. Med.* 14, 209–220.
- Aurich, F., Dahmann, C., 2016. A Mutation in *fat2* Uncouples Tissue Elongation from Global Tissue Rotation. *Cell Rep* 14, 2503–2510. doi:10.1016/j.celrep.2016.02.044
- Baena-López, L.A., Baonza, A., García-Bellido, A., 2005. The orientation of cell divisions determines the shape of *Drosophila* organs. *Current Biology* 15, 1640–1644. doi:10.1016/j.cub.2005.07.062
- Barone, V., Lang, M., Krens, S.F.G., Pradhan, S.J., Shamipour, S., Sako, K., Sikora, M., Guet, C.C., Heisenberg, C.-P., 2017. An Effective Feedback Loop between Cell-Cell Contact Duration and Morphogen Signaling Determines Cell Fate. *Developmental Cell*. doi:10.1016/j.devcel.2017.09.014
- Bazin-Lopez, N., Valdivia, L.E., Wilson, S.W., Gestri, G., 2015. Watching eyes take shape. *Current Opinion in Genetics & Development* 32, 73–79. doi:10.1016/j.gde.2015.02.004
- Behrndt, M., Salbreux, G., Campinho, P., Hauschild, R., Oswald, F., Roensch, J., Grill, S.W., Heisenberg, C.-P., 2012. Forces driving epithelial spreading in zebrafish gastrulation. *Science* 338, 257–260. doi:10.1126/science.1224143
- Benham-Pyle, B.W., Pruitt, B.L., Nelson, W.J., 2015. Mechanical strain induces E-cadherin-dependent Yap1 and β -catenin activation to drive cell cycle entry. *Science* 348, 1024–1027. doi:10.1126/science.aaa4559
- Bertet, C., Sulak, L., Lecuit, T., 2004. Myosin-dependent junction remodelling controls planar cell intercalation and axis elongation. *Nature* 429, 667–671. doi:10.1038/nature02590
- Black, S.D., Vincent, J.P., 1988. The first cleavage plane and the embryonic axis are determined by separate mechanisms in *Xenopus laevis*. II. Experimental dissociation by lateral compression of the egg. *Developmental Biology* 128, 65–71.

- Bogdanović, O., Delfino-Machín, M., Nicolás-Pérez, M., Gavilán, M.P., Gago-Rodrigues, I., Fernández-Miñán, A., Lillo, C., Ríos, R.M., Wittbrodt, J., Martínez-Morales, J.R., 2012. Numb/Numbl-Opo antagonism controls retinal epithelium morphogenesis by regulating integrin endocytosis. *Developmental Cell* 23, 782–795. doi:10.1016/j.devcel.2012.09.004
- Boone, E., Colombani, J., Andersen, D.S., Léopold, P., 2016. The Hippo signalling pathway coordinates organ growth and limits developmental variability by controlling *dilp8* expression. *Nature Communications* 7, ncomms13505. doi:10.1038/ncomms13505
- Bort, R., Signore, M., Tremblay, K., Barbera, J.P.M., Zaret, K.S., 2006. Hex homeobox gene controls the transition of the endoderm to a pseudostratified, cell emergent epithelium for liver bud development. *Developmental Biology* 290, 44–56. doi:10.1016/j.ydbio.2005.11.006
- Bosveld, F., Markova, O., Guirao, B., Martin, C., Wang, Z., Pierre, A., et al. (2016). Epithelial tricellular junctions act as interphase cell shape sensors to orient mitosis. *Nature*, 530(7591), 495–. <http://doi.org/10.1038/nature16970>
- Bosveld, F., Bonnet, I., Guirao, B., Tlili, S., Wang, Z., Pétitalot, A., et al. (2012). Mechanical control of morphogenesis by Fat/Dachsous/Four-jointed planar cell polarity pathway. *Science (New York, N.Y.)*, 336(6082), 724–727. <http://doi.org/10.1126/science.1221071>
- Bothma, J.P., Levine, M., Boettiger, A., 2010. Morphogen Gradients: Limits to Signaling or Limits to Measurement? *Current Biology* 20, R232–R234. doi:10.1016/j.cub.2010.01.040
- Britton, J.S., Edgar, B.A., 1998. Environmental control of the cell cycle in *Drosophila*: nutrition activates mitotic and endoreplicative cells by distinct mechanisms. *Development* 125, 2149–2158.
- Brown, N.H., 2011. Extracellular matrix in development: insights from mechanisms conserved between invertebrates and vertebrates. *Cold Spring Harb Perspect Biol* 3, a005082–a005082. doi:10.1101/cshperspect.a005082
- Bryant, P.J., Levinson, P., 1985. Intrinsic growth control in the imaginal primordia of *Drosophila* and the autonomous action of a lethal mutation causing overgrowth. *Developmental Biology* 107, 355–363. doi:10.1016/0012-1606(85)90317-3
- Burkel, B.M., Dassow, von, G., Bement, W.M., 2007. Versatile Fluorescent Probes for Actin Filaments Based on the Actin-Binding Domain of Utrophin. *Cell motility and the cytoskeleton* 64, 822–832. doi:10.1002/cm.20226
- Burridge, K., Guilluy, C., 2016. Focal adhesions, stress fibers and mechanical tension. *Experimental Cell Research* 343, 14–20. doi:10.1016/j.yexcr.2015.10.029
- Cabochette, P., Vega-Lopez, G., Bitard, J., Parain, K., Chemouny, R., Masson, C., Borday, C., Hedderich, M., Henningfeld, K.A., Locker, M., Bronchain, O., Perron, M., 2015. YAP controls retinal stem cell DNA replication timing and genomic stability. *eLife* 4, e08488. doi:10.7554/eLife.08488
- Cadart, C., Monnier, S., Grilli, J., Attia, R., Terriac, E., Baum, B., Cosentino-Lagomarsino, M., Piel, M., 2017. Size control in mammalian cells involves modulation of both growth rate and cell cycle duration. *bioRxiv* 152728. doi:10.1101/152728
- Calderwood, D.A., Ginsberg, M.H., 2003. Talin forges the links between integrins and actin. *Nature Cell Biology* 5, 694–697. doi:10.1038/ncb0803-694
- Calegari, F., 2005. Selective lengthening of the cell cycle in the neurogenic subpopulation of neural progenitor cells during mouse brain development. *J. Neurosci.* 25, 6533–6538. doi:10.1523/JNEUROSCI.0778-05.2005
- Camenisch, T.D., Biesterfeldt, J., Brehm-Gibson, T., Bradley, J., McDonald, J.A., 2001. Regulation of cardiac cushion development by hyaluronan. *Exp Clin Cardiol* 6, 4–10. doi:10.1016/bs.ircmb.2016.02.004
- Campinho, P., Behrndt, M., Ranft, J., Risler, T., Minc, N., Heisenberg, C.-P., 2013. Tension-oriented cell divisions limit anisotropic tissue tension in epithelial spreading during zebrafish epiboly. *Nature Cell Biology* 15, 1405–1414. doi:10.1038/ncb2869
- Chan, E.H., Shivakumar, P.C., Clément, R., Laugier, E., Lenne, P.-F., 2017. Patterned cortical tension mediated by N-cadherin controls cell geometric order in the *Drosophila* eye. *eLife* 6, e22796. doi:10.7554/eLife.22796
- Chen, A., Beetham, H., Black, M.A., Priya, R., Telford, B.J., Guest, J., Wiggins, G.A.R., Godwin, T.D., Yap, A.S., Guilford, P.J., 2014. E-cadherin loss alters cytoskeletal organization and adhesion in non-malignant breast cells but is insufficient to induce an epithelial-mesenchymal transition. *BMC Cancer* 14, 3756. doi:10.1186/1471-2407-14-552

- Cheng, L.Y., Bailey, A.P., Leever, S.J., Ragan, T.J., Driscoll, P.C., Gould, A.P., 2011. Anaplastic Lymphoma Kinase Spares Organ Growth during Nutrient Restriction in *Drosophila*. *Cell* 146, 435–447. doi:10.1016/j.cell.2011.06.040
- Christian, J.L., 2011. Morphogen gradients in Development: from form to function. Wiley interdisciplinary reviews. *Developmental biology* 1, 3–15. doi:10.1002/wdev.2
- Clendenon, S.G., Shah, B., Miller, C.A., Schmeisser, G., Walter, A., Gattone, V.H., II, Barald, K.F., Liu, Q., Marrs, J.A., 2009. Cadherin-11 controls otolith assembly: Evidence for extracellular cadherin activity. *Developmental Dynamics* 238, 1909–1922. doi:10.1002/dvdy.22015
- Collinet, C., Rauzi, M., Lenne, P.-F., Lecuit, T., 2015. Local and tissue-scale forces drive oriented junction growth during tissue extension. *Nature Cell Biology* 17, ncb3226–1258. doi:10.1038/ncb3226
- Colombani, J., andersen, D.S., Léopold, P., 2012. Secreted peptide Dilp8 coordinates *Drosophila* tissue growth with developmental timing. *Science* 336, 582–585. doi:10.1126/science.1216689
- Conlon, I., Raff, M., 1999. Size Control in Animal Development. *Cell* 96, 235–244. doi:10.1016/S0092-8674(00)80563-2
- Cooper, M.S., Szeto, D.P., Sommers-Herivel, G., Topczewski, J., Solnica-Krezel, L., Kang, H.-C., Johnson, I., Kimelman, D., 2005. Visualizing morphogenesis in transgenic zebrafish embryos using BODIPY TR methyl ester dye as a vital counterstain for GFP. *Dev. Dyn.* 232, 359–368. doi:10.1002/dvdy.20252
- Cory, S., Huang, D.C.S., Adams, J.M., 2003. The Bcl-2 family: roles in cell survival and oncogenesis. *Oncogene* 22, 8590–8607. doi:10.1038/sj.onc.1207102
- Cox, C.D., Bae, C., Ziegler, L., Hartley, S., Nikolova-Krstevski, V., Rohde, P.R., Ng, C.-A., Sachs, F., Gottlieb, P.A., Martinac, B., 2016. Removal of the mechanoprotective influence of the cytoskeleton reveals PIEZO1 is gated by bilayer tension. *Nature Communications* 7, 10366. doi:10.1038/ncomms10366
- Crest, J., Diz-Munoz, A., Chen, D.-Y., Fletcher, D. A., & Bilder, D. (2017). Organ sculpting by patterned extracellular matrix stiffness. *Elife*, 6. <http://doi.org/10.7554/eLife.24958>
- Delanoue, R., Slaidina, M., Léopold, P., 2010. The steroid hormone ecdysone controls systemic growth by repressing dMyc function in *Drosophila* fat cells. *Developmental Cell* 18, 1012–1021. doi:10.1016/j.devcel.2010.05.007
- del Rio, A., Perez-Jimenez, R., Liu, R., Roca-Cusachs, P., Fernandez, J. M., & Sheetz, M. P. (2009). Stretching Single Talin Rod Molecules Activates Vinculin Binding. *Science (New York, N.Y.)*, 323(5914), 638–641. <http://doi.org/10.1126/science.1162912>
- Delva, E., Tucker, D.K., Kowalczyk, A.P., 2009. The Desmosome. *Cold Spring Harb Perspect Biol* 1, a002543–a002543. doi:10.1101/cshperspect.a002543
- Di Gregorio, A., Bowling, S., Rodriguez, T.A., 2016. Cell Competition and Its Role in the Regulation of Cell Fitness from Development to Cancer. *Developmental Cell* 38, 621–634. doi:10.1016/j.devcel.2016.08.012
- Di Talia, S., Skotheim, J.M., Bean, J.M., Siggia, E.D., Cross, F.R., 2007. The effects of molecular noise and size control on variability in the budding yeast cell cycle. *Nature* 448, 947–951. doi:10.1038/nature06072
- Diaz de la Loza, M.C., Thompson, B.J., 2017. Forces shaping the *Drosophila* wing. *Mechanisms of Development* 144, 23–32. doi:10.1016/j.mod.2016.10.003
- Diaz-Benjumea, F.J., Cohen, S.M., 1993. Interaction between dorsal and ventral cells in the imaginal disc directs wing development in *Drosophila*. *Cell* 75, 741–752.
- Diez del Corral, R., Aroca, P., Gomez-Skarmeta, J.L., Cavodeassi, F., Modolell, J., 1999. The Iroquois homeodomain proteins are required to specify body wall identity in *Drosophila*. *Genes Dev.* 13, 1754–1761.
- Discher, D.E., 2005. Tissue Cells Feel and Respond to the Stiffness of Their Substrate. *Science* 310, 1139–1143. doi:10.1126/science.1116995
- Diz-Muñoz, A., Fletcher, D.A., Weiner, O.D., 2013. Use the force: membrane tension as an organizer of cell shape and motility. *Trends in Cell Biology* 23, 47–53. doi:10.1016/j.tcb.2012.09.006
- Domínguez-Giménez, P., Brown, N.H., Martín-Bermudo, M.D., 2007. Integrin-ECM interactions regulate the changes in cell shape driving the morphogenesis of the *Drosophila* wing epithelium. *J Cell Sci* 120, 1061–1071. doi:10.1242/jcs.03404

- Dong, J., Feldmann, G., Huang, J., Wu, S., Zhang, N., Comerford, S. A., et al. (2007). Elucidation of a Universal Size-Control Mechanism in *Drosophila* and Mammals. *Cell*, 130(6), 1120–1133. <http://doi.org/10.1016/j.cell.2007.07.019>
- Dubatolova, T.D., Dorogova, N.V., Omel'yanchuk, L.V., Chang, L.S., 2011. Duration of the cell cycle phases in mutants for the tumor suppressor Merlin in *Drosophila melanogaster*. *Russ J Genet* 47, 404–408. doi:10.1134/S1022795411040041
- Dumont, S., Prakash, M., 2014. Emergent mechanics of biological structures. *Mol. Biol. Cell* 25, 3461–3465. doi:10.1091/mbc.E14-03-0784
- Dye, N.A., Popović, M., Spann, S., Etournay, R., Kainmueller, D., Myers, E.W., Jülicher, F., Eaton, S., 2017. Cell Dynamics Underlying Oriented Growth Of The *Drosophila* Imaginal Wing Disc. bioRxiv 140038. doi:10.1101/140038
- Dzafic, E., Strzyz, P.J., Wilsch-Bräuninger, M., Norden, C., 2015. Centriole Amplification in Zebrafish Affects Proliferation and Survival but Not Differentiation of Neural Progenitor Cells. *Cell Rep* 13, 168–182. doi:10.1016/j.celrep.2015.08.062
- Edmondson, R., Broglie, J.J., Adcock, A.F., Yang, L., 2014. Three-Dimensional Cell Culture Systems and Their Applications in Drug Discovery and Cell-Based Biosensors. *Assay and Drug Development Technologies* 12, 207–218. doi:10.1089/adt.2014.573
- Eisenhoffer, G.T., Loftus, P.D., Yoshigi, M., Otsuna, H., Chien, C.-B., Morcos, P.A., Rosenblatt, J., 2012. Crowding induces live cell extrusion to maintain homeostatic cell numbers in epithelia. *Nature* 484, 546–549. doi:10.1038/nature10999
- Eom, D.S., Amarnath, S., Agarwala, S., 2013. Apicobasal Polarity and Neural Tube Closure. *Development, growth & differentiation* 55, 164–172. doi:10.1111/dgd.12030
- Etournay, R., Popović, M., Merkel, M., Nandi, A., Blasse, C., Aigouy, B., Brandl, H., Myers, G., Salbreux, G., Jülicher, F., Eaton, S., 2015. Interplay of cell dynamics and epithelial tension during morphogenesis of the *Drosophila* pupal wing. *eLife* 4, e07090. doi:10.7554/eLife.07090
- Fankhauser, G., 1945. Maintenance of Normal Structure in Heteroploid Salamander Larvae, Through Compensation of Changes in Cell Size by Adjustment of Cell Number and Cell Shape. *J. Exp. Zool.* 100, 445–455.
- Fish, J.L., Dehay, C., Kennedy, H., Huttner, W.B., 2008. Making bigger brains—the evolution of neural-progenitor-cell division. *J Cell Sci* 121, 2783–2793. doi:10.1242/jcs.023465
- Fletcher, G.C., Elbediwy, A., Khanal, I., Ribeiro, P.S., Tapon, N., Thompson, B.J., 2015. The Spectrin cytoskeleton regulates the Hippo signalling pathway. *The EMBO Journal* 34, 940–954. doi:10.15252/embj.201489642
- Florio, M., Huttner, W.B., 2014. Neural progenitors, neurogenesis and the evolution of the neocortex. *Development* 141, 2182–2194. doi:10.1242/dev.090571
- Frisch, S.M., Francis, H., 1994. Disruption of epithelial cell-matrix interactions induces apoptosis. *J Cell Biol* 124, 619–626.
- Fuhrmann, S., 2010. Eye Morphogenesis and Patterning of the Optic Vesicle. *Current topics in developmental biology* 93, 61–84. doi:10.1016/B978-0-12-385044-7.00003-5
- Gaiano, N., Fishell, G., 2002. The role of notch in promoting glial and neural stem cell fates. *Annu. Rev. Neurosci.* 25, 471–490. doi:10.1146/annurev.neuro.25.030702.130823
- Gallet, A., 2011. Hedgehog morphogen: from secretion to reception. *Trends in Cell Biology* 21, 238–246. doi:10.1016/j.tcb.2010.12.005
- García, M.T., Chang, Y., Arai, Y., Huttner, W.B., 2016. S-phase duration is the main target of cell cycle regulation in neural progenitors of developing ferret neocortex. *J. Comp. Neurol.* 524, 456–470. doi:10.1002/cne.23801
- Garelli, A., Gontijo, A.M., Miguéla, V., Caparros, E., Dominguez, M., 2012. Imaginal discs secrete insulin-like peptide 8 to mediate plasticity of growth and maturation. *Science* 336, 579–582. doi:10.1126/science.1216735
- Geldmacher-Voss, B., Reugels, A.M., Pauls, S., Campos-Ortega, J.A., 2003. A 90-degree rotation of the mitotic spindle changes the orientation of mitoses of zebrafish neuroepithelial cells. *Development* 130, 3767–3780.
- Gibson, M.C., 2005. Extrusion and Death of DPP/BMP-Compromised Epithelial Cells in the Developing *Drosophila* Wing. *Science* 307, 1785–1789. doi:10.1126/science.1104751
- Gibson, W. T., Veldhuis, J. H., Rubinstein, B., Cartwright, H. N., Perrimon, N., Brodland, G. W., et al. (2011). Control of the Mitotic Cleavage Plane by Local Epithelial Topology. *Cell*, 144(3),

- 427–438. <http://doi.org/10.1016/j.cell.2010.12.035>
- Gilbert, S.F., 2013. *Developmental Biology*, 10 ed. Sinauer Associates.
- Gilson, H., 2008. Leonardo da Vinci's Embryological Annotations. *Embryo Project Encyclopedia* (2008-08-19). ISSN: 1940-5030 [WWW Document]. embryo.asu.edu. URL <https://embryo.asu.edu/pages/leonardo-da-vincis-embryological-annotations> (accessed 9.7.17).
- Ginzberg, M.B., Kafri, R., Kirschner, M., 2015. Cell biology. On being the right (cell) size. *Science* 348, 1245075. doi:10.1126/science.1245075
- Giraldez, F., Represa, J.J., Borondo, L., Barbosa, E., 1987. Polarization and density of Na-pumps in the inner ear of the chick embryo during early stages of development. *Development* 100, 271–278.
- Gomez, G.A., McLachlan, R.W., Yap, A.S., 2011. Productive tension: force-sensing and homeostasis of cell–cell junctions. *Trends in Cell Biology* 21, 499–505. doi:10.1016/j.tcb.2011.05.006
- Gong, Y., Mo, C., Fraser, S.E., 2004. Planar cell polarity signalling controls cell division orientation during zebrafish gastrulation. *Nature* 430, 689–693. doi:10.1038/nature02796
- Goodwin, K., Ellis, S.J., Lostchuck, E., Zulueta-Coarasa, T., Fernandez-Gonzalez, R., Tanentzapf, G., 2016. Basal Cell-Extracellular Matrix Adhesion Regulates Force Transmission during Tissue Morphogenesis. *Developmental Cell* 39, 611–625. doi:10.1016/j.devcel.2016.11.003
- Graham, A., Francis-West, P., Brickell, P., Lumsden, A., 1994. The signalling molecule BMP4 mediates apoptosis in the rhombencephalic neural crest. *Nature* 372, 684–686. doi:10.1038/372684a0
- Greene, N.D.E., Copp, A.J., 2014. Neural Tube Defects. *Annu. Rev. Neurosci.* 37, 221–242. doi:10.1146/annurev-neuro-062012-170354
- Grego-Bessa, J., Bloomekatz, J., Castel, P., Omelchenko, T., Baselga, J., Anderson, K.V., Gleeson, J.G., 2016. The tumor suppressor PTEN and the PDK1 kinase regulate formation of the columnar neural epithelium. *eLife* 5, e12034. doi:10.7554/eLife.12034
- Grill, S.W., Gönczy, P., Stelzer, E.H., Hyman, A.A., 2001. Polarity controls forces governing asymmetric spindle positioning in the *Caenorhabditis elegans* embryo. *Nature* 409, 630–633. doi:10.1038/35054572
- Grosse, A.S., Pressprich, M.F., Curley, L.B., Hamilton, K.L., Margolis, B., Hildebrand, J.D., Gumucio, D.L., 2011. Cell dynamics in fetal intestinal epithelium: implications for intestinal growth and morphogenesis. *Development* 138, 4423–4432. doi:10.1242/dev.065789
- Guignard, L., McDole, K., Clack, N., Amat, F., Branson, K., Keller, P., 2017. The Digital Mouse Embryo – towards an atlas of cellular dynamics from gastrulation to early organogenesis. *Mechanisms of Development* 145, S70. doi:10.1016/j.mod.2017.04.161
- Gurley, K.A., Rink, J.C., Alvarado, A.S., 2008. β -Catenin Defines Head Versus Tail Identity During Planarian Regeneration and Homeostasis. *Science* 319, 323–327. doi:10.1126/science.1150029
- Gutzman, J.H., Graeden, E.G., Lowery, L.A., Holley, H.S., Sive, H., 2008. Formation of the zebrafish midbrain–hindbrain boundary constriction requires laminin-dependent basal constriction. *Mechanisms of Development* 125, 974–983. doi:10.1016/j.mod.2008.07.004
- Haigo, S. L., & Bilder, D. (2011). Global tissue revolutions in a morphogenetic movement controlling elongation. *Science (New York, N. Y.)*, 331(6020), 1071–1074. <http://doi.org/10.1126/science.1199424>
- Haigo, S.L., Hildebrand, J.D., Harland, R.M., Wallingford, J.B., 2003. Shroom Induces Apical Constriction and Is Required for Hingepoint Formation during Neural Tube Closure. *Current Biology* 13, 2125–2137. doi:10.1016/j.cub.2003.11.054
- Han, M.K.L., de Rooij, J., 2016. Converging and Unique Mechanisms of Mechanotransduction at Adhesion Sites. *Trends in Cell Biology* 26, 612–623. doi:10.1016/j.tcb.2016.03.005
- Harris, W. A., & Hartenstein, V. (1991). Neuronal determination without cell division in *Xenopus* embryos. *Neuron*, 6(4), 499–515.
- Harunaga, J.S., Doyle, A.D., Yamada, K.M., 2014. Local and global dynamics of the basement membrane during branching morphogenesis require protease activity and actomyosin contractility. *Developmental Biology* 394, 197–205. doi:10.1016/j.ydbio.2014.08.014
- Hayward, P., Kalmar, T., Arias, A.M., 2008. Wnt/Notch signalling and information processing during

- development. *Development* 135, 411–424. doi:10.1242/dev.000505
- He, J., Zhang, G., Almeida, A.D., Cayouette, M., Simons, B.D., Harris, W.A., 2012. How variable clones build an invariant retina. *Neuron* 75, 786–798. doi:10.1016/j.neuron.2012.06.033
- Hertwig, O., 1893. Ueber den Werth der ersten Furchungszellen für die Organbildung des Embryo Experimentelle Studien am Frosch-und Tritonei. *Archiv f. mikrosk. Anat.* 42, 662–807. doi:10.1007/BF02976796
- Hodkinson, P.S., Elliott, P.A., Lad, Y., McHugh, B.J., MacKinnon, A.C., Haslett, C., Sethi, T., 2007. Mammalian NOTCH-1 activates beta1 integrins via the small GTPase R-Ras. *J. Biol. Chem.* 282, 28991–29001. doi:10.1074/jbc.M703601200
- Hoijman, E., Rubbini, D., Colombelli, J., Alsina, B., 2015. Mitotic cell rounding and epithelial thinning regulate lumen growth and shape. *Nature Communications* 6, 7355. doi:10.1038/ncomms8355
- Homem, C.C.F., Steinmann, V., Burkard, T.R., Jais, A., Esterbauer, H., Knoblich, J.A., 2014. Ecdysone and mediator change energy metabolism to terminate proliferation in *Drosophila* neural stem cells. *Cell* 158, 874–888. doi:10.1016/j.cell.2014.06.024
- Order, T., 2001. *History of Developmental Biology*, eLS. John Wiley & Sons, Ltd, Chichester, UK. doi:10.1038/npg.els.0003080
- Hu, D.J.-K., Baffet, A.D., Nayak, T., Akhmanova, A., Doye, V., Vallee, R.B., 2013. Dynein Recruitment to Nuclear Pores Activates Apical Nuclear Migration and Mitotic Entry in Brain Progenitor Cells. *Cell* 154, 1300–1313. doi:10.1016/j.cell.2013.08.024
- Hu, M., Easter, S.S., Jr., 1999. Retinal Neurogenesis: The Formation of the Initial Central Patch of Postmitotic Cells. *Developmental Biology* 207, 309–321. doi:10.1006/dbio.1998.9031
- Hufnagel, L., Teleman, A.A., Rouault, H., Cohen, S.M., Shraiman, B.I., 2007. On the mechanism of wing size determination in fly development. *Proc. Natl. Acad. Sci. U.S.A.* 104, 3835–3840. doi:10.1073/pnas.0607134104
- Huttner, W.B., Brand, M., 1997. Asymmetric division and polarity of neuroepithelial cells. *Current Opinion in Neurobiology* 7, 29–39. doi:10.1016/S0959-4388(97)80117-1
- Icha, J., Kunath, C., Rocha-Martins, M., Norden, C., 2016. Independent modes of ganglion cell translocation ensure correct lamination of the zebrafish retina. *The Journal of Cell Biology* 215, 259–275. doi:10.1083/jcb.201604095
- Icha, J., Weber, M., Waters, J.C., Norden, C., 2017. Phototoxicity in live fluorescence microscopy and how to avoid it. *BioEssays* 39. doi:10.1002/bies.201700003
- Ichikawa, T., Nakazato, K., Keller, P.J., Kajjura-Kobayashi, H., Stelzer, E.H.K., Mochizuki, A., Nonaka, S., 2013. Live Imaging of Whole Mouse Embryos during Gastrulation: Migration Analyses of Epiblast and Mesodermal Cells. *PLoS ONE* 8, e64506. doi:10.1371/journal.pone.0064506
- Inoue, D., Wittbrodt, J., 2011. One for All—A Highly Efficient and Versatile Method for Fluorescent Immunostaining in Fish Embryos. *PLoS ONE* 6, e19713. doi:10.1371/journal.pone.0019713
- Irvine, K. D., & Wieschaus, E. (1994). Cell Intercalation During *Drosophila* Germband Extension and Its Regulation by Pair-Rule Segmentation Genes. *Development*, 120(4), 827–841.
- Iulianella, A., Sharma, M., Durnin, M., Heuvel, G.B.V., Trainor, P.A., 2008. Cux2 (Cutl2) integrates neural progenitor development with cell-cycle progression during spinal cord neurogenesis. *Development* 135, 729–741. doi:10.1242/dev.013276
- Jansen, A., Andermann, E., 2005. Genetics of the polymicrogyria syndromes. *Journal of Medical Genetics* 42, 369–378. doi:10.1136/jmg.2004.023952
- Jeanes, A., Gottardi, C.J., Yap, A.S., 2008. Cadherins and cancer: how does cadherin dysfunction promote tumor progression? *Oncogene* 27, 6920–6929. doi:10.1038/onc.2008.343
- Jeong, J., McMahon, A.P., 2005. Growth and pattern of the mammalian neural tube are governed by partially overlapping feedback activities of the hedgehog antagonists patched 1 and Hhip1. *Development* 132, 143–154. doi:10.1242/dev.01566
- Joel B Miesfeld, B.A.L., 2014. Establishment of transgenic lines to monitor and manipulate Yap/Taz-Tead activity in zebrafish reveals both evolutionarily conserved and divergent functions of the Hippo pathway. *Mechanisms of Development* 0, 177–188. doi:10.1016/j.mod.2014.02.003
- Johnston, L.A., Prober, D.A., Edgar, B.A., Eisenman, R.N., Gallant, P., 1999. *Drosophila* myc regulates cellular growth during development. *Cell* 98, 779–790. doi:10.5167/uzh-740

- Jusuf, P.R., Harris, W.A., 2009. Ptf1a is expressed transiently in all types of amacrine cells in the embryonic zebrafish retina. *Neural Development* 2012 7:1 4, 34. doi:10.1186/1749-8104-4-34
- Katoh, H., Fujita, Y., 2012. Epithelial Homeostasis: Elimination by Live Cell Extrusion. *Current Biology* 22, R453–R455. doi:10.1016/j.cub.2012.04.036
- Kay, J.N., Finger-Baier, K.C., Roeser, T., Staub, W., Baier, H., 2001. Retinal Ganglion Cell Genesis Requires *lakritz*, a Zebrafish atonal Homolog. *Neuron* 30, 725–736. doi:10.1016/S0896-6273(01)00312-9
- Kay, J.N., Link, B.A., Baier, H., 2005. Staggered cell-intrinsic timing of *ath5* expression underlies the wave of ganglion cell neurogenesis in the zebrafish retina. *Development* 132, 2573–2585. doi:10.1242/dev.01831
- Kerridge, S., Munjal, A., Philippe, J.-M., Jha, A., las Bayonas, de, A.G., Saurin, A.J., Lecuit, T., 2016. Modular activation of Rho1 by GPCR signalling imparts polarized myosin II activation during morphogenesis. *Nature Cell Biology* 18, 261–270. doi:10.1038/ncb3302
- Kim, D.-H., Sarbassov, D.D., Ali, S.M., King, J.E., Latek, R.R., Erdjument-Bromage, H., Tempst, P., Sabatini, D.M., 2002. mTOR interacts with raptor to form a nutrient-sensitive complex that signals to the cell growth machinery. *Cell* 110, 163–175.
- Knights, A.J., Funnell, A.P.W., Crossley, M., Pearson, R.C.M., 2012. Holding Tight: Cell Junctions and Cancer Spread. *Trends in cancer research* 8, 61–69.
- Knox, A.L., Brown, N.H., 2002. Rap1 GTPase Regulation of Adherens Junction Positioning and Cell Adhesion. *Science* 295, 1285–1288. doi:10.1126/science.1067549
- Koontz, L.M., Liu-Chittenden, Y., Yin, F., Zheng, Y., Yu, J., Huang, B., Chen, Q., Wu, S., Pan, D., 2013. The Hippo effector Yorkie controls normal tissue growth by antagonizing scalloped-mediated default repression. *Developmental Cell* 25, 388–401. doi:10.1016/j.devcel.2013.04.021
- Kosodo, Y., Suetsugu, T., Suda, M., Mimori-Kiyosue, Y., Toida, K., Baba, S.A., Kimura, A., Matsuzaki, F., 2011. Regulation of interkinetic nuclear migration by cell cycle-coupled active and passive mechanisms in the developing brain. *The EMBO Journal* 30, 1690–1704. doi:10.1038/emboj.2011.81
- Kühn, K., 1995. Basement membrane (type IV) collagen. *Matrix Biology* 14, 439–445. doi:10.1016/0945-053X(95)90001-2
- Kwan, K.M., Fujimoto, E., Grabher, C., Mangum, B.D., Hardy, M.E., Campbell, D.S., Parant, J.M., Yost, H.J., Kanki, J.P., Chien, C.-B., 2007. The Tol2kit: a multisite gateway-based construction kit for Tol2 transposon transgenesis constructs. *Dev. Dyn.* 236, 3088–3099. doi:10.1002/dvdy.21343
- Kwan, K.M., Otsuna, H., Kidokoro, H., Carney, K.R., Saijoh, Y., Chien, C.-B., 2012. A complex choreography of cell movements shapes the vertebrate eye. *Development* 139, 359–372. doi:10.1242/dev.071407
- LaFoya, B., Munroe, J.A., Mia, M.M., Detweiler, M.A., Crow, J.J., Wood, T., Roth, S., Sharma, B., Albig, A.R., 2016. Notch: A multi-functional integrating system of microenvironmental signals. *Developmental Biology* 418, 227–241. doi:10.1016/j.ydbio.2016.08.023
- Lamb, T.D., 2013. Evolution of phototransduction, vertebrate photoreceptors and retina. *Progress in Retinal and Eye Research* 36, 52–119. doi:10.1016/j.preteyeres.2013.06.001
- Lamb, T.D., Collin, S.P., Pugh, E.N., 2007. Evolution of the vertebrate eye: opsins, photoreceptors, retina and eye cup. *Nature Reviews Neuroscience* 8, 960–976. doi:10.1038/nrn2283
- Lamouille, S., Xu, J., Derynck, R., 2014. Molecular mechanisms of epithelial-mesenchymal transition. *Nature Reviews Molecular Cell Biology* 15, 178–196. doi:10.1038/nrm3758
- Lander, A.D., 2011. Pattern, Growth and Control. *Cell* 144, 955–969. doi:10.1016/j.cell.2011.03.009
- Lange, C., Huttner, W.B., Calegari, F., 2009. Cdk4/CyclinD1 Overexpression in Neural Stem Cells Shortens G1, Delays Neurogenesis and Promotes the Generation and Expansion of Basal Progenitors. *Cell Stem Cell* 5, 320–331. doi:10.1016/j.stem.2009.05.026
- Lawrence, P.A., Shelton, P.M., 1975. The determination of polarity in the developing insect retina. *J Embryol Exp Morphol* 33, 471–486.
- Lecuit, T., Le Goff, L., 2007. Orchestrating size and shape during morphogenesis. *Nature* 450, 189–192. doi:10.1038/nature06304
- Lecuit, T., Lenne, P.-F., 2007. Cell surface mechanics and the control of cell shape, tissue patterns

- and morphogenesis. *Nature Reviews Molecular Cell Biology* 8, 633–644. doi:10.1038/nrm2222
- Lecuit, T., Yap, A.S., 2015. E-cadherin junctions as active mechanical integrators in tissue dynamics. *Nature Cell Biology* 17, 533–539. doi:10.1038/ncb3136
- LeGoff, L., Lecuit, T., 2015. Mechanical Forces and Growth in Animal Tissues. *Cold Spring Harb Perspect Biol* a019232. doi:10.1101/cshperspect.a019232
- Leong, K.G., Hu, X., Li, L., Nosedá, M., Larrivé, B., Hull, C., Hood, L., Wong, F., Karsan, A., 2002. Activated Notch4 inhibits angiogenesis: role of beta 1-integrin activation. *Mol. Cell. Biol.* 22, 2830–2841.
- Leung, L., Klopper, A.V., Grill, S.W., Harris, W.A., Norden, C., 2012. Apical migration of nuclei during G2 is a prerequisite for all nuclear motion in zebrafish neuroepithelia. *Development* 139, 2635–2635. doi:10.1242/dev.085456
- Leung, L., Klopper, A.V., Grill, S.W., Harris, W.A., Norden, C., 2011. Apical migration of nuclei during G2 is a prerequisite for all nuclear motion in zebrafish neuroepithelia. *Development* 138, 5003–5013. doi:10.1242/dev.071522
- Levine, E.M., Green, E.S., 2004. Cell-intrinsic regulators of proliferation in vertebrate retinal progenitors. *Seminars in Cell & Developmental Biology* 15, 63–74. doi:10.1016/j.semcdb.2003.09.001
- Lienkamp, S. S., Liu, K., Karner, C. M., Carroll, T. J., Ronneberger, O., Wallingford, J. B., & Walz, G. (2012). Vertebrate kidney tubules elongate using a planar cell polarity-dependent, rosette-based mechanism of convergent extension. *Nature Genetics*, 44(12), 1382–1387. <http://doi.org/10.1038/ng.2452>
- Liu, W., Mo, Z., Xiang, M., 2001. The Ath5 proneural genes function upstream of Brn3 POU domain transcription factor genes to promote retinal ganglion cell development. *Proc. Natl. Acad. Sci. U.S.A.* 98, 1649–1654. doi:10.1073/pnas.98.4.1649
- Loganathan, R., Rongish, B.J., Smith, C.M., Filla, M.B., Czirok, A., Bénazéraf, B., Little, C.D., 2016. Extracellular matrix motion and early morphogenesis. *Development* 143, 2056–2065. doi:10.1242/dev.127886
- Lowery, L.A., Sive, H., 2005. Initial formation of zebrafish brain ventricles occurs independently of circulation and requires the *nagie oko* and *snakehead/atp1a1a.1* gene products. *Development* 132, 2057–2067. doi:10.1242/dev.01791
- Ma, M., Cao, X., Dai, J., Pastor-Pareja, J.C., 2017. Basement Membrane Manipulation in *Drosophila* Wing Discs Affects Dpp Retention but Not Growth Mechanoregulation. *Developmental Cell* 42, 97–106.e4. doi:10.1016/j.devcel.2017.06.004
- MacDonald, R.B., Randlett, O., Oswald, J., Yoshimatsu, T., Franze, K., Harris, W.A., 2015. Müller glia provide essential tensile strength to the developing retina. *J Cell Biol* 210, 1075–1083. doi:10.1083/jcb.201503115
- Mammoto, T., Ingber, D.E., 2010. Mechanical control of tissue and organ development. *Development* 137, 1407–1420. doi:10.1242/dev.024166
- Mao, Y., Tournier, A. L., Bates, P. A., Gale, J. E., Tapon, N., & Thompson, B. J. (2011). Planar polarization of the atypical myosin Dachs orients cell divisions in *Drosophila*. *Genes & Development*, 25(2), 131–136. <http://doi.org/10.1101/gad.610511>
- Mao, Y., Tournier, A.L., Hoppe, A., Kester, L., Thompson, B.J., Tapon, N., 2013. Differential proliferation rates generate patterns of mechanical tension that orient tissue growth. *The EMBO Journal* 32, 2790–2803. doi:10.1038/emboj.2013.197
- Marinari, E., Mehonic, A., Curran, S., Gale, J., Duke, T., Baum, B., 2012. Live-cell delamination counterbalances epithelial growth to limit tissue overcrowding. *Nature* 484, 542–545. doi:10.1038/nature10984
- Marlow, H.Q., Srivastava, M., Matus, D.Q., Rokhsar, D., Martindale, M.Q., 2009. Anatomy and development of the nervous system of *Nematostella vectensis*, an anthozoan cnidarian. *Developmental Neurobiology* 69, 235–254. doi:10.1002/dneu.20698
- Martin, A.C., Goldstein, B., 2014. Apical constriction: themes and variations on a cellular mechanism driving morphogenesis. *Development* 141, 1987–1998. doi:10.1242/dev.102228
- Martinez-Morales, J.R., Rembold, M., Greger, K., Simpson, J.C., Brown, K.E., Quiring, R., Pepperkok, R., Martín-Bermudo, M.D., Himmelbauer, H., Wittbrodt, J., 2009. ojolano-mediated basal constriction is essential for optic cup morphogenesis. *Development* 136, 2165–2175. doi:10.1242/dev.033563

- Maung, S.M.T.W., Jenny, A., 2011. Planar cell polarity in *Drosophila*. *Organogenesis* 7, 165–179. doi:10.4161/org.7.3.18143
- Meighan, C.M., Schwarzbauer, J.E., 2008. Temporal and spatial regulation of integrins during development. *Current opinion in cell biology* 20, 520–524. doi:10.1016/j.ceb.2008.05.010
- Metcalf, D., 1964. Restricted Growth Capacity of Multiple Spleen Grafts. *Transplantation* 2, 387–392.
- Metcalf, D., 1963. The autonomous behaviour of normal thymus grafts. *Aust J Exp Biol Med Sci* 41, SUPPL437–47.
- Meyer, E.J., Ikmi, A., Gibson, M.C., 2011. Interkinetic Nuclear Migration Is a Broadly Conserved Feature of Cell Division in Pseudostratified Epithelia. *Current Biology* 21, 485–491. doi:10.1016/j.cub.2011.02.002
- Mickoleit, M., Schmid, B., Weber, M., Fahrbach, F.O., Hombach, S., Reischauer, S., Huisken, J., 2014. High-resolution reconstruction of the beating zebrafish heart. *Nat. Methods* 11, 919–922. doi:10.1038/nmeth.3037
- Miesfeld, J.B., Gestri, G., Clark, B.S., Flinn, M.A., Poole, R.J., Bader, J.R., Besharse, J.C., Wilson, S.W., Link, B.A., 2015. Yap and Taz regulate retinal pigment epithelial cell fate. *Development (Cambridge, England)* 142, 3021–3032. doi:10.1242/dev.119008
- Miyata, T., Okamoto, M., Shinoda, T., Kawaguchi, A., 2015. Interkinetic nuclear migration generates and opposes ventricular-zone crowding: insight into tissue mechanics. *Front. Cell. Neurosci.* 8, 673. doi:10.3389/fncel.2014.00473
- Moeller, M.E., Nagy, S., Gerlach, S.U., Soegaard, K.C., Danielsen, E.T., Texada, M.J., Rewitz, K.F., 2017. Warts Signaling Controls Organ and Body Growth through Regulation of Ecdysone. *Current Biology* 27, 1652–1659.e4. doi:10.1016/j.cub.2017.04.048
- Morin, P.J., 1999. β -catenin signaling and cancer. *BioEssays* 21, 1021–1030. doi:10.1002/(SICI)1521-1878(199912)22:1<1021::AID-BIES6>3.0.CO;2-P
- Morrissey, M.A., Sherwood, D.R., 2015. An active role for basement membrane assembly and modification in tissue sculpting. *J Cell Sci* 128, 1661–1668. doi:10.1242/jcs.168021
- Munjal, A., Philippe, J.-M., Munro, E., Lecuit, T., 2015. A self-organized biomechanical network drives shape changes during tissue morphogenesis. *Nature* 524, 351–355. doi:10.1038/nature14603
- Nagele, R.G., Lee, H.-Y., 1979. Ultrastructural changes in cells associated with interkinetic nuclear migration in the developing chick neuroepithelium. *J. Exp. Zool.* 210, 89–105. doi:10.1002/jez.1402100110
- Nakano, T. ando, S., Takata, N., Kawada, M., Muguruma, K., Sekiguchi, K., Saito, K., Yonemura, S., Eiraku, M., Sasai, Y., 2012. Self-Formation of Optic Cups and Storable Stratified Neural Retina from Human ESCs. *Cell Stem Cell* 10, 771–785. doi:10.1016/j.stem.2012.05.009
- Nasonkin, I.O., Lazo, K., Hambright, D., Brooks, M., Fariss, R., Swaroop, A., 2011. Distinct nuclear localization patterns of DNA methyltransferases in developing and mature mammalian retina. *Journal of Comparative Neurology* 519, 1914–1930. doi:10.1002/cne.22613
- Nelson, C.M., Jean, R.P., Tan, J.L., Liu, W.F., Sniadecki, N.J., Spector, A.A., Chen, C.S., 2005. From the Cover: Emergent patterns of growth controlled by multicellular form and mechanics. *Proc. Natl. Acad. Sci. U.S.A.* 102, 11594–11599. doi:10.1073/pnas.0502575102
- Ninov, N., Chiarelli, D.A., Martin-Blanco, E., 2007. Extrinsic and intrinsic mechanisms directing epithelial cell sheet replacement during *Drosophila* metamorphosis. *Development* 134, 367–379. doi:10.1242/dev.02728
- Norden, C., 2017. Pseudostratified epithelia - cell biology, diversity and roles in organ formation at a glance. *J Cell Sci* 130, 1859–1863. doi:10.1242/jcs.192997
- Norden, C., Young, S., Link, B.A., Harris, W.A., 2009. Actomyosin Is the Main Driver of Interkinetic Nuclear Migration in the Retina. *Cell* 138, 1195–1208. doi:10.1016/j.cell.2009.06.032
- Onder, T.T., Gupta, P.B., Mani, S.A., Yang, J., Lander, E.S., Weinberg, R.A., 2008. Loss of E-Cadherin Promotes Metastasis via Multiple Downstream Transcriptional Pathways. *Cancer Res* 68, 3645–3654. doi:10.1158/0008-5472.CAN-07-2938
- Paluch, E. K., Nelson, C. M., Biaias, N., Fabry, B., Moeller, J., Pruitt, B. L., et al. (2015). Mechanotransduction: use the force(s). *BMC Biology*, 13(1), 935. <http://doi.org/10.1186/s12915-015-0150-4>
- Paluch, E., Heisenberg, C.-P., 2009. Biology and Physics of Cell Shape Changes in Development.

- Current Biology 19, R790–R799. doi:10.1016/j.cub.2009.07.029
- Palyanov, A., Khayrulin, S., Larson, S.D., 2016. Application of smoothed particle hydrodynamics to modeling mechanisms of biological tissue. *Advances in Engineering Software* 98, 1–11. doi:10.1016/j.advengsoft.2016.03.002
- Paoli, P., Giannoni, E., Chiarugi, P., 2013. Anoikis molecular pathways and its role in cancer progression. *Biochimica et Biophysica Acta (BBA) - Molecular Cell Research* 1833, 3481–3498. doi:10.1016/j.bbamcr.2013.06.026
- Parker, J., Struhl, G., 2015. Scaling the Drosophila Wing: TOR-Dependent Target Gene Access by the Hippo Pathway Transducer Yorkie. *PLOS Biol* 13, e1002274. doi:10.1371/journal.pbio.1002274
- Parker, N.F., Shingleton, A.W., 2011. The coordination of growth among Drosophila organs in response to localized growth-perturbation. *Developmental Biology* 357, 318–325. doi:10.1016/j.ydbio.2011.07.002
- Pasakarnis, L., Frei, E., Caussinus, E., Affolter, M., Brunner, D., 2016. Amnioserosa cell constriction but not epidermal actin cable tension autonomously drives dorsal closure. *Nature Cell Biology* 18, 1161–1172. doi:10.1038/ncb3420
- Pastor-Pareja, J.C., Xu, T., 2011. Shaping Cells and Organs in Drosophila by Opposing Roles of Fat Body-Secreted Collagen IV and Perlecan. *Developmental Cell* 21, 245–256. doi:10.1016/j.devcel.2011.06.026
- Perrimon, N., Pitsouli, C., Shilo, B.-Z., 2012. Signaling Mechanisms Controlling Cell Fate and Embryonic Patterning. *Cold Spring Harb Perspect Biol* 4, a005975–a005975. doi:10.1101/cshperspect.a005975
- Petridou, N.I., Skourides, P.A., 2014. FAK transduces extracellular forces that orient the mitotic spindle and control tissue morphogenesis. *Nature Communications* 5, ncomms6240. doi:10.1038/ncomms6240
- Petridou, N.I., Spiró, Z., Heisenberg, C.-P., 2017. Multiscale force sensing in development. *Nature Cell Biology* 19, 581–588. doi:10.1038/ncb3524
- Picker, A., Cavodeassi, F., Machate, A., Bernauer, S., Hans, S., Abe, G., Kawakami, K., Wilson, S.W., Brand, M., 2009. Dynamic coupling of pattern formation and morphogenesis in the developing vertebrate retina. *PLOS Biol* 7, e1000214. doi:10.1371/journal.pbio.1000214
- Pilot, F., Lecuit, T., 2005. Compartmentalized morphogenesis in epithelia: From cell to tissue shape. *Developmental Dynamics* 232, 685–694. doi:10.1002/dvdy.20334
- Pittman, A.J., Law, M.-Y., Chien, C.-B., 2008. Pathfinding in a large vertebrate axon tract: isotopic interactions guide retinotectal axons at multiple choice points. *Development* 135, 2865–2871. doi:10.1242/dev.025049
- Polyakov, O., He, B., Swan, M., Shaevitz, J.W., Kaschube, M., Wieschaus, E., 2014. Passive Mechanical Forces Control Cell-Shape Change during Drosophila Ventral Furrow Formation. *Biophysical Journal* 107, 998–1010. doi:10.1016/j.bpj.2014.07.013
- Porazinski, S., Wang, H., Asaoka, Y., Behrndt, M., Miyamoto, T., Morita, H., Hata, S., Sasaki, T., Krens, S.F.G., Osada, Y., Asaka, S., Momoi, A., Linton, S., Miesfeld, J.B., Link, B.A., Senga, T., Castillo-Morales, A., Urrutia, A.O., Shimizu, N., Nagase, H., Matsuura, S., Bagby, S., Kondoh, H., Nishina, H., Heisenberg, C.-P., Furutani-Seiki, M., 2015. YAP is essential for tissue tension to ensure vertebrate 3D body shape. *Nature* 521, 217–221. doi:10.1038/nature14215
- Provenzano, P.P., Keely, P.J., 2011. Mechanical signaling through the cytoskeleton regulates cell proliferation by coordinated focal adhesion and Rho GTPase signaling. *J Cell Sci* 124, 1195–1205. doi:10.1242/jcs.067009
- Randlett, O., MacDonald, R.B., Yoshimatsu, T., Almeida, A.D., Suzuki, S.C., Wong, R.O., Harris, W.A., 2013. Cellular Requirements for Building a Retinal Neuropil. *Cell Rep* 3, 282–290. doi:10.1016/j.celrep.2013.01.020
- Randlett, O., Poggi, L., Zolessi, F.R., Harris, W.A., 2011. The Oriented Emergence of Axons from Retinal Ganglion Cells Is Directed by Laminin Contact In Vivo. *Neuron* 70, 266–280. doi:10.1016/j.neuron.2011.03.013
- Rapaport, D.H., Wong, L.L., Wood, E.D., Yasumura, D., LaVail, M.M., 2004. Timing and topography of cell genesis in the rat retina. *J. Comp. Neurol.* 474, 304–324. doi:10.1002/cne.20134
- Razavi, M.J., Zhang, T., Liu, T., Wang, X., 2015. Cortical Folding Pattern and its Consistency

- Induced by Biological Growth. *Sci Rep* 5, srep14477. doi:10.1038/srep14477
- Reya, T., Duncan, A.W., Ailles, L., Domen, J., Scherer, D.C., Willert, K., Hintz, L., Nusse, R., Weissman, I.L., 2003. A role for Wnt signalling in self-renewal of haematopoietic stem cells. *Nature* 423, 409–414. doi:10.1038/nature01593
- Rodriguez, D., Braden, B.P., Boyer, S.W., Taketa, D.A., Setar, L., Calhoun, C., Maio, A.D., Langenbacher, A., Valentine, M.T., De Tomaso, A.W., 2017. In vivo manipulation of the extracellular matrix induces vascular regression in a basal chordate. *Mol. Biol. Cell* 28, 1883–1893. doi:10.1091/mbc.E17-01-0009
- Rosenblatt, J., Raff, M.C., Cramer, L.P., 2001. An epithelial cell destined for apoptosis signals its neighbors to extrude it by an actin- and myosin-dependent mechanism. *Current Biology* 11, 1847–1857. doi:10.1016/S0960-9822(01)00587-5
- Ross, S.E., Greenberg, M.E., Stiles, C.D., 2003. Basic helix-loop-helix factors in cortical development. *Neuron* 39, 13–25.
- Röper, K., 2015. Integration of cell-cell adhesion and contractile actomyosin activity during morphogenesis. *Cellular Adhesion in Development and Disease, Current Topics in Developmental Biology* 112, 103–127. doi:10.1016/bs.ctdb.2014.11.017
- Röper, K., 2013. Supracellular actomyosin assemblies during development. *Bioarchitecture* 3, 45–49. doi:10.4161/bioa.25339
- Rubin, H., Stoker, M.G.P., 1967. Density Dependent Inhibition of Cell Growth in Culture [WWW Document]. *nature.com*. URL <https://www.nature.com/nature/journal/v215/n5097/pdf/215171a0.pdf> (accessed 8.28.17).
- Rujano, M.A., Sanchez-Pulido, L., Pennetier, C., le Dez, G., Basto, R., 2013. The microcephaly protein Asp regulates neuroepithelium morphogenesis by controlling the spatial distribution of myosin II. *Nature Cell Biology* 15, 1294–1306. doi:10.1038/ncb2858
- Sai, X., Ladher, R.K., 2008. FGF Signaling Regulates Cytoskeletal Remodeling during Epithelial Morphogenesis. *Current Biology* 18, 976–981. doi:10.1016/j.cub.2008.05.049
- Salbreux, G., Charras, G., Paluch, E., 2012. Actin cortex mechanics and cellular morphogenesis. *Trends in Cell Biology* 22, 536–545.
- Sandquist, J.C., Larson, M.E., Hine, K.J., 2016. Myosin-10 independently influences mitotic spindle structure and mitotic progression. *Cytoskeleton* 73, 351–364. doi:10.1002/cm.21311
- Sauer, F.C., 1935. Mitosis in the neural tube. *J. Comp. Neurol.* 62, 377–405. doi:10.1002/cne.900620207
- Sawyer, J.M., Harrell, J.R., Shemer, G., Sullivan-Brown, J., Roh-Johnson, M., Goldstein, B., 2010. Apical constriction: a cell shape change that can drive morphogenesis. *Developmental Biology* 341, 5–19. doi:10.1016/j.ydbio.2009.09.009
- Schindelin, J., Arganda-Carreras, I., Frise, E., Kaynig, V., Longair, M., Pietzsch, T., Preibisch, S., Rueden, C., Saalfeld, S., Schmid, B., Tinevez, J.-Y., White, D.J., Hartenstein, V., Eliceiri, K., Tomancak, P., Cardona, A., 2012. Fiji: an open-source platform for biological-image analysis. *Nat. Methods* 9, 676–682. doi:10.1038/nmeth.2019
- Schluck, T., Nienhaus, U., Aegerter-Wilmsen, T., Aegerter, C.M., 2013. Mechanical Control of Organ Size in the Development of the Drosophila Wing Disc. *PLoS ONE* 8, e76171. doi:10.1371/journal.pone.0076171
- Schoenwolf, G.C., Alvarez, I.S., 1989. Roles of neuroepithelial cell rearrangement and division in shaping of the avian neural plate. *Development* 106, 427–439.
- Sernagor, E., Eglén, S., Harris, B., Wong, R., 2009. *Retinal Development*. Cambridge University Press, Cambridge. doi:10.1017/CBO9780511541629
- Shen, J., Dahmann, C., 2005. Extrusion of Cells with Inappropriate Dpp Signaling from Drosophila Wing Disc Epithelia. *Science* 307, 1789–1790. doi:10.1126/science.1104784
- Shraiman, B.I., 2005. Mechanical feedback as a possible regulator of tissue growth. *Proc. Natl. Acad. Sci. U.S.A.* 102, 3318–3323. doi:10.1073/pnas.0404782102
- Sidhaye, J., Norden, C., 2017. Concerted action of neuroepithelial basal shrinkage and active epithelial migration ensures efficient optic cup morphogenesis. *eLife* 6, 73. doi:10.7554/eLife.22689
- Sinha, B., Köster, D., Ruez, R., Gonnord, P., Bastiani, M., Abankwa, D., Stan, R.V., Butler-Browne, G., Védie, B., Johannes, L., Morone, N., Parton, R.G., Raposo, G., Sens, P., Lamaze, C., Nassoy, P., 2011. Cells Respond to Mechanical Stress by Rapid Disassembly of Caveolae.

- Cell 144, 402–413. doi:10.1016/j.cell.2010.12.031
- Slattum, G., McGee, K.M., Rosenblatt, J., 2009. P115 RhoGEF and microtubules decide the direction apoptotic cells extrude from an epithelium. *J Cell Biol* 186, 693–702. doi:10.1083/jcb.200903079
- Slattum, G., Rosenblatt, J., 2014. Tumour cell invasion: an emerging role for basal epithelial cell extrusion. *Nature reviews. Cancer* 14, 495–501. doi:10.1038/nrc3767
- Smart, I.H., 1973. Proliferative characteristics of the ependymal layer during the early development of the mouse neocortex: a pilot study based on recording the number, location and plane of cleavage of mitotic figures. *J. Anat.* 116, 67–91. doi:10.1111/(ISSN)1469-7580
- Smart, I.H., 1972. Proliferative characteristics of the ependymal layer during the early development of the spinal cord in the mouse. *J. Anat.* 111, 365–380. doi:10.1111/(ISSN)1469-7580
- Spear, P.C., Erickson, C.A., 2012. Apical movement during interkinetic nuclear migration is a two-step process. *Developmental Biology* 370, 33–41. doi:10.1016/j.ydbio.2012.06.031
- Stadler, J.A., Shkumatava, A., Norton, W.H.J., Rau, M.J., Geisler, R., Fischer, S., Neumann, C.J., 2005. Histone deacetylase 1 is required for cell cycle exit and differentiation in the zebrafish retina. *Dev. Dyn.* 233, 883–889. doi:10.1002/dvdy.20427
- Streichan, S. J., Hoerner, C. R., Schneidt, T., Holzer, D., & Hufnagel, L. (2014). Spatial constraints control cell proliferation in tissues. *Proceedings of the National Academy of Sciences of the United States of America*, 111(15), 5586–5591. <http://doi.org/10.1073/pnas.1323016111>
- Strzyz, P.J., Lee, H.O., Sidhaye, J., Weber, I.P., Leung, L.C., Norden, C., 2015. Interkinetic nuclear migration is centrosome independent and ensures apical cell division to maintain tissue integrity. *Developmental Cell* 32, 203–219. doi:10.1016/j.devcel.2014.12.001
- Strzyz, P.J., Matejcic, M., Norden, C., 2016. Heterogeneity, Cell Biology and Tissue Mechanics of Pseudostratified Epithelia: Coordination of Cell Divisions and Growth in Tightly Packed Tissues. *Int Rev Cell Mol Biol* 325, 89–118. doi:10.1016/bs.ircmb.2016.02.004
- Stückemann, T., Cleland, J.P., Werner, S., Thi-Kim Vu, H., Bayersdorf, R., Liu, S.-Y., Friedrich, B., Jülicher, F., Rink, J.C., 2017. Antagonistic Self-Organizing Patterning Systems Control Maintenance and Regeneration of the Anteroposterior Axis in Planarians. *Developmental Cell* 40, 248–263.e4. doi:10.1016/j.devcel.2016.12.024
- Sui, L., Pflugfelder, G.O., Shen, J., 2012. The Dorsocross T-box transcription factors promote tissue morphogenesis in the *Drosophila* wing imaginal disc. *Development* 139, 2773–2782. doi:10.1242/dev.079384
- Sun, Z., Amourda, C., Shagirov, M., Hara, Y., Saunders, T.E., Toyama, Y., 2017. Basolateral protrusion and apical contraction cooperatively drive *Drosophila* germ-band extension. *Nature Cell Biology* 19, 375–383. doi:10.1038/ncb3497
- Swaminathan, V., Waterman, C.M., 2016. The molecular clutch model for mechanotransduction evolves. *Nature Cell Biology* 18, 459–461. doi:10.1038/ncb3350
- Szigeti, B., Gleeson, P., Vella, M., Khayrulin, S., Palyanov, A., Hokanson, J., Currie, M., Cantarelli, M., Idili, G., Larson, S., 2014. OpenWorm: an open-science approach to modeling *Caenorhabditis elegans*. *Front. Comput. Neurosci.* 8, 708. doi:10.3389/fncom.2014.00137
- Tabata, T., Takei, Y., 2004. Morphogens, their identification and regulation. *Development* 131, 703–712. doi:10.1242/dev.01043
- Tada, M., Heisenberg, C.-P., 2012. Convergent extension: using collective cell migration and cell intercalation to shape embryos. *Development* 139, 3897–3904. doi:10.1242/dev.073007
- Tang, H.Y., Smith-Caldas, M.S.B., Driscoll, M.V., Salhadar, S., Shingleton, A.W., 2011. FOXO Regulates Organ-Specific Phenotypic Plasticity In *Drosophila*. *PLOS Genet* 7, e1002373. doi:10.1371/journal.pgen.1002373
- Thompson, D.W., 2014. *On Growth and Form*. Cambridge University Press.
- Tsai, J.-W., Lian, W.-N., Kemal, S., Kriegstein, A.R., Vallee, R.B., 2010. Kinesin 3 and cytoplasmic dynein mediate interkinetic nuclear migration in neural stem cells. *Nature Neuroscience* 13, 1463–1471. doi:10.1038/nn.2665
- Tumaneng, K., Schlegelmilch, K., Russell, R.C., Yimlamai, D., Basnet, H., Mahadevan, N., Fitamant, J., Bardeesy, N., Camargo, F.D., Guan, K.-L., 2012. YAP mediates crosstalk between the Hippo and PI(3)K–TOR pathways by suppressing PTEN via miR-29. *Nature Cell Biology* 14, 1322–1329. doi:10.1038/ncb2615
- Twitty, V.C., Schwind, J.L., 1931. The growth of eyes and limbs transplanted heteroplastically

-
- between two species of *Amblystoma*. *Journal of Experimental Zoology Part A: Ecological Genetics and Physiology* 59, 61–86. doi:10.1002/jez.1400590105
- van de Wetering, M., Sancho, E., Verweij, C., de Lau, W., Oving, I., Hurlstone, A., van der Horn, K., Batlle, E., Coudreuse, D., Haramis, A.-P., Tjon-Pon-Fong, M., Moerer, P., van den Born, M., Soete, G., Pals, S., Eilers, M., Medema, R., Clevers, H., 2002. The β -Catenin/TCF-4 Complex Imposes a Crypt Progenitor Phenotype on Colorectal Cancer Cells. *Cell* 111, 241–250. doi:10.1016/S0092-8674(02)01014-0
- Villa-Cuesta, E., González-Pérez, E., Modolell, J., 2007. Apposition of iroquois expressing and non-expressing cells leads to cell sorting and fold formation in the *Drosophila* imaginal wing disc. *BMC Dev Biol* 7, 106. doi:10.1186/1471-213X-7-106
- Vinson, C.R., Adler, P.N., 1987. Directional non-cell autonomy and the transmission of polarity information by the frizzled gene of *Drosophila*. *Nature* 329, 549–551. doi:10.1038/329549a0
- Weber, I.P., Ramos, A.P., Strzyz, P.J., Leung, L.C., Young, S., Norden, C., 2014. Mitotic position and morphology of committed precursor cells in the zebrafish retina adapt to architectural changes upon tissue maturation. *Cell Rep* 7, 386–397. doi:10.1016/j.celrep.2014.03.014
- Widmann, T.J., Dahmann, C., 2009a. Dpp signaling promotes the cuboidal-to-columnar shape transition of *Drosophila* wing disc epithelia by regulating Rho1. *J Cell Sci* 122, 1362–1373. doi:10.1242/jcs.044271
- Widmann, T.J., Dahmann, C., 2009b. Wingless signaling and the control of cell shape in *Drosophila* wing imaginal discs. *Developmental Biology* 334, 161–173. doi:10.1016/j.ydbio.2009.07.013
- Winder, S.J., Ayscough, K.R., 2005. Actin-binding proteins. *J Cell Sci* 118, 651–654. doi:10.1242/jcs.01670
- Woolner, S., O'Brien, L.L., Wiese, C., Bement, W.M., 2008. Myosin-10 and actin filaments are essential for mitotic spindle function. *The Journal of Cell Biology* 182, 77–88. doi:10.1083/jcb.200804062
- Wu, S., Liu, Y., Zheng, Y., Dong, J., Pan, D., 2008. The TEAD/TEF family protein Scalloped mediates transcriptional output of the Hippo growth-regulatory pathway. *Developmental Cell* 14, 388–398. doi:10.1016/j.devcel.2008.01.007
- Xie, Z., Moy, L.Y., Sanada, K., Zhou, Y., Buchman, J.J., Tsai, L.-H., 2007. Cep120 and TACCs Control Interkinetic Nuclear Migration and the Neural Progenitor Pool. *Neuron* 56, 79–93. doi:10.1016/j.neuron.2007.08.026
- Yamaguchi, M., Tonou-Fujimori, N., Komori, A., Maeda, R., Nojima, Y., Li, H., Okamoto, H., Masai, I., 2005. Histone deacetylase 1 regulates retinal neurogenesis in zebrafish by suppressing Wnt and Notch signaling pathways. *Development* 132, 3027–3043. doi:10.1242/dev.01881
- Yang, Z., Ding, K., Pan, L., Deng, M., Gan, L., 2003. Math5 determines the competence state of retinal ganglion cell progenitors. *Developmental Biology* 264, 240–254. doi:10.1016/j.ydbio.2003.08.005
- Yonemura, S., Wada, Y., Watanabe, T., Nagafuchi, A., & Shibata, M. (2010). α -Catenin as a tension transducer that induces adherens junction development. *Nature Cell Biology*, 12(6), 533–U35. <http://doi.org/10.1038/ncb2055>
- Yu, F.-X., Zhao, B., Guan, K.-L., 2015. Hippo Pathway in Organ Size Control, Tissue Homeostasis and Cancer. *Cell* 163, 811–828. doi:10.1016/j.cell.2015.10.044
- Yurchenco, P.D., 2011. Basement Membranes: Cell Scaffoldings and Signaling Platforms. *Cold Spring Harb Perspect Biol* 3, a004911–a004911. doi:10.1101/cshperspect.a004911
- Zecca, M., Basler, K., Struhl, G., 1995. Sequential organizing activities of engrailed, hedgehog and decapentaplegic in the *Drosophila* wing. *Development* 121, 2265–2278. doi:10.5167/uzh-1053
- Zhao, B., Wei, X., Li, W., Udan, R. S., Yang, Q., Kim, J., et al. (2007). Inactivation of YAP oncoprotein by the Hippo pathway is involved in cell contact inhibition and tissue growth control. *Genes & Development*, 21(21), 2747–2761. <http://doi.org/10.1101/gad.1602907>
- Zuber, M.E., 2010. Eye Field Specification in *Xenopus laevis*. *Current topics in developmental biology* 93, 29–60. doi:10.1016/B978-0-12-385044-7.00002-3

APPENDIX

CONTENTS

- 1 Strzyz, P.J., **Matejic, M.**, Norden, C. (2016). Heterogeneity, Cell Biology and Tissue Mechanics of Pseudostratified Epithelia: Coordination of Cell Divisions and Growth in Tightly Packed Tissues. *International Review of Cell and Molecular Biology*, 325, 89-118
- 2 HDAC1 mutants genotyping protocol

Heterogeneity, Cell Biology and Tissue Mechanics of Pseudostratified Epithelia: Coordination of Cell Divisions and Growth in Tightly Packed Tissues

P.J. Strzyz*, **M. Matejic**, **C. Norden***

Max Planck Institute of Molecular Cell Biology and Genetics, Dresden, Germany

*Corresponding authors. E-mail address: paulina.strzyz@gmail.com

Contents

1. Introduction	2
1.1 Widespread Presence of Pseudostratified Epithelia in Diverse Developmental Contexts	4
1.2 Heterogeneity of Pseudostratified Epithelia	4
2. Apical Nuclear Migration in Pseudostratified Epithelia	6
2.1 Machineries Responsible for PRAM	7
2.2 Nuclear Migration in Tightly Packed Tissue	9
2.3 PRAM and Its Links to Cell Cycle	10
2.4 PRAM and Establishment of Proliferative Zone at Apical Surface	11
2.5 PRAM and Mitotic Entry	13
2.6 PRAM and Centrosome Position	14
2.7 PRAM and Efficient Cell Reintegration Into Tissue Following Division	15
3. Tissue-Wide Properties of PSE	16
3.1 PSE Tissue Packing	16
3.2 Packing Increase in PSE	19
3.3 Linking Mechanical Stimulation to PSE Responses	21
3.4 Hippo Pathway as Example of Mechanosensitive Signaling Pathway	22
3.5 Piezo Channel as Example of Mechanosensitive Cellular Response Element	23
3.6 Possible Origins and Effects of Mechanical Forces in PSE	24
4. Conclusions	26
Acknowledgments	26
References	26

Abstract

Pseudostratified epithelia (PSE) are tightly packed proliferative tissues that are important precursors of the development of diverse organs in a plethora of species, invertebrate and vertebrate. PSE consist of elongated epithelial cells that are attached to the apical and basal side of the tissue. The nuclei of these cells undergo interkinetic nuclear migration (IKNM) which leads to all mitotic events taking place at the apical surface of the epithelium. In this review, we discuss the intricacies of proliferation in PSE, considering cell biological, as well as the physical aspects. First, we summarize the principles governing the invariability of apical nuclear migration and apical cell division as well as the importance of apical mitoses for tissue proliferation. Then, we focus on the mechanical and structural features of these tissues. Here, we discuss how the overall architecture of pseudostratified tissues changes with increased cell packing. Lastly, we consider possible mechanical cues resulting from these changes and their potential influence on cell proliferation.



1. INTRODUCTION

Pseudostratified epithelia (PSE) are proliferative tissues that feature elongated epithelial cells. These cells are organized into a single, tightly packed epithelial layer (Fig. 1). PSE give rise to various tissues in a wide range of invertebrate and vertebrate organisms. The term pseudostratified arose from initial observations of PSE, where the various positions that the nuclei of these epithelia occupy along the apico-basal axis were interpreted as cell stratification. However, it later became clear that despite its stratified appearance, all cells within the epithelial sheet are attached to both the apical and basal surfaces of the tissue (Sauer, 1935; Smart, 1972) (Fig. 1). The nuclei in PSE are dynamic and perform apico-basal movements correlated with the cell cycle. These nuclear movements are known as interkinetic nuclear migration (IKNM) (Sauer, 1935). IKNM consists of different modes of nuclear movement: Shortly before mitosis, nuclei move to the apical surface in a rapid and directed manner (Kosodo et al., 2011; Norden et al., 2009; Strzyz et al., 2015; Tsai et al., 2010). This apical migration is highly conserved among organisms and appears in all cells within PSE before cell division. Consequently, all mitotic events in PSE are localized to the apical surface of the tissue. Following division, daughter nuclei are displaced from the apical surface and localize to more basal positions. In most systems studied so far this basal translocation is slower than apical migration (Kosodo et al., 2011; Norden et al., 2009).

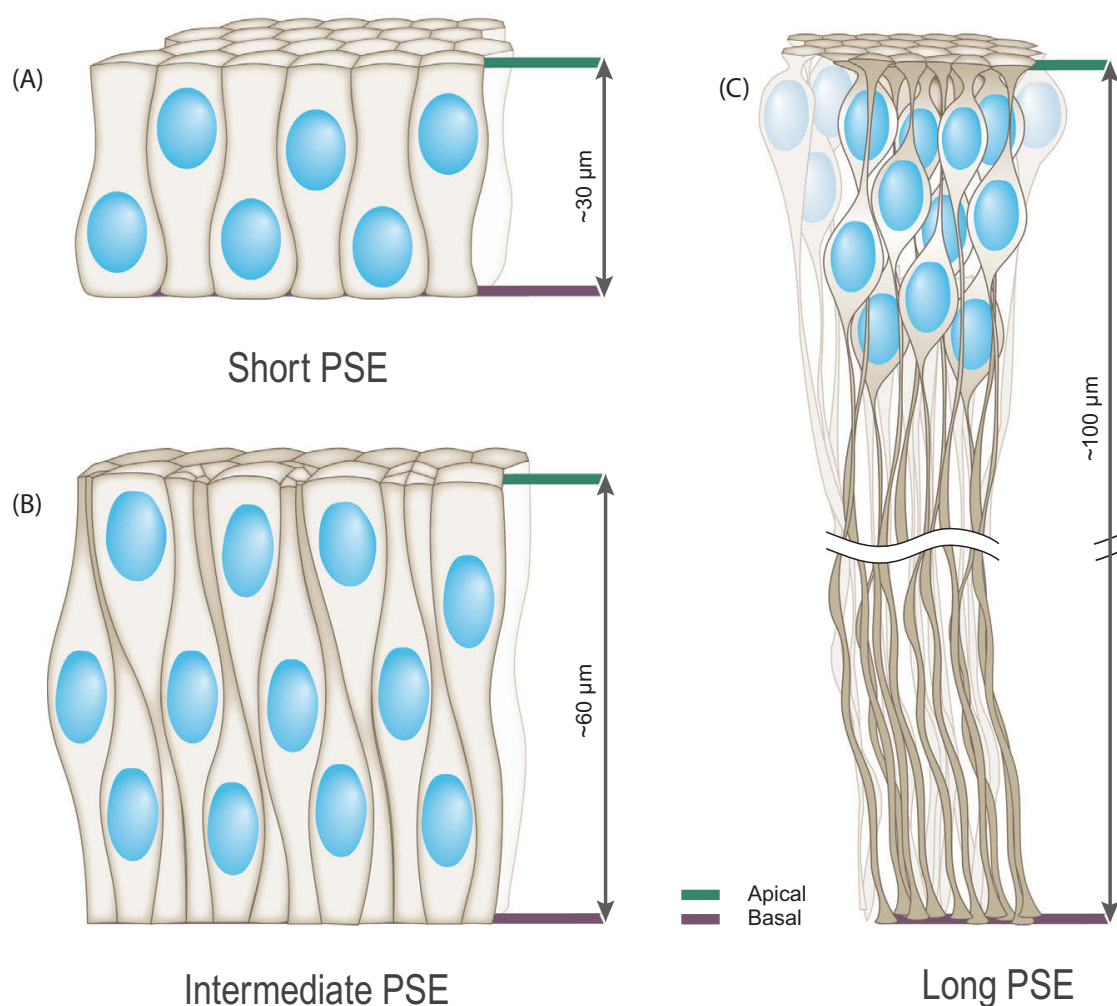


Figure 1 Pseudostratified epithelia (PSE) can be categorized into three major types. (A) The short PSE in which cells are 20–30 μm long and their nuclei organize into two to three layers inside the tissue. Examples include the vertebrate endodermal organ buds (Bort et al., 2006) and the *Drosophila* optic lobe (Rujano et al., 2013). (B) The intermediate PSE [eg, fly imaginal discs (Meyer et al., 2011) and zebrafish retinal neuroepithelium (Norden et al., 2009)] in which cells are up to 60 μm long and the tissue typically has four to five nuclear layers. (C) The long PSE found in, for example, in the neural tube of higher vertebrates at later stages of development. This tissue comprises eight or more nuclear layers and its cells span up to 100 μm (Smart, 1972). An example of extremely thin and elongated PSE is found in the developing neocortex, where the length of the radial glial cells exceeds 200 μm (Taverna and Huttner, 2010).

As cells within pseudostratified tissues are arranged in a tightly packed epithelial sheet, it has to be considered that nuclear movements during IKNM do not occur in isolation. On the contrary, nuclei move and divide within a tissue, which progressively expands and increases its cell density with every round of division. As cells proliferate, their morphology within the PSE also changes. They progressively elongate and decrease their apical

surface (Smart, 1972). As a consequence, proliferation in pseudostratified tissues influences the overall tissue organization and most likely has implications for tissue maturation, and consequently, continued proliferation might affect the tissue-scale mechanical properties and responses to mechanical stimuli in the PSE (Humphrey, 2003). Even though research has just touched upon it in the PSE, mechanical stimuli are well known to modulate cellular behavior, including proliferation [see (Benham-Pyle et al., 2015; Pathak et al., 2014)]. Changes in cell numbers occurring upon proliferation might therefore directly influence the mechanical properties of PSE, thereby creating a regulatory loop that feeds back to proliferation and/or differentiation.

1.1 Widespread Presence of Pseudostratified Epithelia in Diverse Developmental Contexts

PSE are commonly seen during the development of many different species. In vertebrates, they give rise to a plethora of tissues, including the liver, lung and pancreas buds, gut, nasal placode epithelia, otic placode/vesicle, lens placode/vesicle and the central nervous system. Recently, this list has been further expanded by showing that PSE also play important roles during very early mammalian development, for example by forming the epiblast of the gastrulating mouse embryo (Ichikawa et al., 2013). Furthermore, pseudostratified tissues are not restricted to vertebrates. They are also found building the embryonic ectoderm of the sea anemone *Nematostella* (Meyer et al., 2011), imaginal discs of fly larvae [precursors of legs, wings and antennae (Meyer et al., 2011)], as well as the fly optic lobe neuroepithelium [precursor of the visual processing centers of the fly brain (Rujano et al., 2013)]. This means that pseudostratified tissues precede the formation of many organs in both vertebrates and invertebrates. Therefore, studying their biology should generate insights on how these organs originate and develop. Additionally, most likely the tissues described as PSE to date do not exhaust the full spectrum of pseudostratification occurring in nature. Thus, further studies of various organisms and tissues at different developmental stages are needed to fully understand the role these tissues play during ontogenesis.

1.2 Heterogeneity of Pseudostratified Epithelia

As mentioned previously, PSE can be found throughout the animal kingdom. Although all PSE share the dispersed, “layered” nuclear arrangement, they can largely vary with respect to their cell length. Different PSE can span apico-basal distances from less than 30 micrometers to hundreds of

micrometers and even millimeters (Fig. 1). Furthermore, the degree of pseudostratification of a PSE, which describes how many nuclear layers are stacked within the epithelial sheet, can also vary. In the remainder of the review we will refer to this layering feature as tissue packing. One of the most prominent and most studied pseudostratified tissues is the developing neocortex in rodents and other mammals. During the development of the cortex, cells progressively elongate and their length is highly dependent on their developmental stage (Huttner and Brand, 1997; Florio and Huttner, 2014; Schoenwolf and Alvarez, 1989; Sauer, 1935). Therefore, we will use the central nervous system as an example to illustrate the large variability of cell lengths in pseudostratified tissues and to subdivide PSE into categories with varying degrees of cell elongation and nuclear stacking.

The vertebrate central nervous system originates from the neural plate (Schoenwolf and Alvarez, 1989; Sauer, 1935; Smith and Schoenwolf, 1989; Smith et al., 1994). Cells forming the neural plate are relatively short, measuring 20–30 μm and their nuclei arrange into only two to three nuclear layers. A similar tissue organization is found in the neuroepithelium of the optic lobes in *Drosophila* (Rujano et al., 2013), vertebrate otic vesicle (Clendenon et al., 2009; Hoijman et al., 2015), and endodermal organ buds (Bort et al., 2006). In all these tissues in which nuclei are stacked into only two or three layers, cells show a rather columnar morphology. For the purpose of this review, we will refer to these tissues as short PSE (Fig. 1A).

As the development of the brain progresses, the neural plate forms the neural tube and the brain vesicles. These structures are built from proliferative neuroepithelial cells, initially spanning apico-basal distances of 30–60 μm . In these more elongated epithelia compared to the short PSE, progenitor nuclei arrange on average into four to five layers (Jeong and McMahon, 2005; Nagele and Lee, 1979). A similar tissue organization is observed in retinal and hindbrain neuroepithelia of the zebrafish (Leung et al., 2011; Norden et al., 2009), the epithelium of the developing mouse intestine (Grosse et al., 2011), the fly imaginal discs (Meyer et al., 2011) and the ectoderm of the sea anemone *Nematostella* (Meyer et al., 2011). Cells in these tissues are discernibly less columnar than those in simple PSE; however, they still retain some cytoplasm in their apical and basal processes. In this review, they will be referred to as intermediate length PSE (Fig. 1B).

At later stages of development, intermediate length neural progenitors elongate further. For example, in the neural tube and the retina of higher vertebrates, these cells reach a final length of up to 100 μm , arranging their nuclei into eight or even more layers (Iulianella et al., 2008;

Nasonkin et al., 2011; Smart, 1972). We will define these as long PSE (Fig. 1C, upper half). In the developing neocortex, PSE elongation is even more extensive and accompanied by specification of neuroepithelial cells and their transformation into the radial glial cells (Bystron et al., 2008). These cells can be extremely elongated, measuring mms in primates (Miyata, 2008; Rakic, 1972). The ratio of their length to width is very high and their processes contain very little cytoplasm. The only bulky region of the cell is found around the nucleus. This gives radial glial cells a “bead on a string” appearance (Taverna and Huttner, 2010). Markedly, the nuclei in radial glia are not dispersed along the entire apico-basal axis of these highly elongated cells, but reside in a restricted zone within 150 μm of the apical surface, where they are densely packed, exceeding ten layers (Miyata, 2008; Okamoto et al., 2014; Smart, 1972) (Fig. 1C). Radial glial cells achieve extreme degrees of cell elongation that are not comparable to any other pseudostratified tissue described here, and we will therefore consider them separately.

In sum, PSE are a diverse and heterogeneous group of tissues, exhibiting a wide spectrum of cell lengths and nuclear layering. The differences in cell length can be correlated to differences in the overall cell architecture and nuclear stacking within the tissue. More specifically, cell elongation seems to correlate with a thinning of apical and basal processes. Additionally, in more elongated cells, nuclei are stacked into more layers, leading to increasing pseudostratification of the tissue. During development, both the degree of tissue pseudostratification and cellular length increase, with the most extreme example of this change being found in the neural tissue of higher vertebrates.

Despite the heterogeneity of PSE, one common characteristic of all PSE is that their nuclei move toward the apical side before mitosis. This apical nuclear migration occurs irrespectively of cell length or initial nuclear position. As a result, all divisions in PSE take place at the apical surface. How this nuclear movement is accomplished in diverse PSE will be discussed in the following sections. Additionally, we will consider potential explanations of its conservation in all PSE.



2. APICAL NUCLEAR MIGRATION IN PSEUDOSTRATIFIED EPITHELIA

In the 1930s, it was first noted by Sauer that nuclei in PSE move to the apical surface before mitosis (Sauer, 1935). Since then many studies focused on characterizing the phenomenon of nuclear movements in PSE. It is now

clear that apical nuclear migration is an active process dependent on cell intrinsic forces generated by cytoskeletal components (Norden et al., 2009; Spear and Erickson, 2012a; Strzyz et al., 2015; Tsai et al., 2010). Furthermore, apical nuclear movements have been shown to occur in a fast, persistent and directional manner in many systems (Kosodo et al., 2011; Norden et al., 2009; Okamoto et al., 2014, 2013). Additionally, apical nuclear movements are linked to cell cycle progression and occur specifically in the G2 phase of the cell cycle (Hu et al., 2013; Kosodo et al., 2011; Leung et al., 2011; Spear and Erickson, 2012a). It was suggested that this apical nuclear migration can cause passive displacement of other surrounding nuclei following division (Kosodo et al., 2011; Leung et al., 2011). Together, this means that the apical surface represents the “proliferative zone” of the tissue, in which mainly mitotic nuclei reside. Consequently, apical nuclear migration appears to be a key event, responsible for the spatial organization of proliferation in the PSE. For this reason, we propose the introduction of a novel term to refer to this important phenomenon. This will highlight the link between apical nuclear migration and mitosis and distinguish it from other nuclear motion occurring during IKNM. As nuclei migrate apically, only shortly before mitosis and this movement is characterized by high directionality and fast kinetics, we suggest the term *Pre-mitotic Rapid Apical Migration (PRAM)*. Further, we will depict in more detail how PRAM occurs and discuss its importance for proliferation in PSE.

2.1 Machineries Responsible for PRAM

Although PRAM occurs in all PSE observed so far, the molecular mechanisms driving nuclear movements vary depending on the tissue investigated. They can either depend on microtubules (MTs) or the actomyosin contractile system or a combination of both. MTs drive PRAM in radial glia of the rodent neocortex (Hu et al., 2013; Tsai et al., 2010; Xie et al., 2007) as well as in the elongated neuroepithelial cells of the chick neural tube (Spear and Erickson, 2012a). In brief, PRAM in these systems occurs via dynein recruitment to the nuclear envelope. This is followed by the active transport of the nucleus along MTs toward their minus ends which are anchored at the apically localized centrosome (Baffet et al., 2015; Hu et al., 2013; Kosodo et al., 2011; Tsai et al., 2010). In radial glia cells this dynein recruitment is a two-step process that involves two nuclear envelope components in combination with their respective adaptor proteins. Notably, both these pathways are activated consecutively and are both necessary to ensure that nuclei reach

the apical surface for mitosis (Hu et al., 2013). In the chick neural tube, PRAM also occurs in two steps. However here, the second part of the nuclear movement is driven by actomyosin and not by dynein recruitment (Spear and Erickson, 2012a).

Interestingly, in short and intermediate length PSE actomyosin contractility has been shown to be the major force generator of PRAM (Meyer et al., 2011; Norden et al., 2009; Rujano et al., 2013). However, the exact molecular mechanisms underlying actomyosin-driven apical migration are so far not well understood. What is known is that in preparation for mitosis, cells undergo extensive remodeling of the actomyosin cytoskeleton, resulting in the acquisition of a rounded cell shape [reviewed in (Heng and Koh, 2010)]. As apical nuclear migration and mitotic rounding occur at about the same cell cycle stages and both depend on actomyosin contractility, it has been suggested that apical nuclear translocation represents mainly an initial step of cell rounding before mitosis (Meyer et al., 2011; Nagele and Lee, 1979; Spear and Erickson, 2012b). Although this might be the case in shorter PSE cells, it was recently demonstrated that PSE cells of intermediate length in the zebrafish retina can enter mitosis and undergo cell rounding at nonapical positions (Strzyz et al., 2015). Additionally, in zebrafish retinal neuroepithelia (Strzyz et al., 2015) as well as the epithelium of *Drosophila* wing disc (Liang et al., 2014), apical nuclear migration was still observed after mitotic entry at basal positions. This indicates that at least in intermediate length PSE apical migration of nuclei and mitotic rounding in preparation for mitosis are separate processes.

In addition to the question how exactly actomyosin generates the forces resulting in PRAM, it is furthermore not understood how and why different machineries underlying PRAM in different kinds of PSE arose. To date, MT-based PRAM has been mainly observed in long PSE, whereas actomyosin-based PRAM is more prominent in short and intermediate PSE. This might indicate that the differences in the PRAM machinery are related to different PSE tissue thickness. What could be the reason for this switch in PRAM machineries upon increasing cell elongation? It is tempting to speculate that the two different cytoskeletal machineries are able to generate different amounts of forces to bring nuclei to the apical side. It is, for example, possible that the forces generated by actomyosin are sufficient to drive nuclear migration over relatively short distances. Following this line of argument, it can be imagined that in the short PSE of the *Drosophila* optic lobe for example, actomyosin-based cell rounding is sufficient to move nuclei apically. However, with progressive cell elongation and the need of nuclei to cover

longer distances before reaching the apical side, PRAM might have emerged as a separate nuclear translocation mechanism independent of mitotic rounding. In the intermediate length epithelia, actomyosin seems to be sufficient to generate such movements. Once PSE further elongated, reaching the length scales of radial glia cells and having processes almost devoid of cytoplasm, it is possible that actomyosin is not able to generate enough force any longer to cover the increasing length scales of PRAM. In these cases, dynein-dependent migration along MTs might have evolved as the more effective force generator to drive nuclei toward the apical side. This would imply that tissues which display progressive changes in the degree of pseudostratification during development switch from moving nuclei in concert with cell rounding to actomyosin-driven PRAM and finally to MT-based PRAM. It would be very exciting to test this hypothesis in forthcoming studies in tissues ideally from the same organism but with increasing ratios of elongation.

2.2 Nuclear Migration in Tightly Packed Tissue

As mentioned earlier, a striking hallmark of PSE is that the nuclei are tightly packed into multiple layers and cells are elongated, with high length to width ratios. Consequently, nuclei in PSE cells do not move in isolation. On the contrary, migration to the apical side in G2 from within the depths of the PSE tissue necessitates the movement of the translocating nucleus through the crowded environment in which neighboring cells also feature bulky nuclei moving in different directions. Despite this crowded tissue packing, nuclei undergoing PRAM keep their directed, apical trajectory. To achieve this, the cytoplasm and organelles of the cell undergoing PRAM are likely to be displaced and neighboring nuclei rearranged. Furthermore, the plasma membrane of the PRAM-cell, as well as of the adjacent cells, will be deformed by the moving nuclei. This means that proliferation in PSE leads to significant local nuclear and tissue rearrangements (Fig. 3).

So far, it is not known whether and how nuclear dynamics and rearrangements in the PSE correlate to tissue packing. It is possible that the dynamicity of nuclei is needed to generate pseudostratification in the first place, for example, by allowing nuclear displacements within columnar cells. However, it is also possible that nuclear movements are a consequence and not a cause of pseudostratification. To date, multiple functions of overall apico-basal nuclear dynamics in PSE have been proposed, including a role in cell fate specification (Baye and Link, 2007; Del Bene et al., 2008), a role in

shaping the developing organs (Hojjman et al., 2015; Langman et al., 1966) and optimizing proliferation by preventing local cell over-crowding (Okamoto et al., 2013). Here, we will focus on the function of PRAM during the proliferative phase in which an expansion of the PSE takes place. As mitosis in these tissues is directly preceded by PRAM, in the next paragraphs we will first discuss links of PRAM to cell cycle events and revisit the current hypotheses of how PRAM might influence proliferation in different PSE.

2.3 PRAM and Its Links to Cell Cycle

So far, we described the machineries responsible for PRAM in different types of PSE. Another important question is how these machineries are regulated to reproducibly move nuclei apically exclusively before mitosis. Recently, different groups provided evidence that PRAM is tightly linked to cell cycle progression via the activity of the cell cycle kinase CDK1 (Baffet et al., 2015; Leung et al., 2011; Strzyz et al., 2015). CDK1 is a master regulator of cell cycle continuation and plays a role in the transition from the G2 phase into mitosis (reviewed in Vermeulen et al., 2003). It was shown that CDK1 activity is both necessary and sufficient for PRAM (Strzyz et al., 2015). Interestingly, CDK1 has been demonstrated to play a role in PRAM of both, intermediate length neuroepithelia of the zebrafish retina as well as in the long epithelium in neocortex (Baffet et al., 2015; Strzyz et al., 2015). Hence, it seems that CDK1 can link cell cycle dynamics to the cytoskeleton independently of which cytoskeletal element is used for nuclear translocation. How exactly does CDK1 regulate PRAM in these different tissues? CDK1 phosphorylates multiple cytoskeleton related proteins [(Sivars et al., 2003) reviewed in (Enserink and Kolodner, 2010)] and thus influences their localization and function. In the radial glia cells CDK1 directly phosphorylates a specific nuclear envelope protein, and only this phosphorylated protein can efficiently bind to a dynein adaptor protein and recruit dynein. CDK1 activity has been further shown to influence subcellular localization of another adaptor protein of the dynein complex, regulating its cytoplasmic distribution, which defines whether it binds to the nuclear envelope or is sequestered within the nucleus (Baffet et al., 2015). Most likely, similar mechanisms of modifying protein interactions and their localization by CDK1 phosphorylation also operate during actomyosin-driven PRAM and allow localized actomyosin contractility. However, the details of these interactions still need to be explored.

Therefore, PRAM is a phenomenon that depends on cell cycle progression and invariably occurs in the G2 phase of the cell cycle. Notably, CDK1 activation is a key step necessary for the initiation of PRAM, despite differences in cytoskeletal components responsible for nuclear movement, making it a common regulator of PRAM in different systems.

Together, we so far illuminated the cytoskeletal machineries that drive PRAM and how they are linked to cell cycle progression. However, an important question remains: Why do all PSE move their bulkiest organelle, the nucleus, toward the apical side to undergo mitosis? Why is this apical nuclear migration, which might at first sight appear as a waste of energy, found in all PSE studied to date? In the next chapters, we will outline some possible explanations for this seemingly counterintuitive phenomenon.

2.4 PRAM and Establishment of Proliferative Zone at Apical Surface

As cells acquire a rounded morphology in preparation for cell division, they occupy more lateral space during mitosis than in the interphase (Smart, 1972). For this reason, it has been suggested that nuclei move to the apical surface because it might provide more space for mitotic events (Fig. 2B). Consequently, by alleviating the constraints of tight nuclear packing, this apical restriction of mitotic nuclei achieved by the reproducibility of PRAM could help these cells to proliferate (Fish et al., 2008; Schenk et al., 2009). In some PSE, like the neuroepithelium of the retina, due to its tissue curvature, the apical surface indeed provides more space for the mitotic nuclei than the basal surface. In PSE with a flat apical surface, however, which is seen for most other types of central nervous system neuroepithelia, the basal side and the apical side harbor the same amount of space, and the conservation of the apical surface as the mitotic zone of the tissue cannot be explained by providing more space. This becomes even clearer when we look at the apical surfaces of the brain that have a negative curvature. Here, the apical surface is much smaller than the basal surface, but the nuclei undergo PRAM despite the apparent low apical-to-basal surface ratio. Additionally, cell rounding should be considered, which is a robust process that increases surface tension and decreases adhesion. It is to be expected that in such a tissue, in which the actomyosin cortex of the surrounding cells is not as rigid as in the mitotic cells, the mitotic cell can easily “make space” by the process of rounding and thereby deform neighboring cells (Fig. 2B and C). Hence, robust division in the tightly packed tissue would not require the formation of an apical

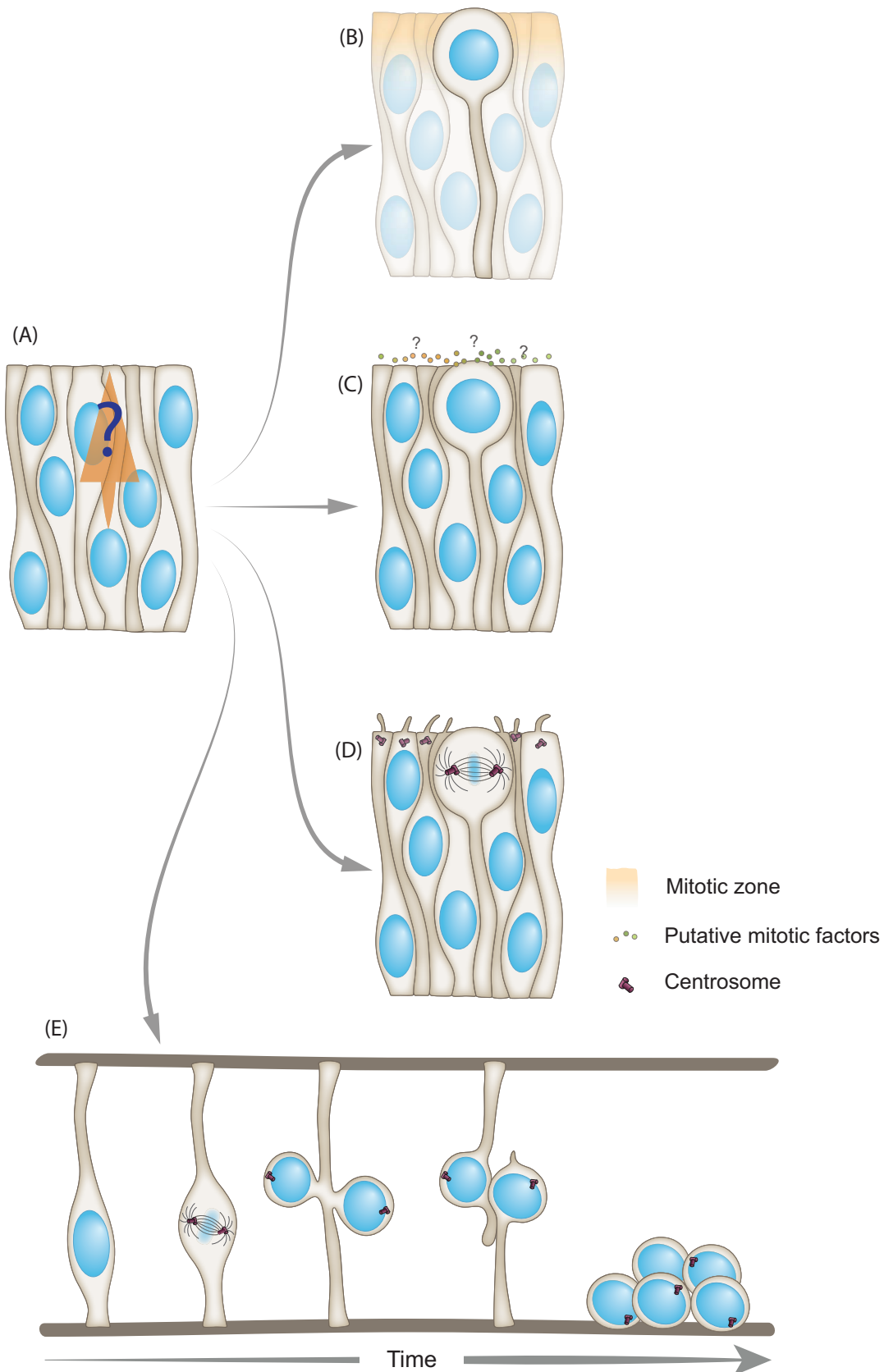


Figure 2 Theories on the purposes of PRAM and apical mitosis. (A) The nucleus of a PSE cell will rapidly migrate through the tightly packed tissue prior to mitosis (indicated by the *gray arrow*), in order to divide at the apical surface. (B) More space for cell rounding

“mitotic only zone” (Fig. 2B). This argument is supported by data which has demonstrated that in some contexts cells can divide at nonapical locations, despite tight nuclear packing (Strzyz et al., 2015; Weber et al., 2014).

Thus, compartmentalization of mitotic nuclei to a particular apical zone might not be absolutely necessary for successful cell proliferation in PSE. Still, such a restriction of mitotic nuclei to a defined tissue region of the apical side, from which interphase nuclei are usually displaced, might allow cells to divide more freely, without the interfering presence of nonmitotic nuclei in the vicinity. Therefore, moving nuclei apically might contribute to the optimization of cell proliferation in a densely packed tissue.

2.5 PRAM and Mitotic Entry

In rat radial glial cells it was observed that when PRAM was blocked during the final stages of nuclear movement, just before the nucleus had reached the subapical region, the cells were not able to enter mitosis and remained in a premitotic state (Hu et al., 2013). On the basis of these observations, it was speculated that the apical side might provide some signals essential for mitotic entry (Fig. 2C). This would mean that successful PRAM is critical for the proliferation of cells in the PSE, as it would represent a prerequisite for mitotic entry. However, in other systems including the mouse neocortex, chick neural tube, as well as the intermediate lengths PSE of the *Drosophila* wing disc and the zebrafish retina, it has been shown that cells within the intact PSE can enter mitosis also at nonapical locations (Liang et al., 2014; Spear and Erickson, 2012a; Strzyz et al., 2015; Tsuda et al., 2010; Yang et al., 2012). Therefore, it seems that PRAM is not absolutely necessary for mitotic

-
- ◀ at the apical side than within the tissue. Due to the apical endfeet attachments and/or displacement of interphase nuclei from this region upon rounding, a mitotic zone devoid of neighbor nuclei might thereby be created apically and aid in PSE proliferation (Fish et al., 2008; Schenk et al., 2009). (C) By entering mitosis at the apical surface, a cell might gain contact to putative factors that ensure proper completion of mitotic events (Hu et al., 2013). The identity of such factors, as well as whether they are intra- or extracellular is so far unknown. (D) PRAM might be important to allow contact between the nucleus and the apical centrosome (Fish et al., 2008; Miyata, 2008). In vertebrates, the centrosome is associated with the primary cilium at the apical side of the cell during interphase. Upon mitotic entry, the cilium is resorbed and the centrosome participates in spindle formation. (E) Apically dividing proliferative cells have a horizontally aligned spindle, and both daughters reintegrate into the tissue after mitosis. Nonapical divisions, however, impede cellular reintegration and cause perturbations in PSE architecture, suggesting that PRAM helps to maintain tissue integrity (Strzyz et al., 2015).

entry in many PSE. Nevertheless, certain signals stimulating mitotic entry might be provided by the apical surface and some tissues might rely more on these signals than others.

2.6 PRAM and Centrosome Position

In PSE the centrosome remains apically of the nucleus during the whole cell cycle (Fig. 2D). In vertebrates, this apical centrosome is involved in nucleating the primary cilium, which serves as a signaling hub during interphase (Chen et al., 1998; Miyata, 2008; Müsch, 2004; Rodriguez-Boulan and Macara, 2014). Although in cuboidal and columnar epithelia the distance between nucleus and centrosome is often in the range of one to five micrometers, in PSE these distances can reach up to tens of micrometers depending on nuclear position before PRAM (Fig. 2A). In mitosis however, the centrosome and the nucleus need to meet, as centrosomes are important factors for the organization of the mitotic spindle (Nigg and Raff, 2009). Consequently, it has been speculated that one reason for the occurrence of PRAM is to bring the nucleus into the vicinity of the apically localized centrosome for mitosis (Fig. 2D). This, in turn, would ensure that the centrosome can serve as a basal body for the primary cilium in interphase and as a spindle organizer in mitosis (Fish et al., 2008; Miyata, 2008, 2015; Schenk et al., 2009). Therefore, it was suggested that the apical position of the centrosome is the major cause for PRAM. This indeed seems to be the case in elongated PSE as well as neocortical radial glia, since in these tissues the apical centrosome is involved in arranging the MT tracks, along which the nucleus is transported apically. However, in intermediate length PSE, PRAM has been shown to occur independently of centrosome position. It was recently demonstrated that in the zebrafish retinal neuroepithelium PRAM still occurs following centrosome mispositioning or ablation. It even ensues after nonapical centrosome-nucleus association (Strzyz et al., 2015). Similarly, in the *Drosophila* wing disc apical mitoses take place even in the absence of centrosomes (Poulton et al., 2014), indicating that also in this tissue PRAM occurs independently of centrosome position or existence. This means that apical centrosome localization is not an absolute prerequisite for PRAM in intermediate length PSE. Nevertheless, by moving nuclei apically to meet the centrosome in the control scenario, mitotic entry is most likely facilitated. As the constant apical position of the centrosome is important for robust signaling from the primary cilium, this might enable the cell to orchestrate signaling and mitotic events (Fig. 2D).

It is further possible that the apical position of the centrosome also has additional functions in interphase independent of primary cilia function, as cells in *Drosophila* PSE lack primary cilia, but still show apical positions of centrosomes throughout the cell cycle (Meyer et al., 2011). In this context, it is imaginable that apical centrosomes are important for maintaining the characteristic apico-basal organization of the MT cytoskeleton observed in PSE (Norden et al., 2009; Z. Xie et al., 2007; Yang et al., 2012) and thereby for intracellular trafficking and organelle positioning in these tissues.

2.7 PRAM and Efficient Cell Reintegration Into Tissue Following Division

Despite the fact that in many PSE nuclei can enter mitosis and even divide nonapically (Liang et al., 2014; Spear and Erickson, 2012a; Strzyz et al., 2015; Tsuda et al., 2010; Yang et al., 2012), PRAM and subsequent apical divisions are highly conserved in all PSE. A hallmark of cell divisions during progenitor expansion in PSE is the perpendicular cleavage plane orientation with respect to the apical surface (Cui et al., 2007; Das et al., 2003; Kosodo et al., 2004; Nakajima et al., 2013; Sauer, 1935; Y. Xie et al., 2013) (Fig. 2D). This control of the cleavage plane positioning is important for the bisection of the apical membrane and thereby can influence the distribution of apical components into both daughter cells. In some examples of PSE, namely mouse radial glia cells, the chick neural tube and the *Drosophila* wing disc, perturbation of cleavage plane orientation can cause one daughter cell to lose its apical attachment leading to cell delamination (Konno et al., 2007; Morin et al., 2007; Nakajima et al., 2013). Importantly, components such as aPKC, LGN, NuMa, SCRIB/DLG, which regulate cleavage plane orientation in various PSE localize apically in these tissues (Cui et al., 2007; Horne-Badovinac et al., 2001; Konno et al., 2007; Morin et al., 2007). Consequently, PRAM appears to be necessary to ensure perpendicular divisions and thus the generation of two daughter cells that both inherit parts of the apical cellular compartment. Additionally, it has recently been suggested that the importance of PRAM in maintaining overall PSE integrity reaches beyond the need of cleavage plane orientation. It was shown in the intermediate length PSE of the zebrafish retina that here the interference with the mitotic cleavage plane does not induce cell delamination while the inhibition of PRAM does. In this case, perturbation of PRAM led to non-apical mitotic entry followed by nonapical cell division. This in turn resulted in the generation of cells that were not able to efficiently reintegrate into the

tissue following division. Consequently, cell delamination and ectopic proliferation were observed (Fig. 2C). Such ectopic divisions majorly interfered with retinal layer formation and subsequent organ morphogenesis (Strzyz et al., 2015). Together, these insights reveal that by ensuring apical mitosis, PRAM allows the cells in diverse PSE to maintain or reestablish their apical contact following division. Thus, PRAM serves as a mechanism that safeguards PSE tissue integrity and architecture (Fig. 2E).

In conclusion, while it is clear that PRAM allows cells to reproducibly divide at the apical location, the impact of interference with this process varies depending on tissue type. Generally, PRAM appears to optimize the proliferative output of the tissue, support mitotic entry and allow the centrosomes to meet the nucleus apically for mitosis. Furthermore, PRAM seems to play a major role in maintaining PSE tissue integrity as well as preventing cell delamination (Fig. 2). However, further cross-organismal studies are necessary to better understand functions of PRAM.



3. TISSUE-WIDE PROPERTIES OF PSE

To date, most studies of PSE focused on single cells and their dynamics, as discussed in the previous chapters. Tissue scale mechanical properties, however, are so far only scarcely explored, but tissue-wide understanding of proliferation, mechanical properties, and responses to stimuli is necessary to fully comprehend the development and function of these important tissues. In the final part of this review we will therefore offer some ideas regarding the crosstalk between tissue architecture, mechanics and cell proliferation, aiming to open new grounds for future studies in the field of PSE biology.

3.1 PSE Tissue Packing

As noted previously, PSE are tightly packed, increasing cell density with increasing PSE elongation. When cells round up at the apical side in order to undergo mitosis, they take up several times more apical surface area than their apical endfeet do during interphase (Smart, 1972) (Fig. 3B). Because of this, the available apical area could represent a constraint to PSE proliferation and division rates. This means that the number of layers of interphase nuclei that will eventually divide apically must be coordinated with the availability of this apical surface and packing of the PSE might serve as readout of proliferative

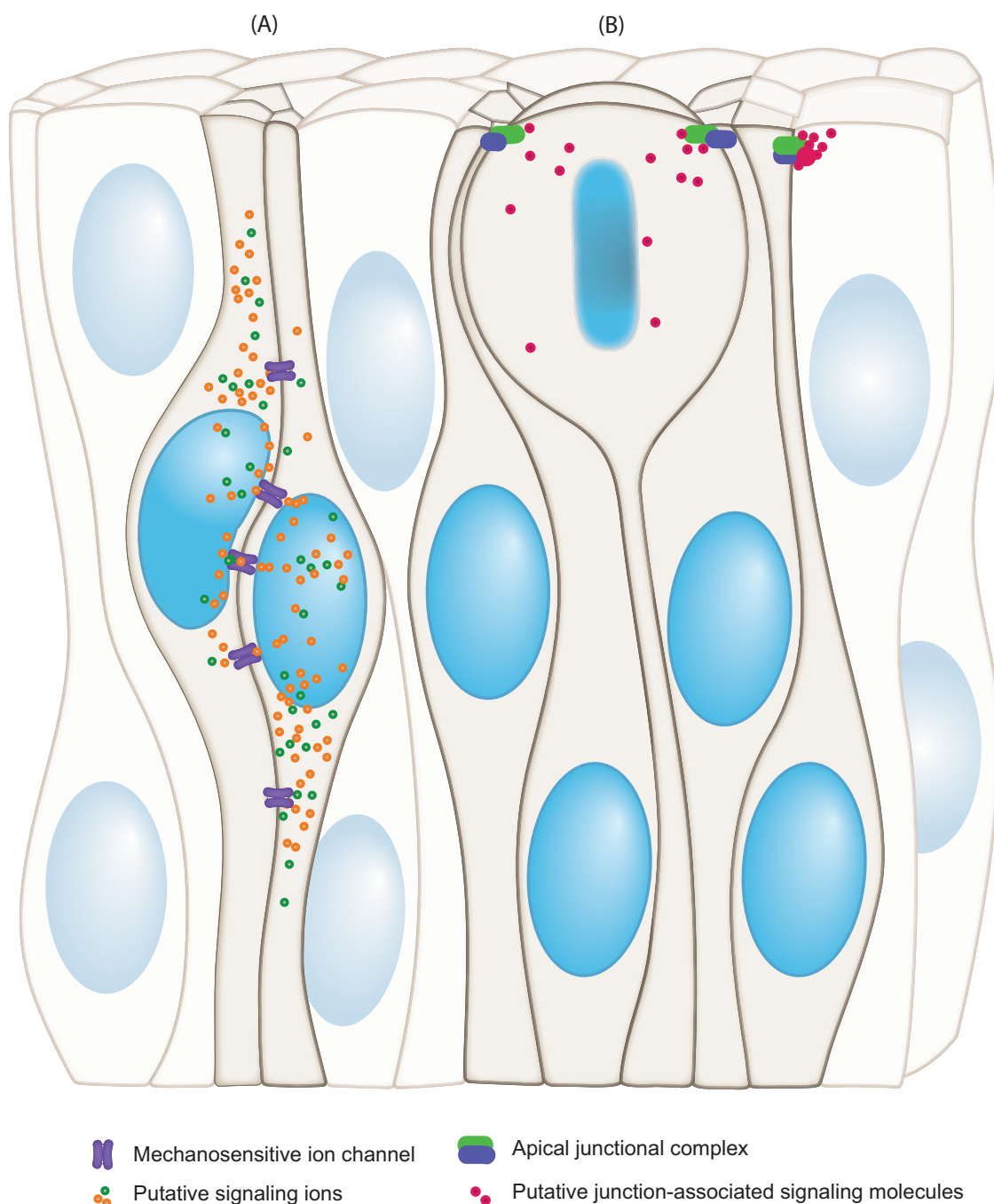


Figure 3 Mechanical stimulation and responses to it can originate in cell deformation during PRAM and mitosis. (A) By mechanosensitive ion channels such as Piezo localized throughout the lateral cell membranes, lateral forces arising during PRAM might regulate proliferation and proliferation-driven growth of the PSE. (B) Upon mitosis, the rounded cell has increased surface tension (Stewart et al., 2010) and takes up several times more space at the apical side than the endfoot of an interphase cell (Smart, 1972, 1973). In this way, rounding might displace apical junctions between the rounded cell and neighboring, interphase cells. Depending on the amplitude of this displacement, rounding could result in the release of a junction-bound signaling molecule, such as a components of the Hippo pathway (Benham-Pyle et al., 2015), signaling to the cell cycle machinery and thus controlling proliferation rates throughout the tissue.

capacity. To understand the limitations to PSE proliferation and the maximal number of nuclear layers that can make up a specific PSE, it is important to know how much of the apical space a mitotic cell inhabits and for how long it occupies this apical surface unit. Additionally, it is important to identify how long interphase nuclei need to reach the apical surface. Building upon this idea [Fish et al. \(2008\)](#) defined the optimal packing as the maximal number of proliferative layers that can be packed under the apical surface of a specific PSE, without altering its cell cycle parameters. This number of nuclear layers is expected to be proportional to the total cell cycle length and inversely proportional to the length of mitosis. It is important to note that Fish et al. treat proliferation as the only contributor to PSE packing. With respect to this, one might argue that both proliferation and minimization of cell extrusion/death lead to increased packing. However, cell death is not widespread in most PSE investigated to date ([Dzafic et al., 2015](#); [Milán et al., 1997](#); [Naruse and Keino, 1995](#)) and might often be negligible when it comes to its effect on total cell number and growth. Proliferation, on the other hand, is the major contributor to PSE cell numbers and we will thus continue our discussion with the assumption that cell extrusion/death can be neglected.

Due to the fact that M phase and total cell cycle length, as well as the size of the rounded, mitotic cell can differ between tissues, the optimal packing introduced previously will also vary between different PSE. As a simple illustration of this difference, one can consider two theoretical PSE tissues, A and B, that both have a packing level of 10 (ie, they harbor 10 layers of nuclei stacked in an apico-basal tissue column). We assume that A and B both have equal cell cycle and M phase lengths of respectively 12 h and 30 min. What they differ in, though, is the relative size of mitotic cells. In tissue A, the mitotic cell is relatively small compared to tissue B—it takes 2 times more apical surface than an interphase nucleus does, whilst in tissue B the M-phase cell takes up three times as much apical surface as an interphase nucleus. Taking these facts together this would mean that PSE A has the highest proliferative efficiency at its packing optimum of 12 layers, and PSE B at the optimal 8 layers. Since they both harbor 10 nuclear layers, PSE A would result as *under-* and PSE B as *overpacked*. The underpacked tissue might occur earlier in development and could further increase its proliferative efficiency by packing more nuclear layers. Here, a positive feedback loop mechanism might act, sensing the tissue packing state and allowing cells in these tissues to further increase their proliferative capacity. Conversely, tissue B, because it is overpacked, might be a more developed PSE at the onset of differentiation. In this scenario the apical surface might become overcrowded with mitotic

cells and consequently hinder its own proliferation through a negative feedback loop. Still, tissue B could potentially reach its optimal packing level, provided that M-phase is shortened and/or overall cell cycle length prolonged. In conclusion, packing of the PSE might serve as readout of proliferative capacity as mentioned previously, but only if the tissue's optimal packing level is already known from measuring all cell cycle parameters. Following this rationale [Fish et al. \(2008\)](#) calculated the packing level that allows maximal proliferation of mammalian radial glia cells. Using values of cell cycle parameters and M-cell size obtained from fixed samples, they concluded that, in the PSE of the mammalian cortex, radial glia proliferation seems most efficient when eight layers of nuclei are stacked in a nuclear column beneath the apical surface. This layering thus represents the optimal packing level of this particular PSE tissue ([Fish et al., 2008](#)).

However, so far these thoughts are merely theoretical. It would therefore be now important to experimentally verify whether packing of different PSE tissues follows these predictions. This can be achieved by examining proliferation in presumably over-, under-, and optimally packed PSE, as well as by investigating the links between packing and tissue development. As PSE tissue packing has so far not been systematically analyzed, many fundamental questions regarding this feature remain: Whether, and, if so, how does the proliferation rate in different PSE scale with this increase in tissue packing? Can PSE sense and increase their packing levels? Assuming that changes in packing also affect PSE mechanical properties, can this feed back to proliferation control mechanisms? If yes, how could this mechanofeedback be regulated? As suggested here and in the example above, intricate feedback loops might be at the center of coordinating growth and cell cycle parameters to keep proliferation of a PSE at its intrinsic optimum. It would be fascinating if such mechanisms would indeed be identified, and the upstream cues and downstream molecular cascades involved in their regulation dissected. Further, we provide a discussion on how PSE packing under spatial constraints could potentially be controlled raising outlooks for future studies.

3.2 Packing Increase in PSE

In the *underpacked* state, the apical surface unit might accept a higher mitotic frequency, meaning that the tissue could robustly proliferate and further increase its packing, as illustrated in the previous section. More nuclear layers could, in turn, result in growth by increasing tissue thickness. This might

further raise the tissue's proliferative capacity and total cell number. Therefore, it could be beneficial for the developing PSE to maximize its packing by increased proliferation instead of remaining in the underpacked state.

However, as this way of packing more nuclear layers would eventually lead to overall tissue expansion, it might be most efficient only in case when growth is spatially unrestrained. Additionally, with increased number of cells and packing, proliferation would rise as well, resulting in the need for more (apical) space to accommodate mitotic cells. Tissue growth is, however, typically limited in the developing organism, for example, it might be internally restricted by the tissue's apical surface tension (Okamoto et al., 2013). Consequently, proliferation and packing within the PSE might be affected by significant external spatial constraints (Streichan et al., 2014) imposed by the limited space in which the tissue develops. Hence, in order to increase packing, these limiting effects would need to lessen (LeGoff and Lecuit, 2015). Cell elongation and/or cell volume decrease could be potential strategies that might be employed to increase packing upon constrained growth. It is known that PSE tissues indeed elongate and pack more nuclear layers as they mature. In Smart's 1972 study of the mouse diencephalon, a 10-day-post-conception (E10) PSE had a thickness of 90 μm with six layers of nuclei. At day 11 the tissue was 110 μm thick, with eight nuclear layers, to grow up to 150 μm in thickness and a twelve-layer pseudostratification at day 12 (Smart, 1972). In order to undergo such changes in degrees of pseudostratification, cells would have to undergo multiple structural rearrangements. Specifically, they would need to elongate and thin their cellular processes, reorder their nuclei as well as decrease the attached endfeet areas (Miyata, 2015) in a tissue-wide, coordinated manner. With respect to this, mechanical tests have shown that apical endfeet are contractile in the PSE of the mouse cerebral wall (Okamoto et al., 2013). Active deformations such as endfoot shrinkage would thus most likely be mediated by actomyosin cortex contractions, which are known to play a central role in controlling cell shape (Salbreux et al., 2012). Such changes might also be largely enhanced by the abundant dynamicity of neighboring cells. Cell elongation, on the other hand, might be a more complex change, as it would imply both thinning of cellular processes, and elongation leading to the thickening of the entire tissue. Thus, cell elongation might require greater forces and might be governed by both cortical contractions/rearrangements, and microtubule polymerization throughout the cell body. However, cell elongation as a packing strategy might be an option only if spatial constraints acting perpendicular to the tissue plane are mild, as it would also result in tissue growth

and an increase of tissue thickness. With even further increase in packing prior to reaching the maximum, these constraints might become impossible to overcome. At this point, a decrease in cell and nuclear volume might be the only strategy allowing further increase in layering. With respect to this, it seems that cells do possess autonomous mechanisms to measure and adjust their size in accordance to the environment and cell cycle ([Ginzberg et al., 2015](#)). With this in mind, introducing cell size-related research to the PSE field and relating it to tissue-wide packing studies would largely contribute to our understanding of mechanisms governing PSE proliferation.

Because of the phenomenon of packing, growth in the PSE might not be directly coupled to proliferation, making research both experimentally and theoretically challenging. Nevertheless, it would be fascinating to understand how proliferation, elongation and volume decrease relate to each other and temporally overlap. So far nothing is known about the mechanisms behind any of these three possible packing strategies or about their developmental regulation in the PSE. Hence, multiscale, tissue-wide developmental studies, focusing on architectural changes in different PSE, are needed to link proliferation, elongation, and volume decrease to tissue expansion.

3.3 Linking Mechanical Stimulation to PSE Responses

The research field of tissue mechanics emerged in the 19th century, founded by D'Arcy Thompson, who was interested in the mechanical forces shaping biological systems. During the last decade it has reemerged as a highly multidisciplinary field of developmental biology ([Mammoto and Ingber, 2010](#)), owing to advances in live imaging and biophysical methods. It is now well known that diverse mechanical stimuli play major roles in proliferation, tissue development and function. Examples of animal development being affected by sensing mechanical stimuli include the developing zebrafish heart and nephrons, the developing mouse lung, and chick neural tube closure (reviewed in ([LeGoff and Lecuit, 2015](#); [Mammoto and Ingber, 2010](#))). The PSE, a highly dynamic epithelium with tightly packed elongated cells could serve as a model system providing novel insights into the role of mechanical cues in tissue development and function.

Recently, more pathways underlying the mechanisms of translating mechanical stimuli into cellular responses have been unraveled ([Provenzano and Keely, 2011](#)). In the recent years, studies have also touched upon mechanosensation in different pseudostratified tissues

(Mao et al., 2013; Porazinski et al., 2015; Schluck et al., 2013). Upon the application of force the studied PSE altered their proliferation levels or exhibited developmental changes. For example, a study of a fish mutant in the Hippo signaling pathway demonstrated organism-wide responses to gravitational force (mechanostimulation) (Porazinski et al., 2015). The mutant developed malformed (flattened) and misaligned organs, including the neural tube and optic cup, both of which derive from a PSE. In another study, direct links between mechanical strain and PSE proliferation were investigated (Schluck et al., 2013). By mechanically stretching *Drosophila* wing disc epithelia, it was confirmed that a proliferation increase by mechanical tension can exist in this PSE. With these two studies in mind, we can speculate that PSE are indeed mechanosensitive and can respond to mechanical forces such as strain by changing proliferation rates or other developmental parameters. Furthermore, several studies have dealt with mechanosensation by the cell nucleus (Dahl et al., 2008). This central organelle might be a possible mechanotransducing element in the PSE due to the tight packing of nuclear arrangement. Further, we discuss two exemplary mechanosensing pathways that might also be important regulators of PSE proliferation.

3.4 Hippo Pathway as Example of Mechanosensitive Signaling Pathway

The Hippo signaling pathway is well known to play a central role in regulating cell proliferation through its response to mechanical stimuli. Because its constituents have also been found to affect the development of PSE tissues (Porazinski et al., 2015), we believe that more detailed research focusing on the PSE could provide interesting insights into how Hippo regulates proliferation of complex tissues.

The Hippo pathway [reviewed in (Yu and Guan, 2014)] is conserved across the animal phylogeny, with orthologous genes studied in models ranging from *Drosophila* to mouse. It comprises a signaling cascade that affects tissue growth and homeostasis by controlling cell number by proliferation, growth, differentiation and death. As a result of these essential functions, the constituents of the Hippo pathway, their cascades and activities are extensively studied. Many Hippo signaling components localize to the cellular junctions (eg, PAR6, β -catenin) and several have been confirmed to interact with the cytoskeleton (eg, α -catenin, Zyxin) in both mouse and *Drosophila* (Yu and Guan, 2014). Upstream factors known to affect this

pathway are cell polarity, G-protein-coupled receptor (GPCR) signaling and mechanotransduction. In the latter, the master mediators of signal transduction seem to be cellular tension and the actin cytoskeleton (Yu and Guan, 2014). A mechanotransduction pathway following the cascade formed by tension sensors, Hippo and proliferation (Fig. 3B) is of special interest to this review because of the tightly packed state of the pseudostratified tissue. Therefore, a crowded, dynamic and polarized environment such as the PSE, with its PRAM and apical mitoses, likely provides a plethora of mechanical stimuli and the need for their efficient transduction throughout the tissue (Fig. 3).

It has recently been demonstrated in an epithelial cell culture study that mechanical strain controls proliferation via junction-associated YAP and β -catenin (Benham-Pyle et al., 2015). Stretching quiescent epithelial sheets resulted in the relocation of β -cat and YAP from the tight junctions to the nucleus. This, in turn, resulted in the activation of transcription leading to cell cycle reentry and increased proliferation. In an epithelial tissue such as the PSE, with the important feature of highly efficient proliferation, a similar Hippo-associated pathway might play a role and mediate cell cycle responses to proliferation, packing or nuclear dynamics (Fig. 3). In this regard, it would be helpful to have tension-sensing and strain-inducing in vivo methods in the PSE, to serve as read-out of the tissue's physical properties and test its Hippo pathway response to mechanical stimulation.

3.5 Piezo Channel as Example of Mechanosensitive Cellular Response Element

As another possible PSE mechanosensitive mechanism, we here describe the Piezo mechanosensitive ion channel (Coste et al., 2012). Although not yet studied in the PSE, Piezo might be distributed along lateral cell membranes and act as the mechanoresponsive element able to respond to forces arising from PRAM,

Mechanosensitive channels (Guharay and Sachs, 1984) are membrane-bound force-transducing molecules, whose working principles rely on their ability to respond to a wide range of external and internal local mechanical stimuli {eg, flows, (osmotic) pressure changes, stretching or position information} [reviewed in (Kung, 2005)]. Following the stimulus, diffusion of ions (cations in eukaryotes) through the channel triggers an intracellular signaling cascade. Two current principal models of their gating mechanism are (1) the lipid bilayer tension or stretch model, in which

membrane tension induces a conformational change and opens the pore and (2) the spring-like tether model, in which tethers connect the channel to the ECM or the cytoskeleton (Lumpkin and Caterina, 2007), and the channel opens upon their displacement by local extra- or intracellular forces.

The Piezo is a pore forming protein of a mechanosensitive cation channel, conserved in mouse, zebrafish, and *Drosophila* (Coste et al., 2012; Eisenhoffer et al., 2012). With its highly specific structure, this channel opens upon changes in membrane tension, allowing the influx of Ca^{2+} ions. By promoting subsequent nuclear localization of YAP (Benham-Pyle et al., 2015; Pathak et al., 2014), Piezo represents another link of mechanical force transduction to cellular responses via the Hippo pathway. In the highly proliferative PSE, a mechanosensitive ion channel such as Piezo might form a signaling cascade involving Hippo, as well as downstream cell cycle regulators (Fig. 3). By localizing mechanosensitive ion channels throughout the lateral cell membranes, the tissue could respond to mechanical stimuli that are not directly related to apical junction displacements (Fig. 3A). In this way, lateral forces might also regulate proliferation and proliferation-driven growth of the PSE.

3.6 Possible Origins and Effects of Mechanical Forces in PSE

As mentioned previously, mechanosensing plays an important role in proliferation control of the *Drosophila* wing disc and development of the zebrafish neural tube and optic cup. Employing both junctional localization of Hippo pathway components and lateral membrane localization of mechanosensitive channels such as Piezo, the dynamic PSE would be “fully equipped” to respond to mechanostimuli originating anywhere along the apico-basal cell axis (Fig. 3). These tension-altering stimuli in the PSE might arise from local events such as PRAM (Fig. 3A), apical mitotic cell rounding (Fig. 3B), or from more global events such as crowding of the apical surface or increased tissue packing. For example, during apical mitosis, the rounded mitotic PSE cells could change their physical properties by increasing surface tension and weakening the junctions, similar to cells in culture (Stewart et al., 2010). Rounded cells could influence their neighbors as well, by compressing their apical endfeet. Furthermore, lateral membranes of the elongated PSE cells are subject to various deformations resulting from nuclear dynamics. Together, apical mitosis and PRAM might cause displacements and tension changes in the membrane-bound

apical polarity components (Fig. 3B), as well as in the neighboring cell lateral membranes under tension (Fig. 3A). Such shape changes could act as powerful signaling sources by, for example, changing the tension of plasma membranes (Tsuji et al., 2015). Additionally, overall changes in tissue packing result in significant alterations of PSE architecture as discussed previously, and could feed into mechanosensitive pathways. An important first step in future studies should be to investigate whether Piezo and/or other mechanosensitive channels act in the PSE. Furthermore, it will be important to demonstrate if and how PSE-specific events mentioned previously influence junctional components and the localization of Hippo pathway constituents such as YAP.

Altogether, mechanical stimulation in the PSE could lead to specific, tissue-wide coordinated cellular responses that affect proliferation. Recent work done on mechanosensing via the Hippo pathway and the Piezo channel opened new exciting research possibilities for PSE mechanobiology. Furthermore, research focusing on the localization, dynamics and function of Hippo components and mechanosensitive channels in the PSE will most likely shed light on the mechanical control of proliferation and growth. To accomplish this, developmental cell biological *in vivo* studies should be complemented with PSE *in vitro* research. Both *in vivo* and *in vitro* studies in the PSE, however, have their own advantages and limitations. Tissue-scale studies represent a challenge for live imaging due to the very tight packing and tissue thickness, but would allow unprecedented insights into tissue-wide dynamics of, for example, YAP or ion currents upon mechanical stimulation. On the other hand, maintaining a PSE as epithelial sheets or organoids *in vitro* is possible, but by no means trivial (Eiraku et al., 2011). These cells exhibit most of the PSE features (IKNM, differentiation) and might ease both imaging and manipulations. In the future, reproducible biophysical methods including tension sensors and packing alterations, together with powerful live imaging methods, would help to understand local and global physical properties of this tissue in both *in vivo* and *in vitro* environments. Further, investigation of possible feedback loops between mechanical forces and proliferation and growth at both the tissue as well as the cellular levels will be important. We believe that the PSE with its tight packing, nuclear dynamicity and developmental relevance represents an excellent model to expand our knowledge of tissue mechanics to more complex epithelial tissues and will provide new insights into general regulation of cell proliferation and tissue growth.



4. CONCLUSIONS

Until now studies of PSE mainly focused on single-cell behavior. As a result, we gathered a significant understanding of the PSE cell biology, including valuable insights into nuclear dynamics occurring in these cells as well as their importance for cell and tissue proliferation. What we need to explore in much more detail, however, is how the dynamic events occurring in single-cells, such as PRAM and apical mitoses translate to tissue-wide changes. Future studies of mechanisms linking mechanics to PSE proliferative dynamics are essential to fully comprehend the development and function of these tissues. In addition, large-scale comparative quantitative studies are necessary to understand the versatility of PSE types and their packing levels. Finally, we believe that a transition toward a more mechanobiological approach, together with a shift toward a more comparative, tissue-scale perspective in the field of PSE biology should be underway. These additional routes in PSE research will result in unprecedented insights into the developmental and evolutionary causes and consequences of pseudostratification itself.

ACKNOWLEDGMENTS

We would like to thank Anna Erzberger and the Norden lab for helpful discussions and comments on the manuscript. We are grateful to Franziska Friedrich (PhotoLab, MPI-CBG) for helping us with the figures. C.N. is supported by the Human Frontier Science Program (CDA-00007/2011) and the German Research Foundation (DFG).

REFERENCES

- Baffet, A.D., Hu, D.J., Vallee, R.B., 2015. Cdk1 activates pre-mitotic nuclear envelope dynein recruitment and apical nuclear migration in neural stem cells. *Devel* 1–15.
- Baye, L.M., Link, B.A., 2007. Interkinetic nuclear migration and the selection of neurogenic cell divisions during vertebrate retinogenesis. *J. Neurosci.* 27 (38), 10143–10152.
- Benham-Pyle, B.W., Pruitt, B.L., Nelson, W.J., 2015. Cell adhesion. Mechanical strain induces E-cadherin-dependent Yap1 and β -catenin activation to drive cell cycle entry. *Science* 348 (6238), 1024–1027.
- Bort, R., Signore, M., Tremblay, K., Barbera, J.P.M., Zaret, K.S., 2006. Hex homeobox gene controls the transition of the endoderm to a pseudostratified, cell emergent epithelium for liver bud development. *Dev. Biol.* 290 (1), 44–56.
- Bystron, I., Blakemore, C., Rakic, P., 2008. Development of the human cerebral cortex: Boulder Committee revisited. *Nat. Rev. Neurosci.* 9 (2), 110–122.
- Chen, J., Knowles, H.J., Hebert, J.L., Hackett, B.P., 1998. Mutation of the mouse hepatocyte nuclear factor/forkhead homologue 4 gene results in an absence of cilia and random left-right asymmetry. *J. Clin. Invest.* 102 (6), 1077–1082.
- Clendenon, S.G., Shah, B., Miller, C.A., Schmeisser, G., Walter, A., Gattone II., V.H., et al., 2009. Cadherin-11 controls otolith assembly: evidence for extracellular cadherin activity. *Dev. Dyn.* 238 (8), 1909–1922.

- Coste, B., Xiao, B., Santos, J.S., Syeda, R., Grandl, J., Spencer, K.S., et al., 2012. Piezo proteins are pore-forming subunits of mechanically activated channels. *Nature* 483 (7388), 176–181.
- Cui, S., Otten, C., Rohr, S., Abdelilah-Seyfried, S., Link, B.A., 2007. Analysis of aPKC λ and aPKC ζ reveals multiple and redundant functions during vertebrate retinogenesis. *Mol. Cell. Neurosci.* 34 (3), 431–444.
- Dahl, K.N., Ribeiro, A.J.S., Lammerding, J., 2008. Nuclear shape, mechanics, and mechanotransduction. *Circ. Res.* 102 (11), 1307–1318.
- Das, T., Payer, B., Cayouette, M., Harris, W.A., 2003. In vivo time-lapse imaging of cell divisions during neurogenesis in the developing zebrafish retina. *Neuron* 37 (4), 597–609.
- Del Bene, F., Wehman, A.M., Link, B.A., Baier, H., 2008. Regulation of neurogenesis by interkinetic nuclear migration through an apical-basal notch gradient. *Cell* 134 (6), 1055–1065.
- Dzafic, E., Strzyz, P.J., Wilsch-Bräuninger, M., Norden, C., 2015. Centriole amplification in Zebrafish affects proliferation and survival but not differentiation of neural progenitor cells. *CellReports* 13 (1), 168–182.
- Eiraku, M., Takata, N., Ishibashi, H., Kawada, M., Sakakura, E., Okuda, S., et al., 2011. Self-organizing optic-cup morphogenesis in three-dimensional culture. *Nature* 472 (7341), 51–56.
- Eisenhoffer, G.T., Loftus, P.D., Yoshigi, M., Otsuna, H., Chien, C.-B., Morcos, P.A., Rosenblatt, J., 2012. Crowding induces live cell extrusion to maintain homeostatic cell numbers in epithelia. *Nature* 484 (7395), 546–549.
- Enserink, J.M., Kolodner, R.D., 2010. An overview of Cdk1-controlled targets and processes. *Cell Div.* 5 (1), 11–41.
- Fish, J.L., Dehay, C., Kennedy, H., Huttner, W.B., 2008. Making bigger brains—the evolution of neural-progenitor-cell division. *J. Cell. Sci.* 121 (Pt 17), 2783–2793.
- Florio, M., Huttner, W.B., 2014. Neural progenitors, neurogenesis and the evolution of the neocortex. *Development* 141 (11), 2182–2194.
- Ginzberg, M.B., Kafri, R., Kirschner, M., 2015. On being the right (cell) size. *Science* 348 (6236), 1245075.
- Grosse, A.S., Pressprich, M.F., Curley, L.B., Hamilton, K.L., Margolis, B., Hildebrand, J.D., Gumucio, D.L., 2011. Cell dynamics in fetal intestinal epithelium: implications for intestinal growth and morphogenesis. *Development* 138 (20), 4423–4432.
- Guharay, F., Sachs, F., 1984. Stretch-activated single ion channel currents in tissue-cultured embryonic chick skeletal muscle. *J. Physiol.* 352, 685–701.
- Heng, Y.-W., Koh, C.-G., 2010. Actin cytoskeleton dynamics and the cell division cycle. *Int. J. Biochem. Cell Biol.* 42 (10), 1622–1633.
- Hojjman, E., Rubbini, D., Colombelli, J., Alsina, B., 2015. Mitotic cell rounding and epithelial thinning regulate lumen growth and shape. *Nat. Commun.* 6, 7355.
- Horne-Badovinac, S., Lin, D., Waldron, S., Schwarz, M., Mbamalu, G., Pawson, T., et al., 2001. Positional cloning of heart and soul reveals multiple roles for PKC λ in zebrafish organogenesis. *Curr. Biol.* 11 (19), 1492–1502.
- Hu, D.J.-K., Baffet, A.D., Nayak, T., Akhmanova, A., Doye, V., Vallee, R.B., 2013. Dynein recruitment to nuclear pores activates apical nuclear migration and mitotic entry in brain progenitor cells. *Cell* 154 (6), 1300–1313.
- Humphrey, J.D., 2003. Review paper: continuum biomechanics of soft biological tissues. *Proc. R. Soc. A* 459, 3–46.
- Huttner, W.B., Brand, M., 1997. Asymmetric division and polarity of neuroepithelial cells. *Curr Opin Neurobiol.* 7 (1), 29–39.
- Ichikawa, T., Nakazato, K., Keller, P.J., Kajiura-Kobayashi, H., Stelzer, E.H.K., Mochizuki, A., Nonaka, S., 2013. Live imaging of whole mouse embryos during gastrulation: migration analyses of epiblast and mesodermal cells. *PLoS ONE* 8, e64506.

- Iulianella, A., Sharma, M., Durnin, M., Vanden Heuvel, G.B., Trainor, P.A., 2008. *Cux2* (*Cutl2*) integrates neural progenitor development with cell-cycle progression during spinal cord neurogenesis. *Development* 135 (4), 729–741.
- Jeong, J., McMahon, A.P., 2005. Growth and pattern of the mammalian neural tube are governed by partially overlapping feedback activities of the hedgehog antagonists *patched 1* and *Hhip1*. *Development* 132 (1), 143–154.
- Konno, D., Shioi, G., Shitamukai, A., Mori, A., Kiyonari, H., Miyata, T., Matsuzaki, F., 2007. Neuroepithelial progenitors undergo LGN-dependent planar divisions to maintain self-renewability during mammalian neurogenesis. *Nat. Cell Biol.* 10 (1), 93–101.
- Kosodo, Y., Röper, K., Haubensak, W., Marzesco, A.-M., Corbeil, D., Huttner, W.B., 2004. Asymmetric distribution of the apical plasma membrane during neurogenic divisions of mammalian neuroepithelial cells. *EMBO J.* 23 (11), 2314–2324.
- Kosodo, Y., Suetsugu, T., Suda, M., Mimori-Kiyosue, Y., Toida, K., Baba, S.A., et al., 2011. Regulation of interkinetic nuclear migration by cell cycle-coupled active and passive mechanisms in the developing brain. *EMBO J.* 30 (9), 1690–1704.
- Kung, C., 2005. A possible unifying principle for mechanosensation. *Nature* 436 (7051), 647–654.
- Langman, J., Guerrant, R.L., Freeman, B.G., 1966. Behavior of neuro-epithelial cells during closure of the neural tube. *J. Comp. Neurol.* 127 (3), 399–411.
- LeGoff, L., Lecuit, T., 2015. Mechanical forces and growth in animal tissues. *Cold Spring Harb Perspect Biol.* pii, a019232.
- Leung, L., Klopffer, A.V., Grill, S.W., Harris, W.A., Norden, C., 2011. Apical migration of nuclei during G2 is a prerequisite for all nuclear motion in zebrafish neuroepithelia. *Development* 138 (22), 5003–5013.
- Liang, L., Haug, J.S., Seidel, C.W., Gibson, M.C., 2014. Functional genomic analysis of the periodic transcriptome in the developing *Drosophila* wing. *Devcel* 29 (1), 112–127.
- Lumpkin, E.A., Caterina, M.J., 2007. Mechanisms of sensory transduction in the skin. *Nature* 445 (7130), 858–865.
- Mammoto, T., Ingber, D.E., 2010. Mechanical control of tissue and organ development. *Development* 137 (9), 1407–1420.
- Mao, Y., Hoppe, A., Kester, L., Thompson, B.J., Tournier, A.L., Tapon, N., 2013. Differential proliferation rates generate patterns of mechanical tension that orient tissue growth. *EMBO J.* 32 (21), 2790–2803.
- Meyer, E.J., Ikmi, A., Gibson, M.C., 2011. Interkinetic nuclear migration is a broadly conserved feature of cell division in pseudostratified epithelia. *Curr. Biol.* 21 (6), 485–491.
- Milán, M., Campuzano, S., García-Bellido, A., 1997. Developmental parameters of cell death in the wing disc of *Drosophila*. *Proc. Natl. Acad. Sci. USA* 94 (11), 5691–5696.
- Miyata, T., 2008. Development of three-dimensional architecture of the neuroepithelium: role of pseudostratification and cellular “community.”. *Dev. Growth Differ.* 50 (Suppl 1), S105–S112.
- Miyata, T., 2015. Interkinetic nuclear migration generates and opposes ventricular-zone crowding: insight into tissue mechanics. *Front Cell Neurosci.* 8, 1–11.
- Morin, X., Jaouen, F., Durbec, P., 2007. Control of planar divisions by the G-protein regulator LGN maintains progenitors in the chick neuroepithelium. *Nat. Neurosci.* 10 (11), 1440–1448.
- Müsch, A., 2004. Microtubule organization and function in epithelial cells. *Traffic* 5 (1), 1–9.
- Nagele, R.G., Lee, H.Y., 1979. Ultrastructural changes in cells associated with interkinetic nuclear migration in the developing chick neuroepithelium. *J. Exp. Zool.* 210 (1), 89–105.
- Nakajima, Y.-I., Meyer, E.J., Kroesen, A., McKinney, S.A., Gibson, M.C., 2013. Epithelial junctions maintain tissue architecture by directing planar spindle orientation. *Nature* 500 (7462), 359–362.

- Naruse, I., Keino, H., 1995. Apoptosis in the developing CNS. *Prog. Neurobiol.* 47 (2), 135–155.
- Nasonkin, I.O., Lazo, K., Hambright, D., Brooks, M., Fariss, R., Swaroop, A., 2011. Distinct nuclear localization patterns of DNA methyltransferases in developing and mature mammalian retina. *J. Comp. Neurol.* 519 (10), 1914–1930.
- Nigg, E.A., Raff, J.W., 2009. Centrioles, centrosomes, and cilia in health and disease. *Cell* 139 (4), 663–678.
- Norden, C., Young, S., Link, B.A., Harris, W.A., 2009. Actomyosin is the main driver of interkinetic nuclear migration in the retina. *Cell* 138 (6), 1195–1208.
- Okamoto, M., Namba, T., Shinoda, T., Kondo, T., Watanabe, T., Inoue, Y., et al., 2013. TAG-1-assisted progenitor elongation streamlines nuclear migration to optimize subapical crowding. *Nat. Neurosci.* 16 (11), 1–13.
- Okamoto, M., Shinoda, T., Kawaue, T., Nagasaka, A., Miyata, T., 2014. Ferret–mouse differences in interkinetic nuclear migration and cellular densification in the neocortical ventricular zone. *Neurosci. Res.* 83, 25–32.
- Pathak, M.M., Nourse, J.L., Tran, T., Hwe, J., Arulmoli, J., Le, D.T.T., et al., 2014. Stretch-activated ion channel Piezo1 directs lineage choice in human neural stem cells. *Proc. Natl. Acad. Sci. USA* 111 (45), 16148–16153.
- Porazinski, S., Wang, H., Asaoka, Y., Behrndt, M., Miyamoto, T., Morita, H., et al., 2015. YAP is essential for tissue tension to ensure vertebrate 3D body shape. *Nature* 1–16.
- Poulton, J.S., Cuningham, J.C., Peifer, M., 2014. Acentrosomal *Drosophila* epithelial cells exhibit abnormal cell division leading to cell death and compensatory proliferation. *Devcel* 30 (6), 731–745.
- Provenzano, P.P., Keely, P.J., 2011. Mechanical signaling through the cytoskeleton regulates cell proliferation by coordinated focal adhesion and Rho GTPase signaling. *J. Cell Sci.* 124 (8), 1195–1205.
- Rakic, P., 1972. Mode of cell migration to the superficial layers of fetal monkey neocortex. *J. Comp. Neurol.* 145 (1), 61–83.
- Rodriguez-Boulan, E., Macara, I.G., 2014. Organization and execution of the epithelial polarity programme. *Nat Rev Mol Cell Biol.* 15 (4), 225–242.
- Rujano, M.A., Sanchez-Pulido, L., Pennetier, C., le Dez, G., Basto, R., 2013. The microcephaly protein Asp regulates neuroepithelium morphogenesis by controlling the spatial distribution of myosin II. *Nat Cell Biol.* 15 (11), 1294–1306.
- Salbreux, G., Charras, G., Paluch, E., 2012. Actin cortex mechanics and cellular morphogenesis. *Trends Cell Biol.* 22 (10), 536–545.
- Sauer, F.C., 1935. Mitosis in the neural tube. *J. Comp. Neurol.* 62 (2), 377–405.
- Schenk, J., Wilsch-Bräuninger, M., Calegari, F., Huttner, W.B., 2009. Myosin II is required for interkinetic nuclear migration of neural progenitors. *Proc. Natl. Acad. Sci. USA* 106 (38), 16487–16492.
- Schluck, T., Nienhaus, U., Aegerter-Wilmsen, T., Aegerter, C.M., 2013. Mechanical control of organ size in the development of the *Drosophila* wing disc. *PLoS ONE* 8 (10), e76171–e76179.
- Schoenwolf, G.C., Alvarez, I.S., 1989. Roles of neuroepithelial cell rearrangement and division in shaping of the avian neural plate. *Development* 106 (3), 427–439.
- Sivars, U., Aivazian, D., Pfeffer, S.R., 2003. Yip3 catalyses the dissociation of endosomal Rab–GDI complexes. *Nature* 425 (6960), 856–859.
- Smart, I.H., 1972. Proliferative characteristics of the ependymal layer during the early development of the mouse diencephalon, as revealed by recording the number, location, and plane of cleavage of mitotic figures. *J. Anat.* 113 (Pt 1), 109.
- Smart, I.H., 1973. Proliferative characteristics of the ependymal layer during the early development of the mouse neocortex: a pilot study based on recording the number, location and plane of cleavage of mitotic figures. *J. Anat.* 116 (Pt 1), 67–91.

- Smith, J.L., Schoenwolf, G.C., 1989. Notochordal induction of cell wedging in the chick neural plate and its role in neural tube formation. *J. Exp. Zool.* 250 (1), 49–62.
- Smith, J.L., Schoenwolf, G.C., Quan, J., 1994. Quantitative analyses of neuroepithelial cell shapes during bending of the mouse neural plate. *J. Comp. Neurol.* 342 (1), 144–151.
- Spear, P.C., Erickson, C.A., 2012a. Apical movement during interkinetic nuclear migration is a two-step process. *Dev. Biol.* 370 (1), 33–41.
- Spear, P.C., Erickson, C.A., 2012b. Interkinetic nuclear migration: a mysterious process in search of a function. *Dev. Growth Differ.* 54 (3), 306–316.
- Stewart, M.P., Helenius, J., Toyoda, Y., Ramanathan, S.P., Muller, D.J., Hyman, A.A., 2010. Hydrostatic pressure and the actomyosin cortex drive mitotic cell rounding. *Nature* 469 (7329), 226–230.
- Streichan, S.J., Hoerner, C.R., Schneidt, T., Holzer, D., Hufnagel, L., 2014. Spatial constraints control cell proliferation in tissues. *Proc. Natl. Acad. Sci. USA* 111 (15), 5586–5591.
- Strzyz, P.J., Lee, H.O., Sidhaye, J., Weber, I.P., Leung, L.C., Norden, C., 2015. Interkinetic nuclear migration is centrosome independent and ensures apical cell division to maintain tissue integrity. *Devcel* 32 (2), 203–219.
- Taverna, E., Huttner, W.B., 2010. Neural progenitor nuclei IN motion. *Neuron* 67 (6), 906–914.
- Tsai, J.-W., Lian, W.-N., Kemal, S., Kriegstein, A.R., Vallee, R.B., 2010. Kinesin 3 and cytoplasmic dynein mediate interkinetic nuclear migration in neural stem cells. *Nat. Neurosci.* 13 (12), 1463–1471.
- Tsuda, S., Kitagawa, T., Takashima, S., Asakawa, S., Shimizu, N., Mitani, H., et al., 2010. FAK-mediated extracellular signals are essential for interkinetic nuclear migration and planar divisions in the neuroepithelium. *J. Cell Sci.* 123 (Pt 3), 484–496.
- Tsujita, K., Takenawa, T., Itoh, T., 2015. Feedback regulation between plasma membrane tension and membrane-bending proteins organizes cell polarity during leading edge formation. *Nat. Cell Biol.* 17 (6), 749–758.
- Vermeulen, K., Van Bockstaele, D.R., Berneman, Z.N., 2003. The cell cycle: a review of regulation, deregulation and therapeutic targets in cancer. *Cell Prolif.* 36 (3), 131–149.
- Weber, I.P., Ramos, A.P., Strzyz, P.J., Leung, L.C., Young, S., Norden, C., 2014. Mitotic position and morphology of committed precursor cells in the zebrafish retina adapt to architectural changes upon tissue maturation. *CellReports* 7 (2), 386–397.
- Xie, Z., Moy, L.Y., Sanada, K., Zhou, Y., Buchman, J.J., Tsai, L.-H., 2007. Cep120 and TACCs control interkinetic nuclear migration and the neural progenitor pool. *Neuron* 56 (1), 79–93.
- Xie, Y., Jüschke, C., Esk, C., Hirotsune, S., Knoblich, J.A., 2013. The phosphatase PP4c controls spindle orientation to maintain proliferative symmetric divisions in the developing neocortex. *Neuron* 79 (2), 254–265.
- Yang, Y.-T., Wang, C.-L., Van Aelst, L., 2012. DOCK7 interacts with TACC3 to regulate interkinetic nuclear migration and cortical neurogenesis. *Nat. Neurosci.* 15 (9), 1201–1210.
- Yu, F.X., Guan, K.L., 2014. Transcription and processing: multilayer controls of RNA biogenesis by the Hippo pathway. *EMBO J.* 33 (9), 942–944.

HDAC1 genotyping

Pt.1: DNA extraction by finclipping

(modified Utrecht protocol)

Lysisbuffer:	final	stock
	100 mM Tris HCl pH 8.8	1 M Tris HCl pH 8.5
	200 mM NaCl	5 M NaCl
	0.2% SDS	10% SDS
	5 mM EDTA	0.5 M EDTA
		10 mg/ml ProteinaseK
	prepare and keep at RT	
	add ProteinaseK (final	
	concentration: 100 µg/ml)	
	just before the preparation	
	starts	

Day1

- anaesthetise fishes in MESAB/fishwater (4.2 ml MESAB/Tricaine in 100 ml fishwater)
- clip fins and directly transfer them into precooled Eppendorf tubes or deep well plates, kept on dry ice
- finish all clips before continue with isolation

- add 500 µl lysisbuffer (incl. ProteinaseK), - **take care when thawing** (not too cold but do not leave it at RT for too long)
plates: seal carefully, and spin to make sure that all fins are in the lysisbuffer
eppis: close, check that fin is in the lysisbuffer
- incubate ON at 55°C, vortex from time to time (important in the beginning)

Day2

- spin down debris at
deep well-plates: 4.600 rpm* (3761 g) for 1h (and transfer supernatant to new plate - optional and very tedious)
eppis: 8.000 rpm for 10 min, (transfer supernatant into new tubes)
- add 400 µl Isopropanol,
deep-well plates: seal with alu-foil, mix by inverting several times (check if foil still seals tightly), seal with new sheet of foil
eppis: just invert several times
- *deep-well plates*: spin at 3761g for 1h at RT, discard supernatant immediately
eppis: spin at 13.000 rpm (full-speed) for 15 min at RT, discard supernatant immediately
- wash once with 300 ul 70% ethanol, seal with alu-foil, invert several times, (seal with fresh foil)
- *deep-well plates*: spin at 3761g for 30 min, discard supernatant immediately
eppis: spin at 13.000 rpm for 15 min at RT, discard supernatant immediately
- 2nd washing step optional
- dry several minutes at RT (5min upside down + 20min open)
- add 200 µl TE (library), vortex and shake for several hours at RT, store at -20°C ---

Day3

- check 5ul of genomic DNA on 0.7% agarose gel, use λHindIII digested as length marker (separate 2,4,8 ul of marker on the agarose gel)
- for PCRs dilute genomic DNA 1:50

- take out 70 ul of genomic DNA and generate masterplate (kept at -20°C), the deep well plate is the working plate
- - Multifuge 3S-R, Swing-out rotor 7500 6445, microtiterplates: 4600 rpm (= 3761g) is max speed
 - deep well plates: Nerbe 1.1 ml deep well plates , order no. 04-072-0000

HDAC Genotyping

Pt. 2: Restriction Fragment Length Polymorphism

(modified ZIRC assay)

***Bfal* digestion**

	name	seq
Primer(fwd):	#655 HDAC-Bfal	ttcagctggtgcggtgaaactcaacaac
Primer(rev):	#647 hdac1 R1	GAAATAACTTGATGTTAGAGC

PCR reaction:	1X (µl)
10 mM dNTPs	0.6
10µM primer	0.6
10µM primer	0.6
PCR buffer	3.0
ddH2O	10.05
Taq	0.15
DNA from lysis	15.0
Vt	30.0

use 10ul of PCR product to check on gel

PCR Profile:	Step	Temp	Time
	1	94°C	2 min
	2	94°C	15 sec
	3	55,1°C	20 sec
	4	72°C	20 sec
	5	repeat steps 2-4 for 30 cycles	
	6	72°C	1 min
	7	store at 4°C	

Precipitation: work in 96well PCR plates

add 2ul 3M NaOAc to 20ul of PCR product and mix by shaking
add 66ul 100% EtOH and mix by shaking
store at -80°C for 15 min or at -20°C for 1 hr
centrifuge at 3760 RZB for 1 hr and remove carefully the supernatant
wash with 100ul 70% EtOH
centrifuge at 3760 RZB for 30 min and remove carefully the supernatant
dry the pellets and dissolve in 10ul H2O
shake for 2 hrs

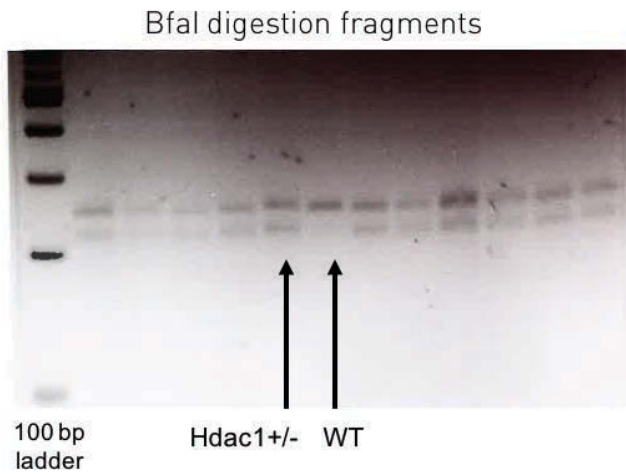
Bfal digestion:		@ 37°C
	1X (µl)	
ddH2O	8.0	
10X NEB Cutsmart	1.5	
PCR product	5.0	
Bfal	0.5	
Vt=	15.0	

Run products out on 3% agarose TAE gel:
 (2% Lonza Metaphor Agarose and 1% Agarose)

PCR product size = 250bp

Mut = 220bp + 250bp

Wt = 250bp



SUPPLEMENTAL MOVIES AND SCRIPTS

On the link below and on attached CD.



QR-code links to cloud.mpi-cbg.de

DATA

All data can be found at DOI: [10.5281/zenodo.1316912](https://doi.org/10.5281/zenodo.1316912)